Versatile biosensor for deciphering glycoenzymatic activities

Daniel Márquez-Martín

THÈSE

Pour obtenir le grade de

DOCTEUR DE L'UNIVERSITÉ GRENOBLE ALPES

Spécialité : Chimie Biologie

Arrêté ministériel : 25 mai 2016

Présentée par

Daniel MÁRQUEZ-MARTÍN

Thèse dirigée par **Didier GASPARUTTO**,Dir. Recherche CEA, Université Grenoble Alpes
et co-encadrée par **Olivier LEROUXEL**,enseignant-chercheur et **Aurelie BOUCHET-SPINELLI**, UNIVERSITE GRENOBLE ALPES

préparée au sein du **Laboratoire Systèmes Moléculaires et Nano Matériaux pour l'Énergie et la Santé**
dans **l'École Doctorale Chimie et Sciences du Vivant**

Biocapteur polyvalent pour décrypter les activités glycoenzymatiques

Versatile biosensor for deciphering glycoenzymatic activities

Thèse soutenue publiquement le **16 mars 2021**,
devant le jury composé de :

Monsieur DIDIER GASPARUTTO
INGENIEUR HDR, CEA GRENOBLE, Directeur de thèse
Madame MURIEL BARDOR
PROFESSEUR DES UNIVERSITES, UNIVERSITE DE ROUEN - HAUTE NORMANDIE, Rapporteure
Monsieur CARMELO DI PRIMO
CHARGE DE RECHERCHE HDR, INSERM DELEGATION NOUVELLE-AQUITAINE, Rapporteur
Madame Carole CHAIX-BEAUVAIS
DIRECTRICE DE RECHERCHE, CNRS DELEGATION RHONE AUVERGNE, Examinatrice
Monsieur OLIVIER RENAUDET
PROFESSEUR DES UNIVERSITES, UNIVERSITE GRENOBLE ALPES, Président

Résumé

À ce jour, les glycosyltransférases (GT) sont une famille essentielle d'enzymes mal caractérisées à la fois structurellement et mécaniquement, ce qui constitue une limitation majeure dans le domaine des glycosciences. Ces enzymes jouent un rôle crucial dans les organismes vivants en catalysant le transfert stéréo- et régio-spécifique d'un sucre donneur activé vers une molécule acceptrice, pour construire des oligosaccharides complexes à la surface des cellules. La mise au point de nouveaux outils analytiques est nécessaire pour analyser et caractériser les interactions entre ces enzymes et les glycanes, dans une approche à haut débit. Dans ce contexte, l'imagerie par résonance plasmonique de surface (SPRi) apparait comme une méthodologie adaptée et polyvalente pour répondre à cette demande de criblage de ligands et de suivi des interactions biomoléculaires, en temps réel et sans marquage.

Par conséquent, ce projet de recherche multidisciplinaire est organisé en trois axes principaux : dans un premier temps, nous abordons l'expression hétérologue et la purification d'une fucosyltransférase de la plante *Arabidopsis thaliana* (AtFUT1) qui participe à la dernière étape de la biosynthèse du ligand xyloglucan (XyG). Ensuite, les approches d'immobilisation spécifiques des résidus glycanes sur surface ont motivé la conception de stratégies chimiosélectives pour conjuguer les entités XyG à des échafaudages oligonucléotidiques avec de bons rendements. La polyvalence des structures ODN conjuguées aux glycanes fournit des informations et propriétés précieuses pour les étapes de purification et de caractérisation des glycanes, ainsi que pour leur immobilisation. Enfin, le troisième axe est consacré à la conception et à la construction d'une glyco-puce XyG polyvalente, par une approche d'immobilisation spécifique dirigée par l'ADN (DDI). Cette stratégie conduit au développement final d'un outil analytique original basé sur la puissante technique SPRi, qui permet la visualisation et la caractérisation des interactions biomoléculaires en temps réel et sans marquage.

Abstract

To date, glycosyltransferases (GTs) are an essential family of enzymes poorly characterized both structurally and mechanistically which is being a major bottleneck in Glycoscience. They play a crucial role in living organisms catalysing the stereo- and regiospecific transfer of an activated donor sugar to an acceptor moiety to build up complex oligosaccharides onto the cell surface. New analytical tools are required to screen enzyme-glycan interactions in high-throughput manner. In this context, Surface Plasmon Resonance imaging (SPRi) has spread as a versatile methodology to overcome this glycoscientific demand for ligands screening and biomolecular interaction monitoring at real time and without any labels.

Therefore, this multidisciplinary project is organized in three main axes: first, we address the heterologous expression of a fucosyltransferase from the plant *Arabidopsis thaliana* (AtFUT1) (CAZy family GT37) that participates in the last step in the biosynthesis of xyloglucan (XyG) ligand. Then, specific immobilization approaches using DNA architectures motivate the design of chemoselective strategies to conjugate XyG building-blocks to oligonucleotidic scaffolds in good yields. The versatility of having ODN structures conjugated to glycans provides powerful insights for glycan purification, characterization and also immobilization approaches on solid support. In this matter, the third axis is dedicated towards the conception and construction of a versatile XyG glycochip for its specific immobilization approach by DNA-Directed Immobilization (DDI). This strategy is envisioned through the powerful SPRi technique that allows the simultaneous visualization of binding events without using any label molecule in real time measurements.

Acknowledgements

Either the destiny or love led me make the decision to travel and discover what will be one of the places that have left an unforgettable mark on my life: Grenoble. Those three years of Ph.D student helped me to mature and be a better person both professionally and personally. And it is for these details what I want to thank all those people who made it possible to make my dreams come true.

First and foremost, this project would not have been carried out without the help of my supervisors. That is why my gratitude goes to Olivier, Aurelie and Didier. Together, we have been able to discover and work on a multidisciplinary project combining the knowledge of three disciplines (biology, chemistry and biophysics) into one. Thanks to you and your support, I was able to learn a lot about the different challenges and concerns involved in working on multiple areas of science. This has triggered on me a much more open and critical mentality as a scientist. You have been an example of professionalism, closeness, camaraderie and tolerance; and I feel very proud to have been a part of it.

All of this, of course, is accompanied by two magnificent laboratories where I have had the real pleasure of being involved like a family. The Glycobiologie molécularie et structurale (GBMS) team at CERMAV and the Chimie pour la Reconnaisance et l'étude d'assemblages biologiques (CREAB) team at CEA. The amazing high human level within these two groups is immeasurable and I felt so lucky from the first time I was there: a small chemist surrounded by a world of biologist and physicist.

I thank the entire GBMS group, you honor your entity as the theme of the laboratory: *Strong binding and affinity effect* within the members of the group. I could met wonderful and amazing people like Aurora, Oriane, Sima, Dania, Rafael, Lukas, François, Dylan, Kanhaya, Sue, Marguerita that showed me how important a good work environment and friendship are necessary in a team. Thanks a lot. Moreover, I would like to highlight the important contribution to the advancement of this project to Emilie, Isaty and Marion in the protein purification and characterization by ITC. Finally, I would like to thank Valerie and Ferielle for your unconditional help both in technical and administrative support within my first year.

Similarly, I thank the entire CREAB team represented by the entity of *Gold people*. It is a team that shine everywhere they go and whose value is always immense. People like Jon, Lucile, Charlotte, Eric, Milagros, Annette, Maud, Larry, Oleski, Marie, Marielle, Elise, Ere, Sophie, Ricardo and Marine. I will never forget you! I will highlight the great atmosphere that we got during the coffee breaks, the sortie de ski (Amazing! although I was always the petit canard), or Christmas lunch. Unforgettable! I specially thank Christine to "fight" with me in the purification, characterization and analysis of the chemical structure of Xyloglucan "monster" with a conjugated DNA. This work it could not be possible without your help. Likewise, I would like to thank Raph for your help in the SPRi experiments and also my friend Jose that helped me a lot to settle down in the lab and make feel "safe & comfy" with the French bureaucracy. Finally, I take with me some special moments with Chacha, Jon and Eric playing squash until getting exhausted or playing music in the pure pop rock style or dancing bachata latino with Ricardo to disconnect from our daily routines.

In parallel to my work family, I am really fortunate to have met and involved within such a wonderful group of people who call themselves *Grenoble New Generation*. If a person arrives to Grenoble and find this group of people, fun is guaranteed. That was my case. I can't imagine a better reception than the one I had. I need to thank all these amazing people like Jorge, Marie Laure, Alvaro, Ricardo, Ines, Tomas, Rob, Marila, Vanni, Raquel, Xenia, Kike, Jaione, Javi, Maddi, Isa, Ana, Mark, Eugenia and Niko for their friendship, incredible moments, a very strong linkage that makes being away from home just a memory. Although our paths have been separated, I will keep in memory all those unforgettable experiences that a great family of friends can have. However, there are two people who have made me grow as a person and have an incredible vision of life. They are Jorge and Marie Laure. We have managed to create a special link so big and beautiful, that I have no words to express it. You were a guide in my beginnings in Grenoble and you are still a guide to me nowadays. We have shared countless adventures together (magical randos, ski, kayak, rackets...), amazing discussions about hotspot social problems (we will change the world) and thankfully, it will continue to be that way for a long time to come. I hope infinite. Everything would have been more difficult without you around.

I would like to thank as well Ines and Ricardo for their close engagement, deep discussions and their adventurous spirit. Thanks a lot!. And also, a big thank you to Alvaro, the king of the tortilla de patatas and my flatmate just for three months. However, we only needed a few days to realize the good feeling that exist between us. Thanks a lot bro (get the party going).

Luckily, this group still live evolving towards a *Grenoble New Generation 2.0* with amazing people having the same feeling, enthusiasm and energy to do a lot of things together. I have to thank Maria, Gonzalo, Miren, Angel, Jesus, Maria (2) and Alvaro (2) for all these moments doing barbecues, randos (taking and eating les ail des ourses, myrtilles) like kids, and having a really warm friendship environment.

I would also like to remember all wonderful people from the Neel institute like Roberto, Gotham, Estelle, Riadh, Priyank, Kazi, William also pretty nice football players.

En este punto, quiero dar un salto en el tiempo y en el espacio para agradecer a todos aquellas personas que han compartido conmigo etapas muy importantes en mi vida, y que de alguna manera, me han llevado hasta donde estoy ahora. Quiero agradecer a mis fieles amigos de Arganda Víctor, Tito, Méndez (mi banda Crash Rush), Panero, Naten, Virginia, Coty y Rebe, que a pesar de la distancia siempre hemos seguido muy unidos. Por supuesto, a mis compañeros de la universidad, Ana, Iris, Sandra, Clemens, Elena, Víctor, Kike y al nuevo integrante de la manada, el pequeño Matiño. Gracias por todos esos momentos fantásticos, de viajes y celebraciones de tesis (salvo la nuestra eh Victor, nos la deben) o de cenas de Navidad que espero no cesen nunca de ocurrir. Sois los mejores.

Y por supuesto, todo este proyecto no hubiera sido posible sin el pilar imprescindible de mi familia. Agradecer a mi padre, mi madre y mi hermano Álvaro, que son un orgullo y un ejemplo a seguir de motivación, confianza, optimismo y superación para sobreponer la dureza de la distancia, y vivir cada día como si estuvieran a mi lado. Sois la pieza base y el apoyo que sustenta toda mi carrera tanto personal como profesional. De igual forma a mis tíos y primos que tanto aprecio y que han estado ahí animando y empujando desde atrás para seguir mirando hacia adelante. Igualmente, quiero agradecer también a mis padres políticos Pepe y Ana por todo vuestro apoyo y entrega que habéis tenido hacia nosotros en esta dura etapa.

Por último, cierro los agradecimientos referenciando la primera frase que abrió esta sección, agradeciendo a mi compañera de viaje y de aventuras, la cual tengo la gran suerte de que sea mi novia: Ana Cristina (o Ana, que te gusta más). Cómo hubiera cambiado nuestra vida de saber que empezaríamos esta aventura del doctorado separados. Pero fue algo más que el destino lo que me condujo a tomar la decisión de viajar a Grenoble desde Bristol (siempre estará en mi recuerdo, gracias Prof. Carmen Galan y a todo su grupo), y no me arrepiento de lo ocurrido. Haber podido desarrollar esta primera etapa de independencia contigo, me ayuda a mirar al futuro con grandes perspectivas. Gracias por estar al pie del cañón en todo momento, por tu ayuda incondicional, tus esquemas organizativos, tu capacidad de síntesis e ir siempre al grano (guiño, guiño a la tesis), por tu cariño, tu apoyo y tu aguante en momentos delicados. Mérito enorme pasar una pandemia con una persona escribiendo una tesis. Espero de corazón seguir a tu lado compartiendo infinidad de retos, de aventuras y deseos en un camino futuro que se abre ante nosotros.

A todos, mil gracias!

Thesis Layout

Before starting, I would like to provide a guideline reading that might explain to the reader on how this manuscript has been organized.

This project dives into the Glycoscience framework moving at the interfaces between biology, chemistry and physics. The motivation of this multidisciplinary project is determined by the complexity of each scientific domain and therefore, it requires an equitable treatment throughout this manuscript. Thus, I prepared this thesis research into six chapters organized as follows:

The first chapter will be dedicated to provide a general overview about the world of carbohydrates, the biological machinery of enzymes responsible on their fabrication, and one emerging technology to monitor their interactions.

The following three chapters will entail the core of this project and they will be dedicated to explore the three scientific domains aforementioned. Each of these chapters will be introduced by a scientific context about the state-of-the-art, followed by a proposed strategy and the most relevant results obtained for that purpose. Finally, they will be closed by a general conclusions.

Then, a fifth chapter will be devoted to a detailed description of the materials and experimental procedures carried out in this project. Finally, the thesis closes with a sixth chapter that will provide the general conclusions and some future perspectives.

Contents

List of abbreviations

A	Adenine
Asp	Aspartate
AtFUT1	Arabidopsis thaliana fucosyltransferase 1
ATP	Adenosine triphosphate
BCN	bicyclononyne
BPB	bromophenol blue
C	Cytosine
CAZy	Carbohydrate Active enZyme Database
CCD	Charge-Coupled Device
CG	Cytosine-Guanine pair
COCs	Carbohydrate-Oligonucleotide Conjugates
cODN	complementary Oligodeoxynucleotide
ConA	Concanavalin A
COV	Coronavirus
CSLC	Cellulose synthase-like C
CuAAC	Copper(I)-catalyzed alkyne-azide cycloaddition
DBCO	Dibenzocyclooctyne amine
DDI	DNA-directed immobilization
DHB	2,5-Dihydroxybenzoic acid
DIBAC	Dibenzo-aza-cyclooctyne
DIBO	Dibenzocyclooctyne
DIFO	Difluorinated cyclooctyne
DIMAC	Dimethoxy-azacyclooctyne
DMT	4,4'-dimethoxytrityl
DNA	Deoxyribonucleic acid
dsDNA	Duplex DNA
FUT1	Fucosyltransferase 1
G	Guanine
GalTs	Galactosyltransferase(s)
GBP	Glycan-binding proteins
GDP	Guanosine diphosphate

GDP-Fuc	Guanosine diphosphate fucose
Glc	Glucose
Glu	Glutamate
GTs	Glycosyltransferase(s)
HEPES	2-[4-(2-hydroxyethyl)piperazin-1-yl]ethanesulfonic acid
Hi5	High-five insect cells
HIA	Hemagglutination inhibition
HIV-I	Human immunodeficiency virus
HPA	3-hydroxypicolinic acid
ITC	Isothermal Titration Calorimetry
kDa	kiloDaltons
LC MS	Liquid chromatography Mass-spectrometry
MALDI-Tof	Matrix-Assisted Laser Desorption/Ionization Time-of-flight
MC	Millions of cell
MOI	Multiplicity of infection
MS	Mass-spectrometry
MUR	Arabidopsis mutant collection
NGC	Natural gas chromatography
NHS	N-hydroxysuccinimide
ODN	Oligodeoxynucleotide
OGT	O-linked N-acetylglucosamine transferase
PAGE	Polyacrylamide-based gel
PCW	Primary cell wall
PyNAC	Pyrrole-nucleic acid conjugates
QCM	Quartz crystal microbalance
R.U	Refectivity units
RCA 120	Ricinus Communis Agglutinin 120
RNA	Ribonucleic acid
ROI	Regions of interest
RP HPLC	Reverse Phase High Performance Liquid Chromatography
SAMDI	SAM on gold with the MALDI-Tof MS analysis
SAMs	Self-assembly monolayers
SDS-Page	Sodium dodecyl sulphate-Polyacrylamide gel electrophoresis
SEC	Size-exclusion chromatography

SPAAC	Strain-promoted azide-alkyne cycloaddition
SPR	Surface Plasmon Resonance
SPRi	Surface Plasmon Resonance imaging
ssODN	Single-strand Oligonucleotide
STD-NMR	Saturation-Transfer Diference NMR
T	Thymine
T10	Thymine spacer
TEG	Triethylenglycol
TIR	Total internal reflection
Tm	Melting temperature
TS	Transition state
TXyG	Tamarind xyloglucan
UDP	Uracil diphosphate
UDP-Glc	Uridine diphosphate glucose
XC	Xylene cyanol
XLT	Xyloglucan L-side chain galactosyl transferase
XXT	Xylosyltransferase
XyG	Xyloglucan
Xyl	Xylose
XyNAC	Xyloglucan nucleic acid conjugates

1 General Introduction

The world is sweet!! Sugars are considered one of the most abundant macromolecules found on Earth. They have become to a central family of molecules playing unique roles in living organisms. From Hermann E. Fisher, "a new line of study emerged gathering fundamental research fields to understand this new language of life: the Glycoscience." This chapter outlines general information regarding the world of sugars, a pivotal family of enzymes that synthesise them called glycosyltransferases and a powerful biosensing tool that enable their biochemical characterization.

Contents

1.1 The central language of carbohydrates

In the past, there were only three main research areas in biochemistry that have concentrated the major attention within the scientific community: the nucleic acids, the proteins and the lipids. Additionally, it existed a family of natural macromolecules named carbohydrates that are concealed in the anonymity only admittedly as a useful function to provide energy or mechanic strength. However, because of their structural complexity and they are not part of the genome, the study of carbohydrates has been recently emphasized as a new biological target of communication language in Nature. The lack of information and the discovery of new structural and biochemical implications in modulating biomolecular recognition for pathological process, inflammation responses or immune system activation have promoted the origin of a new research discipline called Glycoscience.[1–4]

1.1.1 The Study of Carbohydrates in Glycoscience

Glycoscience is a scientific interdisciplinary area involved in the study of one of the most abundant biomolecules found on Earth: the carbohydrates. Within this wide research field, it combines a global community of biologists, chemists, biochemists, microbiologists, engineers, computational scientists and informatics to provide a deep knowledge towards the better understanding of the biological information and potential applications behind these interesting macromolecules.[3,5]

The term carbohydrate has been historically interchanged with sugars just to define a carbohydrate molecule that exhibit sweetness flavour in taste. Moreover, this organic molecule has adopted generic names such as glycans (Greek prefix of sugar), saccharides or sugars, all of them perfectly validated within the Glycoscience community.

Carbohydrates belong to a fundamental family of macromolecules that are composed by carbon and hydrogen atoms (literally hydrates of carbon) with the empirical formula ($Cn(H_2O)n$) as the smallest template unit. However, it exists a huge variety of carbohydrates biomolecules that encompasses the simplest units named monosaccharides and the combination of each monosaccharide unit to form more complex structures so called disaccharides (two monosaccharides) or polysaccharides (more than thirteen monosaccharides).

The large variety of carbohydrates structures resides in their versatility as chemical composition. In the Figure 1.1 a model of trisaccharide is illustrated with a description of all the chemical information contained within their structure.

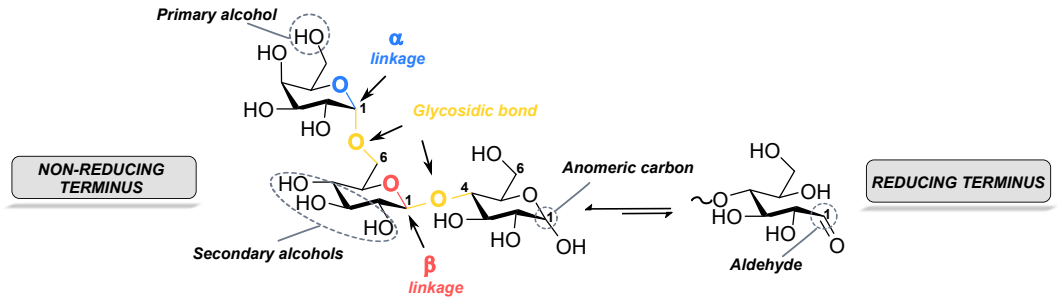

Figure 1.1: Chemical structure of a model of trisaccharide. Chemically, two different functional groups are distinguished: the free alcohol groups (primary and secondary alcohols) and the aldehyde group, generally in the close form as hemiacetal. The active point of reactivity from the aldehyde form determines the reducing end of the glycan. On the other hand, the hydroxyl groups are the oxidized form within the glycan structure, and therefore, they define the non-reducing end. The reaction of both chemical groups from different glycans yields the coupling of the structures through a glycosidic bond (in yellow) with a fixed stereochemistry (either α- in blue or β- in red) and the reactive points of linkage (regiochemistry) within the glycosidic bond (1,4 and 1,6).

The general attachment of monosaccharides is a result from the chemical reaction between the aldehyde form of one monosaccharide unit with an alcohol from another residue to yield an acetal bond. This linkage is called glycosidic bond and the chemical process is known as glycosylation.

In this example, the trisaccharide is described by the formation of two glycosidic bonds (Figure 1.1- in yellow). Each glycosidic linkage at the anomeric carbon can be differentiated by the spatial orientation (stereochemistry) and the reaction position (regiochemistry) of each sugar molecule linked to the next one. Thus, the sterochemistry of the glycosidic bond can be defined either β-in red (H-axial) or α-in blue (H-equatorial), and the regiochemistry between the two reactive partners (hydroxyl group and the potential aldehyde form) both 1,4 ad 1,6 in this trisaccharide.
Similarly to a single strand DNA or RNA architectures wherein the nucleotides are orientated based on a directionality 5'-end to 3'-end on the ribose sugar (phosphodiester bonds), or to peptides sequences in which are defined an N-terminal residue and a C-terminal residue (amide bonds), the carbohydrates also exhibit their own orientation motif described by the reducing terminus region located at the aldehyde position (easy to be reduced) and the non-reducing terminus from the free alcohols (Figure 1.1).

The versatility of a single monosaccharide provides access to multiple reactive points in its linkage with other monomers. That assumption contributes to the

structural complexity of these compounds compared to nucleotides or proteins that possess only one type of linkage (either phosphodiesters or amide bonds respectively) giving linear polymers orientation. Instead, this inherent chemical feature is a direct result of finding a huge variety of glycans that can lead to the formation of both linear and branched structures with a critical active roles in Nature.

A couple of examples illustrated in the Figure 1.2 demonstrate the versatility in the 3-D conformation of carbohydrate structures that determine the final functionality (cellulose vs starch) from the single glucose sugar.

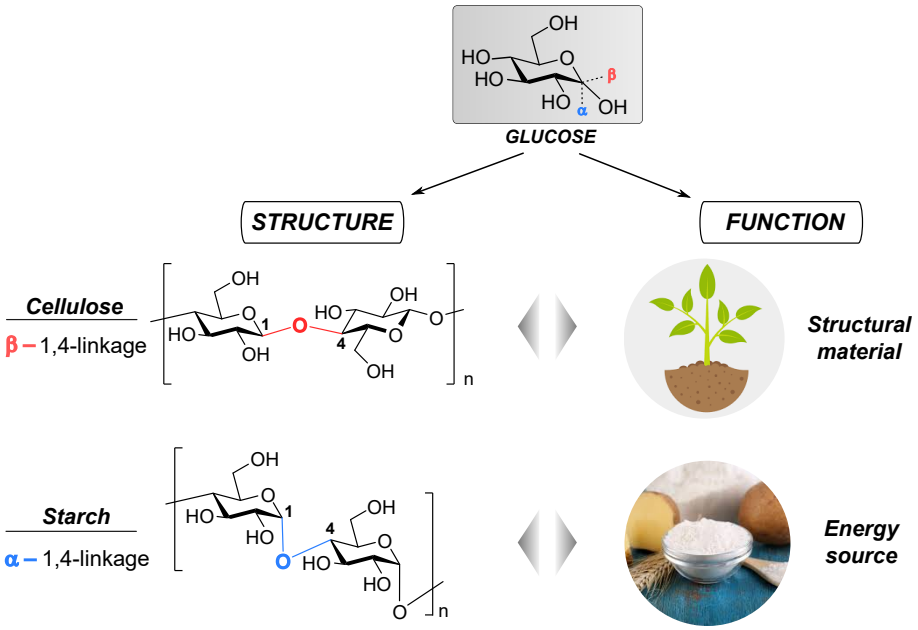

Figure 1.2: Examples of the variety of glycan structures with completely different functionalities sharing the same unit molecule of glucose. On the top, it is illustrated a couple of glycan examples forming a β-1,4-linkage: the cellulose polysaccharide. At the bottom, it is illustrated a couple of glycan examples forming α-1,4-linkage: the starch polysaccharide.

As we already described, the spacial arrangement is dominated by the stereochemistry of glycosidic linkages along with intermolecular hydrophobic and hydrophilic interactions.

Thus, the cellulose polysaccharide (the most abundant compound in nature) is a natural product synthesised by plants that is composed by D-glucose molecules joint through a β-1,4-glucosidic bonds (Figure 1.2-up). This alternating rotation of

the glucose sugar allows the formation of fiber piles by hydrogen bonds that provide a robust and insoluble structure that plants utilize as a structural material. On the other hand, the same glucose arrangement with α-1,4-glucoside linkage (Figure 1.2-down) reveals the family of starch polysaccharide. Instead, because of this stereochemistry of the glycosidic bond at α-position, the starch macromolecules lack on intermolecular hydrogen bonds which increases the water-solubility that facilitate their hydrolysis and final glucose distribution as an energy source.

Is in this framework wherein the glycoscience is aimed to address the comprehension within the mechanism of synthesis and degradation of these macromolecules as well as their structural heterogeneity that is displayed in living organisms. Moreover, the glycoscience framework is also dedicated to explore the biological systems involved within the glycan interactions. These families are mainly binding proteins called lectins and enzyme-catalysed named glycosyltransferases which represent a pivotal biological magnitude towards a better understanding one of the central language of life.[3]

1.1.2 Information behind the glycans. The sweet outcome in the glycome era

Glycans are ubiquitous in living organisms decorating the cell membrane within a particular region called glycocalyx (Figure 1.3) most of them conjugated with proteins (glycoproteins) and lipids (glycolipids). This external shield of glycans represents a strategic location out of the surface that opens the possibilities to interact with different biological residues and modulate many biological pathways including cell signalling and cell-cell interaction, inflammation, viral and bacteria host infections or immunity system activation.[4,6]

In eukaryotic cells, protein modifications generally occur after the translation process in the biosynthetic pathway of proteins where different functional groups are covalently attached to them. This process is called posttranslational modification (PTM) and in this case, the glycosylation process (attachment of glycans to form glycoconjugates) is considered one of the most common and diverse PTM of proteins or lipids that could explain the great relevance of carbohydrates towards increasing the biological complexities throughout the genome.[4,7]

The presence of glycan structures shielding the cell surface renders biological relevance into the glycosylation processes which represent a potential target towards therapy development.[4] To highlight the scope of the biological roles of glycans within living organisms, a couple of examples are briefly mentioned below and illustrated in the Figure 1.4.

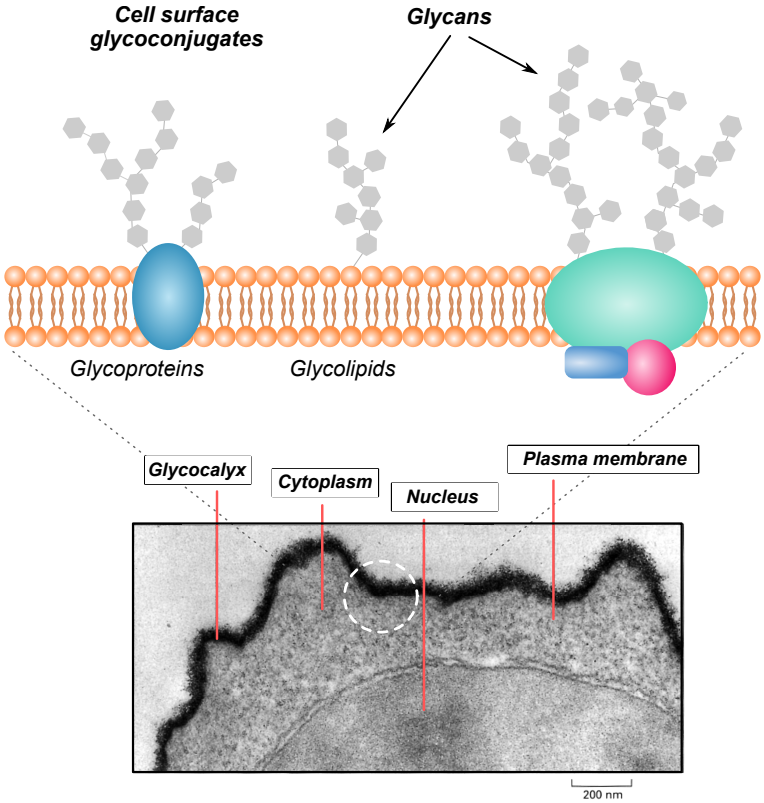

Figure 1.3: Model of a cell membrane with a dark meshwork of coated carbohydrates forming the glycocalyx. The zoom image illustrates a cartoon with some of the different glycoconjugates potentially found decorating the cell surface.

One of the most important milestone for the human immune system was the discovery of the ABO blood antigens in human cells by Karl Landsteiner awarded with the Nobel Prize in Physiology or Medicine, 1930. Briefly, the human red blood cells were codified by one specific glycan sequence decorating the cell surface called antigen H. The classification of ABO(H) blood types is promoted by further glycosylation of this basal structure encoded by specific glycosyltransferases (Figure 1.4-a) to get four blood types candidates: the O, A, B and AB. Thus, human cells with O-type means that the antigen H has not been modified by any glycosyltransferase. The blood type A refers to the glycosylation of the antigen H by adding one N-acetyl-D-galactosamine sugar with a particular glycosyltransferase ("GT-A"). Then, the blood type B this antigen is glycosylated by adding a galactose sugar with another glycosyltransferase ("GT-B"). Finally, the tpye AB presents a mixture of antigen H glycosylated by both glycosyltransferases ("GT-A" and "GT-B").

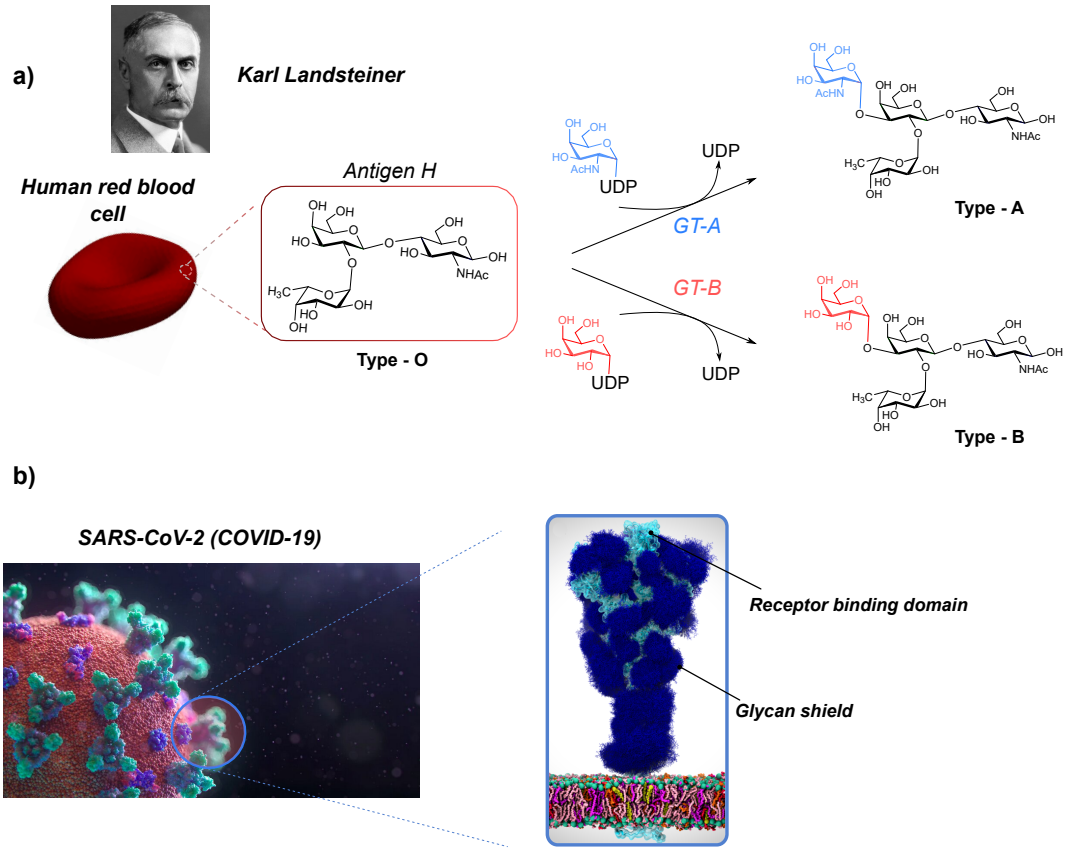

Figure 1.4: Schematic illustration of some relevant examples where the glycosylation process gain importance nowadays. a) Human type blood cell classification is defined by glycosylation of the antigen H either by GT-A to provide a blood type-A or by GT-B to provide a blood type-B or both. b) Spike protein model covered by a glycan shield from the SARS-CoV-2 (COVID-19) virus protein. This glycan shield is used by the virus particles to evade the immune system.

It is important to remark that this process is more complicated and not only promoted by the ABO system. However, this example stands here to highlight that small differences in only one specific sugar, and more precisely in a single chemical functional group within each transfer sugar, is sufficient to trigger a response of the immune system to reject the blood. Therefore, understanding the classification of the ABO blood types was the winning strategy to avoid incompatibilities in blood transfusions nowadays.

Another example is illustrated in Figure 1.4-b and it can explain the relevance of this macromolecules in our daily life. In 2019, a global pandemic caused by a coronavirus (CoV) named COVID-19 has posed in check the human health inducing an infectious disease in the respiratory system with a massive number of human life lost. Huge efforts from all the scientific community have been deployed to decode the virus mechanism towards the development of a proper vaccine and treatments that returns to normality. Many different research lines have been explored to date with several approaches. However, we refer for this topic the recent study developed by Casalino *et al.*[8] wherein they reported the viral structures from COVID-19 decorated with carbohydrates that help evade our immune system response. In particular, they fully described a molecular dynamic simulations of the glycosylated SARS-CoV-2 (virus that causes COVID-19) spikes proteins in the viral membrane as a critical target for vaccine design.

The glycan implication as we have reported in these model examples, either can serve to control our immune system to avoid a mismatch in blood transfusion or to act as camouflage by adding a glycan shield for helping viral proteins to be recognized.

The most interesting assertion is that glycan building-blocks are not natural products encoded by the genome contrary to proteins, and it does not exist a template code. It indicates that the biological information that modulates binding interactions should be retained within the sugar structure itself or behind the glycan assembly taken place by a machinery of glycosidases and glycosyltransferases at the level of Golgi apparatus.[7] Moreover, the glycosylation pathway is considered as a dynamic process wherein the nature of the glycan structures are variable and highly dependant on the environmental conditions, cell-type or organism to be exposed.[3] Thus, all these remarkable features encoded inside the large and complex network of glycan architectures have entailed the beginning of a new era coined glycomics (analogous to proteomics or genomics) to envision the complete elucidation of the totally collection of glycans: the glycome.

1.2 The biological machinery to build-up glycans: the Glycosyltransferase enzymes

Understanding the glycosylation process comprises one of the major challenge in glycoscience. A myriad of biomolecules such as glycans, proteins or lipids are glycosylated to form glycoconjugates that modulate their final function.[4] The glycosylation process to build-up complex glycan structures occurs mainly at endoplasmic

reticulum and Golgi apparatus and it is controlled by a machinery of enzymes called glycosyltransferases.[7]

1.2.1 Definition and structures

Glycosyltransferases, GTs (EC 2.4.x.y) are a large family of enzymes responsible in the biosynthesis of glycans in nature. This type of enzymes catalyse the formation of glycosydic linkages by transferring an activated glycosyl moiety (donor) to an acceptor molecules.[9,10] The nature of the glycosyl donor residues are mostly nucleoside phosphate groups, such as uridine diphosphate glucose (UDP-Glc) or Guanosine diphosphate fucose (GDP-Fuc), that work as a good leaving group to promote the binding reaction. On the other hand, acceptor substrates are typically other sugars in the form of mono-di-oligo-polysaccharides but also, other biomolecules such as proteins or lipids.[10] In the Figure 1.5 is depicted the enzymatic transfer reaction from a generic donor to a different acceptor substrates.

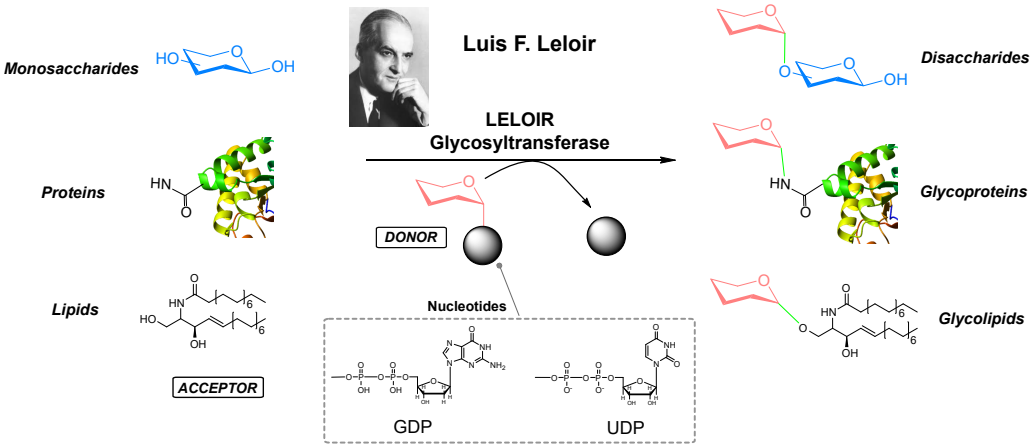

Figure 1.5: Generic representation of a Leloir glycosyltransferase transfer reaction from the generic form of sugar donor to the three different acceptor substrates (monosaccharides, proteins and lipids). Examples of nucleotide phosphate to activate the sugar moiety are depicted as grey circle (UDP and GDP). The final transfer products are illustrated as generic conjugates as disaccharides, glycoproteins and glycolipids.

Typically, the nucleotide-dependant glycosyltransferases are referred with the name of Leloir enzymes in reference to Luis F. Leloir (Nobel Prize in Chemistry, 1970), author of one of the most important discovery of sugar nucleotides and their implication in the biosynthetic pathway of carbohydrates (Figure 1.5).[10]

The crystal structures and X-ray analysis of these Leloir GTs revealed two predominant canonical fold-type based on the nucleotide binding domain called GT-A and GT-B, although a third protein folding GT-C has been described.[9–13] The Figure 1.6 illustrates a ribbon diagram of the two main types of Leloir GTs folding determined by their catalytic domain.

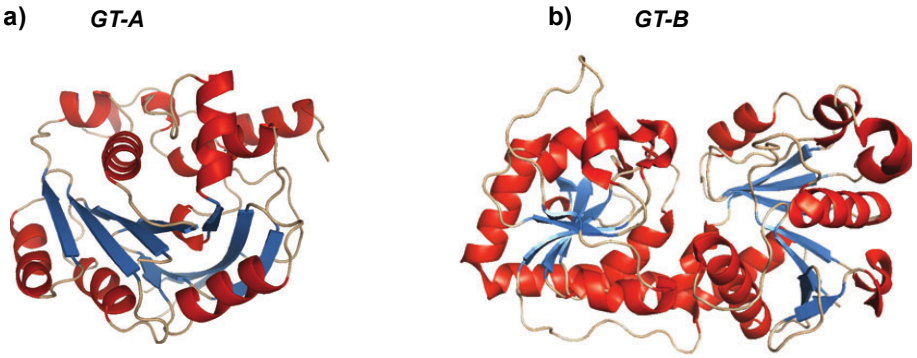

Figure 1.6: Ribbon diagram of the two predominant types of folding determined for the glycosyltransferase enzyme catalytic domain. a) Model of GT-A fold adopted by the enzyme SpsA from *Bacillus subtilus*, Protein Data Bank (pdb) 1qgq. b) Model of GT-B fold observed in a bacteriophage T4 β-glucosyltransferase, pdb 1jg7. Taken from Lairson *et al.*[10]

These two main Leloir GT fold-types fall into the structural similarity of displaying at least one Rossmann-type folding in the catalytic domain.[9] This Rossmann fold can be defined as a $\alpha/\beta/\alpha$ sandwiches to create the active site typically found in many Leloir GT enzymes. In particular, the GT-A fold contains a single Rossmann-like motif that interacts with the nucleotide sugar donor (Figure 1.6-a). Furthermore, most of the GT-A enzymes have been found to require divalent cations (generally Mn^{2+} or Mg^{2+}) coordinated through a common DxD motif (Asp-any residue-Asp) for activity. On the other hand, the GT-B enzymes display two Rossmann-like folded domains separated by a large cleft wherein the active site is located (Figure 1.6-b). Contrary to the GT-A fold, the GT-B enzymes are not metal-ion-dependent and they do not contain a DxD motif for activity.

Typically, most of GT enzymes exhibit a type-II membrane topology. This spacial arrangement at surface level implies a globular catalytic domain (C-terminal) localized at the Golgi lumen which is connected by a stem region to a single-cross transmembrane domain to conclude with a short N-terminal facing the cytosol region.[14–16] The Figure 3.2 exemplifies this model.

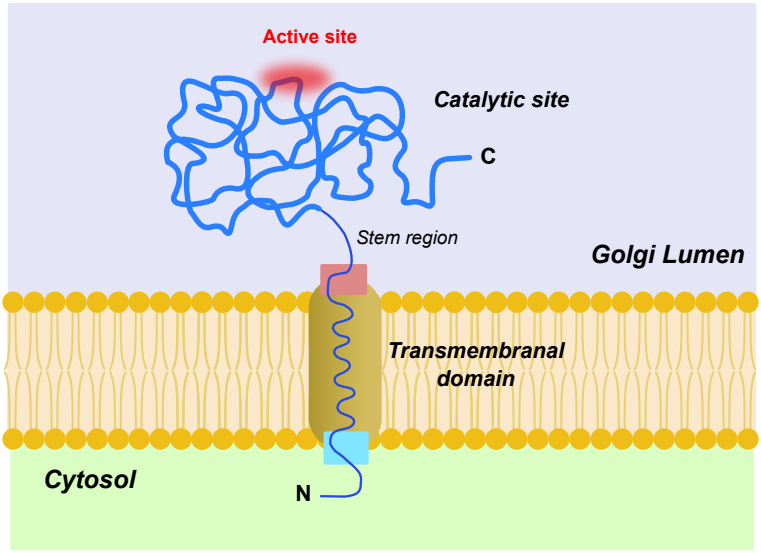

Figure 1.7: Model of a type-II membrane topology typically found for most of GTs. The catalytic site is located at Golgi lumen which it is connected ith a single transmembrane domain. Image inspired from Oikawa*et al.*[16]

1.2.2 Classification and Reaction Mechanisms

Approximately, around 1-2 % of the gene production are encoded a GTs families of any organism. They are organised in the Carbohydrate Active enZyme Database (CAZy, http://www.cazy.org/Glycosyltransferase.html) along with other carbohydrate-active enzymes such as glycoside hydrolases or polysaccharide lyases.[17]

The GTs are classified according to the stereochemical outcomes on the anomeric carbon of the substrate donor involved in the transfer reaction. Thus, they can modulate two types of stereochemistry over the new glycosylated product: retaining or inverting configurations are depicted in the Figure 1.8.[10,18]

By analogy with the organic chemistry, the glycosylation reaction can be observed as a nucleophilic attack over the anomeric position of the sugar donor bearing a nucleotide phosphate leaving group. The preservation or modification of the anomeric configuration within the final product might suggest different catalytic mechanisms.[19]

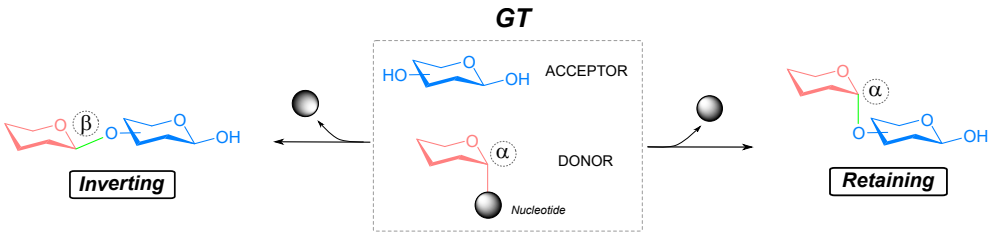

Figure 1.8: Schematic diagram of the final configuration adopted from the GT transfer reaction. The retaining GTs preserve the stereochemistry of the glycosidic bond (α to α). The inverting GTs permute the stereochemistry of the glycosidic bond (α to β). Adapted from Lairson *et al.* 10

Most of inverting GTs operate through a single-displacement transfer mechanism *via* bimolecular nucleophilic substitution (S_N2) as shown in the Figure 1.9-a. The mechanism proceeds when a catalytic base residue (typically Glutamate, Histidine or Aspartate) activates the acceptor molecule by taking a proton from an hydroxyl group. It increases the nucleophilicity and promotes the nucleophilic attack over the anomeric position mediated with the formation of an oxocarbenium ion-like transition state. This attack is produced from the opposite site of the nucleotide phosphate leaving group to displace it yielding a glycosilated product with an inversion in the anomeric configuration. However, other inverting GTs are mediated through a unimolecular nucleophilic substitution (S_N1) catalytic mechanism with no base catalyst participation.[20] This is the case of the fucosyltransferase 1 (FUT1) from plant cell wall in which an oxygen from the GDP-Fucose donor participates in the deprotonation process to activate the hydroxyl group from the acceptor molecule. Then, a water molecule mediate the protonation state of the GDP and the acceptor hydroxyl group (Figure 1.9-b).

On the other hand, the understanding of retaining GTs has been considered a great challenge and a strong debate.[21] However, recent structural studies of the catalytic mechanism of retaining GTs have validated important insights.[22,23] Generally, this catalytic mechanism of GTs is addressed by two different approaches: a double-displacement *via* S_N2 or a stepwise front-face mechanism.

The mechanism of double-displacement suggests a first stage where one aminoacid residue (Glu or Asp) participates in a nucleophilic attack over the donor sugar (anomeric carbon) generating a covalent glycosylated intermediate between the enzyme and the donor sugar. This complex shields by steric hindrance the nucleophilic attack by the acceptor molecule towards the opposite side retaining the final glycosidic bond configuration in the second stage (Figure 1.10-c).

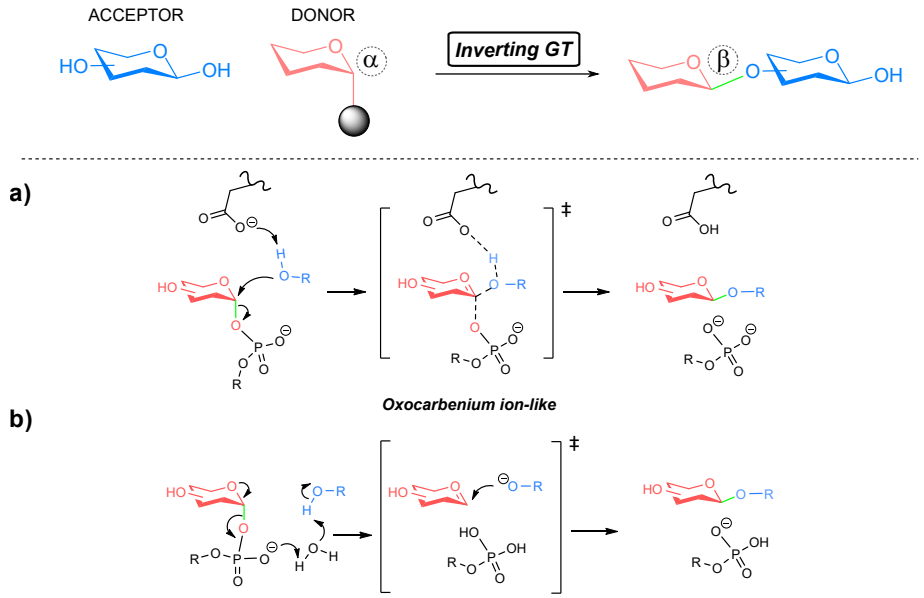

Figure 1.9: Schematic diagram of the reaction mechanisms of inverting GTs. a) Single-displacement via S_N2 by base-catalyst activation. b) S_N1 mechanism by water-mediated transfer catalyst. All reaction mechanisms exhibit the formation of an oxocarbenium ion-like transition state. The glycosidic bonds broken and formed are represented in green. Mechanism inspired from Ardèvol *et al.* 19

Regarding the second approach, the stepwise front-face is modulated by the phosphate group from the sugar donor modulate in a dual manner. First, this group deprotonates the incoming hydroxyl group from the acceptor molecule leaving an oxocarbenium-like transition state within a short-lived period. Then, the attack is produced from the same side leaving the phosphate group and retaining the final configuration (Figure 1.10-d).[19]

Overall, we notice that in all four transfer mechanisms, the hydroxyl group from the acceptor molecule is activated by deprotonation to increase the nucleophilicity. Either a basic aminoacid, a phosphate group or a water molecule enhance the nucleophilic attack through an oxocarbenium ion-like transition state.

Even though we have briefly reviewed the general mechanisms of inverting and retaining GTs, this study represents a major challenge that proves the necessity of seeking a better understanding about enzyme-substrate recognition.

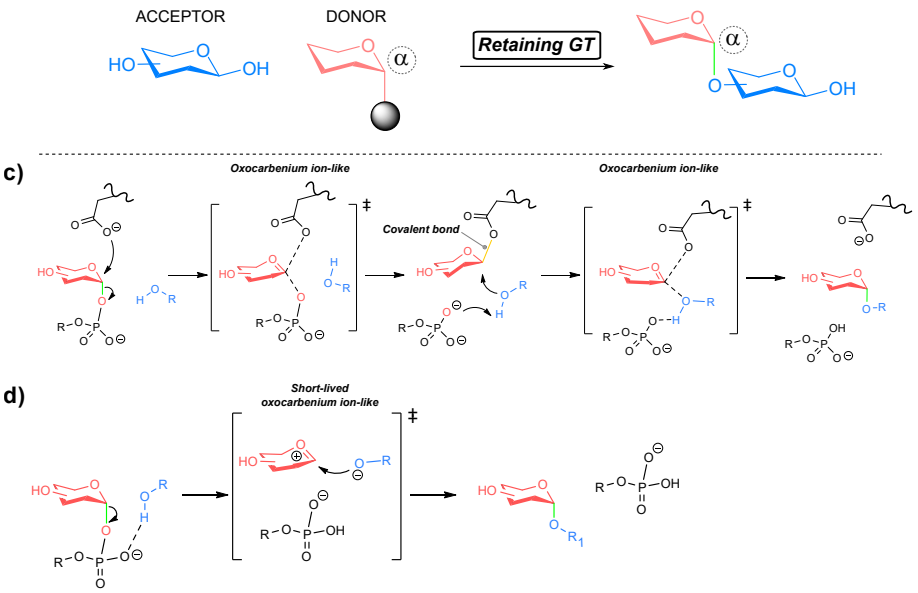

Figure 1.10: Schematic diagram of the reaction mechanisms of retaining GTs. a) Double-displacement *via* S_N2. A first displacement is produced forming a covalent glycosidic bond through an oxocarbenium ion-like transition state. A second displacement is generated after the nucleophilic attack by the acceptor molecule b) Stepwise front-face mechanism. The phosphate group is liberated and deprotonates the acceptor molecule through a short-lived oxocarbenium ion-like transition state. The glycosidic bonds broken and formed are represented in green. An intermediate glycosidic bond is drawn in yellow. Mechanism inspired from Ardèvol *et al.* 19

1.3 Bio-analytical tools for the interrogation of glycoenzymatic interactions

Glycosyltransferases represent a family of enzymes responsible for the glycosylation process in nature. The genomic and crystallographic analysis along with 3D modelling can help to describe putative GTs, but functional tools to address glycosylation patterns are yet required. The complexity and diversity of glycan structures make to these enzymes an attractive landmark to be interrogated as a possible target molecules that could contribute to decipher the glyco-code.

A variety of screening methodologies have been explored to address GT interactions and activity monitoring including radiolabelling,[24] chromatography[25] or mass spectrometry[26] among others.[27] However, the development of new biophysical and biochemical methodologies has offered a future line of understanding glycan-GT interactions.[28] The main idea of these bio-analytical tools resides in reproducing the nature distribution of enzymes and glycans interactions by displaying these tar-

get probes on a solid surface to detect biomolecular binding events. In the field of carbohydrates, this concept was defined as glyco-array platforms and a detailed description of this technique is presented in the Chapter 5 on this project.

1.3.1 Biosensors. General Principle and Major Advantages

Within the last decades, the concept of biosensing has congregated a great progress towards multiple research fields such as chemistry, biochemistry, biotechnology and biomedicine among others.[29] A biosensor can be defined as an analytical device that utilizes an integrated bioreceptor element for sensing specific analytical probes (Figure 1.11). This bioreceptor element is generally formed by high specificity biomolecules (antibodies, enzymes, nucleic acids or small molecule receptors) intimately in contact to the transducer and exposed to outside. Owing to the interaction of both components, a transducer converts the biochemical interaction into a physical signal (electrochemical, optical, heat, piezoelectric, etc) that is amplified, identified and processable.[30]

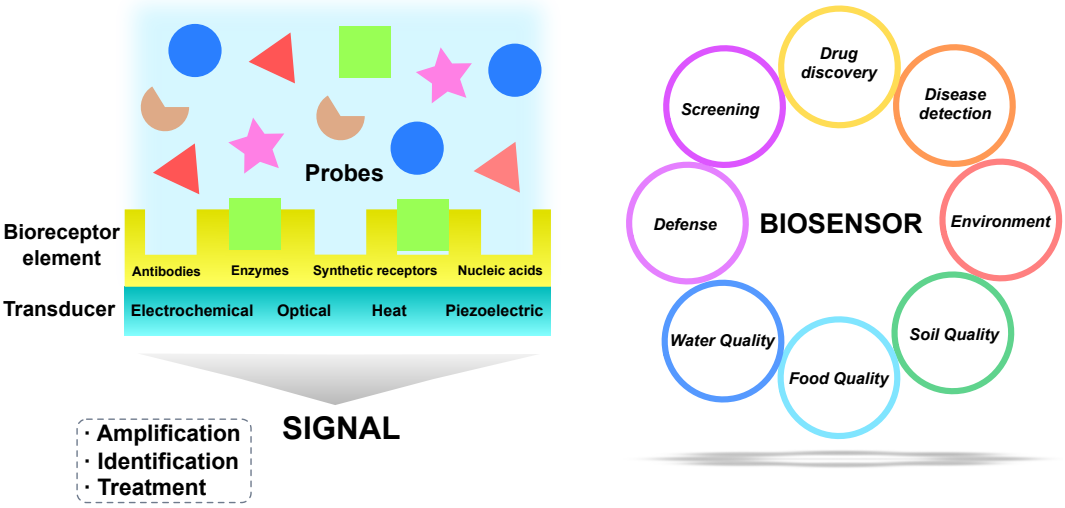

Figure 1.11: Model of the biosensor and potential applications. Adapted from Bhalla *et al.* 31

The widespread use of these versatile devices aims to overcome the major challenges in biochemical detection methods providing a simple platform for rapid analysis, reproducibility, under simultaneous monitoring for both quantitative and qualitative measurements. The higher selectivity and substrate specificity of biological targets have become a frame of reference to explore a wide areas of research towards drug discovery, disease detection, environmental monitoring, food quality and po-

tentially defence applications among others depicted in the Figure 1.11.[31]

In the field of glycoscience, the design of biosensors has been dedicated towards the monitoring of glycan-protein interactions wherein glycans or glycoproteins probes are immobilized on a solid support, namely glyco-arrays.[32] Advances in the development of miniaturization technologies in combination to high-detection methods make the carbohydrates micro-arrays technology a leading-edge tools for the simultaneous assessment of small sample quantities. Moreover, they can be adapted for a range of glycans and affinity proteins.[33]

1.3.2 Optical Biosensor Technique

Optical biosensors have emerged rapidly as one of the most representative model of biosensor.[34] The principle of this detection method is to monitor changes in the optical field as a consequence of a biorecognition event. As shown in the Figure 1.11, the bioreceptor integrated with an optical transducer device will provide an optical response proportionate to the concentration of the analyte recognised. Within this family of transduction techniques, there is one that has become the most popular: the surface plasmon resonance (SPR) and the updated version using an imaging detector named SPR imaging (SPRi). For a detailed description of the physical phenomena of SPR methodology refers to Homola.[35,36]

Surface Plasmon Resonance biosensor

SPR biosensor is an optical method that enables the direct analysis of interacting biomolecules in real-time measurements without labelling.[34] The SPR principle uses the electromagnetic waves generated on a metallic surface (generally gold) when a polarized-light illuminates the surface (Figure 1.12). The energy coupling between the incident light and the free electromagnetic waves at specific angle (resonance angle) induces the formation of plasmons at the surface level and as a consequence, a drop in the total energy (total internal reflection, TIR). When a binding analyte interacts with the biological element, a shift in the optical response (reflectivity) is triggered proportionate until a certain point to the successive number of bound molecules on the surface. The SPR transduction is based on the detection of the local changes in reflectivity closeness to the gold surface over a few hundred nanometers.[37]

A new version of SPR, called surface plasmon resonance imaging (SPRi), allows the detection of a hundreds or thousands samples simultaneously on a single chip and further analysis thanks to the high resolution charge-couple device (CCD) camera. SPRi represents the forefront of multiplexed analysis in a high-throughput manner to address binding interaction in real-time.

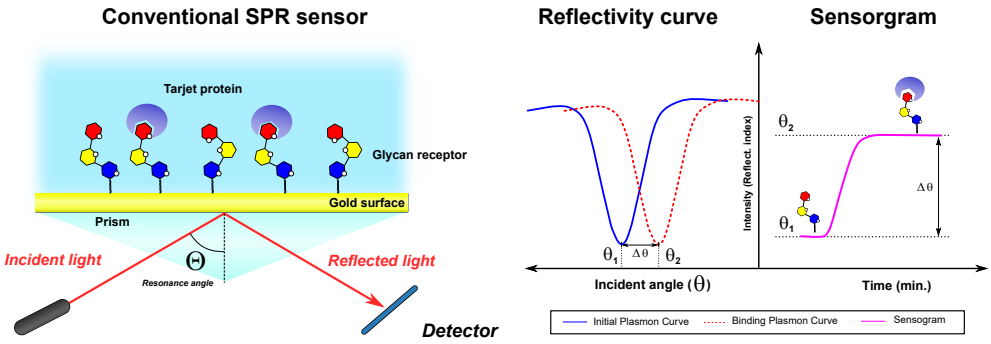

Figure 1.12: Principle of a conventional SPR biosensor (left side). The target binding to the glycan receptor induces a shift of the initial resonance angle $\theta 1$ to $\theta 2$ in the reflective curve. The angle interrogation monitoring provides a real-time measurement about kinetic binding events. Adapted from Prabowo *et al.* 38

The approach in the use of SPRi biosensors is mainly due to the great potential advantages of this technology. Owing to the optical light measurements do not interfere on the sample solution or the recognition events, the SPRi device can be adapted to many different sample probes specially suitable for biological analytes which native states need to be preserved. Furthermore, the direct analysis, label-free and real-time detection features along with the high specificity and selectivity of biological systems make this optical devices so attractive to explore biorecognition elements such as DNA,[39] RNA,[40] antibodies,[41] proteins, enzymes and other type of biomolecules like glycans.[42] Moreover, its versatility is expanded towards the solid-gas interface to explore many other applications such as bioelectronics sensors to detect volatile compounds.[43]

1.4 Aim of this Thesis

Glycosylation or attachment of glycans is considered one of the most important post-translational modification developed in living organisms. A large family of enzyme named glycosyltransferases are intimately responsible for the catalytic assembly and processing of these glycan structures to build-up more complex glyco-architectures that contribute to the dynamic information package of the glycome. However, the lack of biochemical information and characterization of these glycosyltransferases is actually a major bottleneck in Glycoscience.

Under this premises, my PhD research is involved in a multidisciplinary project that aims at the elaboration of a versatile glycochip for monitoring glycoenzymatic interactions. This approach is explored by SPR imaging biosensor technique to provide a fast, original and easy-adapted screening tool for real-time and label-free detection assays.

To that end, the design of this glycochip is divided into three main correlated chapters that tackle three main blocks: the target probe (enzyme), the bioreceptor molecule (ligand) and the transducer element (technique) based on glycoenzymatic biosensing detection.

A first general introduction is presented in Chapter 1 about the pivotal role of glycans, the glycosyltransferases as a precise machinery of glycosylation and the SPRi as a powerful deciphering technique.

The Chapter 2 is dedicated to the expression and purification of a specific target probe. In this study, a fucosyltransferase from *Arabidopsis thaliana* (AtFUT1) is used as a model of glycosyltransferase previously described in our group at CERMAV laboratory.[44,45] The AtFUT1 is expressed active and soluble in insect cells under heterologous expression and purified by nickel affinity at milligram scale.

On the other hand, the Chapter 3 focuses on the production and chemical modification of the bioreceptor molecule. For this specific enzymatic system, the tamarind xyloglucan (TXyG) is the AtFUT1 ligand. This large polysaccharide is digested into a set of smaller building-blocks that are chemoselectively modified with an oligonucleotide structure (XyG-DNA) for further immobilization approach. In parallel, a complementary strand is conjugated using a pyrrole group to address surface immobilization.

Finally, the Chapter 4 prepares the glycochip fabrication by collecting all the partners previously obtained and monitoring the interactions by SPRi assays. Thus, this chapter describes the implementation of grafting xyloglucan-DNA probes through specific DNA/DNA hybridization named DNA-Directed immobilization (DDI) approach. Then, the accessibility of XyG probes on the chip are validated using LM24 antibody (Anti-XyG) on the chip. Finally, preliminary assays of AtFUT1 and XyG interaction is explored on glycochip using SPRi technique.

2 The AtFUT1: developing a clear-cut Xyloglucan Fucosyltransferase

Within this chapter, we will explore a model of glycosyltransferase from Arabidopsis thaliana, AtFUT1, through a scientific context. Then, we will develop an heterologous expression, purification and characterization of the AtFUT1 in insect cells adapted for large-scale production. Finally, a novel GDP-Glo™assay will be performed to determine the enzymatic activity of AtFUT1.

Contents

2.1 Scientific context

2.1.1 Native Glycosyltransferases Involved in the Xyloglucan biosynthesis

Thinking about plants, it always comes to mind the name cellulose, one of the most abundant and studied compound involved the primary cell wall (PCW). However, a plethora of polysaccharides compounds walk along with the cellulose such as pectins, xylans or xyloglucan among others,[46] building-up a template of cross-linked network of polymers never found in other living organisms. In particular, the xyloglucan polysaccharide (XyG) belongs to the family of hemicelluloses (cellulose core-like) and it is considered as one of the major component in PCW in dicots. The XyG is responsible for having a strong non-covalent hydrogen bond interactions within the cellulose microfibrils leading to a noteworthy meaning in regulatory stages involving growth, elongation and cell wall stiffness in plants.[47] Within the biosynthetic mechanism of the XyG structure at Golgi apparatus level,[16,48,49] many Leloir glycosyltransferases (GTs) have been identified in Arabidopsis Thaliana as we depicted in the Figure 2.1.[50] In several stages, these enzymes are able to build the final core of the xyloglucan through the transfer of sugar moieties from an activated sugar (nucleotide sugars) such as uracil di-phosphate (UDP) and guanosine di-phospate (GDP), to the native polymer chain forming a new glycosidic bond.

From a general overview, these glycosyltransferases can be classified based on the specific function in the biosynthetic pathways towards the formation of the final XyG structure in two main lines: the glucosyl backbone template and the side-chain decorated with branched sugar residues. For the first one, the glucan polymer consists of a sequencing β-1,4-glucose linkages that are synthesized by a cellulose synthase-like C (CSLC) family-type GT2. It uses UDP-Glucose to form the glycosidic bond and promote the entrance of the backbone into the Golgi apparatus. The activity of this enzyme was described for the AtCSLC4 in Arabidopsis by Cocuron *et al.*[51]

Additionally, the side-chain modification starts with the α-1,6 addition of a xylose moiety to the glucose backbone in position 1, 2 and 3 by the xylosyltransferase (XXT) activity.[52] This family of enzymes belongs to the GT34 and the enzymatic activity has been described for XXTs 1-5 in Arabidopsis,[53–55] but its mechanism is yet not well-understood. However, great evidences endorse the cooperative behaviour between CSLC and XXTs in the construction of the xyloglucan structure.[50]

Once the xylose molecules are attached, another GT continues decorating the XyG core by transferring D-Galactose moieties *via* UDP-Gal onto the xylose ac-

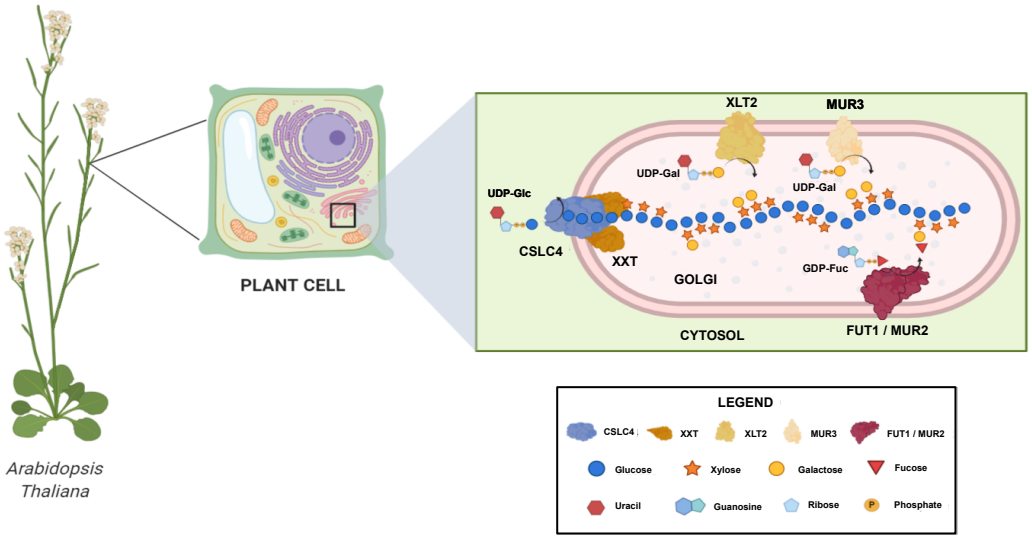

Figure 2.1: Schematic representation of the pivotal glycosyltransferases involved the xyloglucan (XyG) biosynthetic pathway in the Golgi apparatus of *Arabidopsis*. The combined action mechanism of synthase and glycosyltransferase enzymes induces the transportation of nucleotide sugar inside the Golgi apparatus to form the XyG. Image inspired from M. Pauly and Keegstra, reference 50.

ceptors forming a β-1,2-galactose linkages. From the initial structure of XyG-type (XXXG, one-letter code nomenclature[56]), enzymatic activity assays proved that two galactose sugars were transferred over different xylose molecules in the XXXG core-type, and therefore, two different galactosyltransferases (GalTs) participate on this transfer. MUR3 (*Arabidopsis* mutants) was the first identified GalT to be responsible for the specific transfer on the xylose residue in the third position converting the initial XXXG core into XXLG.

Moreover, the xyloglucan L-side chain galactosyl transferase 2 (XLT2) was identified as an homologue of MUR3. This GalT regulates the selective transfer of a galactosyl unit at the second position, modifying the initial XXXG core into XLXG. Both GalTs belongs to GT47 family[57] and its enzymatic activities have been predicting in *Arabidopsis* mutants according to the literature.[58,59]

Finally, the first GT of all to be identified in Arabidopsis by Perrin *et al.*[60] in 1999, which entails the last step in the XyG biosynthetic pathway. The specific GT catalyses the transfer of one L-Fucose sugar *via* GDP-Fuc donor, to the galactose moiety on the XyG core.[61] This fucosylation reaction is carried out by the

fucosyltransferase (FUT1) enzyme forming an α-1,2 fucose linkage to the galactose side chain residue at the third position, giving a final XXFG or XLFG core-type structures.[62]

In the following table, we collect all the different families of GTs identified so far in *Arabidopsis* and pea from the critical review made by Amos *et al.*[63]

Enzyme or family	Sugar transfer	Activity	GT CAZy GT family	Acceptor	Activity notes	Homology / redundancy (Arabidopsis)	References
CSLC	D-Glc	β-1,4-Glc XyG backbone	2	Unknown: endogenous acceptors or de novo synthesis in P. Pastoris.	Unknown elongation size; limited solubility of β-glucan oligosaccharides with chain lengths larger than DP 6. High MW polymerization unknown.	Five-member family. Activity for CSLC4 only.	Cocuron *et al.*, 2007; Davis *et al.*, 2010
XXT	D-Xyl	α-1,6-Xyl side chain initiation on XyG backbone X Side chain	34	XyG backbone oligosaccharides, DP 4–6. DP 3 acceptor tested, no activity detected.	Single addition to GGGGGG synthesizes GGXGGG. Less efficient second product, GGXXGG. DP $\geq$ 4 acceptor required for activity. DP 6 acceptor preferred to DP 5.	Five-member family. Activity for XXT1, 2, 4, and 5.	Faik *et al.*, 2002; Cavalier and Keegstra, 2006; Vuttipongchaikij *et al.*, 2012; Culbertson *et al.*, 2016, 2018; Ruprecht *et al.*, 2018
MUR3	D-Gal	β-1,2-Gal addition to X side chain (Xyl residue transferred by XXT) L Side chain	47	XG oligosaccharides extracted from mur3-deficient plants with acceptor sites for Gal transfer, unknown size/DP.	Single addition to XXXG synthesizes XXLG.	One homolog: XLT2. Activity predicted from mutant phenotype	Madson et al., 2003
FUT1 MUR2	L-Fuc	α-1,2-Fuc addition to L side chain (Gal residue transferred by MUR3) F side chain	37	XG oligosaccharides with acceptor sites for Fuc transfer, DP 4: XXLG or XLLG.	Single addition to XXLG synthesizes XXFG. Single addition to XLLG synthesizes XLFG.	10-member FUT family. XG-related activity for FUT1 only. FUT4 and FUT6 transfer Fuc to AGP side chains.	Perrin et al., 1999; Faik et al., 2000; Vanzin et al., 2002; Ciceron et al., 2016; Rocha et al., 2016; Urbanowicz et al., 2017

Table 2.1: Summary of the main GTs determined by heterologous expression that are involved in the biosynthesis of the xyloglucan structure. Table taken from Amos *et al.*[63]

2.1.2 State of the art: the Xyloglucan fucosyltransferase AtFUT1

As we mentioned in the Table 2.1, there are four main families of GTs that participate in the synthesis of the xyloglucan structure. Specifically, we will focus our attention to the *Arabidopsis thaliana* α-1,2-fucosyltransferase (AtFUT1), a well-studied GT that gets involved in the last step of the XyG synthesis before being secreted into the lumen.

In 1999, Perrin *et al.*[60] identified and purified the first xyloglucan fucosyltransferase from pea epicotyls named PsFUT1. The information from the peptide sequence served as a reference to clone this gene from *Arabidopsis thaliana* (AtFUT1)

and from Pea (PsFUT1). The homologous and heterologous expression of these genes enable the confirmation of its enzymatic fucose transfer activity and the XyG-FUT1 specificity.[52,60,64–66] The breakthrough in the discovery of the *A. thaliana* AtFUT1 enzymatic function gave rise to the creation of the GT37 family comprising a total of 10 different genes among which 3 have a characterized fucosyltransferase activity that has been proven (FUT1, FUT4 and FUT6).[67]

FUT1 is localized at the Golgi compartment as a type II membrane topology (Figure 3.2). It catalyses the regiospecific transfer of a L-fucose sugar from the nucleotide GDP-fucose, known as glycosyl donor, to a D-galactose side-chain on the XyG body. Moreover, studies in *Arabidopsis* revealed that the fucose transfer occurs precisely in a single addition to the first galactosyl residue within the XXLG or XLLG cores of xyloglucan acceptor to yield the α-bond structure in the way of XXFG or XLFG respectively.[60,62,64,66]

Additional biochemical characterization studies has been performed for this particular enzyme. Biochemical assays suggested a size-dependant affinity behaviour of the AtFUT1 for its XyG substrate since shorter xyloglucan units might function as inhibitors for the enzyme.[44,64] The analysis of AtFUT1 kinetic parameters have been addressed on pea (*Pisum sativum*)[64] and in *Arabidopsis*[44] showed in the Table 2.2. These kinetic results revealed a close proximity in the final values of K_M for the GDP-fucose donor and XyG acceptor in both systems, differing considerably in the V_{max} values.

	Faik *et al.*[64] (standard enzymatic assay) *Pisum sativum*		Cicerón *et al.*[44] (GDP-Glo assay kit, Promega) *Arabidopsis thaliana*	
Substrate	Km (μM)	Vmax (mM/h·μg)	Km (μM)	Vmax (mM/h·μg)
GDP-Fucose	30	0.15	42	12
Tamarin xyloglucan	0.46	0.2	0.31	9

Table 2.2: Comparative studies of the kinetic parameters determined for AtFUT1 enzyme from pea and insect cells.

Recent studies have been successfully developed regarding the production and characterization of FUT1 in *Arabidopsis*. Cicerón *et al.*[44] in 2016 reassessed the biochemical condition of FUT1 heterologous expression and purification in a large-scale production. They cloned, expressed and purified a truncated recombinant gene of AtFUT1 (the catalytic region lacking 68 aminoacids corresponding to the transmembrane domain) using a baculovirus expression system in insect cells. This

strategy provided a high production yield of a soluble and an active form of AtFUT1 enzyme (4 mg/L of culture). Moreover, the biochemical characterization of this enzyme by size-exclusion chromatography (SEC) and dynamic light scattering confirmed that the truncated form of AtFUT1 exhibits a noncovalent homo-dimer behaviour (around 150 kDa) involving intramolecular disulphide bonds interactions between monomers.

A crystal structure has been successfully resolved for the catalytic domain of AtFUT1 enzyme to determine the activity, specificity and mechanistic analysis.[20,45] It has been classified as a member of the GT-B superfamily characterized by two canonical Rossmann-type domains (N-terminal and C-terminal) separated by a large cleft containing the metallo-independent catalytic site.[9,10] However, a variant of this canonical GT-B fold never found in any other fucosyltransferase has been recently described.[45] Briefly, the AtFUT1 structure was crystallized in complex with the GDP and XyG monomer (XLLG) at 2.2 Å to tackle the enzyme:donor:acceptor interactions. The crystal structure of the AtFUT1 enzyme in complex with the binding donor:acceptor substrates is depicted in the Figure 2.2-a wherein the N-terminal domain is described in blue, the C-terminal in green and the stem region in red.

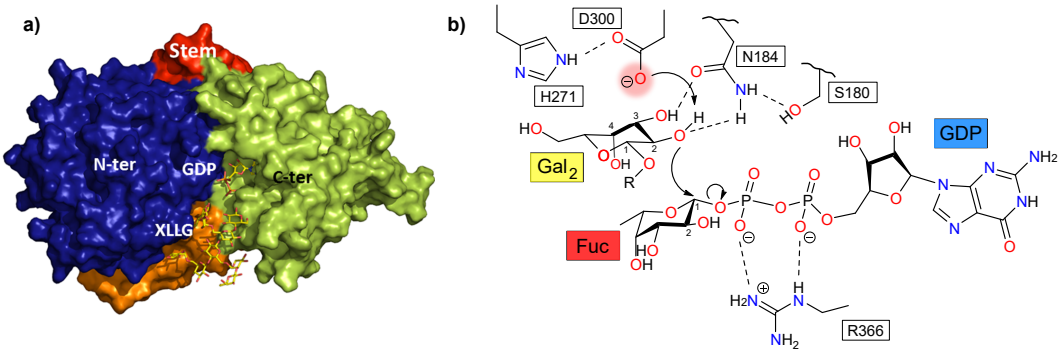

Figure 2.2: Representation of the monomer FUT1:GDP:XLLG Ternary Complex and mechanism. a) Surface representation of AtFUT1 in the complex with XLLG and GDP-fucose. The N-domain (N-ter) is depicted in blue, the C-domain is in green, the stem region is in red and the extra C-domain in orange. This latest explains the specificity of FUT1 enzyme upon the XyG substrate in terms of stabilization and biding process. (b) FUT1 inverting mechanism *via* oxocarbenium ion-like (S_N2) transition state. The D300 (aspartate) aminoacid induces a deprotonation over the galactose molecule from the XyG acceptor to promote the subsequent nucleophilic attack to the anomeric position of the activated GDP-fucose donor. Images taken and adapted from Rocha *et al.* 45.

However, this crystallography study revealed an extra C-terminal domain described in orange located on the opposite site to the stem region. This catalytic domain of the AtFUT1 enzyme appears to be involved in the pivotal role of stabilization and binding process of the XyG substrate.[45]

Regarding the mechanism behind the enzymatic catalysis in the fucosylation event is still ongoing. Following the FUT1 crystal structure analysis reported critical insights in the fucosylation mechanism of the xyloglucan ligand. Within the same publication, Rocha *et al.*[45] suggested that the fucosylation process leads up to the formation of an α-1,2-glycosidic linkage through an inverting mechanism assisted by an aspartate-base group from D300 within the catalytic pocket as it is shown in the Figure 2.2-b. This anionic aminoacid deprotonates the hydroxyl group in position 2 of the galactose sugar, increasing the nucleophilicity of the OH group so that it promotes in a single step a bimolecular nucleophilic substitution (S_N2) *via* an oxocarbenium ion-like transition state.[10,21,45]

Overall, the data obtained from this study confirmed the GT-B folding in this families of plants GTs but also, it revealed a variant of GT-B fold-type with an structural organization unique in this family.

A comparative study of FUT1 mechanism was carried out by Urbanowicz et al.[20] that consider another type of mechanism (Figure 2.3-a). In this research, they provided *in silico* studies by molecular dynamic (MD) that suggest the AtFUT1 transfer mechanism is mediated by a water molecule in the catalytic site. Under this approach, the water molecule is localized in the middle of the transfer interactions to promote an acid/base catalysis. This joint action both deprotonates the hydroxyl group of the galactose moiety in position 2 and protonate the phosphate group (base) within the transition-state (TS) as shown in the Figure 2.3-b. Therefore, they proposed an unimolecular nucleophilic substitution (S_N1-like) mechanism in which the D366 (Arginine 366) seems to be a key aminoacid of binding and catalysis since it stabilizes the phosphate group to promote the transfer in the TS.

In summary, the AtFUT1 belongs to a family of carbohydrate-active enzymes involved in the plant cell wall biosynthetic pathway. Nowadays, plant FUTs studies of activity and fucosylation diversity offers a primary insights across many organisms.[67] However, identification and characterization of new putative FUTs is yet a challenge and it would provide a better understanding of the biological role of fucosylation process in plant cell wall polysaccharides with high-market applications in drug discovery, bioenergy or food.[68–70]

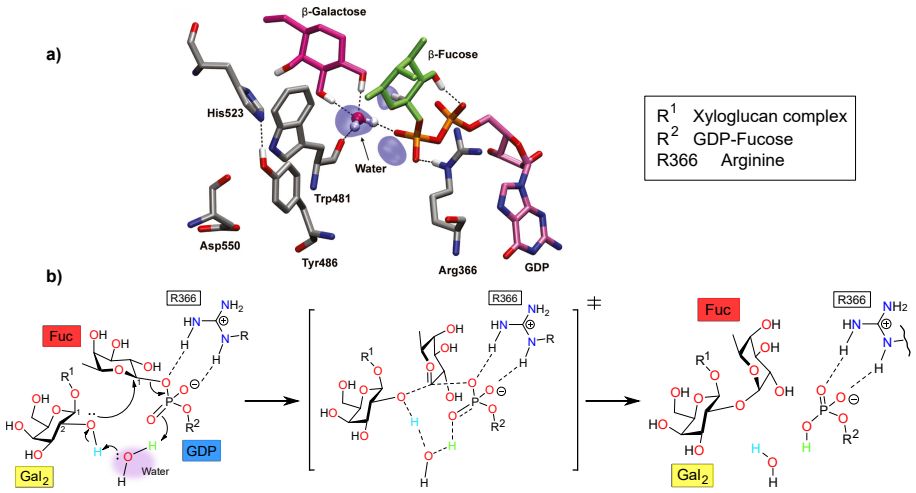

Figure 2.3: (a) Molecular modelling of the fucosylation transfer mechanism within the binding pocket of FUT1 enzyme depicted in licorice representation. The fucose molecule is in green with a β-conformation, the GDP is in light pink with the phosphate groups in orange, the galactose is in dark pink in β-conformation and the water molecule is centred to induce the acid/base catalysis. (b) Water-mediated transfer mechanism *via* S_N1-like . Images taken and adapted from Urbanowicz *et al.* 20

2.1.3 Proposed strategy

Glycosyltransferases represents essential pieces of the puzzle in the dynamic framework of plant cell wall polysaccharides. The majority of this type of enzymes have supposed an important challenge in the field, making difficult the evaluation and demonstration of enzymatic activities, catalytic mechanisms or structural analysis. This is mainly due to the poor solubility of these enzymes and the very low amount and purity that are generally obtained. Herein, we explore the heterologous expression of a truncated form of AtFUT1 ($His_{\Delta 68}$-AtFUT1) which correspond to the catalytic domain of the enzyme. This form of AtFUT1 is expressed active in solution and in a large-scale production according to the literature.[44] To make it possible, an insect cell line is selected to guarantee post-translational modifications (PTM), proper folding of the final FUT1 enzyme conformation and, hopefully active form of FUT1 in solution. Furthermore, the N-terminal domain of the AtFUT1 sequence is tagged with six histidine aminoacids for purification purposes.

Therefore, the expression and purification of the AtFUT1 enzyme are documented and organized in three stages: first, within a large-scale production, the recombinant form $His_{\Delta 68}$-AtFUT1 is expressed in insect cells by an heterologous expression of using a baculovirus vector system; then, a purification step by Nickel affinity

chromatography. Finally, a novel methodology of monitoring enzymatic activity is addressed by a GDP-Glo™assay from Promega.

2.2 Heterologous Expression of His$_{\Delta 68}$-AtFUT1 in insect cells

Eukaryotic enzymes like FUT1 demands expression systems that enable PTM during the biosynthesis of the enzyme. These chemical changes in the enzyme may drive to the proper folding conformation and therefore, to obtain a suitable enzymatic activity.

Insect cell lines are complex systems that offer the opportunity to guarantee secretory pathways to enable these PTMs towards the final protein synthesis. In this study, we optimized the recombinant expression of the AtFUT1 enzyme in a large-scale production using insect expression system. In particular, High-five (Hi5, Invitrogen) insect cell line was chosen to grow and produce the AtFUT1 enzyme in suspension culture. This type of cell line is originated from the ovarian cells of the cabbage looper from *Trichoplusia ni*. They provide high quality properties for the recombinant expression of proteins within a serum-free medium and flexible to suspension culture method.

2.2.1 High-Five Cell Line Culture under Production-loop Process

The cell line production started with the adaptation of the Hi5 cells to a suspension culture under sterile conditions in a laminar hood. These cells were cultivated using 10 mL of a serum-free Ex-cell 405 culture medium at pH 6.2 with a cell density around 0.8 millions of cell (MC) per mL having a cell mortality over 15%. The culture medium was supplemented with the antibiotic gentamicin that inhibits bacterial protein synthesis. Typically, the Hi5 cells were cultivated at 22 °C and mixed with an orbital shaker at 130 rpm to oxygenate the solution and reduce the formation of aggregates.

Considering that cell growing is exponential in time, the initial cell density was diluted by adding fresh culture medium in a fresh-sterile flask. The capacity of the flask containing the cells need to be large enough for adequate aeration with around 1/4 to 1/3 of the total flask volume.

This process was systematically controlled to avoid the overexpression of the cells up to the suitable cell density (3 MC/mL) and the formation of aggregates that could reduce the cell viability. Therefore, when the cell density was around 1-2 MC/mL

the cell culture was split by supplying fresh Ex-cell 405 medium to provide enough nutrients for the proper growth.

Starting from 10 mL of culture volume, the insect cells were grown until 1.2 L of culture medium with an optimal cell density around 2 MC/mL prior infection.
In the Table 2.3 below, the first cell production was registered before the infection step. The suspension cells counting was measured with a Neubauer chamber or hemocytometer using Trypan blue stain under microscope at 100x magnification. The cell viability was calculated as the average living cells divided by the total number of cells. All the cells that were stained by Trypan blue were considered as dead cells; and the rest non-stained cells were defined as living cells.

CELL LINE PRODUCTION				
Day	Vol.cells (mL)	Vol. fresh medium (mL)	Cell density (MC/mL)	Cell viability (%)
1	1	9	0.8	84
3	10	10	0.5	93
6	20	30	2.3	91
9	50	50	1.9	93
13	100	200	1.4	94
14	300	200	1.1	92
15	500	200	1.5	93
16	700	500	3.0	93

Table 2.3: Cell line production estimation of the High-five insect cells in a period of 16 days determined by hemocytometer prior Baculovirus infection.

We observed in the first cell line of production that the viability obtained were up to 90 %. The addition of fresh culture media was adjusted to maintain a minimum dilution factor of 2 to keep the cell line of production within the proper cell density. Although few cell aggregates were formed within the culture medium, the Hi5 cells were grown healthy and robust in time using Ex-cell 405 culture medium.

Throughout three non-stop weeks, we produced the first bulk of insect cells with a density around 3.0 MC/mL in a 1.2 L of culture medium. In order to keep the cell line in a continuous production-loop, a volume of 50 mL of culture medium was taken at the end of each cell growth production and re-cultivated with fresh culture

medium. Overall, four different stocks of 0.60, 0.95, 1.1 and 1.20 L of insect cells culture were obtained to express the AtFUT1 in solution.

2.2.2 Baculovirus infection of High-five cell line culture

As we mentioned at the beginning of the chapter, the AtFUT1 enzyme expression was promoted by the infection of the High-five cells cultivated earlier using a Baculovirus expression vector system. This type of virus was produced and optimized within our laboratory (CERMAV) to induce the specific production of the AtFUT1 enzyme. In particular, a truncated form of the enzyme in which 68 amino acid residues were removed from the N-terminus of the protein sequence (catalytic domain) along with the addition of six histidine amino acids for purification purposes. Previous research have successfully demonstrated the production of a soluble and active FUT1 structure using this truncated form maintaining its catalytic site.[44]

The Figure 2.4 illustrates schematically and briefly, the general process of preparing the recombinant virus containing the genetic expression of our protein AtFUT1.

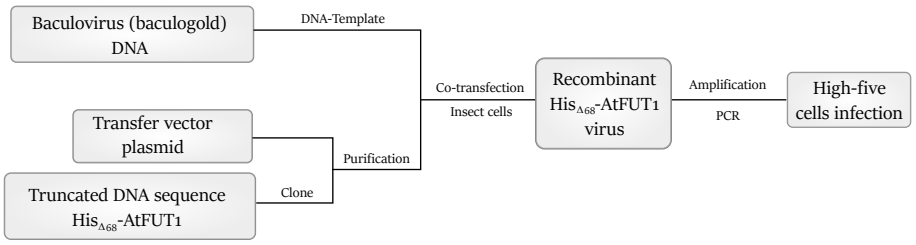

Figure 2.4: General diagram for the construction of the recombinant baculovirus bearing the truncated His$_{\Delta 68}$-AtFUT1 DNA sequence.

To begin the production, the modified-DNA sequence encoding the His$_{\Delta 68}$-AtFUT1 needs to be cloned into a circular DNA plasmid called transfer vector. This recombinant vector is co-transfected with the linear baculovirus DNA (Baculogold) and amplified afterwards by PCR (Polymerase Chain Reaction) in insect cells to build-up the virus particles after titration. The value for the titre stock was estimated at 2.7 x 10^8 pfu/mL. This parameter determine the number of virus particles able to infect a host cell forming plaque units per millilitre.

Therefore, 1.2 litres of the Hi5 cell line previously produced with a density around 3 MC/mL was incubated in presence of this recombinant baculovirus containing the gen-of-interest inside an incubator at 27 °C under orbital shaker for 7 days. The

ratio of virus particles per cells, also known as multiplicity of infection (MOI), was estimated to be optimal between 2 and 5. This parameter determined the volume of virus required to infect the insect cells according to the cell density and culture volume. The data in the table below showed the infection parameters for the different cell cultures produced resulting in maximum production of AtFUT1.

High-five production	Vol.culture (L)	Cell density (MC/mL)	MOI (virus/cell)	Vol. virus (mL)
1	1,2	3,0	2	26,7
2	1,1	2,0	5	40,7
3	0,9	1,0	3	10,6
4	0,6	1,2	2,5	6,7

Table 2.4: Data collection of the infection parameters used for the expression of AtFUT1 within the production of High-five cell lines

With the conditions described in the table, we managed to get a percentage of cell viability below 15-20 % between three days and a week of infection. These values concluded that High-five cells were successfully infected by baculovirus system and, therefore, we expected to find presence of AtFUT1 enzyme soluble in the culture medium.

2.2.3 Immunodetection of AtFUT1 enzyme production

As a proof-of-control of the baculovirus infection and consequently, the favourably production of AtFUT1 enzyme, a preliminary immunodetection tests were carried out using a Nickel resin beads and Western blot immunoassay. The assays consisted in taking 1 mL of each production media at 0 and 7 days of infection. Since the enzyme was rigorously modified with a tail of six histidine in its protein sequence, these aminoacids served as a footprint for trapping and detecting the AtFUT1 enzyme. In this context, a sample from the infected culture was placed in contact with nickel beads resin at pH 6.8. The imidazole rings from the histidine bind to the nickel ions forming an organometallic complex able to catch the protein onto the agarose resin. Subsequently, and after several steps of washing, an elution step was carried out using a buffer solution containing imidazole at 500 mM. The higher concentration of imidazole within the elution buffer competes with the histidine tag for the binding site of the nickel-agarose resin and releases the protein from the complex. Finally, the elution fraction was analysed by electrophoresis (SDS-Page) at

10% acrylamide under denaturing conditions of β-mercaptoethanol (β-ME). The resulting gel was transferred onto a nitrocellulose membrane showed in the Figure 2.5.

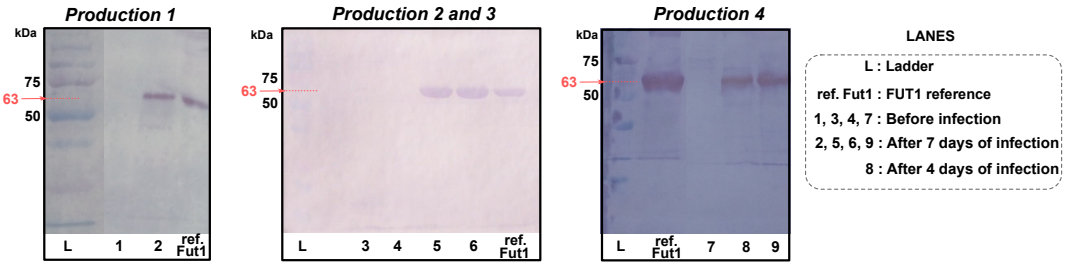

Figure 2.5: Western-blot immunoassays obtained as a proof-of-control for the infection and production of the $His_{\Delta 68}$-AtFUT1 enzyme (MW: 63kDa, red arrow). Reference size of protein in between 75 kDa and 50 kDa from the ladder (L).

The Western-blot revealed the presence of AtFUT1 enzyme (MW: 63 kDa) within the four culture media indicated by the red arrow. A reference of FUT1 was placed in all productions to confirm and monitor the expected fraction of the AtFUT1 enzyme along with a size-reference ladder (lane L) expressed in kilodaltons (kDa). The lanes number 1, 3, 4 and 7 corresponded to the native culture before the infection with baculovirus. On the other hand, the lanes number 2, 5, 6 and 9 gave clear information about the presence of AtFUT1 enzyme with seven days of infection for all set of productions in comparison with the AtFUT1 reference. We included in the production 4, a lane number 8 that revealed the presence of AtFUT1 only after four days of infection. Overall, we successfully accomplished the expression of the truncated $His_{\Delta 68}$-AtFUT1 enzyme in solution by the baculovirus infection over a set of cell production after seven days. Finally, we preserved all the media containing the enzyme at -80 °C ready for further purification.

2.3 Purification of AtFUT1 through Nickel column chromatography

Affinity chromatography was selected as an efficient method to selectively separate the soluble histidine-tag AtFUT1 enzyme from the rest of the matrix. In particular, chelating purification chromatography using nickel metal (IMAC) was applied and optimised for large-scale of production in suspension.

The AtFUT1 was purified under native conditions, which means that the enzyme required to preserve both the tertiary and quaternary structure throughout the whole process of purification. There are many external variables to be considered that are able to interfere in the 3D structure of the enzyme. The pH, the temperature, the ionic strength or even the culture media are crucial parameters to be carefully considered.
Based on preliminary assays performed by a previous Ph.D. student (Felix Cicerón), the strategy for the AtFUT1 purification relied on optimizing the pH and temperature of the culture media. This approach demonstrated that pH values of the Ex-cell 405 culture media greater than 7.1 led to the formation of some precipitated (generally salts) after two hours at 4 °C which clogged the chromatography tubing. Furthermore, the HEPES buffer at pH 8.0 was probed to be suitable and robust to adjust the pH of the culture media containing the enzyme. On the other hand, the temperature effect might also accelerate the precipitation process within the medium. As a result, the culture media was adjusted at pH 6.8 and preserved at 4 °C during the injection through the nickel column. Implications of these results concluded a relevant role of both the pH and temperature for the IMAC purification of the soluble AtFUT1 enzyme in Ex-cell 405 culture.

2.3.1 Preparation of Ex-cell 405 Culture Media containing the AtFUT1 enzyme

Prior to start the purification process, the culture media containing the AtFUT1 enzyme has to be properly conditioned. Thus, three lines of buffers were prepared to optimise the isolation process of the enzyme from the Ex-cell 405 culture media. One line of buffer was dedicated to accommodate the enzyme to the suitable binding conditions at pH 7. The remaining two buffer lines were prepared and fitted on the NGC system to perform the enzyme purification from the affinity column. The chemical composition of the different buffers is described in the Table 2.5.

Composition	Adjust	Wash	Elution
NaCl	-	500 mM	500 mM
HEPES	1 M	25 mM	25 mM
Imidazole	-	-	500 mM
pH	8.0	7.0	7.0
Buffer	pH fitting	A	B

Table 2.5: Chemical composition of running buffers for the NGC purification platform and the pH adjustment of the culture media.

From our production-loop of insect cells growth media and the positive infection with baculovirus expression system, we managed to express a truncated form of fucosyltransferase enzyme in suspension (figure 2.5). All the culture media containing the enzyme with an initial pH of 6.1 were preserved at -80 °C before purification. In a first stage, the sample medium was slowly thawed to 4 °C to prevent the formation of precipitate within the medium, although a white cloudy solution were observed inside afterwards. Therefore, the culture medium was centrifuged under 13000xg at 4 °C to remove the solid particles and recover the supernatant. We analysed the white precipitate by SDS-Page under denature conditions of β-ME to check the presence of AtFUT1 (Figure 2.6).

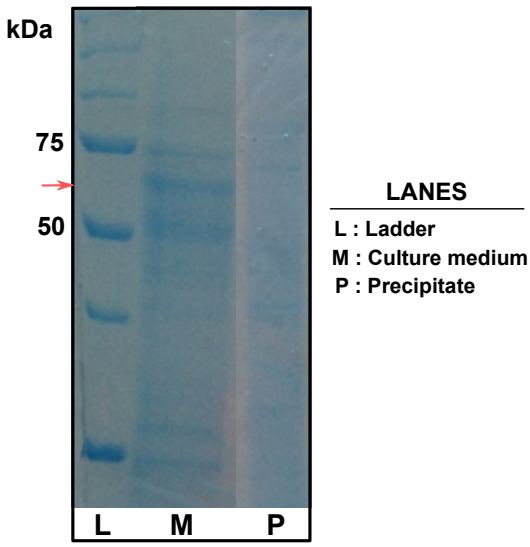

Figure 2.6: SDS-PAGE analysis of white precipitates within the culture medium before IMAC purification step. The lane L (Ladder) is defined in kDa. The lane M (culture media) contains a very subtle fraction of AtFUT1 indicated with the red arrow. The lane P (precipitate) with no presence of AtFUT1 enzyme.

Within the SDS-Page gel, the lane L (ladder) was used to define the size-reference in kDa. The analysis of the culture medium without purification (lane M) revealed very subtle the presence of AtFUT1 enzyme indicated by a red arrow. Furthermore, the lane P clearly proved that the Histidine-tagged AtFUT1 enzyme remained in solution compared to the culture media in lane M. Therefore, the presence of white precipitates was mainly caused by mineral salts from the Hi5 culture medium with no protein containing.

After filtration of the culture media, a solution of HEPES 1M at pH 8.0 (Table 2.5) was used to carefully increase the initial pH from 6.1 to 6.8 in order to enhance a suitable binding of 6xHis-tagged residues to the nickel column. Finally, the supernatant was filtered again through 0.2 μm and degassed prior injection into the column.

2.3.2 Monitoring the FUT1 purification using NGC affinity chromatography

At this point, the culture medium was under optimal conditions to be purified through the nickel affinity column. An NGC™chromatography system was employed to automate and monitor by UV (280 nm) the purification of the His-tagged AtFUT1 enzyme.

This stage of the purification stands on the nickel-histidine affinity interaction that occurs inside the column. The AtFUT1 enzyme was selectively functionalized at the N-terminal with a sequence of six histidine tags. The functional group imidazole of these aminoacids can bind to the nickel ions immobilized on the nitrilotriacetic acid (NTA) resin even at low concentrations. To that end, a 1 mL nickel column HisTrap™and both washing buffer (A) and elution buffer (B) were connected to the NGC system.

Overall, a global NGC curve profile of the entire purification process was depicted in the Figure 2.7 and described in the following sections.

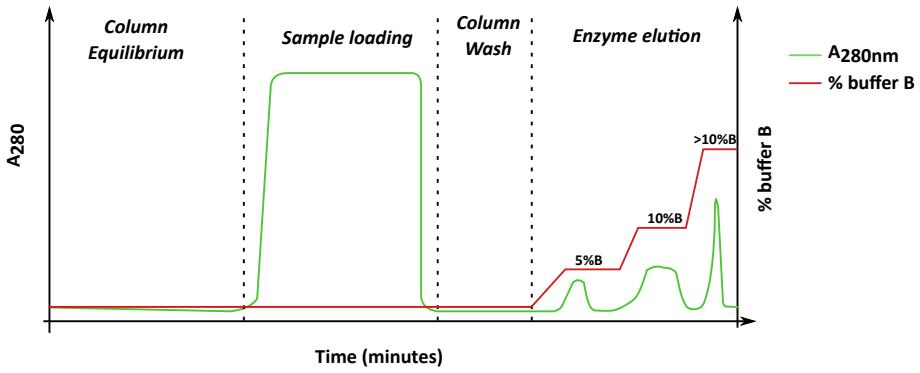

Figure 2.7: Standard profile of the NGC chromatography system involved in the purification of a truncated form of AtFUT1 enzyme. Both UV absorbance at 280 nm (green line) and percentage of buffer B (red line) are simultaneously monitored. Four stages are distinguished within the purification protocol using the NGC system: Column equilibrium, medium loading, column wash and enzyme elution.

In our case, the whole purification process of AtFUT1 was monitored by UV absorbance fixing the wavelength at 280 nm with a flow rate of 1 mL/min and a temperature of 4 °C according to the literature.[44] Further SDS-gel 10 % acrylamide analysis were performed to verify the purification process.

Column Equilibration and Sample Loading containing the AtFUT1 enzyme in solution

Within the first stage, the column was equilibrated by pumping the buffer A at 1 mL/min to maintain the standard condition of pH and salts inside the column (Figure 2.7-column equilibration). Then, a total volume of 650 mL of the stock production 1 was injected at 4 °C through the nickel column overnight with a flow rate of 0.5 mL/min (Figure 2.7-sample loading). Typically, this process led to a drastically increased in the absorbance to the saturation since all the non-tagged proteins presented in the medium exhibited a weaker interaction with the nickel and therefore, were released with the flow out of the column. Only the histidine-tag from the AtFUT1 enzyme can display stronger binding interaction with the nickel to be trapped inside the column.

Column wash prior enzyme elution

In reality, any host protein we can find inside a culture medium could have accessible histidine residues able to bind with the nickel or maybe bind under non-specific manner. These interactions are generally weaker than the polyhistidine tags and can be easily washed away (Figure 2.7-column wash). Consequently, the nickel column was washed by injecting buffer A until the absorbance measure reached roughly the zero-base and remained stable for around 10 minutes. That means we removed non-specific proteins and we established a suitable background for the AtFUT1 elution step.

AtFUT1 enzyme Elution in Gradient Mode of Buffer B

This step could be considered the most relevant of all since it determines the quality of the purification. Generally, a disrupted agent was injected into the column to modify the binding conditions between the histidine-tag from the protein and nickel resin. This disrupted agent could be a pH variation (generally acidic conditions) that changes the pKa of the histidine residue and breaks the interactions within the nickel complex. A major drawback is the pH-sensitivity of the enzyme that could disrupt the native conformation under acidic conditions.

Alternatively, a commonly disrupted agent used in the elution stage is the imidazole substrate. This molecule shares the chemical structure residue from the

histidine group inducing a competition reaction for coordination site of the nickel. In our case, the AtFUT1 enzyme was eluted using buffer B containing 500 mM of imidazole (Table 2.5).

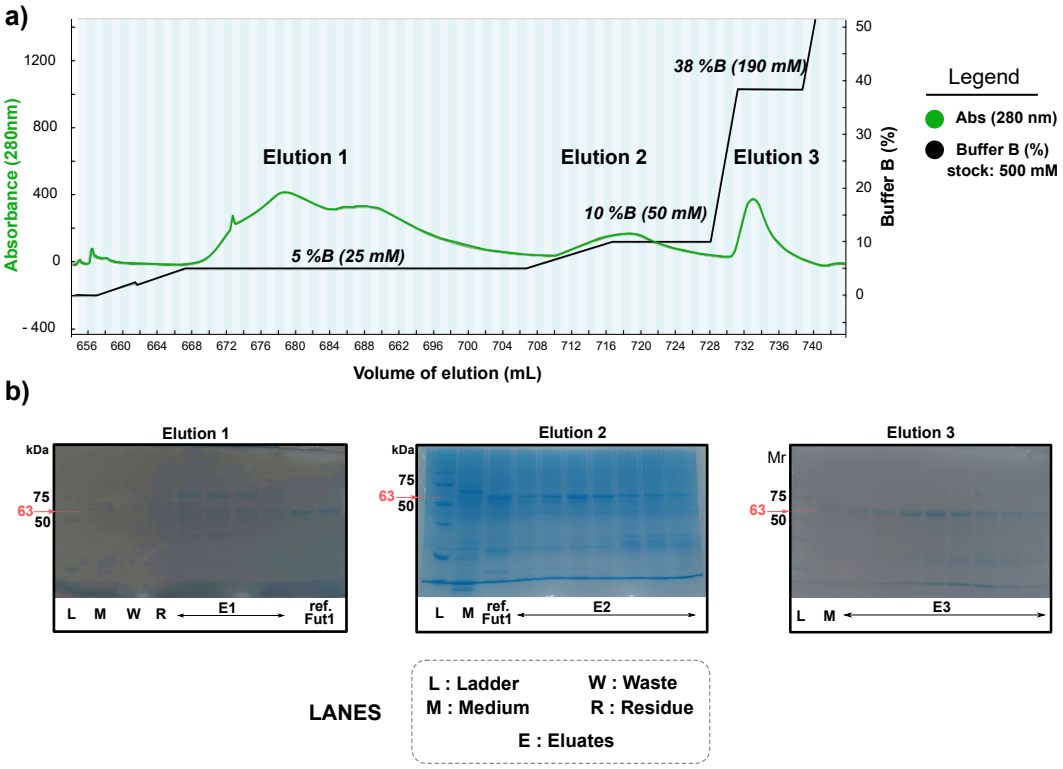

Figure 2.8: Purification under native conditions of his-tag AtFUT1 from 650 mL of culture medium Ex-cell 405 (Production 1) in 1 mL nickel column HisTrap™excel (GE) a) NGC purification monitoring. Both UV absorbance at 280 nm (line green) and percentage of imidazole (line black) readout simultaneously. Three peaks are obtained based on the percentage of imidazole: 5% (25 mM, elution 1), 10% (50 mM, elution 2), 38% (190 mM, elution 3) (b) Electrophoresis gels at 10 % acrylamide of the three different elution stages from the AtFUT1 purification. The expected AtFUT1 size is defined in red (63 kDa) to localized the protein from the eluates (E). A size ladder (L) is also added as a reference. The medium (M) was incorporated to monitor the protein fractions eluates from the column. Elution 1 and 2 provide the AtFUT1 mixed with other proteins (E1 and E2). Elution 3 provides pure AtFUT1 enzyme from the elutes E3.

The elution process was carried out by increasing the concentration of imidazole (in percentage) from lower to higher percentages of buffer B in a gradient mode (Figure 2.7-enzyme elution). Thus, the Figure 2.8 showed three percentage of buffer B carried out to elute the AtFUT1 enzyme: the first one was established from 0 to 5 % (25 mM), the second one from 5 to 10 % (50 mM) and the last one from 10 to 38 % (190 mM) of imidazole (buffer B).

Within the first elution stage at 5 % of imidazole (25 mM) depicted in the Figure 2.8-elution 1, we observed an increase of the absorbance meaning that some protein were released from the column. The analysis of the SDS-Page showed eluates (E1) with a mixture of different proteins wherein the AtFUT1 band was presented in comparison with the reference. The detachment of the AtFUT1 might be attributed to the less accessibility of the polyhistidine tag or a reduced number of histidine residues in their interaction with the nickel. Therefore, the binding effect was weaker enough to be washed away from the column even at lower concentration of buffer B.

Once the system reached the equilibrium and proteins no longer released the column, we proceeded with the injection of 10 % of imidazole (50 mM) through the column (Figure 2.8-elution 2). At this concentration of imidazole, the binding interaction of the proteins with the nickel should be higher to be stuck inside the column. However, the absorbance gently raised up to 200 UA and decreased in the same way to the background. The SDS gel analysis for the elution 2 concluded that most of the protein detected belonged to the AtFUT1enzyme compared to the positive control (FUT1). Similarly, we observed the presence of the enzyme within the gel since the binding interactions did not occur with the full number histidine (in this case six), and thus, this higher concentration of imidazole washed the enzyme away from the column.

Finally, the elution 3 was carried out at 38 % of imidazole (190 mM) wherein the maximum of the curve was observed. Based on the SDS-Page analysis, we obtained the AtFUT1 protein really pure showing an unique band in the eluates (E3).

Overall, both the elution 2 and 3 were selected as a candidate to be concentrated for further biochemical characterization of AtFUT1. Furthermore, it confirmed that the purification process of AtFUT1 by nickel affinity chromatography was successfully addressed.

2.3.3 FUT1 concentration and preservation

Considering the last elution step, we collected the eluates 2 and 3 which produced around 16 mL of total sample volume. This total volume need to be reduced and at the same time, re-purified in order to remove the entire concentration of imidazole. There are several methods in biochemistry to concentrate proteins such as precipitation or salting out, dialysis or even chromatography. We tackled this step using a Vivaspin 30 centrifugal concentrator technique with a membrane cut-off from 90 to 150 kDa since the AtFUT1 was expressed in solution as a dimer with a molecular weight of around 150 kDa. The diluted AtFUT1 enzyme was loaded into the tube

on top of the membrane and the centrifuge effect induced the separation of both the solvent and smaller proteins and molecules that pass through the membrane, leaving retained those proteins with higher molecular weight (see Experimental conditions). This process was repeated eight times to ensure that the imidazole is no loger present in the mixture. The concentrator solution was composed by NaCl 150 mM and HEPES 25 mM at pH 7.0 to replace the elution buffer containing imidazole and higher salts concentration.

Finally, we managed to obtain 400 μL final volume of pure AtFUT1 splitted in eight Eppendorf tubes with 50 μL each containing around 3 mg/mL monitored by Nanodrop 2000 Spectrophotometer (Thermo Scientific). As we noticed in the SDS-gel for the elution 2 and 3, only the AtFUT1 was identified as a highest protein in the mixture. Therefore, we expected to find our AtFUT1 relatively pure. All the stock solutions of AtFUT1 were preserved at -20°C for further experiments.

2.4 Enzymatic Activity Evaluation of AtFUT1 enzyme by GDP-Glo™Assay

A soluble form of $His_{\Delta 68}$-AtFUT1 enzyme was successfully expressed and purified. In order to verify the enzymatic activity of our enzyme, we explore a novel bioluminescence assay using a GDP-Glo™kit from Promega. This assay was adapted for a rapid activity detection and kinetic evaluation of AtFUT1 enzyme.

The principle of GDP-Glo™assay lies on the biochemical detection of the GDP nucleotide released as an enzymatic side-product after the glycosylation event. This GDP is enzymatically transformed by the combination of GDP detection reagent and a luciferase enzyme (Ultra-Glo™Recombinant luciferase) in one-step-addition into ATP to generate bioluminescence light. Based on the Figure 2.9, this indirect assay is able to detect the photon emission which is proportional to the GDP released that correlates with the enzymatic transfer from the AtFUT1 enzyme.

In a first stage, to estimate the amount of GDP that is produced during the transfer reaction, a bioluminescence detection assay from GDP substrate was performed. This allowed the determination of the linearity and sensitivity of the GDP-Glo assay by creating a GDP standard curve in a range of GDP solutions from 0 to 10μM (Figure 2.10-a). Each point represents the mean value of a triplicate bioluminescence readout plotted against the initial concentration of GDP. The linearity response of this GDP standard curve confirms the system stability and the important proportionality of the bioluminescence readout at low concentration of GDP. Therefore,

this equation can be used to extrapolate the luminescence readout to get the GDP concentration produced by the AtFUT1 enzyme in the kinetic assay.

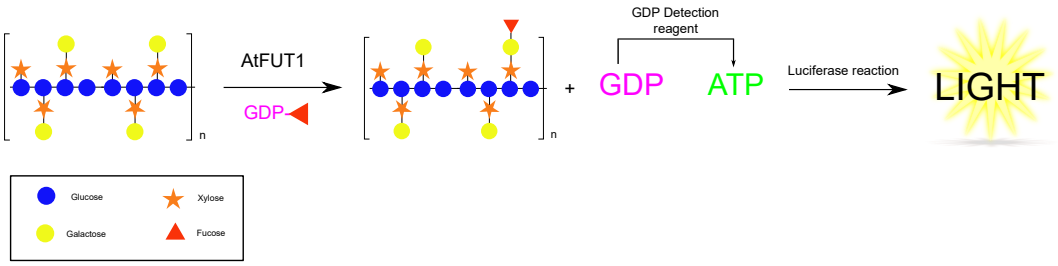

Figure 2.9: Bioluminiscence assay based on the GDP-Glo^{TM} principle for monitoring glycosyltransferase kinetic activity.

Furthermore, a control reagent of the GDP-Glo assay was performed in order to demonstrate the relevance of each partner involved in the transfer reaction to be occurred. Thus, five conditions were depicted in the Figure 2.10-b. Based on the bar chart, it was significantly distinguished the luminescence response in the condition number 5 in which all partners were worked together to promote the transfer activity. However, this was not the case for the rest of the conditions wherein at least one of the partners was missed.

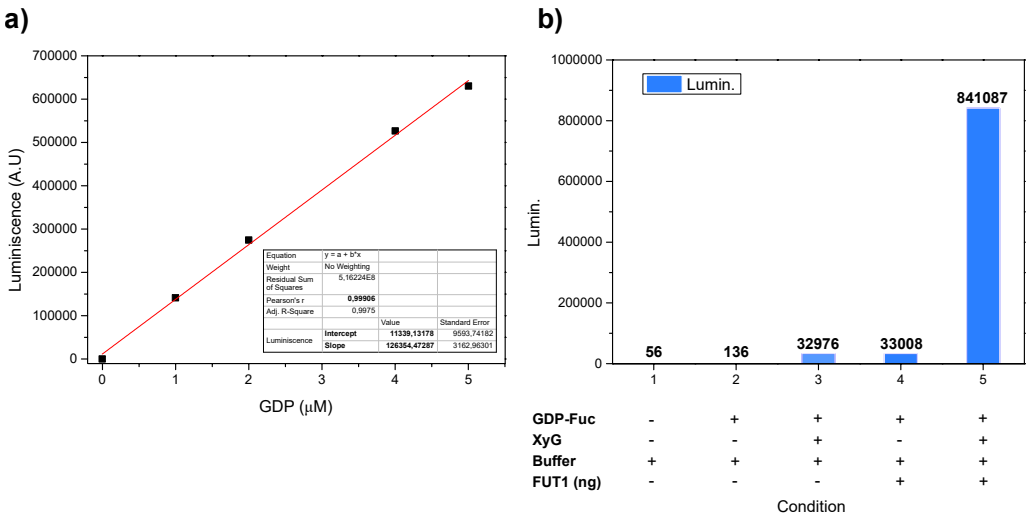

Figure 2.10: Evaluation of the linearity and sensitivity within the GDP-Glo assay. a) GDP standard curve obtained by plotted a mean value from triplicate measurements of bioluminescence response (AU) against the GDP range concentration. b) Experimental conditions to confirm both the sensitivity and transfer activity by detecting the luminescence of GDP.

Finally, a kinetic curve was obtained following the recommended conditions from the supplier. Typically, the estimation of the set values were in the range of 0.2 to 10 times the Michaellis constant. Furthermore, the enzyme concentration was optimized to get speed values around the linear region from the Michaellis curve (half of V_{max}). The data were carried out by triplicate with a plotting curve of the luminescence mean value. For this assay, a concentration of enzyme (150 ng/mL) with 3 mg/mL of xyloglucan ligand and GDP-Fuc concentrations from 62 to 2000 μM was evaluated (Figure 2.11).

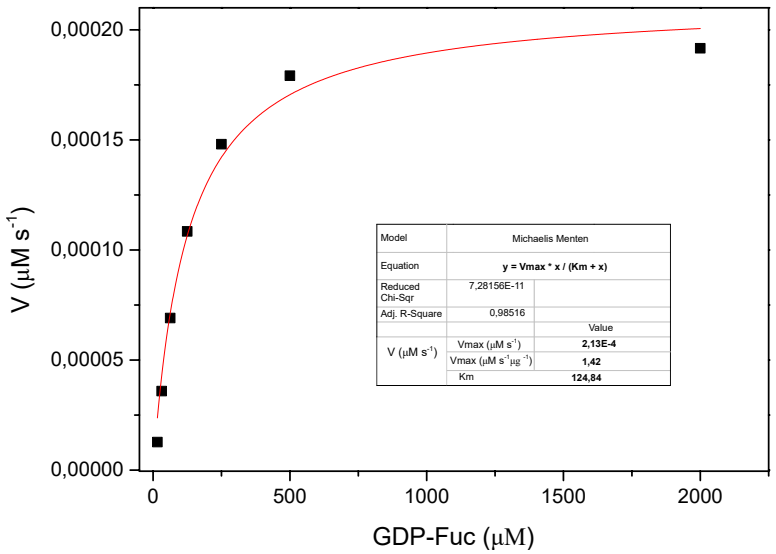

Figure 2.11: Michaelis-Menten curve obtained from the GDP-Glo assay by plotting the reaction speed against the concentration of GDP-Fucose. The values V_{max} and K_M were obtained from the direct from the curve.

The following describes a Michaellis kinetic curve from the GDP-Fucose values. The data fitting provides an estimated values of V_{max} and K_M; 1.42 μM/s·μg and 124.84 μM respectively.

Although our values for the GDP-Fucose molecule differs from the literature (V_{max}: 3.3 μM/s·μg and K_M: 42 μM),[44] they helps us to confirm an active enzyme transfer activity.

2.5 Conclusions

To summarize, in this chapter we focused on the production of an α-1,2- fucosyltransferase 1 as a model of glycosyltransferase enzyme from *Arabidopsis thaliana*. This specific glycosyltransferase plays an important role in the biosynthetic pathway of the xyloglucan polymer, and therefore, a major understanding of GT:sugar specificity would reduce the gap in the study of these special family of enzymes.

In the first part of the chapter, we produced and grew an eukaryotic system of High-five™insect cell in suspension suitable for the expression of complex enzymes like FUT1. This step was optimized using a production-loop of culture media for a large-scale of production (around 1.2 L) according to the literature.[44] Then, we managed to infect the cells with a recombinant baculovirus expression system, containing a truncated form of AtFUT1 with the lack of 68 aminoacids in the gene sequence (catalytic domain), and a tag-sequence of six histidine. The heterologous expression by using baculovirus system offered an easy way to express our AtFUT1 enzyme under native conditions and soluble in a large-scale of production. The evaluation of each cell culture infection by nickel affinity resin followed by SDS-Page and western-blot detection concluded that the AtFUT1 enzyme was successfully produced within the culture media. Finally, we addressed the AtFUT1 purification step from the culture media using nickel affinity chromatography. In accordance with the NGC™chromatogram and the SDS-Page results, we successfully managed to isolate and quantify the AtFUT1 enzyme at milligram scale for further experiments.

Lastly, we demonstrated the positive transfer activity of AtFUT1 using an indirect bioluminescence assays named GDP-Glo™from Promega. This technique offered an alternative detection platform to addressed the kinetic parameters (K_M and V_{max}) involved in a glycosyltransferase transfer activity.

Likewise and in concordance with the literature,[44] implications of the results presented here may facilitate improvements in the development of new compatible methodologies in the biochemical expression and characterization of these challenging group of enzymes.

3 Towards the Chemical Construction of Xyloglucan-DNA conjugates

In this chapter we will explore the construction of carbohydrate-DNA conjugates (COCs) as a powerful and versatile architecture for detection, characterization and immobilization approaches. We will particularize towards the study of the xyloglucan polysaccharide (XyG) as the optimal ligand for the α-1,2-fucosyltransferase (AtFUT1) interaction. We will describe the optimization process to obtain a set of building-blocks of XyG for further conjugation over DNA scaffolds using chemoselective reactions commonly used in organic chemistry. Likewise, we will explore the impact of the DNA structure over a suitable detection and characterization of xyloglucan-DNA conjugates (XyNAC) as a "labelling" compound. Finally, the further immobilization approach on solid support will motivate the chemical construction of complementary DNA architectures.

Contents

3.1 Scientific context

Since the early 1970s, oligonucleotides (ODN) have been used for the development of DNA-based architectures with numerous applications such as diagnostic tools,[71] aptamers,[72] catalysis[73] or DNA biochips[74] among others. Great efforts have been addressed to investigate the synthetic procedures by conjugating oligonucleotides with several important target molecules like proteins, carbohydrates, peptides, lipids or fluorescent derivatives.[75] However, in this context, carbohydrates-oligonucleotide conjugates (COCs) are probably one of the most well studied pattern due to the major participation of glycans in regulating biological processes such as cell-cell recognition, immune defence or signal transduction.[2,76,77]

One example observed in Nature falls to the carbohydrate recognition by specific sugar-binding proteins or lectins. This family of proteins is present decorating the cell surface as membrane receptors to selectively identify carbohydrates from different glycoproteins. The binding interaction triggers a cascade of response leading to the cellular uptake of this glycoproteins through endocytosis as defence mechanism system.[78] Interestingly, this natural process occurs in a multivalent manner. This means the formation of sugars glycoclusters to enhance and increase the protein-binding affinity in comparison to the single-monosaccharide binding, typically weaker in affinity (mM range).

The attractive goal in preparing COCs architectures relies on taking advantage of the ODN-based hybridization properties. This configuration provides rigidity, robustness and solid structures in order to facilitate the carbohydrate recognition, accessibility and spatial rearrangement. Some examples of glycocluster ODN architectures are shown in the Figure 3.1.[79–82]

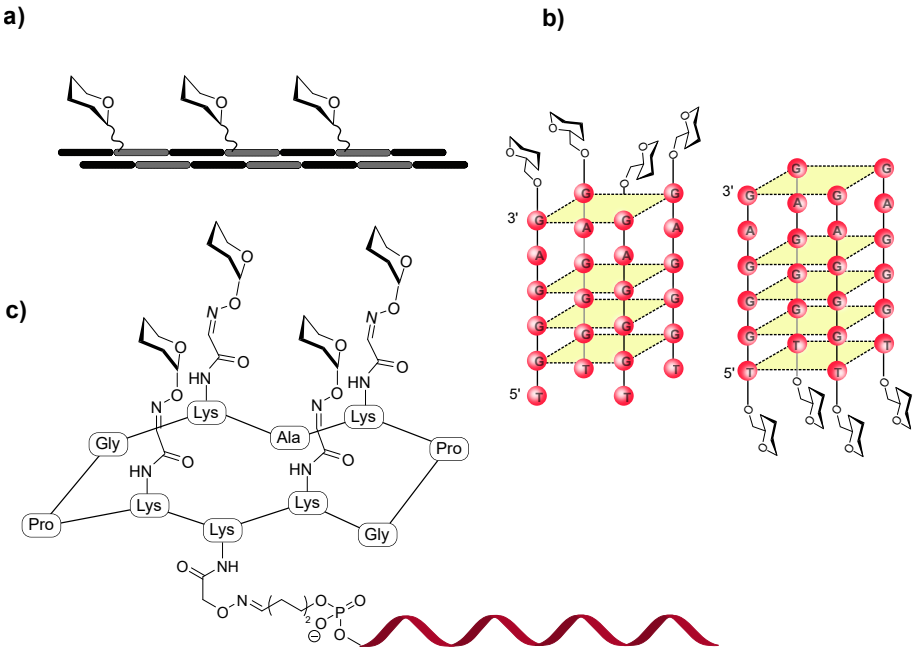

Figure 3.1: General approach of different COCs scaffolds. a) COC formed by concatenation of dsDNA scaffold.[82] b) COC using parallel G-quadruplex scaffolds couple with sugars at 5'-end and 3'-end.[80] c) RAFT Glycocluster formed around a cyclic peptide template[79]

The design of COCs aims to overcome some difficulties in terms of pharmacokinetic and pharmacodynamic properties of bare-ODNs. However, the strategy behind the construction of these architectures is not a simple task because of the intrinsic nature of both biomolecules which are not entirely suitable to be conjugated.

From a general point of view, the COC scaffolds can be classified according to the spatial location of the carbohydrate molecule over the ODN strand. As it is depicted in the Figure 3.2 three types of carbohydrate-oligonucleotide ligations are opened to be functionalized: the 3'-end (a), the 5'-end (b) or located inside the ODN strand.

Typically, the 5'-end and 3'-end are the most common positions to be conjugated due to a better accessibility and less steric hindrance towards hybridization process. In the Figure 3.2a,b both positions are highlighted by a blue arrow. Nevertheless, it exits other points of reactivity at the inner part of the ODN strand (Figure 3.2-c). One is on the deoxyribose sugar or sugar phosphate and the other one is located on the nucleobases, both highlighted as a red arrow within the Figure 3.2. Specifically, the deoxyribose sugar only exhibits a unique reactivity point at the position 2' to be incorporated an external glycan. Alternatively, the nucleobase can offer another

panel of reactivity determined by the nucleobase of study. Thus, the pyrimidine bases (A-G) can react at position 5 and the purine bases at position 7. This is critical to be considered since the glycan position plays a noteworthy role in the final property of the COCs.[83]

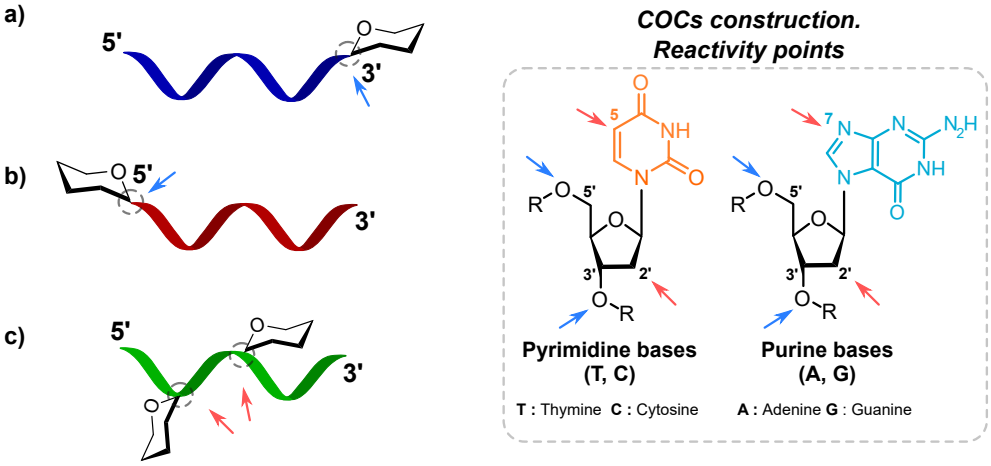

Figure 3.2: Representation of the different points of reactivity towards the COCs construction. a) ODN-glycan modification through the 3'-end. b) ODN-glycan modification through 5'-end. c) Internal ODN-glycan modification either by the deoxyribose sugar at position 2' or by the nucleobase at position 5 (pyrimidine bases A-G) or position 7 (purine bases T-C).

3.1.1 Chemoselective reactions towards the COCs synthesis

The advent and study of regio- and chemoselective reactions have entailed a great improvement towards the construction of new glycomimetic structures. These reactions have become a versatile conjugation strategy to obtain final products in high yields that otherwise, would imply multiple reaction steps. Two main examples are the oxime chemistry and the classical Huisgen 1,3-dipolar cycloaddition reaction.

Oxime Ligation

The oximation reaction belongs to the chemoselective reactions group in which an aminooxy group (formNH_2-OR) reacts with a carbonyl function (either ketone or aldehyde) to form an oxime ether linkage. As we depicted in the Figure 3.3, this reaction is just a particular example of an imine formation but with an adjacent heteroatom oxygen in α position to the nitrogen atom.

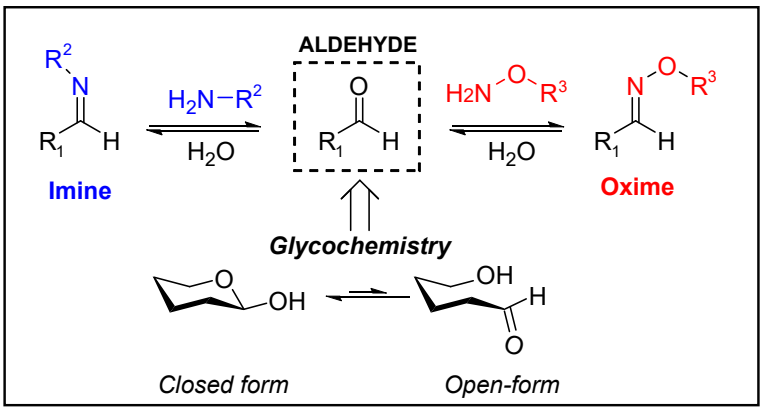

Figure 3.3: Formation of imine (in blue) and oxime (in red) ligations from the addition of free-amine group and amniooxy group to an aldehyde group, respectively. In glycoscience, the aldehyde at the anomeric position can be exposed in the open-form for this chemical modification, although it is typically masked in the closed form (cyclic hemiacetal).

However, these type of ligations are fairly common in the world of glycoscience (Figure 3.3).[84] Sugar molecules, as we reviewed in the Introduction, are special compounds that exhibit multiple functional groups with different points of reactions. This is more highlighted at the anomeric position where a masked open-form exposes a free aldehyde susceptible of being modified by these model of reactions.

Both reactions are in equilibrium under aqueous solutions and consequently, undergo with hydrolysis to revert at the initial state. Interestingly, the oxygen in alpha position induces the higher stability from hydrolysis of the oxime ligation compare to its imine analogue.[85] This phenomena stems from what is called **α-effect** and it can be explained by electronic effects through relative stability in the canonical resonance structures described in the Figure 3.4.

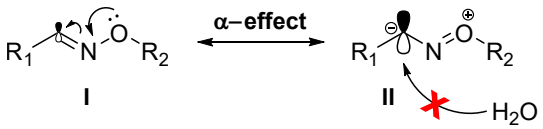

Figure 3.4: Representation of the α-effect in the hydrolytical stabilization of oxime ligation.

Chemically, this stabilizing effect is promoted by the charge-delocalization of the unshared electron pairs from the oxygen towards the nitrogen in conjugation through the double-bond. Thus, the resulting resonance form II exhibits a higher electron density within the sp^2 molecular orbital of the carbon atom which induces an elec-

tronic hindrance towards nucleophilic attack by water. Moreover, the acid-catalyzed hydrolysis is being considerably reduced due to the negative inductive effect (-I) of the oxygen atom in alpha position which decreases the basic capacity of the sp^2 nitrogen atom.[84,86]

Regarding the oxime bond formation, the oximation reaction can be catalyzed under acidic conditions (Figure 3.5-a) based on the important mechanistic studies by Jenks *et al.*[87,88] Typically, this reaction undergoes by acidic protonation of the carbonyl group that facilitates the nucleophilic attack by the aminooxy group. The proton transfer drives the formation of a tetrahedral hemiaminal intermediate. Next, the protonation of the hydroxyl group promotes the release of a water molecule and final yielding of the oxime product after deprotonation step. However, the pH parameter could determine the production of the final product since pH values below 3 would reduce considerable the final rate of the reaction. This is mainly because at lower pH the aminooxy group can be derived in two inactive protonated forms in equilibrium.[89] For that reason, the optimal pH values are in the range of 3 to 7 being the deprotonation step, the rate-limiting reaction.[90]

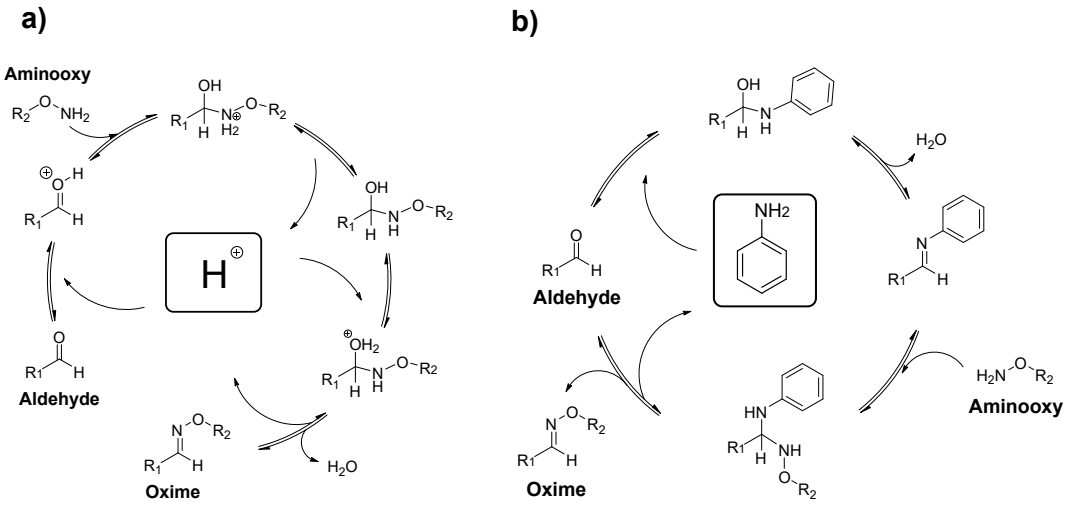

Figure 3.5: Catalytic cycle for the formation of oxime products. a) Oxime reaction *via* acid catalysis b) Oxime reaction *via* aniline as a nucleophilic catalyst.

However, the use of efficient catalysts opens the access to another reaction conditions that boost strongly the versatility of this type of reaction. With this idea, Jencks *et al.* were the first on proposing the use of aniline as a monofunctional catalyst for the semicarbazone formation with 3.5 fold rate.[91] They suggested a mechanism presented in the Figure 3.5-b, where the aniline exhibits a nucleophilic

attack over the carbonyl function first, to generate an aromatic imine, that acts as a new active reagent for the aminooxy nucleophile addition. The intermediate evolves by releasing the catalyst to yield the final oxime product. In this context, several groups have been made a great effort to test many different analogues of aniline catalysts or combinations to enhance the oxime reaction.[92–94,132]

Copper-free click chemistry conjugation

Click chemistry describes a concept conceived by Prof. K. Barry Sharpless and coworkers in 2001 that covers a group of reactions ideally defined by a stringent set of criteria: click reactions should be generated stereospecific byproducts with high yields and easily removed by non-chromatographic methods. In particular, both byproducts and solvents should be inoffensive and water-based scope respectively.[95] Overall, the main concept for Sharpless was to form carbon-heteroatom bonds with high robustness under physiological conditions towards the application to both small-scale and large-scale of production.

Based on their chemical transformation, four main set of reactions are involved in the above criteria:

- ☛ Cycloadditions of unsaturated species such as Diels-Alder reactions or the Huisgen 1,3-dipolar cycloaddition reaction with alkynes.
- ☛ Nucleophilic substitution *via* S_N2 based on ring-opening reactions in epoxides or aziridines
- ☛ Non-aldol type carbonyl chemistry *via* hydrazone and oxime chemistry seen in the last section
- ☛ Addition C-C multiple bonds, in particular epoxidation, aziridination or dihydroxylation

An example of click chemistry "par excellence" is the copper-(I)-catalysed Huisgen 1,3-dipolar cycloaddition using azide-alkynes reagents. This reaction is generally known as *Copper-catalysed Azide-Alkyne Cycloaddition* or CuAAC. Historically, this 1,3-dipolar cycloaddition was firstly described by Huisgen in 1963 (Figure 3.6).[96] However, this reaction required high temperatures to obtain reasonable yields generally with a mixture of 1,4 and 1,5 regioisomers. With this idea, Sharpless and coworkers optimized the scope of this reaction by introducing copper (I) salts that promote a catalytic cycle to yield regioselective 1,4 triazoles hydrolytically and thermically stable (Figure 3.6).[97] However, the mechanism of the copper catalyst in the 1,3-dipolar cycloaddition is still an object of attention, being the most up-to-date

accepted study, the key bridging di-nuclear copper (I,II) μ-alkenylidene intermediate proposed by Worrel *et al.*.[98]

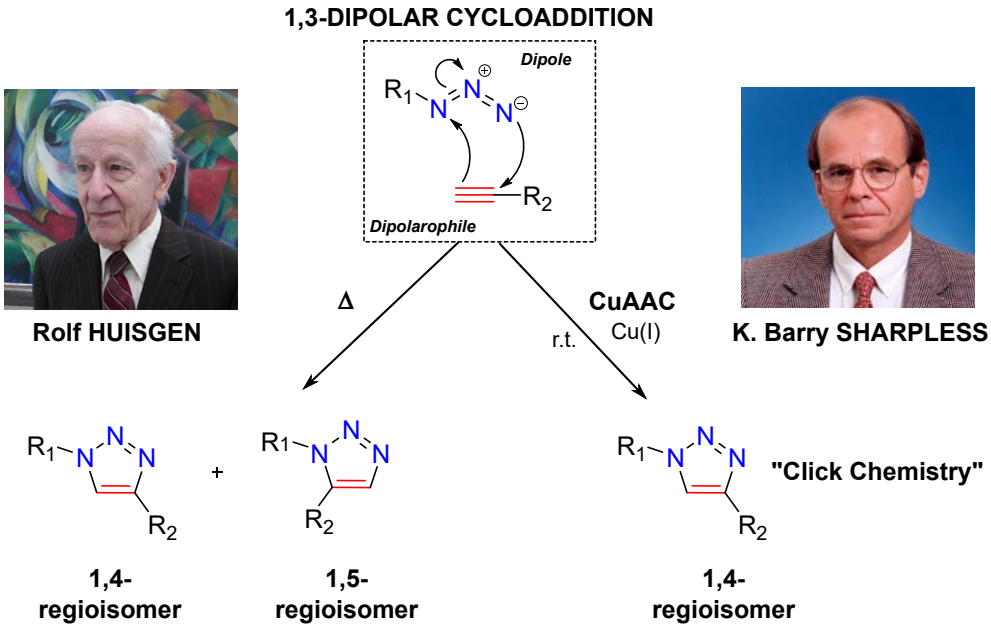

Figure 3.6: Representation of the remarkable 1,3-dipolar cycloaddition firstly discovered by Huisgen[96] and further optimization with Cu(I) salts as a catalyst by Sharpless.[97]

Even though the CuAAC has been fully employed as a versatile, chemoselective and robust chemical tool, this chemistry exhibits some limitations in bioconjugation through biological environs due to the toxicity of the copper catalyst. Therefore, an alternative copper-catalyzed approach of click chemistry has been reported by Bertozzi and coworkers *via* copper-free click reaction.[99] This model of click reaction has been extensively developed in her laboratory towards the design of bioorthogonal reactions in biological systems.[100] Known as strain-promoted azide-alkyne cycloaddition or SPAAC, this biocompatible click chemistry relies on highly strained cycloalkynes (ring strain) as a driving force to trigger the cycloaddition with rising applications in labelling approaches such as lipids,[101] nucleotides[83] and carbohydrates.[102] This spontaneus catalyst-free reaction depicted in the Figure 3.7 generally occurs between cyclooctynes (the minimal cycloalkyne stable in solution) and azide groups by Huisgen dipolar cycloaddition due to the lower distortion energy of the cyclooctyne in the transition state to form the final sp^2 angle compared to terminal alkynes from 160° and 180° respectively.[103]

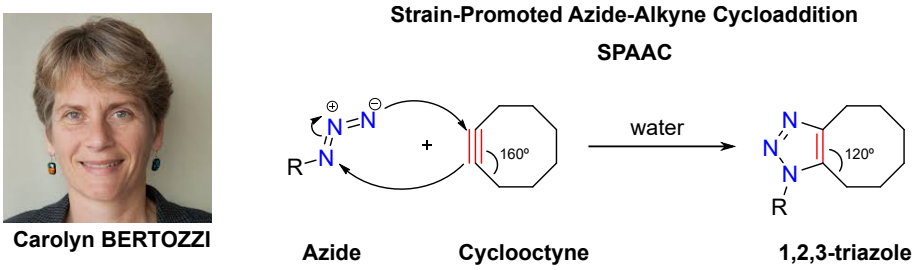

Figure 3.7: General scheme of SPAAC described by C. Bertozzi and coworkers.[100]

A great diversity of cyclooctyne derivatives have been synthesized and optimized in the past decades based on reaction kinetic, hydrophilicity and size. Thus, we can find cyclooctyne structures such as difluorinated cyclooctynes[104,105] (DIFO), bicyclononyne[106] (BCN), dibenzocyclooctyne[107] (DIBO), dimethoxy-azacyclooctyne[108] (DIMAC), dibenzo-aza-cyclooctyne[109] (DIBAC, also named as ADIBO[110] or aza-DBCO[111]), among others.[112]

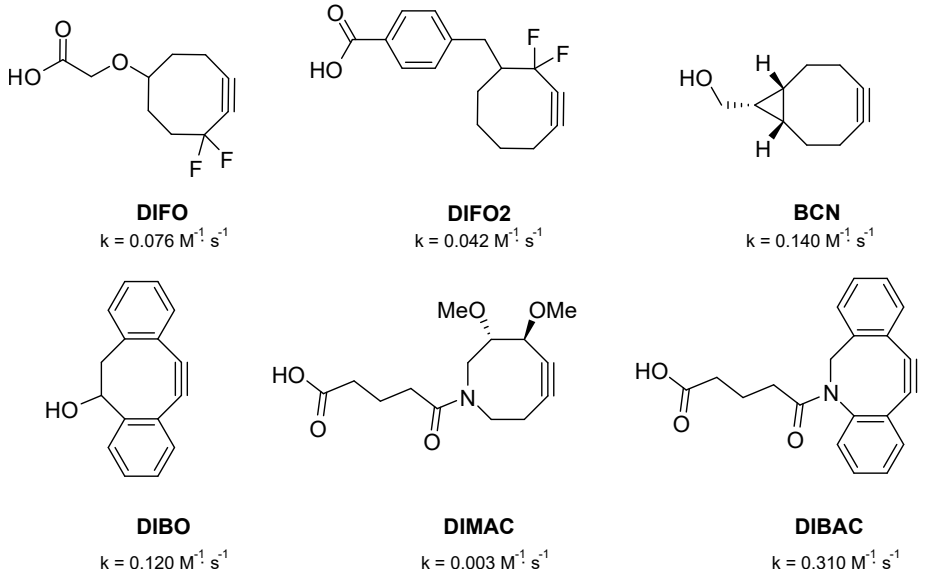

Figure 3.8: Overview of some chemical structures of cyclooctynes synthesized towards the copper-free click chemistry in living systems. DIFO - DIFO2 (difluorinated cyclooctynes[104,105]), BCN (bicyclononyne[106]), DIBO - DIBAC (dibenzocyclooctynes[107,111]).

Thanks to its versatility, these chemical strategies are employed for COCs synthesis both in solution and on solid support.

3.1.2 Common approaches to build-up COCs

According to this spatial distribution of the glyco-moiety, two main streamlines of research have been developed by several groups: on solid support and in solution phase synthesis.[113–115] Herein, we will summarise the most relevant synthetic techniques used so far.

Synthesis of COCs on Solid Support

The principle of this synthetic strategy resides in the addition of modified carbohydrate moieties to the ODN strand using an automated solid-phase synthesis. Commonly on this approach, the sugar is not commercially available and it requires synthetic steps to protect the hydroxyl groups and localize the reactivity on the carbon atom to be anchored. On this regard, the main goal is to seek a the proper linker with a suitable chemical group in order to interact selectively either with the ODN structure or with the solid-phase.

Generally, the most accepted strategy relies on the incorporation of the glycan structures at the 5'-end through phosphoramite chemistry. This synthetic process takes the advantage of using the automated ODN synthesizer to conjugate glycan-phosphoramidite derivatives after the ODN elongation. An example is described by Akhtar *et al.*[116] They synthesized a mannose-phosphoramidite compound which has to be conjugated onto the 5'-end ODN sequence at the anomeric position. On the other hand, the conjugation can be established at the 3'-end position of the ODN by carbohydrates functionalized solid support bearing a DMT (4,4'-dimethoxytrityl) protecting group. The first example was reported by Adinolfi *et al.* where they used a succinyl linker to attach DMT-glucose derivative to the solid-phase.[117]

Applications on this type of linkage is found in the comparative study developed by D'Onofrio *et al.* in which they incorporated three different carbohydrates (glucose, sucrose and mannose) through the two conjugation strategies seen before (3' and 5'-end) to build-up quadruplex structures.[80] Some of these conjugates are quite relevant in biomedicine as antiviral against the HIV-I (human immunodeficiency virus). This study confirmed that 3'-glycoconjugates is more stable in the quadruplex and specifically, the mannose sugar exhibited higher levels of antiviral activity.

Some other clever strategies have been reported in the way of creating COCs. In those cases, the nucleoside-base residue can be directly functionalized by a carbohydrate moiety and added to the ODN using the automated solid-phase DNA synthesis. As we illustrate in the Figure 3.9, the individual base is bearing the

carbohydrate molecule and the pentose is protected by DMT in the 5'-end and activated with phosphoramidite group at the 3'-end.

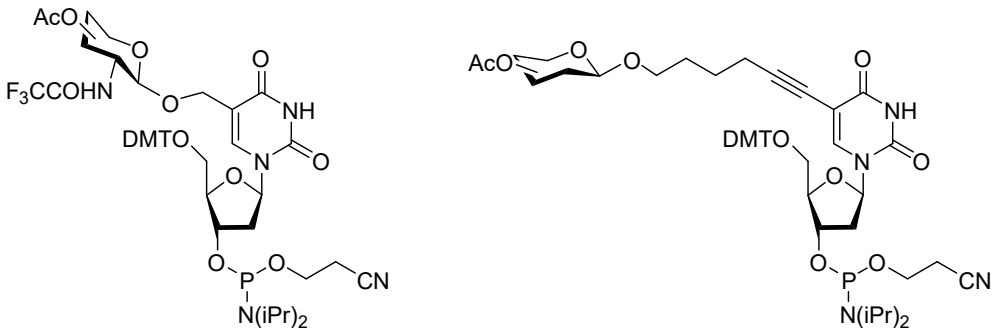

Figure 3.9: Example of glycosylated phosphoramidites monomers used for the oligonucleotide synthesis.[118,119]

In particular on solid-support synthesis, the carbohydrate can be exposed without any modification and re-used throughout multiple cycles to increase the final yield. However, it should be resistant enough to the final cleavage step. Within the oximation conjugation, the aminooxy group is highly selective to react with carbonyl groups, mainly aldehydes, to produce an oxime ligation. Karskela *et al* developed this chemistry by incorporating into the ODN sequence (*via* phosphoramidite approach), an activated linker bearing aminooxy groups. Then, the free-aldehyde from a modified hyaluronic disaccharide yielded the final oxime ligation through the anomeric position.[120]

On the other hand, the CuAAC has been broadly developed in bioconjugation. This chemoselective reaction consists in the 1,3-dipolar cycloaddition between an azide and alkyne group catalysed by Cu(I) to yield 1,2,3-triazoles.[95] This reaction has gained special importance in the COCs synthesis where the azide-alkyne groups is localized either at the sugar moiety or at the ODN strand separately. However, the preference is to functionalize the sugar molecule with azide group and the alkyne group with the ODN. Otherwise, the presence of phosphoramidite and azido groups can be quenched by the Staudinger reaction.[121]

This strategy was reported by Bouillon *et al* where they anchored a propagyl amine (alkyne group) onto the phosphonate group from ON backbone by amidative oxidation with CCl_4 and then, the azidosugar was couple *via* CuAAC click chemistry boosted by microwave radiation.[122]

Synthesis of COCs in solution phase

Contrary to the solid support strategy, the solution chemistry approach tackles the synthesis and purification of COCs scaffolds where both substrates are synthesized separately. Accordingly, this post-synthesis conjugation must be achieved under compatible reaction conditions for both partners to avoid solubility problems or lack of selectivity that may lead to obtain low coupling yields. Therefore, it is particularly useful for this strategy once again, tackling the COCs synthesis by using regio- and chemoselective reactions like oxime and CuAAC seen before, that are water-friendly in bioconjugation reactions. Several types of reactions can lead stable COCs products such as disulfide formation by oxidative coupling of thiol molecules,[123] or imines and hydrazones which similarly to the oxime ligation, react with carbonyl groups (commonly aldehydes) *via* amino and hydrazide groups without using protecting groups.[124] However, the use of oxime ligation or CuAAC click is by far, the most extensible strategy to conjugate carbohydrates to ON strands, as we can see in the Figure 3.1c.[125] Specially it is interesting to remark the possible combinations that can be established between these reactions. For instance, Morvan and coworkers reported a clever bis-conjugation of ON by the sequential combination of oxime ligation and CuAAC where the ON was functionalized with an akyne group at the 5'-end and an aldehyde group at the 3'-end. This strategy allowed the incorporation of carbohydrate moieties in both ends of the ON sequence.[126]

3.2 Proposed strategy

This chapter is dedicated towards the preparation of COCs as a versatile architecture for detection, purification and immobilization approaches for biosensing purposes (Chapter 5). In particular, a complex polysaccharide from plant cell wall named Tamarin Xyloglucan is selected as a probe ligand of the α-1,2-fucosyltransferase (AtFUT1) to monitor protein-glycan interactions. However, the larger size of this molecule (MW: 550 kDa) limits its possibility of being properly handled and characterized. Thus, this substrate is enzymatically digested to obtain a set of building-blocks each of which, are conjugated with an single-strand ODN-1 scaffold. From now, this COCs will be specified as Xyloglucan Nucleic Acid Conjugate (XyNAC). On the other hand, the surface immobilization approach that will be developed in this project suggests the construction of a complementary ODN-2 scaffold modified by a pyrrole molecule for grafting purposes (Chapter 5). Likewise, this ODN conjugate will be named Pyrrole Nucleic Acid Conjugate (PyNAC). A global vision of the main components is depicted in the Figure 3.10 to have a major comprehension and visualization.

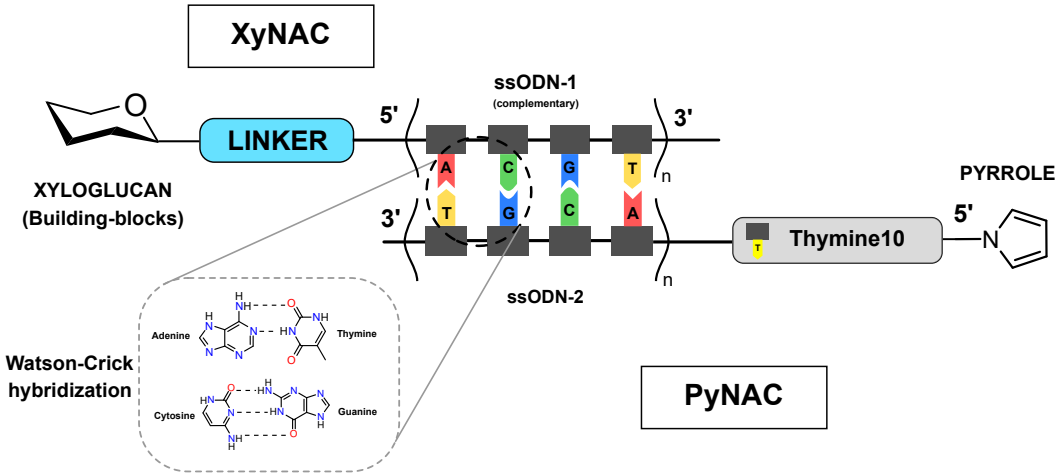

Figure 3.10: Model of the main components from the XyNAC and PyNAC architectures. The XyNAC is formed by the XyG substrate connected to a ssODN-1 through a bifunctional linker at the 5'-end strategy adapted to the synthesis of DNA architectures for DDI of xyloglucan building-blocks on biochips.

On the top, the XyNAC is formed by the XyG ligand (building-blocks) connected through a specific bifunctional linker to the ssODN-1 sequence at the 5'-end. On the other hand, the PyNAC architecture is composed by a ssODN-2 sequence conjugated to a pyrrole molecule at the 5'-end separated by a thymine spacer (T10).

Both ssODN-1 and ssODN-2 are complementary sequences to each other to enable the specific interaction by Watson-Crick hybridization process.

The synthetic strategy to construct both ssODN conjugates requires different approaches depending on the molecule to be conjugated. The overall approach of chemical synthesis and characterization is depicted in the Scheme 3.11.

Regarding the XyNAC architecture (Scheme 3.11-a), this conjugate demands specific chemical reactions to connect the XyG substrate to a ODN sequence. The strategy proposed uses an linear heterobifunctional linker molecule containing two different chemoselective groups at both sides: an aminooxy functional group (H_2N-O) and an azide group. This synthetic approach is chemically developed through a stepwise oximation reaction followed by a copper-free Huisgen cycloaddition reaction. For this last synthetic step, the ssODN-1 is modified at the 5'-end with a dibenzocyclooctyne amine (DBCO) commercially available.

Likewise, the synthetic approach for the construction of PyNAC (Scheme 3.11-b) is based on the nucleophilic substitution *via* S_N2 of the ssODN-2 over an activated pyrrole. In this strategy, the ssODN-2 is modified with an amine group at the 5'-end (commercially available) and the pyrrole is modified by the nitrogen atom with a carbon chain bearing an N-hydroxysuccinimide group (NHS) previously synthesized in our laboratory.

Finally, we propose the study of two relevant techniques highly employed in the field of oligonucleotides: the DNA electrophoresis gel and the melting temperature. The purpose is to evaluate as quality control the ssODN conjugates by DNA electrophoresis, and the effect of the sugar residue over the hybridization process by measuring the melting temperature.

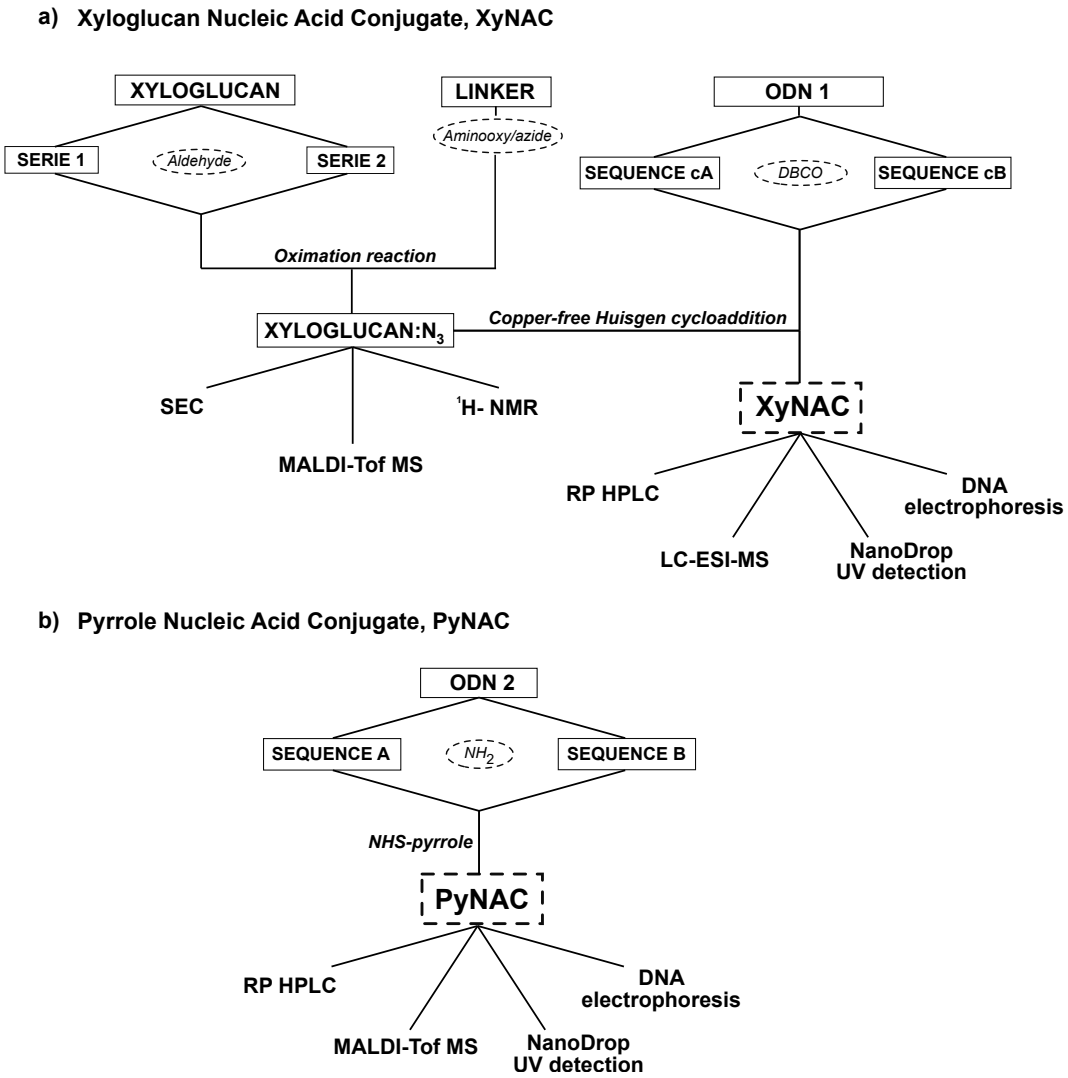

FIGURE 3.11: General overview of the proposed strategy towards the construction and characterization of XyNAC and PyNAC architectures. a) Synthetic route to obtain, purify and characterize the XyNAC product *via* stepwise procedure using an heterobifunctional linker (aminooxy/azide). The xyloglucan is functionalized by oximation reaction to afford the xyloglucan-azide derivative. The subsequent reaction with a DBCO-modified ssODN-1 *via* copper-free Huisgen cycloaddition yield the desire XyNAC product. b) Chemical strategy to obtain, purify and characterize the PyNAC product. An amino-modified ssODN-2 sequence is directly conjugated with an activated pyrrole molecule in the form of NHS-ester to yield the PyNAC product.

3.3 Main Characters involved in the Construction of XyNAC and PyNAC architectures

3.3.1 Understanding the AtFUT1 ligand: the Xyloglucan

The xyloglucan is a branched cellulose derivative from the family of hemicellulose heteropolysaccharides found in higher plants. It comprises an heterogeneous diversity in length and side chain throughout the primary cell wall.[127] Herein, we study the xyloglucan polysaccharide extracted from the Tamarind seeds as a potential ligand of the fucosyltransferase AtFUT1. The chemical structure is illustrated in the Figure 3.12-a,b.

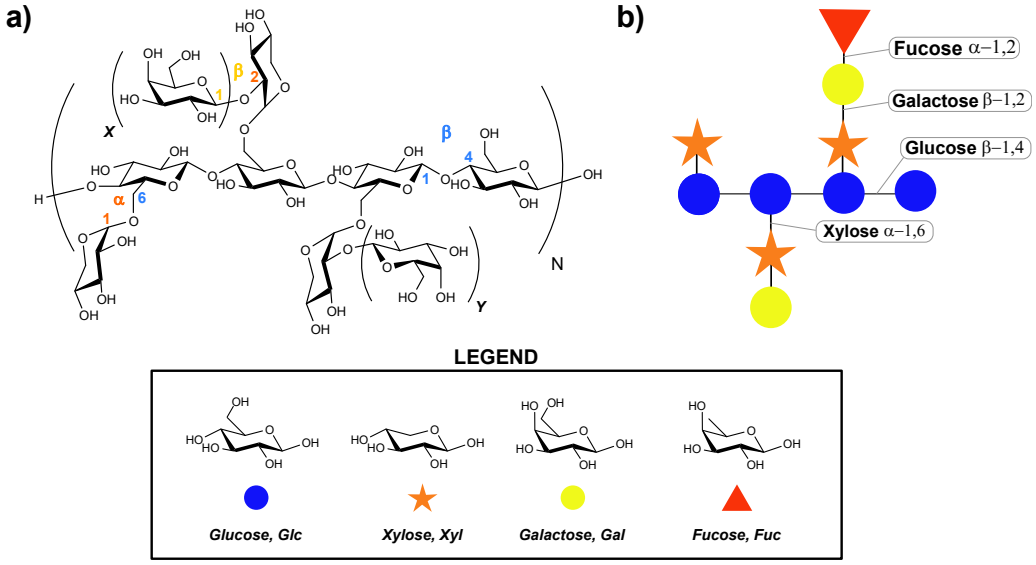

Figure 3.12: Model of the xyloglucan structure. a) Chemical representation of the monomeric unit of XyG showing the glucose molecules (β-1,4-backbone) with side chains made of xylose (α-1,6) and galactose (β-1,2). b) Scheme of xyloglucan linkages depicted by pictorial representation of the different sugars in Glycobiology.

The xyloglucan structure is formed by a cellulose-like backbone composed by four glucose units linked by β-(1,4)-D-glucan bonds. Then, it is regularly substituted by xylopyranosyl sugars linked through an α-(1,6) linkages in three out of four glucose main-chain. Hereafter, the xyloglucan scaffold is already established and further substitutions lead to define different side chains structures and consequently, different plant tissues and species.[127] In the case of xyloglucan obtained from Tamarind seeds, the xylosyl residues are functionalized in position 2 with galactose molecules

by a β-(1,2) linkage. Nevertheless, this xyloglucan composition does not present fucose in the structure, making to this ligand suitable to rationalize the fucose transfer by the AtFUT1 enzyme.

The molecular weight of the entire xyloglucan molecule is around 579 kDa in water at room temperature. Chemically, this heteropolysaccharide exhibits a neutral chemical behaviour under standard conditions and low viscosity.[69] Furthermore, it is a molecule soluble in water but it could form aggregates specially when the polymerization degree (PD) is significantly larger. Moreover, the xyloglucan is stable under mild conditions of temperature and acids and bases mainly due to its high substitution degree.[69]

3.3.2 Choice of the linker

In our main idea of creating COCs architectures, it is always necessary to study how is it chemically possible to connect both biomolecules together. The strategy therefore, was focused on seeking a bifunctional linker able to functionalize the XyG building-blocks and the oligonucleotide scaffold selectively in solution. For this reason, we guided our synthetic approach towards the stepwise chemoselective reactions *via* oxime (XyG) and copper-free conjugation (cODN-1).
Altogether, we found that the aminooxy-triethylenglycol-azide was a nice organic molecule to establish robust connections between the two partners in solution under mild conditions. The chemical structure of the spacer is depicted in the Figure 3.13.

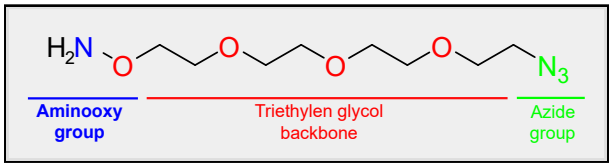

Figure 3.13: Chemical structure of the bifunctional linker. This organic molecule was selected having an aminooxy group (blue) and an azide group (green) separated by a triethylenglycol chain (red).

This organic compound was formed by a triethylenglycol (TEG, in red) backbone to provides flexibility and hydrophilicity to the final molecule. Besides, this bifunctional linker displayed two highly selective and compatible chemical groups at both ends: the aminooxy group (in blue) and the azide group (in green). These dual functions suitable to partake in the chemoselective reactions with the XyG structures and the modified cODN without any chemical modification on those starting molecules.

3.3.3 Chemical composition of cODN-1 sequences

The construction of XyNAC architectures required the participation of an ODN scaffold that facilitated their purification and characterization but also, envisioned the DNA-direct immobilization approach (DDI) of XyG compounds on solid support (Chapter 4).

To this purpose, we proposed two complementary ssODN sequences (cA and cB) presented in the Figure 3.14. The chemical composition of both cODN structures was defined by the incorporation of a dibenzocyclooctyne amine (DBCO) at the 5'-end. This specific functional group was envisioned towards the chemoselective conjugation by SPAAC reaction with the free-azide group presented within the linker structure, previously described. These DBCO-oligonucleotide sequences of 24 base pairs were commercially available from Eurogentec.

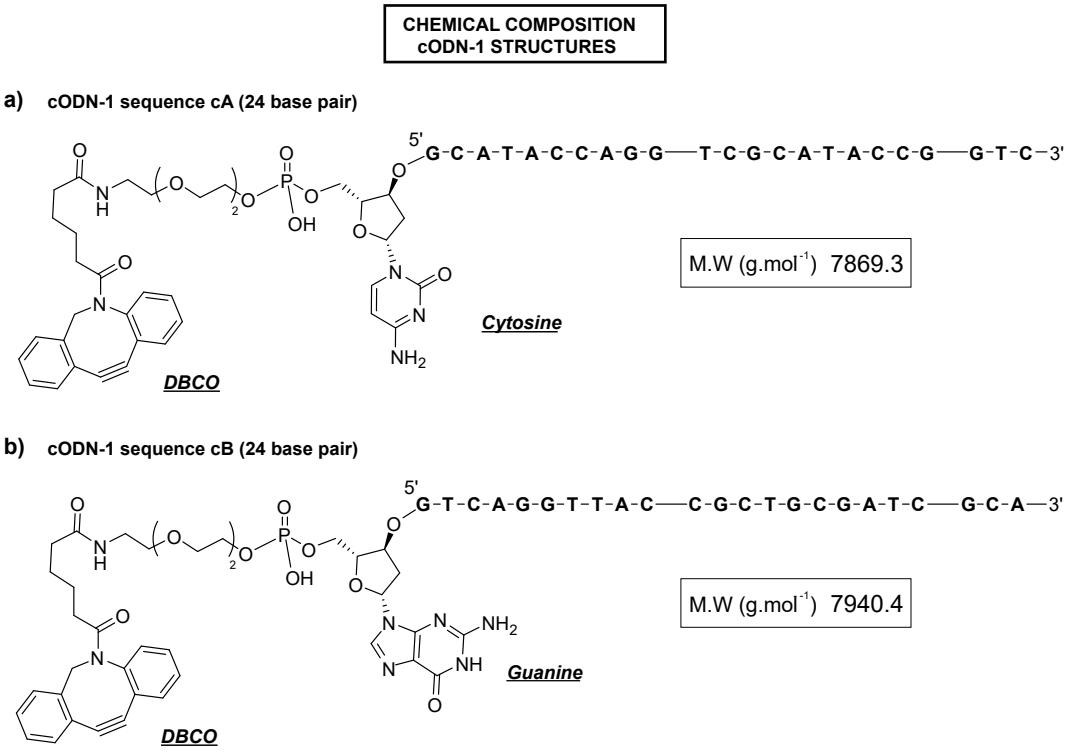

Figure 3.14: Representation of the chemical structure of cODN-1 sequences (24 base pairs) used to prepare XyNAC architectures in solution. a) cODN-1 structure for the sequence A b) cODN-1 structure for the sequence A Second model of ssDNA architecture 1B

The goal of having two different ODN strands repose upon the possibility of generating two families of XyNAC probes to enable the selective immobilization onto a solid surface for further monitoring interactions.

3.3.4 Chemical composition of ODN-2 sequences

Motivated by the surface immobilization approach based on DNA structures, the ODN-2 structures were prepared for surface grafting and specific immobilization binding. Thus, the construction of the ODN-2 structures required the presence of an external pyrrole moiety within the 5'-end (PyNAC). Therefore, this ODN-2 scaffold was specifically modified at the 5'-end with a nucleophile group (amine group) for further coupling reaction. Furthermore, at the 3'-end, the DNA strand was composed by a ten consecutive thymidine chain (T_{10}) to provide a critical separation between the surface and the hybridization region (Figure 3.15).

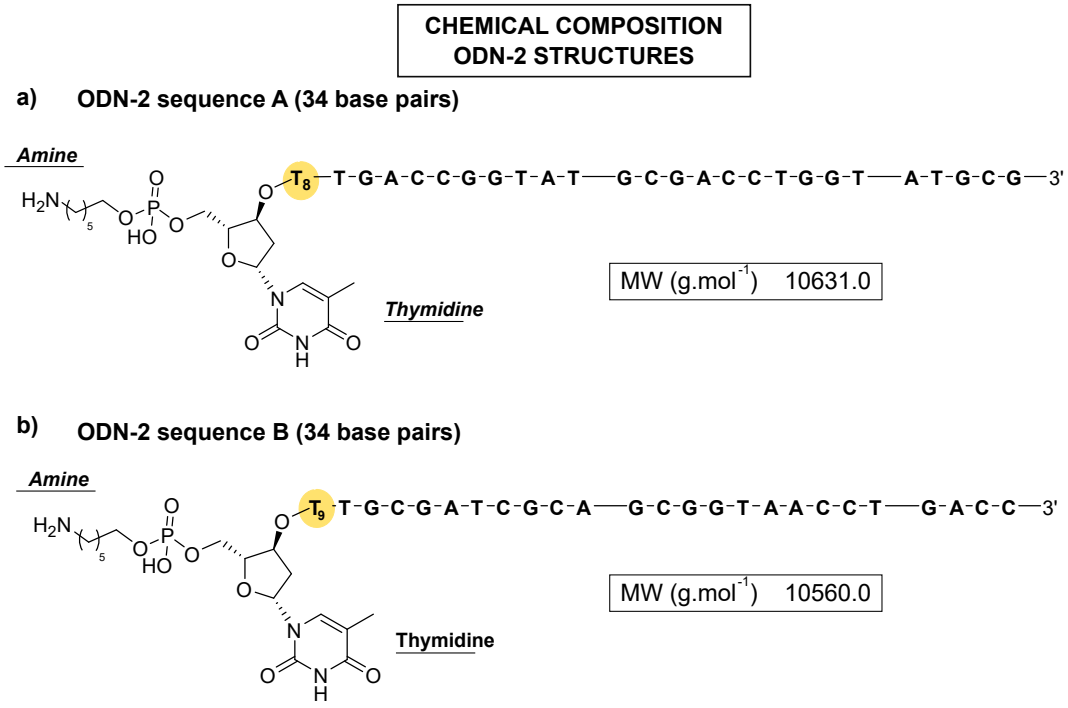

Figure 3.15: Models of commercial amine-DNA architectures sequences used for the NHS-modification. (a) Sequence 2A of the amine-DNA architecture II with a molecular weight of 10631.0 g/mol. (b) Sequence 2B of the amine-DNA architecture II with a molecular weight of 10560.0 g/mol.

To enable a selective hybridization process, the ODN-2 architecture presented two complementary sequences (A and B) over the cODN-1 twin sequences (cA and cB) previously defined (Figure 3.15-a,b). Likewise, the amino-based ssODN-2 were formed by 34 base pairs for hybridization purposes and they were commercially available from Eurogentec.

3.4 Preparation of XyNAC architectures

3.4.1 Elaboration of the xyloglucan starting materials

The Tamarind xyloglucan polysaccharide, among other chemical features, represents a molecule with a molecular weight around 579 kDa. The larger size and complex structure of this polysaccharide make it certainly a difficult molecule to chemically handle. Thus, we have developed an enzymatic reaction in order to cleave the whole Tamarind xyloglucan polymer into a range of different cores (Scheme 3.1).

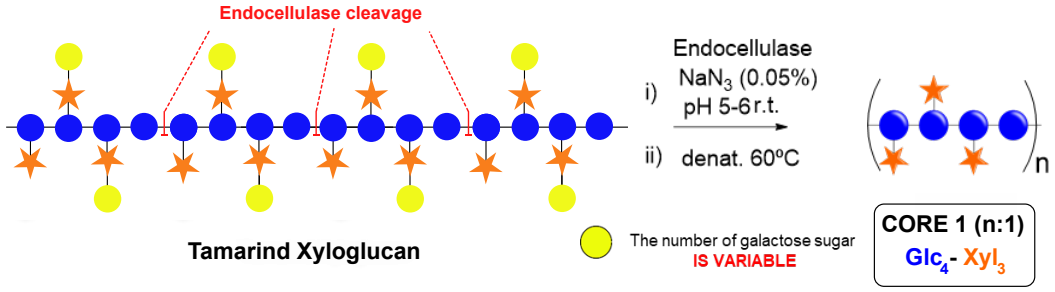

Scheme 3.1: Enzymatic degradation of Tamarin xyloglucan polymer by an endo-cellulase 1,4-β-D-glucanase to obtain a set of different polymerization degrees.

As it is shown in the Scheme 3.1, to prepare a set of different xyloglucan cores, the Tamarind xyloglucan polymer was firstly, enzymatically digested at pH 5 by an endo-cellulase 1,4-β-D-glucanase (1.2 U/μL) from *Aspergillus niger* under 0.05% of sodium azide to preserve the enzyme integrity from bacterial degradation. This type of enzyme particularly hydrolysed the β-1,4-glycosidic bonds of the xyloglucan structure established between the fourth and the fifth glucose main-chain molecules in the polymer from the reducing end. Therefore, the reaction mixture was optimized to obtain larger cores of XyG by controlling both the enzyme exposure time and quantity over the reaction mixture. Finally, to quench the reaction, the temperature was increased up to 80°C to denature the protein.

XyG building-blocks purification by Size-Exclusion Chromatography

The enzymatic digestion of the xyloglucan yielded a mixture of several substrates with a large variety of sizes. The size-exclusion chromatography (SEC) technique also known as gel permeation chromatography, was presented as the candidate technique to purify the XyG fragments. The SEC tackled the separation of the macromolecular components in a mixture based on molecular size through a column of a packed gel filtration resin. In our case, three chromatography columns of Superdex S30 distributed in serie were used. The resin or stationary phase was composed by porous beads with small channels inside where smaller molecules pass through this channels whilst larger molecules flow around the beads and leave the column first. Later, those molecules were detected by refractive index which separate the fractions by molecular weight.

The SEC purification process was performed in two digestion reactions of XyG polysaccharide involving two different enzyme conditions (enzyme concentration and exposure time) to obtain a range of XyG sizes. The first reaction condition (serie 1) was carried out using 2.4 U of the endo-cellulase enzyme for 20 minutes. According to the SEC chromatogram, it showed a profile with much more quantity of smaller molecules than larger molecules. Therefore, an optimization step in a second reaction condition (serie 2) was accomplished under 0.6 U of endo-cellulase enzyme for 5 minutes of exposure before quenching, showing a better peaks distribution in the SEC chromatogram. These results are presented in Figure 3.17 where the larger molecules were eluted from the column at shorter retention times.

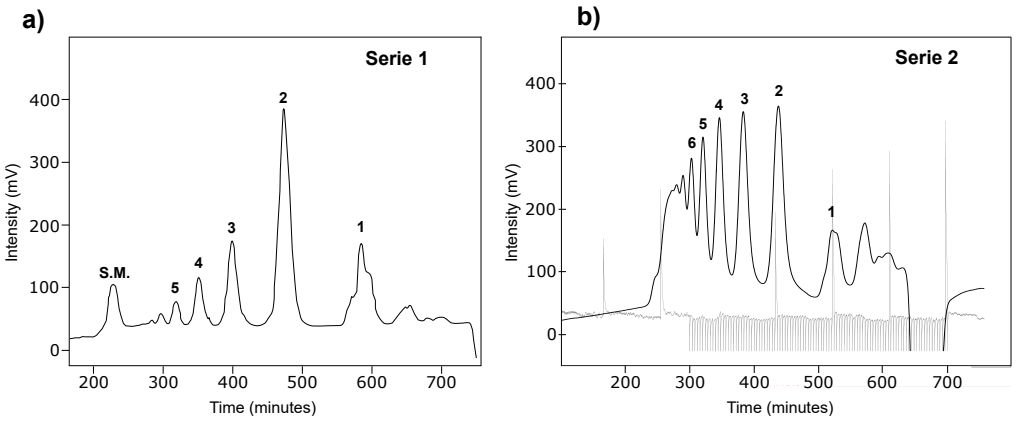

Figure 3.17: Chromatogram of the two different enzymatic conditions series 1 and 2. (a) Serie 1: Tamarind xyloglucan hydrolysis with 2.4 U of endo-glucanase enzyme for 20 minutes. (b) Serie 2: Tamarind xyloglucan hydrolysis with 0.6 U of endo-glucanase enzyme for 5 minutes.

As we expected, series 1 and 2 revealed SEC chromatograms with remarkable variation in the peaks distribution and intensity. On average, the serie 1 showed more presence of smaller molecules compared to the serie 2 due to the higher quantity of enzyme and larger reaction time.Moreover, the presence of the starting material (S.M.) which correspond to the first peak of the chromatogram was observed for the serie 1 of XyG digestion. On the other side, the peaks of the serie 2 were rather similar in terms of intensity, meaning that we managed to quench the reaction on time to get more quantity of the largest one. However, those peaks were relatively overlapped in comparison with the serie 1, making harder the discrimination of the sample tubes. Nevertheless, on average we can conclude that the degree of similarity between the peaks distribution and, in the end, the purification process was successfully obtained by SEC. Regardless of the peaks distribution were detected in the chromatogram, the system only collected the samples in tubes starting at 300 minutes and the peaks before that time were discarded.

Each peak of the SEC labelled in the Figure 3.17 was collected right in the inflection point and lyophilized. It yielded a white cellulose-like appearance solid compound at milligram scale, ready for mass characterization. All of them served as a starting materials for further functionalization with oligonucleotide biomolecules *via* DDI approach.

XyG building-blocks characterization by MALDI-Tof Mass Spectrometry analysis

During the enzymatic hydrolysis of the XyG, we managed to fragment this substrate in a set of XyG building-blocks and to purified them by SEC. The mass spectrometry is our major identification technique to characterize those glycostructures with high accuracy. In particular, *Matrix-Assisted Laser Desorption/Ionization Time-of-Flight* mass spectrometry or MALDI-Tof MS was used to determine qualitatively the structural identity of the different XyG cores isolated through SEC. We evaluated the serie 2 of XyG hydrolysis separately by MALDI-Tof MS technique using 2,5-dihydroxybenzoic acid (DHB) as a crystallization matrix in positive mode.

Based on the Figure 3.18, multiple signals were obtained for each fraction from the SEC analysis. Each peak corresponds to a fixed XyG core (glucose and xylose) along with a variable number of galactose molecules (X). As an example, in the Figure 3.18-a we observed the mass distribution of the three species that belongs to the core 1 of XyG unit formed by 4Glc and 3Xyl; and X number of Gal molecules (X: 0 to 2) to define the final compound. This XyG mass distribution was found for the rest of compound from the serie 2 (Figure 3.18-b to f). Interestingly, we noticed

that all the samples exhibited a Gaussian profile based on the number of galactose molecules within their structures that suggests a random distribution of Gal based on the size of the XyG fragment.

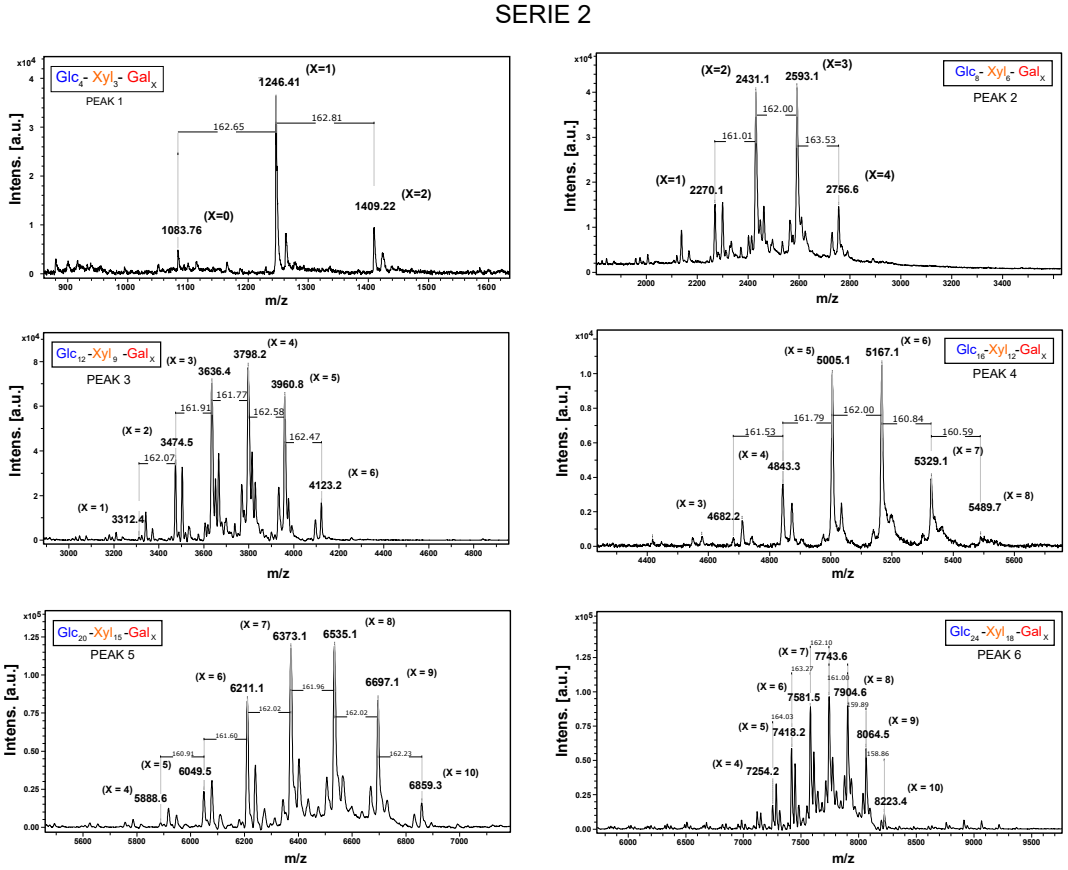

Figure 3.18: MALDI-Tof MS analysis of XyG substrates using DHB matrix in positive mode obtained for the serie 2 from the SEC purification. a) XyG 1 core 4Glc, 3Xyl and XGal (X:0 to 2). b) XyG 2 cores 8Glc, 6Xyl and XGal (X:1 to 4) c) XyG 3 cores 12Glc, 9Xyl and XGal (X:1 to 6) d) XyG 4 cores 16Glc, 12Xyl and XGal (X:3 to 8) e) XyG 5 cores 20Glc, 15Xyl and XGal (X:4 to 10). f) XyG 6 cores 24Glc, 18Xyl and XGal (X:4 to 10).

Considering our previous results, we managed to prepare multiple building-blocks of XyG from an optimized enzymatic hydrolysis of Tamarind XyG using an endo-glucanase (as shown in the Scheme 3.1). The SEC technique along with the MALDI-Tof MS analysis confirmed the pure isolation of XyG building-blocks that will serve as starting materials for the COCs synthesis.

3.4.2 Synthetic Procedure for XyNAC architectures by Chemoselective Reactions

The design and synthesis of glycoconjugates have become an important line of research for the study of carbohydrates interactions within their native environment.[129,130] In this context, the chemoselective reactions have promoted a powerful synthetic tool for the glyco-scientist due to the high selectivity and specificity in reactions with biomolecules *in vivo* and *in vitro*, and their capacity of being stable under physiological conditions.[131]

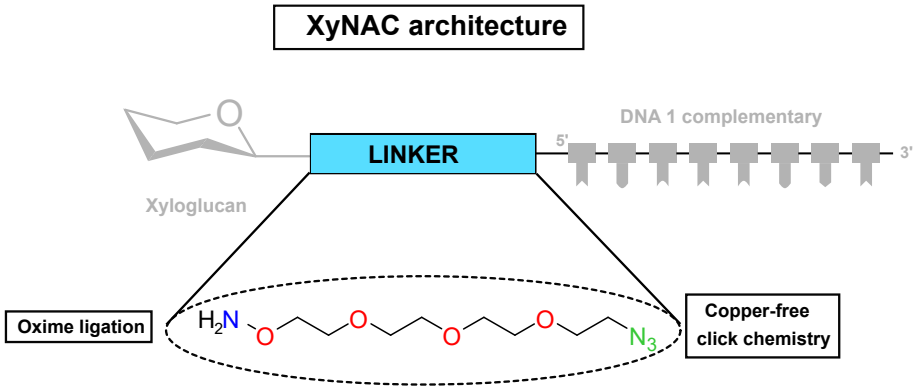

Figure 3.19: Model of the synthetic approach to form XyNAC architectures through chemoselective reactions *via* oxime ligation on the XyG building-blocks followed by copper-free click chemistry on the 5'-end of the ssODN-1 (DBCO).

Based on the functional group within the linker structure depicted in the Figure 3.13, we firstly describe the oximation reaction between the amoniooxy group in the spacer and the XyG anomeric position; and finally, we address the direct coupling between the azide group from the spacer and the aza-DBCO group localized at the 5'-end of the DNA *via* copper-free cycloaddition strategy or strain-promoted Azide-Alkyne cycloaddition (SPAAC).

Oxime reaction

In our synthetic approach, we used the XyG building-blocks to construct new XyNAC architectures *via* oxime ligation from the aminooxylated linker (Figure 3.19).

The Figure 3.20 depicts that the free anomeric position from the glucose molecule in the XyG is in fact an hemiacetal group (close form) in equilibrium with the alde-

hyde group (open form) in the carbohydrate chemistry so called mutarotation. This equilibrium is generally displaced towards the close form of the sugar structure, lower in energy. However, a minimal fraction of this aldehyde is susceptible to be attacked with the α-nucleophile group from the spacer to yield our final XyG-oxime product as a mixture of Z/E stereoisomers.

All the oxime reactions of the different XyG structures were carried out in large excess of the aminooxylated linker (5 equivalents) *via* aniline nucleophilic catalysis at pH 4.5 of sodium acetate (NaOAc) buffer.[132] Since the aniline requires the presence of an aldehyde in the reaction mixture (see Figure 3.5-b), it was necessary to restore the equilibrium in the sugar to the open form by increasing the temperature up to 40 °C. It ensured an increase of the final yield and facilitated the solubility of the aniline in aqueous media. Finally, something to highlight was the avidity of the aminooxy group to carbonyl functions. That made this reaction quite sensitive to exogenous carbonyl sources that may inactivate this reagent for the oximation reaction.

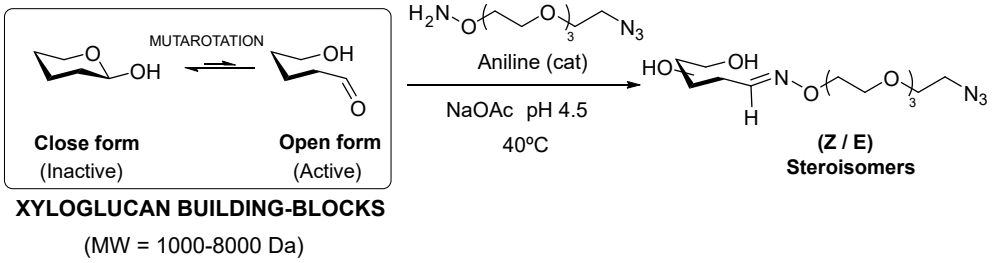

Figure 3.20: Mutarotation phenomena and synthesis of the XyG-oxime conjugates *via* aniline catalysis.

The oxime reaction course was monitored by MALDI-Tof MS with DHB matrix in positive mode. We presented in the following Figure 3.21, an example model of the MALDI-Tof MS profile for the oxime functionalization of the XyG 2 cores previously purified. All data collected in the ANNEXE Chapter 5.

The Figure 3.21 showed a comparative analysis between the starting material for the XyG building-block with 2 cores (orange line) and the final product obtained through oxime ligation (blue line). The MALDI-Tof MS analysis of the XyG 2 cores starting material showed four different m/z peaks regarding the number of galactose molecules on each XyG building-blocks. These XyG compounds with X=1, 2, 3 and 4 galactoses were considered as active reagents for the oxime ligation. After the oximation reaction, the mixture was desalted and purified using PD MiniTrap G-10 (cut-off of 700 Da) to remove the excess of the linker.

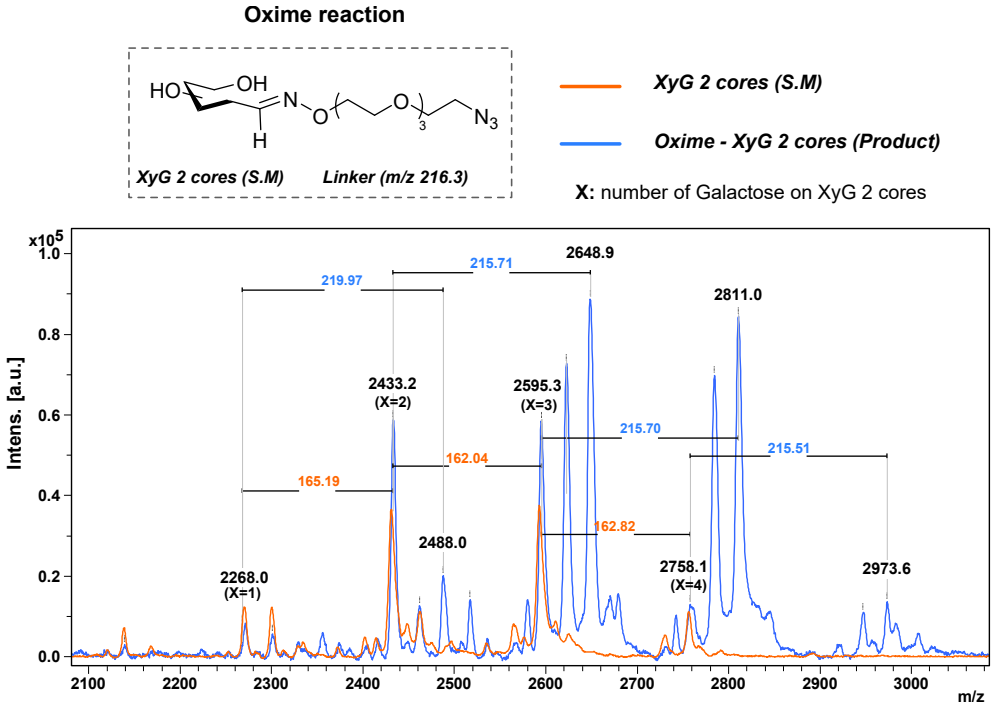

Figure 3.21: MALDI-Tof MS analysis for the oxime reaction involving the XyG 2 cores (X from 1 to 4 galactoses). The orange line represents the XyG 2 cores starting material. The blue line represents the XyG 2 cores oxime product after 48 hours.

The blue line displays the MALDI-Tof MS analysis for the oximation reaction overlapped with the starting material. The oxime products were located at the m/z 2488.0 (X=1), 2648.9 (X=2) and 2811.0 (X=3) and 2973.6 (X=4) as the major components in the reaction mixture. They were found in the MS spectrum as the linker difference (m/z around theoretical value 216.3) between the starting material and the final product. We observed however, the presence of the starting material meaning that the reaction was not fully completed. Nevertheless, we could conclude that the oxime reaction was successfully obtained as the main reaction product and it will be used without further purification.

The oxime substrate exhibits two steroisomers Z and E due to the presence of a double bond as it is depicted in the Figure 3.22. This unsaturated structure can be easily localized by ^{1}H-NMR because of the ring-chain tautomeric form within the α and β pyranose. Those protons are distinctive as doublets around 7 ppm as it is shown in the Figure 3.23.

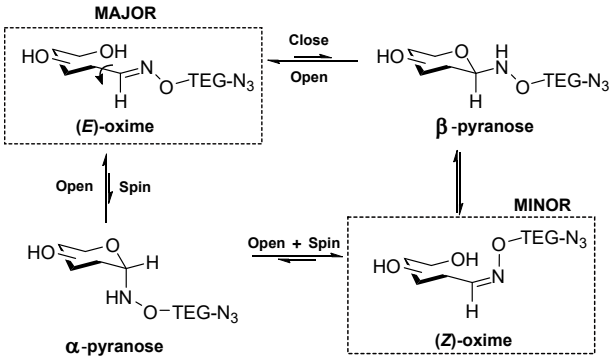

Figure 3.22: Model of the ring-chain mutarotation for the different tautomers and steroisomers of pyranose structure within the oximation reaction products.

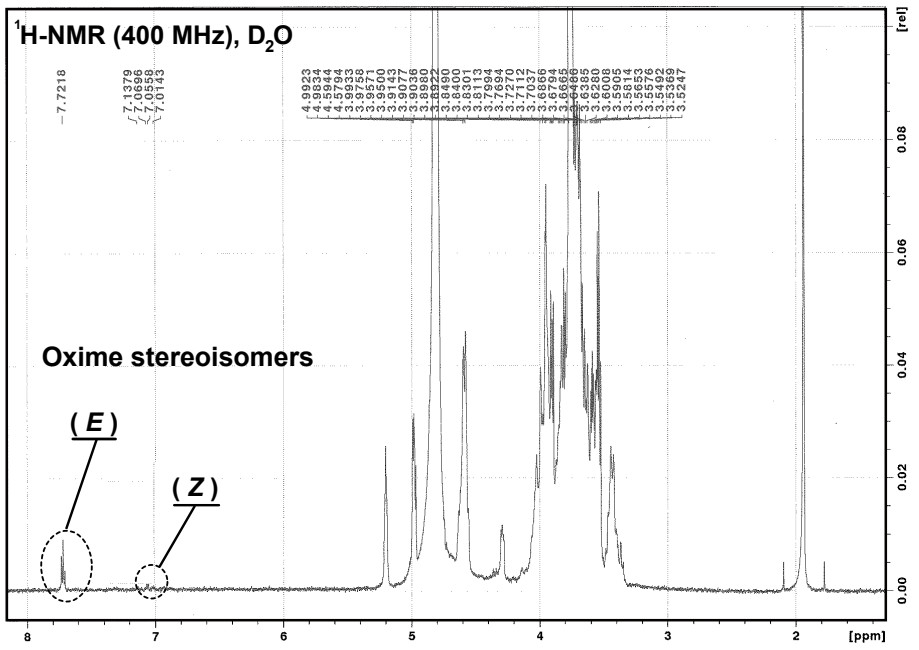

Figure 3.23: ^{1}H-NMR 400 MHz of the XG 2 cores oxime product showing the *Z* and *E* stereoisomers in D_2O.

These results obtained by ^{1}H-NMR along with the MALDI-Tof MS analysis brought to an end the successfully formation of the oxime ligation products. These data allowed to detect the the m/z value and the oxime double-bond formation, which the *E*-oxime substrate is the most abundant steroisomer product.

Copper-free Click chemistry

Our synthetic strategy encompassed the copper-free click reaction between the set of XyG:linker complexes previously functionalized, and the DBCO-based cODN-1 scaffolds according to the Scheme 3.3. The XyG building-blocks with a number of cores from 1 to 3, were conjugated with the cODN-1 using the complementary A sequence (cA). Likewise, the XyG building-blocks with 3 to 6 cores were functionalized with the cODN-1 using the complementary B sequence (cB).

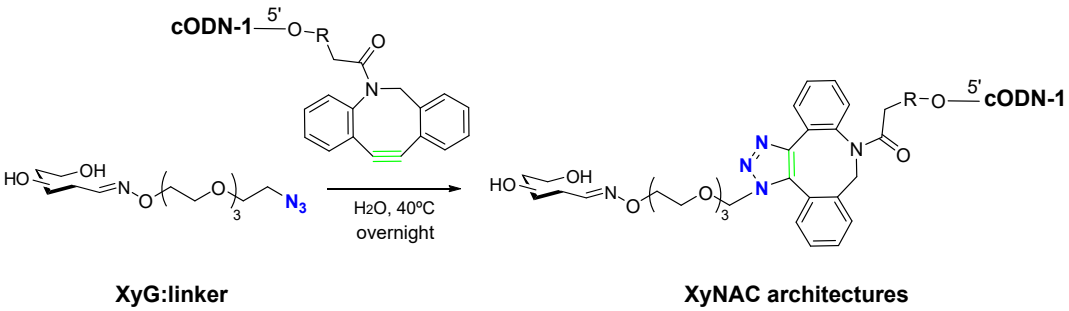

Scheme 3.3: Synthesis of XyNAC architectures *via* SPAAC reaction under aqueous solution at 40^{o}C overnight.

This reaction comes to an end with the formation of covalent 1,2,3-triazole cycle that is quite stable in solution, fixing the entire structure in a robust and well-defined XyNAC architecture.

In the Figure 3.25, we summarized an example of reverse phase HPLC purification and UV detection corresponding to the XyNAC architecture from several XyG core-sizes.

The example of RP HPLC purification of the XyNAC architectures (4-6 cores) taken from the reaction crude (Figure 3.25-c) revealed a single intense peak of absorbance at 260 nm with a retention time around 30 minutes. This large signal came along with several peaks lower in intensity at 35 minutes and a single peak at 28 minutes. They may be related to the secondary cycloaddition reaction between the free-linker molecule and DBCO-cODN starting material. Here, we observed a gradual separation of the XyNAC architectures according to their size. Thus, larger oligosaccharides bearing more hydroxyl groups were eluted from the column with shorter retention times.

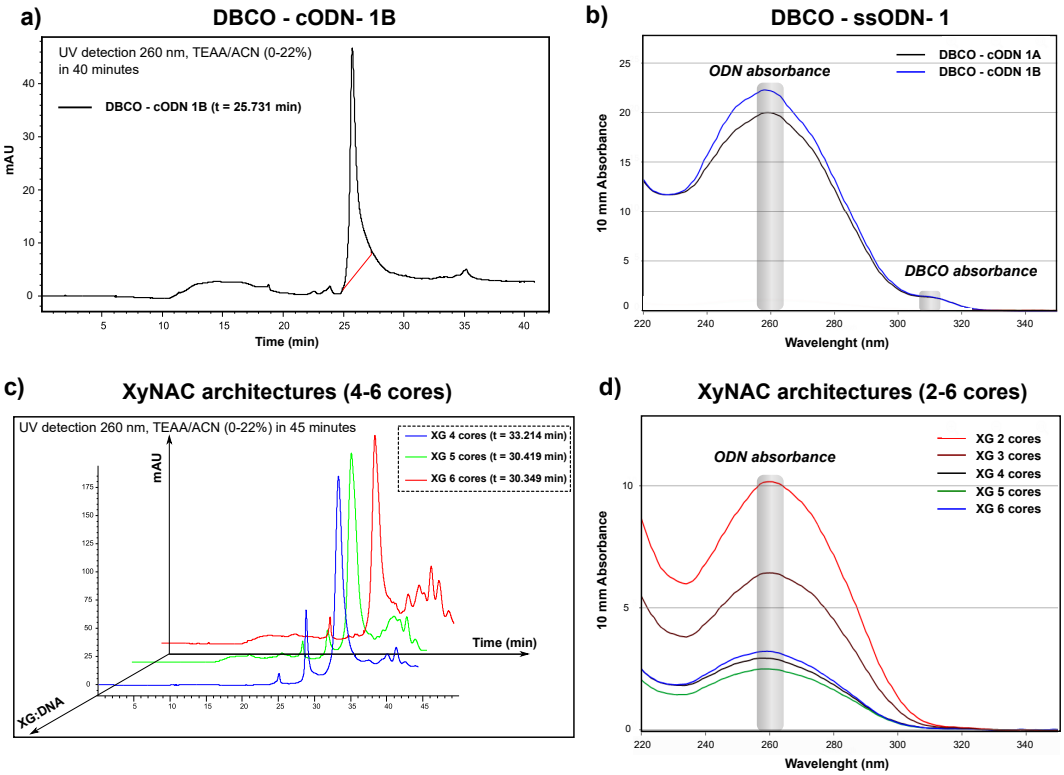

Figure 3.25: RP HPLC purification and UV detection of XyNAC architectures from several core-sizes a) RP HPLC of the starting material DBCO-cODN-1 (cB) monitored at 260 nm with a gradient TEAA/ACN (0-22%) in 40 minutes. b) UV-visible absorbance of the starting materials DBCO-cODN-1 (cA and cB) showing at 260 nm (ODN absorbance) and 310 nm (DBCO absorbance) a fingerprint for the SPAAC reaction detection. c) RP HPLC purification of the set of XyNAC architectures (4-6 cores) monitored at 260 nm with a gradient TEAA/ACN (0-22%) in 45 minutes. d) UV-visible absorbance of the XyNAC products (2-6 cores) showing the absence of the DBCO signal at 310 nm.

In this line of analysis, we noticed that these three peaks exhibited broader peaks in comparison with those of the starting material shown in the Figure 3.25-a. The reason is that the nature of each XyG polysaccharides exhibits different number of galactose molecules per core. The absence of the signal from the starting material within the final chromatogram suggests a fully completed reaction. On the other hand, the absence of the DBCO absorbance at 310 nm (Figure 3.25-d) compared to the UV detection of the DBCO-cODN starting material (Figure 3.25-b) suggests that the SPAAC reaction took place. Finally, a quantitative analysis was performed by the UV-visible measurements. On average, these UV-visible results displayed a total yield for every compound of around 60%.

Then, a qualitative identification of three XyNAC architectures (from 4 to 6 cores) were carried out through *Liquid Chromatography-ElectroSpray Ionization-Mass Spectrometry* (LC-ESI-MS) as shown in the Figure 3.26. The spectra reveal a graphical display of the relative abundance of the final products obtained after RP HPLC purification step. Here, each peak is defined based on its relative abundance. Red peaks refer to the most abundant compound (labelled as A), then the green and purple ones (B and C), and finally the less abundant ones hold the yellow-brownish colour (D). Finally, the chemical composition of each XyNAC analysed substrate is detailed by referring the number of sugar molecule forming the final product. All mass analysis are collected in the ANNEXE Chapter 5.

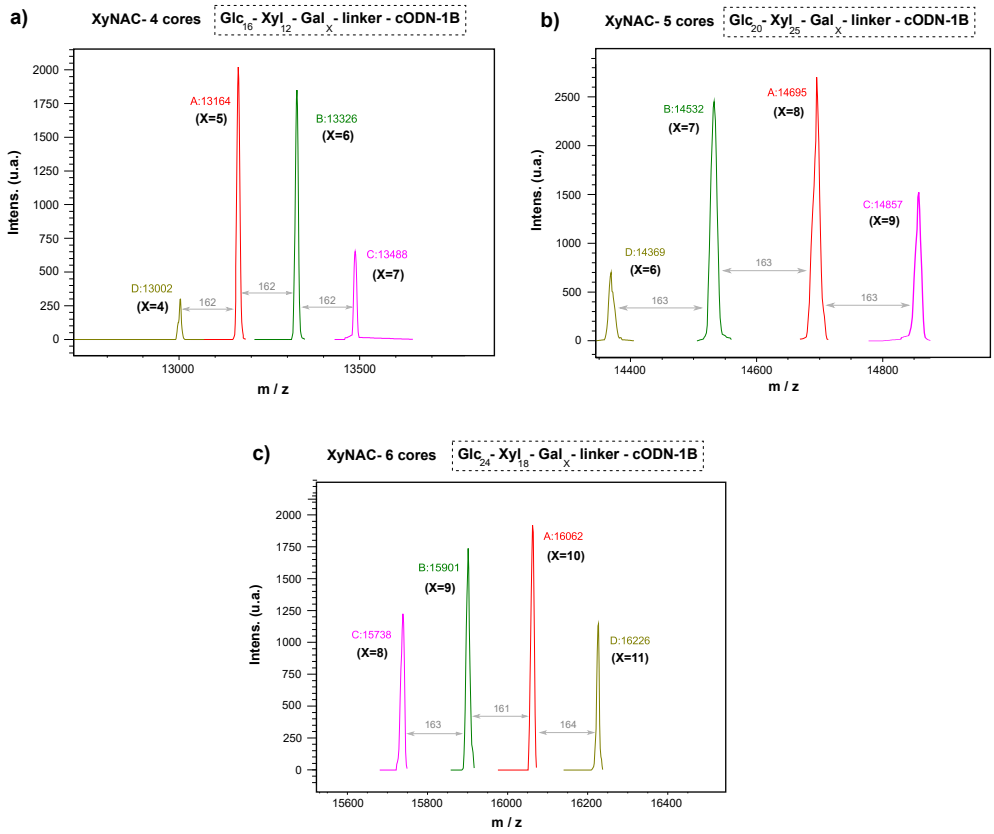

Figure 3.26: LC-ESI-MS de-convoluted spectra of the RP HPLC purification samples described in the Figure 3.25. a) LC-ESI-MS chromatogram of the XyG 4 cores functionalized *via* SPAAC.b) LC-ESI-MS spectrum of the XyG 5 cores functionalized *via* SPAAC. c) LC-ESI-MS spectrum of the XyG 6 cores functionalized *via* SPAAC.

Regarding the mass analysis, four predominant peaks are observed for each XyNAC substrate which correspond to the main core (glucose and xylose) plus a variable number of galactose molecules (X). A comparative analysis with theoretical values helps to the assignment of the number of galactose distributed within the core-size. The theoretical and measured mass values from the XyNAC products shown in the Figure 3.26 are detailed in the Table 3.1. This is also confirmed by the mass difference of 162 units between the peaks.

XyNAC products		
Substrate	Theoretical mass	Measure mass
N=4		
X=4	13000	13002
X=5	13162	13164
X=6	13324	13325
X=7	13486	13488
N=5		
X=6	14368	14369
X=7	14530	14532
X=8	14692	14695
X=9	14854	14857
N=6		
X=8	15737	15738
X=9	15899	15901
X=10	16061	16062
X=11	16223	16226

Table 3.1: ESI-MS assignment found for XyNAC reaction products. The N describes the number of monomeric units (cores) and the X defines the number of galactose molecules within each particular N structure

Overall, we came in to conclusion that the final detection, purification and quantification of the reaction sequence yield a pure DNA architectures at micromolar scale bearing a set of XG cores with different number of galactose molecules.

3.5 Preparation of PyNAC architectures

Moving towards the other part of the synthesis, we address the preparation of the PyNAC architecture that will enable the hybridization and consequent anchoring of

XyNAC probes on the biosensor surface. To make it possible, the SyMMES/CREAB laboratory have designed a clever patterning strategy to immobilize different probes on metallic surfaces, usually gold. The goal of our research team lies in the use of pyrrole molecules to create a uniform films by applying a potential difference that trigger a pyrrole polymerization process on the gold surface.[133] In the Figure 3.27, we detail the chemical structure of the PyNAC architecture to be synthesised.

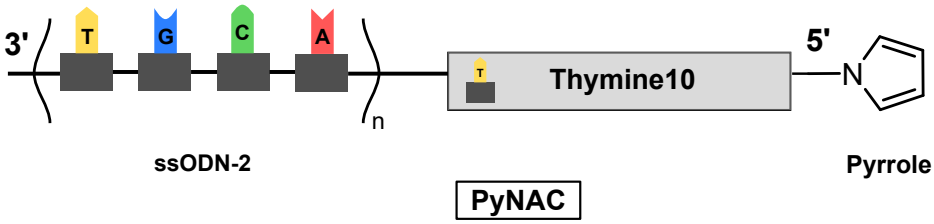

Figure 3.27: Model of the PyNAC architecture composed by a ssODN-2 sequence bearing a pyrrole group at the 5'-end separated by a thymine sequence (T10).

3.5.1 Synthesis of PyNAC *via* NHS-amide coupling

Within our synthetic strategy of preparing PyNAC, an activated pyrrole compound was required to functionalize the ssODN-2. In this context, we explored the chemical coupling of the 5'-amino ssODN structure to the pyrrole moiety through the *N*-hydroxysuccinimide (NHS) activated group. This classical organic compound has been commonly employed to promote the formation of esters or amides (NHS-ester coupling) from activated carboxylic acids. Typically, this type of chemistry on carbonyl groups shows an increase in the reactivity over the Csp_2 towards nucleophilic substitution by S_N2 mechanism.

Therefore, the pyrrole-NHS compound was synthesized by our research group through the Steglich esterification reaction. Then, this substrate is mixed in large excess with the 5'-amino ssODN under aqueous basic conditions (pH 9.3) of potasium carbonate buffer at room temperature overnight as shown in the Scheme 3.4.

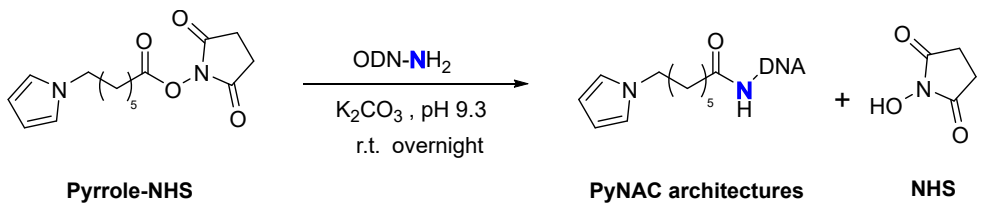

Scheme 3.4: Synthesis of PyNAC using NHS-ester activation *via* nucleophilic substitution by S_N2 mechanism

The NHS-amide coupling procedure begins with the nucleophilic attack by the free electron pairs of amine group over the Csp_2 of the activated ester (better electrophile) as depicted in the Scheme 3.5. This substitution step goes from the initial trigonal starting material towards a trigonal product, through the formation of an unstable tetrahedral intermediate. The latter was easily expelled as negatively charged leaving group.

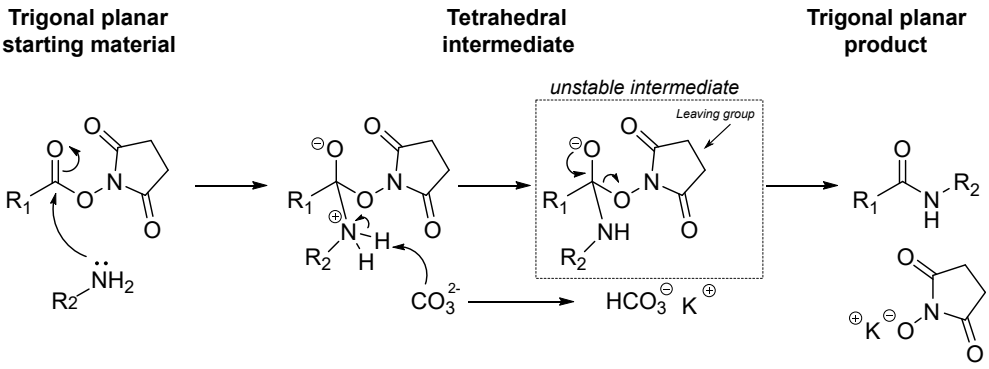

Scheme 3.5: Model of the short reaction mechanism *via* NHS-activating group (leaving group) through a unstable tetrahedral intermediate.

After the addition of the amine starting material, the tetrahedral intermediate was mediated by the base of the medium (in our case the carbonate ion) that removes the proton to give an unstable intermediate. Then, this intermediate undergoes by an elimination step losing the NHS negatively charged as a potassium salts.

At this pH condition, the amine group remained deprotonated, enabling the attack of the free electron pairs over the activated ester. However, the capability of the NHS group makes this type of coupling highly sensitive to the hydrolysis under basic conditions at pH above 10 to form the carboxylic anion salts.

Similarly to the XyNAC, the PyNAC architectures were purified and characterized by RP HPLC C18 column and MALDI-Tof MS analysis as it is shown in the Figure 3.28.

The RP HPLC of the crude reaction mixture from the PyNAC labelling molecule is depicted in the Figure 3.28-a. The results displayed three peaks that at first sight we could easily identified. The first peak was attributed to the DMSO compound present in the pyrrole-NHS starting material (Figure 3.28-a). Then, the second peak at 25.380 minutes was assigned to the non-reactive amine-ssODN-2 remained in the reaction mixture. And lastly, the peak 3 was attributed to the PyNAC compound with a retention time of 33.726 minutes. This third peak was isolated and characterized by MALDI-Tof MS in negative mode with HPA matrix (Figure 3.28-b). The mass analysis revealed the coupling product PyNAC architecture (calc.[M+Na] 10833.1) found in a single peak of 10832.6 corresponding to the M+Na compound.

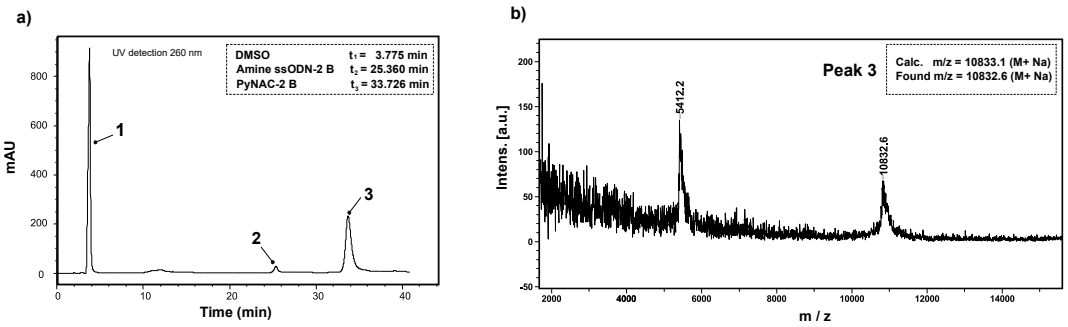

Figure 3.28: RP HPLC analysis and MALDI-Tof MS characterization for the construction of the PyNAC architecture. a) RP HPLC C18 in TEAA 10 mM/ACN (0-18%) at 1mL/min in 40 minutes. b) MALDI-Tof MS analysis with HPA matrix in negative mode.

The PyNAC compounds were finally quantified *via* UV detection at 260 nm to afford an 80% of the total yield at micromolar range.

3.6 Quality Control of DNA-based Architectures

In this section, we conclude the evaluation of XyNAC and PyNAC hybrid architectures by developing two classical methodologies in the ODN biochemistry field: the DNA electrophoresis gel and the melting temperature. These techniques entail a nice complement to our understanding of the ODN glycoconjugates in terms of quality control and duplex stability.

3.6.1 DNA Electrophoresis Gel of single-strand ODN conjugates

DNA biomolecules offer a versatile architecture to track and detect conjugates focused on the oligonucleotide fragment by UV absorbance. Similarly to proteins, this polyanionic biomolecules can be separated and analysed by electrophoresis gel even if some external molecules are attached onto it. The application of an electric field enables the migration of the ODN structures through a gel matrix according to their size.

In our case, we developed a DNA electrophoresis gel as a valuable methodology to visualize the quality of both XyNAC and PyNAC architectures using fluorescence detection. A first DNA electrophoresis assay was addressed using ssODN sequences (10 pmoles) both commercial and synthesised treated under denature conditions. A mixture of bromophenol blue (BPB) / Xylene cyanol (XC) was used as a marker control.

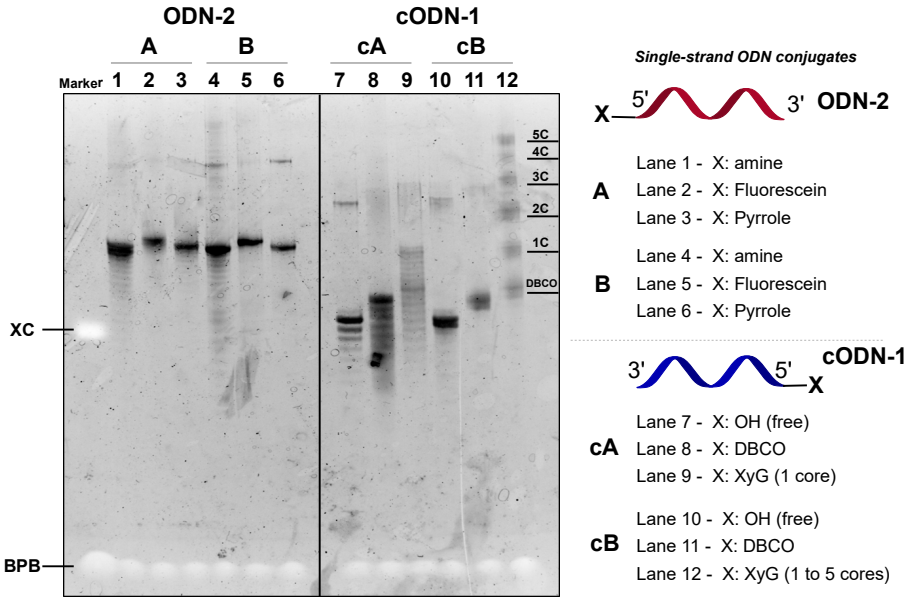

Figure 3.29: DNA electrophoresis gel of the single-strand DNA probes. Both DNA-II sequences (A and B) and complementary DNA-I sequences (cA and cB) were evaluated. The X represents the functional group coupled at the 5' end of each oligonucleotide. The gel was prepared in polyacrylamide gel at 20% and revealed with SYBR-Gold incubation for UV detection.

Based on the Figure 3.29, ODN-2 architectures were injected on the left side of the gel and cODN-1 on the right side of the gel. The X described the functional groups coupled at the 5'-end of each oligonucleotide structure.

Regarding ODN-2 (A and B sequences, lanes 1 to 8), the oligonucleotides showed relatively pure sequences with a unique and major band presence. A subtle bands were revealed in lanes 1 and 4 commercial aminated oligomers below the main band which correspond to the nucleotide bases (n-1 base) from the synthetic process of production. Lanes 2 and 3 (A sequence) and the lanes 5 and 6 (B sequences) represent synthetic products purified by RP HPLC and therefore, they were perfectly defined as a single band as well.

Within the other part of the gel, the cODN-1 (cA and cB sequences, lanes 7 to 12) showed differences between sequences cA (lanes 7 to 9) and cB (lanes 10 to 12). We noticed that both starting materials (X: OH and DBCO) from the sequence cA exhibited bands of impurities of n-1 ODN sequences from the commercial synthetic process. Therefore, it explained the delicate presence of XyG core 1 in lane 9 with the sequence cA. However, the same starting materials from the sequence cB showed an intense pure band in both lane 10 and 11 yielding a clear ladder of XyNAC architectures (1 to 5 cores) in lane 12.

We extended our DNA electrophoresis gel analysis of the XyNAC probes using different sizes of XyG polysaccharide. Thus, the Figure 3.30 illustrates the XyNAC (cB sequences) along with their corresponding starting materials.

The cODN-1 structure with the sequence cB and bearing different moieties (X) was evaluated within a single electrophoresis gel. The gel analysis (Figure 3.30) revealed a clean migration for all the samples injected with a sequential distribution of XyG probes by molecular size from 3 cores to 6 cores respectively (lanes 3 to 7, XyG reference in lane L). Furthermore, the XyG-DNA conjugates with 3, 4 and 5 cores (lanes 3 to 6) as well as the XyG ladder showed a particular band at low molecular weight. The identification of these bands might suggest some impurities from the copper-free cycloaddition (SPAAC) or partially hydrolization of the oxime ligation.

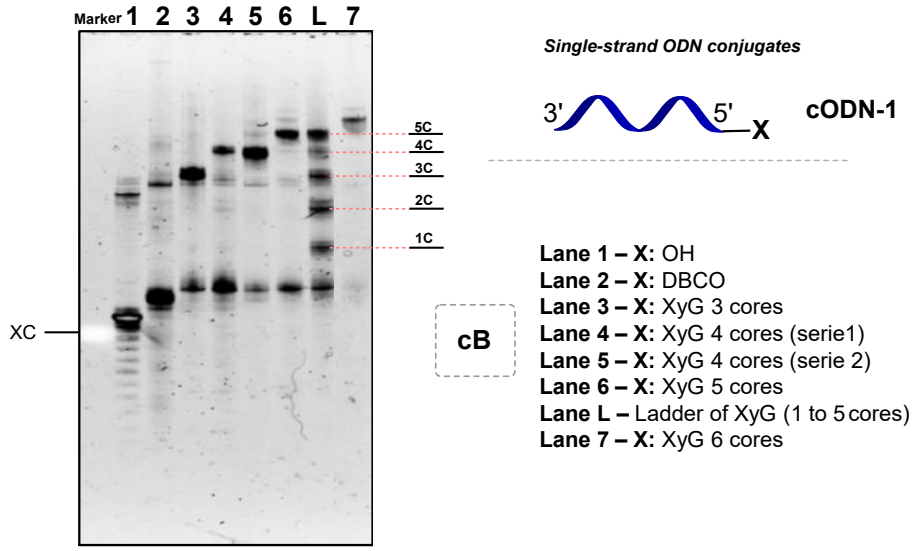

Figure 3.30: DNA electrophoresis gel of single-strand XyNAC with the sequence cB. The X represents the functional group coupled at the 5' end of each complementary oligonucleotide (cB). The gel was prepared in polyacrylamide gel at 20% and revealed with SYBR-Gold incubation for UV detection.

3.6.2 Melting Temperature Determination of the duplex XyNAC/PyNAC

The word "DNA" has always been related to the perfect double-strand association of an oligonucleotide pair molecule. This selective match between DNA strands is known as DNA hybridization or Watson-Crick interaction and it is reversible with the temperature. However, the nature of the nucleic acid components to hybridize can determine the strength or weakness of the DNA duplex. Thus, guanosine-cytosine purine pairs (3 hydrogen bonds) contributes to much higher stabilization than adenosine-thymine pyrimidine pairs (2 hydrogen bonds) (Figure 3.10-Watson-Crick hybridization).

This parameter is determined by the melting temperature (T_m) and it refers to the temperature at which half of the DNA has been denature from the duplex DNA (dsDNA) to ssDNA. The temperature effect induces the transition between two states with different physical properties: dsDNA structures (low absorbance) and ssDNA structures (higher absorbance). Therefore, the T_m can be obtained by monitoring the UV absorbance at 260 nm while the temperature of the sample solution increases (Figure 3.31). At specific temperature, the slope of the curve is maximum (point of inflexion), and the 50% of the dsDNA is transformed into two ssDNA. Is

in this point where the first derivative δAbs/δT provides the critical parameter of DNA melting temperature. Typically, this process is called DNA annealing and it is repeated in multiples cycles of temperatures to obtain a mean value.

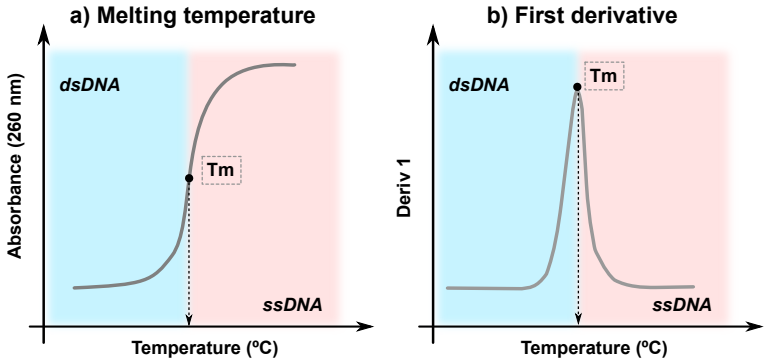

Figure 3.31: Model of a melting temperature and first derivative curves for a duplex DNA. a) Melting temperature curve. The T_m is defined at the inflexion point (maximum slope) of the Absorbance (260 nm) temperature curve where half of the dsDNA is separated into ssDNA. b) First derivative curve. The T_m is obtained by plotting the first derivative at the maximum of the curve.

The T_m parameter is unique for each oligonucleotide pairing and it mainly depends on the nucleotide composition, the length of the DNA and external conditions such as concentration, ionic strength or metal ions. However, within the evaluation of DNA melting temperature with conjugates, the residue attached to the DNA scaffold might interfere in the stabilization or disruption during the annealing process.

In our case, the XyG molecule represents a large branched oligosaccharide that can easily alter negatively to the hybridization process, mainly by steric hindrance. Thus, for this study, we evaluated the DNA melting temperature of two XyNAC architectures with different sizes of XyG molecule (3 and 4 cores) to verify the sugar effect over the DNA hybridization. On the other hand, the amine-based ODN-1 was selected as hybridized molecule. Furthermore, the T_m value for the starting materials cODN-1 (OH / DBCO) was obtained in parallel as a reference values. Additionally, a theoretical value was predicted by the OligoEvaluator from Sigma Aldrich which considered the ODN sequence, the percentage of CG and the length. The DNA melting curves were depicted in the Figure 3.32 and T_m values were described in the Table 3.2.

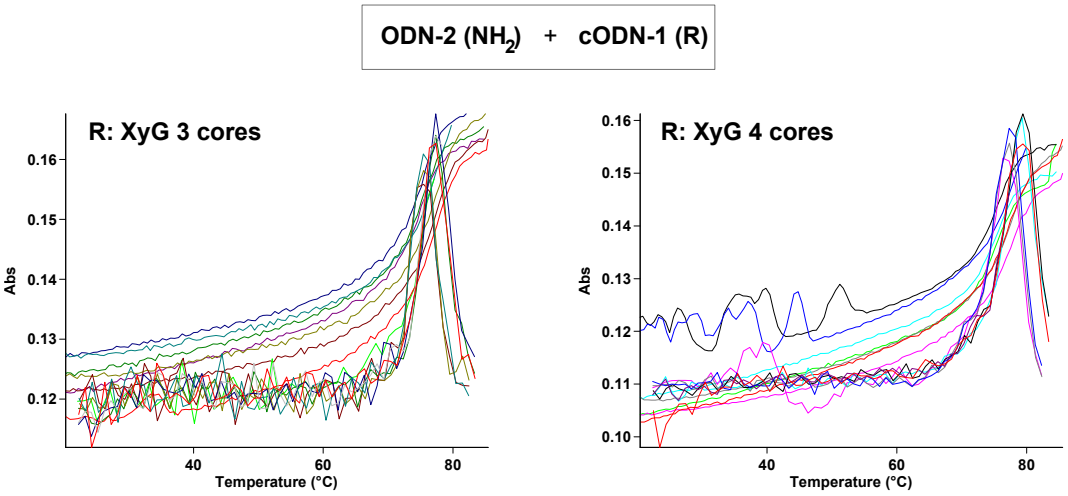

Figure 3.32: Melting temperature and first derivative curves for the XyGNAC 3 and 4 cores. The T_m values were obtained in 4 cycles (increase/decrease) within a range of temperatures from 20 ^{o}C to 80 ^{o}C (1^{o}C/min). First derivative was calculated from the XyNAC melting temperature curve.

Sample	Tm (°C)
Theoretical (B sequence)	78.0
ODN-2/cODN-1 (OH)	76.1
ODN-2/cODN-1 (DBCO)	78.0
ODN-2/cODN-1 (XyG 3 cores)	76.1
ODN-2/cODN-1 (XyG 4 cores)	76.5

Table 3.2: Comparative DNA melting temperatures obtained for the duplex ODN-2/cODN-1 and theoretical from OligoEvaluator (Sigma Aldrich).

Based on the Figure 3.32, both XyNAC structures exhibited DNA melting temperature curves fairly similar. At first sight, both species described a T_m in the range of 75-80°C upon the first derivative curves. The data from the Table 3.2 confirmed very subtle variations in T_m values for both XyNAC substrates (0.0 °C, 3 cores and 0.5 °C, 4 cores) compared to the cODN scaffold without functional group (OH). Therefore, the nature of the XyG fragment did not contribute to destabilize the hybridization process.

On the other hand, the cODN-1 (DBCO) revealed a variation of temperature two points higher in comparison to the rest of the molecules (78.0 °C). However, this difference of temperature was relatively small and it was comparable to the theoretical value (78.0). Therefore, we might not conclude that the DBCO group contributed positively to the stabilization of the duplex form.

Regarding the evidence from this study, the findings concluded that the XyG residue represents a inert molecule for the hybridization event.

3.7 Conclusion

In this chapter we aimed at the construction of two pairing ODN-based conjugates as a versatile and useful architectures for detection, purification, characterization and further immobilization. These two ODN biomolecules were chemically modified in order to obtain both xyloglucan (XyNAC) and pyrrole (PyNAC) conjugates motivated to address the surface immobilization of oligosaccharides for protein binding detection.

Considering the XyNAC architecture, we focused on the development of COCs in solution. The XyNAC hybrid compound was composed by a set of xyloglucan polysaccharide building-blocks, a specific linker and the oligonucleotide scaffold.

The Tamarin xyloglucan polysaccharide was successfully digested and purified by SEC to obtain a range of smaller XyG core sizes. Then, the XyG:ODN conjugation was carried out using an heterobifunctional linker containing both an aminooxy and an azide groups within a triethylenglycol backbone. We chose these particular functional groups to face two stepwise chemoselective synthetic processes that reduce the number of synthetic steps and attain better yields. Therefore, we developed first the oximation ligation between the free aminooxy group from the linker and the masked aldehyde group (open-form) in the anomeric position from the non-protected XyG. This reaction was catalysed by aniline under mild condition of sodium acetate buffer (pH 4.3), purified by SEC and characterized by MALDI-Tof MS analysis. Additionally, a ^{1}H-NMR assay was performed to localize the specific *Z/E*-estereoisomers from the oxime ligation product. Finally, the free azide group from the XyG-linker intermediate was linked to a DBCO-modified ODN structure (commercially availabel) under aqueous conditions to yield the final XyNAC *via* SPAAC reaction. This final product was successfully purified, characterized and quantified by RP HPLC, LC-ESI-MS and UV detection (260 nm and 310 nm) respectively, for further analysis.

Likewise, the PyNAC architecture was composed by an ODN scaffold conjugated with a pyrrole moiety. To prepare this architecture, we developed a classical synthetic strategy to functionalize an amine-based ODN scaffold (commercially available) with a pyrrole moiety through an activated pyrrole-NHS previously synthesized in our laboratory. The PyNAC product was successfully purified and quantified by RP HPLC and UV detection respectively, for further analysis.

Lastly, both XyNAC and PyNAC architectures were explored by classical biochemical methods of DNA analysis: the DNA electrophoresis and DNA melting temperature. These techniques were used to evaluate the target ODN conjugates as a quality control prior use for further assays.

Regarding the DNA electrophoresis gel, a polyacrylamide gel was used to address the migration of both ODN architectures. Thus, we provided a migration panel of ODN starting materials and ODN products to visualize the quality of each sample solution using the ODN scaffold as a labelling biomolecule. This study showed clean DNA gels wherein most of the samples were considerably pure, even though some ODN starting materials appeared to be impure from the beginning. Furthermore, we provided a classical and useful technique to visualize in one gel, a screen of non-modified glycan structures, typically inert molecules, well-distributed by size.

On the hand, the DNA annealing process was addressed by monitoring the melting temperature (T_m). This parameter was analysed in order to evaluate the influence of the xyloglucan fragment containing the ODN conjugates. Thus, the amine-based ODN-2 was used as an hybridized ODN template and T_m values were assessed for XyNAC conjugates (3 and 4 cores) along with ODN starting materials (OH and DBCO). These findings suggested that in general, the xyloglucan compound present in the ODN conjugate (both 3 and 4 cores) did not modified the DNA annealing process with T_m variations around 0.5 to 2 °C.

Overall, we provided a useful chemical strategy to conjugate oligosacccharides with high molecular weight to ODN scaffolds in good yields under aqueous conditions. Furthermore, the versatility of having ODN structures conjugated to glycans will encourage the idea of creating panels of glycoconjugates with huge advantages in detection, purification, characterization, quantification, visualization and also immobilization approaches.

4 Towards a Xyloglucan-based Glycochip Array for deciphering Protein-Xyloglucan interactions using SPRi

In this chapter, we will address the conception of Xyloglucan glycochip based on XyNAC and PyNAC architectures to decipher protein-XyG interactions. The elaboration of this glycochip will be envisioned by DNA hybridization via DDI approach. This process will be achieved in solution by DNA-electrophoresis gel and on chip by SPRi technique. Then, the XyG-based glycochip will be validated using LM24 antibody to prove the accessibility, orientation and integrity of XyG probes by SPRi. Finally, the glycochip will be tackled in a preliminary assay towards the XyG binding recognition upon the AtFUT1 enzyme, prior enzymatic activity test by MALDI-ToF MS analysis.

Contents

4.1 Scientific context

Identifying protein-carbohydrate interactions is a crucial stage to rationalize the mechanism of many biochemical events and to decipher the information encoded within the carbohydrate complexes (glycocode). The development of versatile biosensors has become an emerging field to investigate biomolecular interactions within the glycoscience domain.[134]

In this chapter, we revisit the concept of biosensing techniques committed to the bio-recognition of glycan structures to decipher biochemical interactions using surface plasmon resonance (SPR). In the Figure 4.1 below, we translate the different elements from the general biosensor technique into a glycan biosensing model adapted to SPR detection.

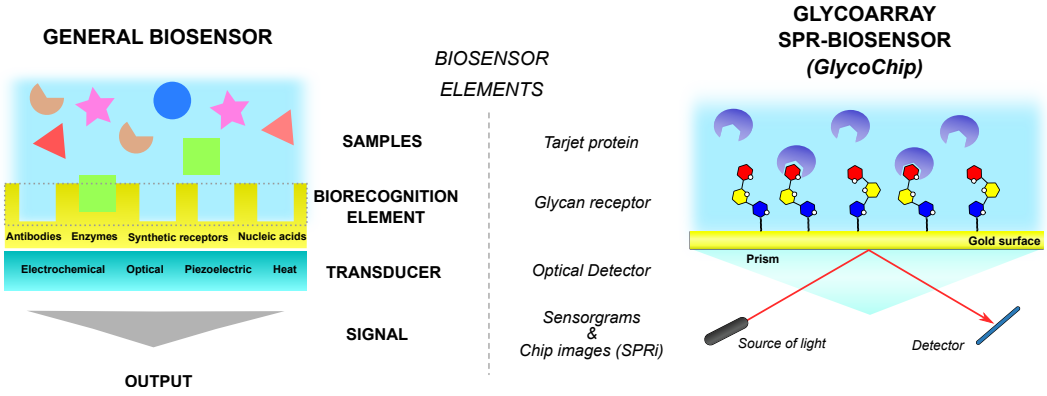

Figure 4.1: Transformation from a general biosensor to a model of glycoarray biosensor compatible for SPR or SPRi detection methods. The biosensor elements are derived as follows: the generic samples are particularise to tarjet proteins; the biorecognition elements are specifically immobilised glycan receptors; the solid support is a gold-based layer adapted to the transducer by optical detection; and the final signal is transformed in a measurable sensorgram.

The model of glycochip particularises the template of a general biosensor into specific elements for the glycan detection by SPR. The sample analytes are generally glycan-binding proteins that interact with glycans bioreceptors immobilised on a solid support (gold-based for SPR). Overall interactions are transduced in an optical response to provide an output signal in the form of sensorgrams and chip images on SPRi in particular.

In this scientific context, we will briefly introduce the glycoarray technology and its implication in glycoscience. We will also explore the different chemical methods linked to the glycans immobilization strategies on solid support (Domain of

Biorecognition elements). Then, we will describe some of the most common techniques used to detect binding interactions on solid support, classified in labelling and label-free detection methods (Domain of transducer). We will emphasise the detection approach towards the SPRi methodology. Finally, we will address complementary techniques in solution that have been deployed in this chapter as a supporting techniques for experimental validation.

4.1.1 Introduction of the Glycoarray Methodology

Glycoarray technology emerged as a one of the major breakthrough for glycoscience research since 2002 with the advent in the glycomics demand.[28,135–137] This powerful tool aims at displaying defined glycan architectures on a solid support to decode the biological mechanisms while interacting with other biomolecules including proteins, antibodies or more complex organisms such as bacteria and viruses. (Figure 4.2).[32]

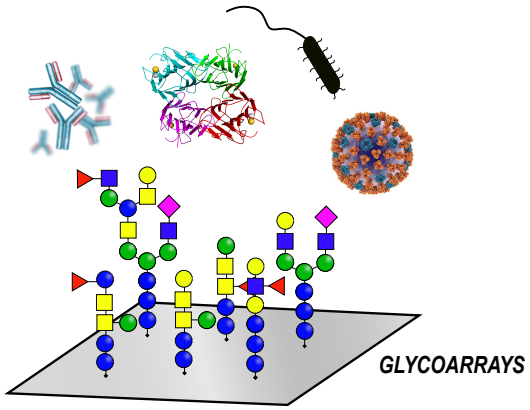

Figure 4.2: Principle of glycan array displaying multiple glycans probes on a single surface. The versatility of this technique opens the scope towards various applications such as screening proteins and antibodies or microorganisms like bacteria and virus particles. A general example of glycan structures is depicted. Adapted from Puvirajesinghe *et al.* 32

For glycoscience, the glycoarray platform achieves the simultaneous exploration of protein interactions with a set of glycosyltated structures. Furthermore, this technique allows the detection of binding interactions using small amounts of samples (glycans and proteins) in the range of pmoles.[138] Finally, displaying multiple glycan structures on the same support facilitates a fast screening method in parallel within a single analytical experiment.[32]

Glycoarray platforms have become a convincing tool in glycobiology to create libraries of glycans and to explore the biochemical recognition and synthesis through glycoenzymatic interactions.[139] This platform also serves as an essential networking between biology, chemistry, biotechnology and medicine with final applications in cell biology, enzyme specificity and kinetics, organic chemistry, sensor studies or plant biochemistry.[33,140,141]

4.1.2 Chemical Methods for Glycan Immobilization. Biorecognition Element

Displaying glycosylated structures on a solid support introduces important approaches for the construction of glycoarrays. In order to address better accessibility and spacial rearrangement of the glycan probes, different strategies of immobilization have been explored. We classify the glycan immobilization on solid surfaces in two categories: direct and indirect immobilization.

Direct Immobilization of Glycans on surfaces

Direct functionalization approaches involve a physico-chemical interaction between the biorecognition element and the solid surface. The initial choice of solid supports has to be addressed based on the type of chemistry to be developed as well as the transducer.[32] Typically, gold-based supports are commonly employed for biomolecular recognition providing a broad compatibility with multiple detection techniques such as MALDI-Tof MS, SPR or Quartz Crystal Microbalance (QCM).[142–144]

- **Electropolymerization of pyrrole**

Among the direct functionalization of surfaces, an immobilization method using polymeric species based on polypyrrole molecules is described.[145] The technique is called electropolymerization of pyrrole and it is typically applied for the physical attachment of binding probes towards biosensing purposes, although applications for cell batteries are also reported.[146] The principle of this technique consists in the direct electrochemically co-polymerisation of pyrrole molecule with the biorecognition molecule containing a pyrrole moiety on its structure (Figure 4.3-a). Some examples of the versatility of this immobilization technique can be found in the literature. We can mention the immobilisation of oligonucleotides to construct DNA biochips,[145,147,148] proteins[149] to assess protein-ligand interactions and carbohydrates for bacteria detection.[150]

Mechanistically, Schweiger *et al.*[151] describes the pyrrole polymerization reaction through the formation of oxidised radical cations after applying a potential difference (Figure 4.3-b). These reactive intermediates rapidly bind together to form

dimeric structures after proton elimination. Successive oxidations increase the size of the polymer to yield an insoluble mesh of pyrrole attached on the gold surface integrating the bioelement of interest.

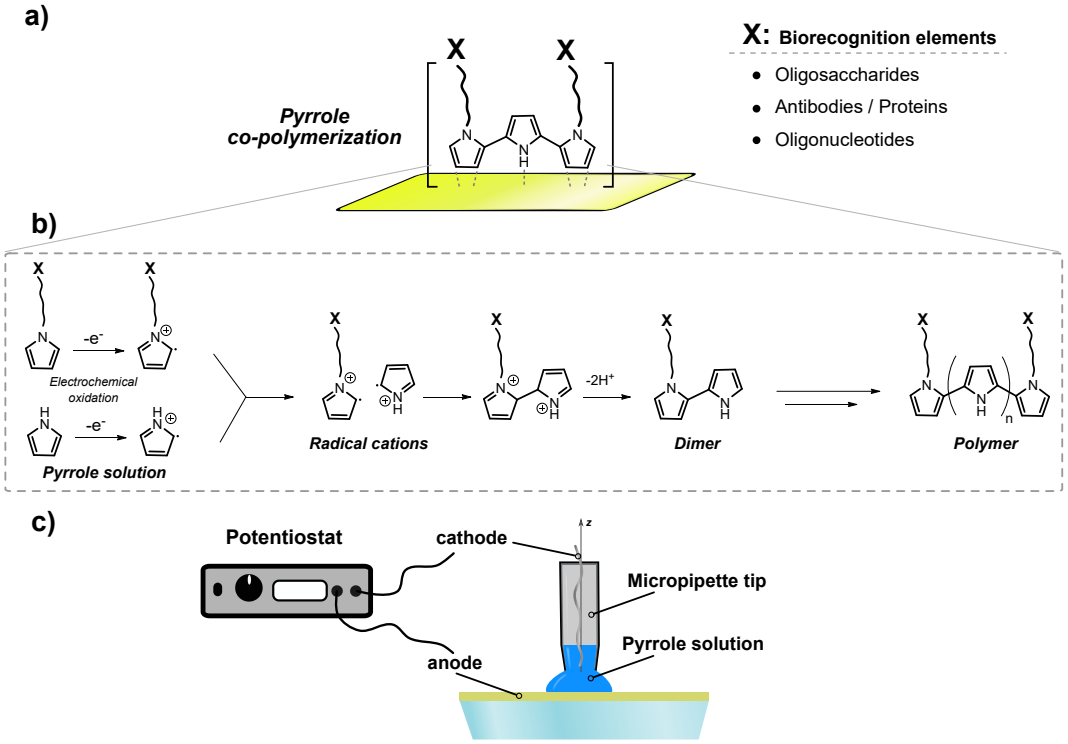

Figure 4.3: Principle for the electropolymerization of pyrrole. a) Pyrrole co-polymerization for the direct surface attachment of bio-recognition elements, X (X:oligosaccharides, antibodies/proteins, oligonucleotides). b) Mechanism of pyrrole electropolymerization by electrochemical oxidation of pyrrole moieties to yield an insoluble polymer (n: even number). c) Example of methodology of electropolymerization compatible for SPRi biosensor.[145]

Precisely on SPRi optical detection technique (Figure 4.3-c), the immobilisation methodology can be addressed by using a two-electrode set up, named electrospotting, developed at CREAB laboratory: one inside a pipette tip containing the pyrrole solution (anode) and the other connected to the metallic surface to be functionalized (cathode). The electric pulse triggers the polymerization reaction in few milliseconds.[149]

Overall, this technique has been shown as an example of a direct functionalization where the pyrrole polymer is directly attached on the material. Furthermore, this

methodology offers the versatility of grafting glycan structures chemo-selectively modified with pyrrole moieties.[152]

- **Self-assembled monolayers, SAMs**

Following the functionalization on gold surfaces, the self-assembled monolayers (SAMs) are one of the most studied systems specially for thiol compounds. SAMs are defined as the spontaneous rearrangement of organic thiolated molecules yielding crystalline and semi-crystalline structures.[153]

Typically on gold surfaces, the thiol groups interact by chemisorption with the metallic surface (Figure 4.4).[154] Gold acts as a weak Lewis acid (electron-pair acceptor) with the lone electron-pair from thiolated compounds (weak Lewis-base) generally substituted by long chains of hybrocarbons or polyethylen glycol. The 2D structures are formed by the spacial crystallization of the lateral chain through intermolecular stabilization interactions such as van der Waals and hydrogen bonds.[155] The combination of the two binding events under specific conditions, is the driving force of the SAMs arrangement.

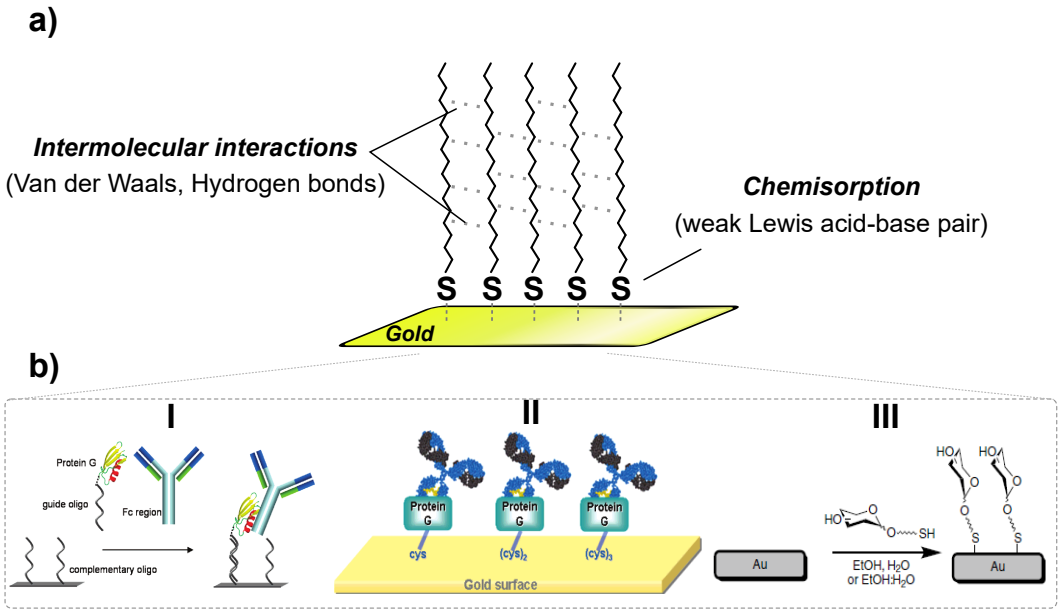

Figure 4.4: Principle of the direct attachment of thiol probes forming SAMs on gold surface. a) Chemical interactions forming the SAMs: intermolecular and Chemisorption. b) Examples of thiol immobilization applied for grafting biomolecules through oligonucleotides (I), cysteines groups (II) and carbohydrates (III).[156–158]

Nevertheless, this direct immobilization can be representative approach for other set of biomolecules containing a thiol groups (Figure 4.4-b). Thus, thiol-modified probes have been used to address arrays platforms for oligonucleotide immobilization[156] (Figure 4.4-b,I), attachment of proteins through cysteine residues genetically introduced[157] (Figure 4.4-b,II) and carbohydrates using thiol linkers (glycan-modify SAMs) at the anomeric position (Figure 4.4-b,III).[158]

- Other strategies for glycan arrays

Although we have covered examples of direct immobilization methods using gold surfaces, it exits other methodologies to construct glycan arrays. In some approaches, the free glycan is passively settled and adsorbed spontaneously on specific surfaces (Figure 4.5). These glycoarrays were developed on supports made of nitrocellulose wherein the glycan structure is immobilised by noncovalent interactions (adsorption) on the surface.[136] However, the effectiveness of the attachment is highly dependant on the contact area with the surface limiting the access of this approach to larger polysaccharides.

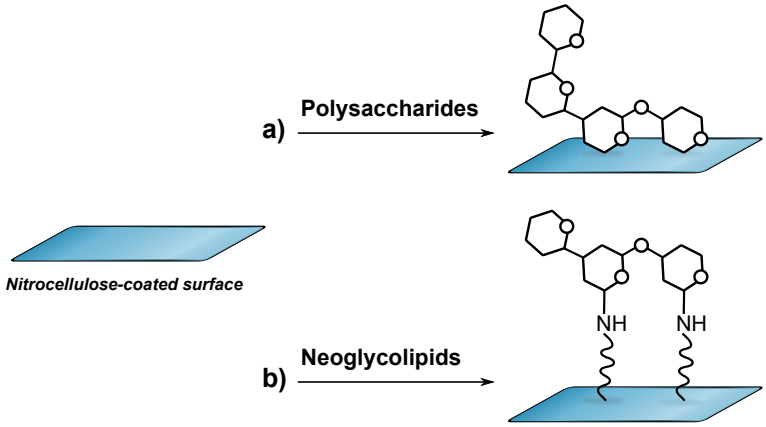

Figure 4.5: Principle of a direct immobilization approach of glycans onto nitrocellulose support. a) Direct attachment of polysaccharides.[136] b) Direct attachment of neoglycolipids.[159] Image inspired from Park *et al.*[33]

Likewise, the immobilization of glycans onto nitrocellulose can also be addressed by neoglycolipids (glycan structures conjugated to lipids).[159,160] The neoglycolip is chemically prepared by reacting the oligosaccharide with an amino-conjugated lipid forming the imine (Shiff base) that is further reduced by reductive amination. The immobilization onto the nitrocellulose platform is produced by hydrophobic ligations (van der Waals) between the lipidic part and the nitrocellulose component (Figure 4.5).

Indirect Immobilization of Glycans on surfaces

Within the indirect functionalization approaches, the immobilization is produced through a complementary pairing groups localized between the biorecognition element and the surface, indicated by an orange dash circle in the Figure 4.6.

In glycoarrays, the immobilization method requires a multi-step process in which both, the surface and the glycan targets are activated by chemical or biochemical complementary groups (X and Y elements). This process is orientated towards the selective coupling interactions to enhance the conjugation process. It exists many different strategies that have been extensively reviewed and published for glycan arrays.[33,161–163] Herein, we tackle the covalent and bioaffinity-based immobilization approaches shown in the Figure 4.6 taken from Song *et al.*[163]

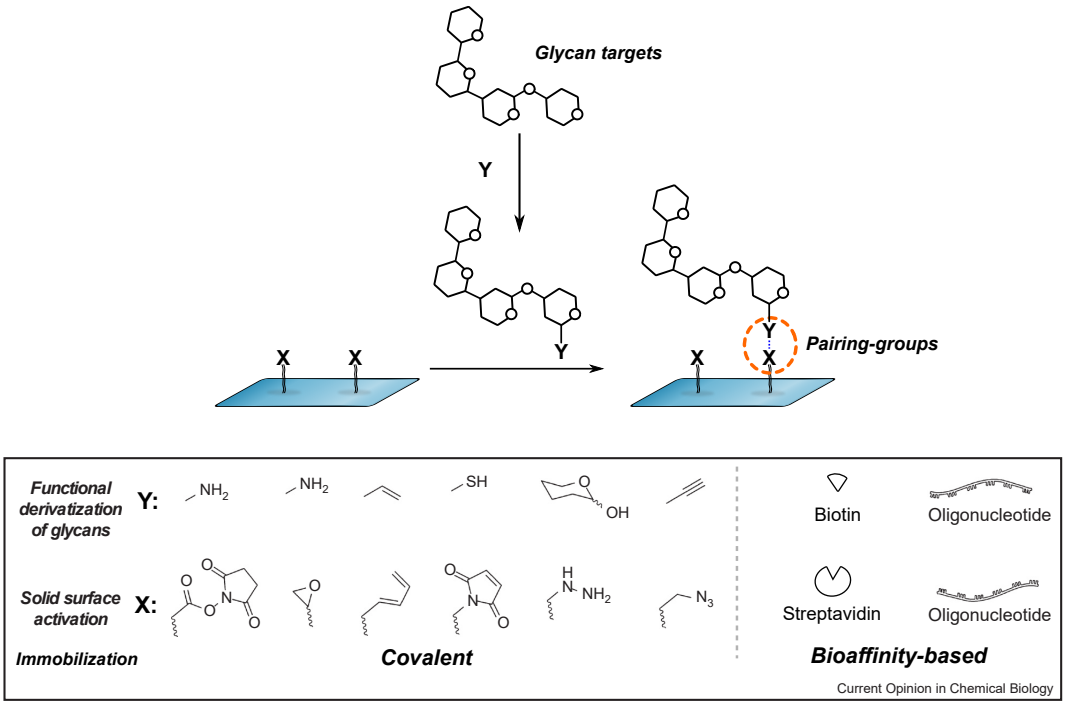

Figure 4.6: Immobilization approaches for glycoarrays. Some chemical pairing-groups (X and Y) are depicted. On the top, the functional groups to derivate the glycan structure are depicted (Y). At the bottom, the activated groups on the surface complementary to the glycan derivative (X). Square taken from Song *et al.*[163]

- **Covalent immobilization**

These types of chemical interactions are mainly based on covalent attachment with functional groups usually employed in organic chemistry (Figure 4.6,Y-X). Typically, the target glycans are chemically modified with functional groups (Y) according to the chemical reaction to be developed on the surface. The pairing-group selection for the surface activation (X) promotes the immobilization of the glycan structure by coupling reactions. We can mention the NHS-activated ester immobilization with relatively robustness and reliability forming an stable amide coupling,[163] the cycloaddition reactions (Diels-Alder and 1,3-azide alkyne cycloadditions) yielding stable cyclic compounds (sometimes an active catalyst is required),[164] and the chemoselective ligation *via* hydrazide among others.

Likewise, the thiol chemistry has been extensively used to immobilize glycans by indirect methodology *via* SAMs formation on gold. The hydrocarbon or polyethylenglycol can be substituted with some chemical groups at the end to enhance the reactivity out of the monolayer. In 2002, Houseman & Mrksich developed a glycan immobilization approach promoted by Diels-Alder reaction *via* SAMs structures.[28] By displaying SAMs containing a benzophenone group, the glycan probes were prepared with a cyclopentadiene moiety to yield the Diels-Alder reaction products on gold surface.

- **Bioaffinity-based immobilization**

This approach consists on the use of pairing biomolecules with site-specific affinity to immobilize glycans on solid support (Figure 4.6). Some examples of this strategy include the strong interaction biotin-streptavidin and DNA/DNA hybridization. Typically, one of the pair biomolecule is coating the surface (streptavidin, single-strand DNA) and the other pair compound (biotin, complementary DNA) is conjugated to a glycan structure.[165–167] This interaction is covalent and highly specific being therefore, harder to recover the final product from the surface.

DNA hybridization is envisioned in this project as a potential approach for glycan immobilization and further surface regeneration and recovery of the final product. This original strategy constitutes an indirect glycan attachment through bioaffinity interactions using DNA scaffolds. This approach is known as DNA-Directed Immobilization or DDI where, the term "Directed" refers to "Guide" the immobilization event.

In the Figure 4.7 it is depicted the schematic illustration of DDI approach. A single-stranded DNA oligomer is displayed onto the surface (yellow dash rectangle)

by different direct functionalization methods (e.g. pyrrole electropolymerization or thiol-oligonucleotides *via* SAMs already described). Then, a complementary sequence of single-stranded DNA oligomer (grey dash rectangle) conjugated to the glycan element (biorecognition element, spheres) is immobilized on the surface forming duplex-DNA architectures (blue dash square).

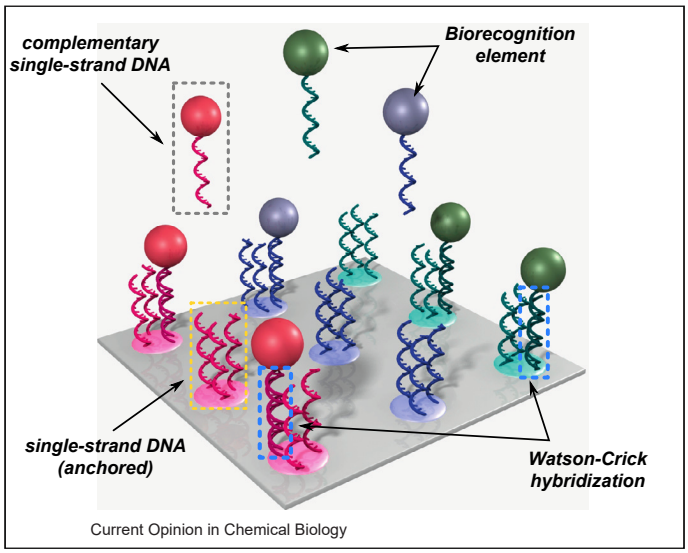

Figure 4.7: Principle representation of DNA-Directed immobilization. The biorecognition elements are depicted as different colour spheres. The grey dash rectangle represents the complementary single-strand DNA bearing the biorecognition element. In yellow dash rectangle indicates the single-strand DNA structures anchored on the surface. The blue dash rectangles show the selective Watson-Crick hybridization process. Image taken from Meyer *et al.*[168]

This type of immobilization strategy provides robust and stable hybridised structures with high substrate selectivity and specificity (selective DNA hybridization). Therefore, it allows the attachment of multiple glycan samples (multiplexed method) in a defined pattern by choosing different DNA sequences to be conjugated with each sugar. Furthermore, the noncovalent nature of the hybridization coupling (hydrogen bonds) offers a great advantage towards reversible processes on solid support compared to the covalent linkages. Thus, it saves time in the surface preparation process having successive hybridization steps in a single assay.[169,170]

The applicability of this technique can be used for glycans structures,[167,170] proteins[171,172] and peptides[114] among others.[168] The framework of DDI approach can be dedicated towards the glycome research, biomedical diagnosis or cell biology domains.[168] Finally, this approach is perfectly compatible with multiple detection methods such as fluorescence,[167] SPRi[41] or MALDI-Tof MS analysis.[173]

4.1.3 Detection Methods on Glycoarrays platform. Transducer Element

In glycan microarrays, the biochemical interaction is intimately joined to the signal response collected by the transducer. Glycosylation reactions will always derive into chemical changes at surface level. Therefore, the great scope is to detect and monitor such changes using powerful analytical techniques. A classification of microarray detection techniques will be briefly explore within two categories: label-demanded and the label-free methods. In the Figure 4.8, a general overview of the main idea of each detection approaches is illustrated.

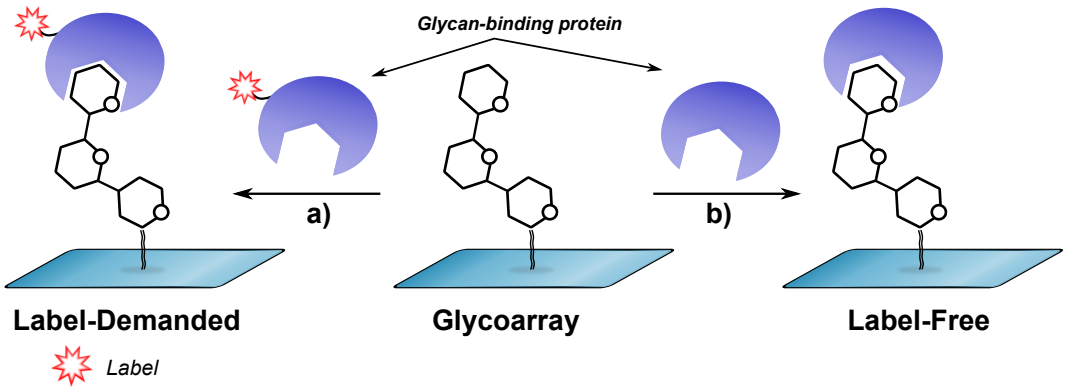

Figure 4.8: Principle of the different approaches to detect binding interactions on glycoarrays. a) Analytical techniques needing a label for indirect binding read-out. b) Label-free techniques for direct binding read-out. Adapted from Gray *et al.*[140]

Within the label-demanded approach (Figure 4.8-a), the samples are depicted as glycan-binding proteins bearing a labelled molecule in the structure. In this method, the binding process is indirectly detected thanks to the tag molecule by fluorescence scanner (fluorophore) or radioactivity (radioactive atoms) at the end of the interaction (endpoint). This procedure provides information about binding yes/no, although it is limiting to the access of kinetic constants. On the other hand, transducing techniques offer alternative approaches to evaluate binding event directly on the surface without using any label compound in real-time measurements, giving access to the kinetic of the reaction. (Figure 4.8-b).

Finally, the election of the solid surface dictates the definition of the detection technique to be explored. Rather than covering an extensive review on each analytical technique,[140] a brief overview of the most relevant ones will be addressed.

Detection Methods needing a label compounds

This group includes a set of analytical techniques that incorporate a label element for the biomolecular interaction readout. These detection method are classified by fluorescence or radioactivity techniques, although electrochemical methods are also involved within this group.[174]

- **Fluorescence detection method**

The most common approach for glycan array detection is the fluorescence method broadly considered as a reference technique for biochemical test. This methodology uses labelled molecules generally called fluorophores, which are organic molecules (dyes) or proteins with the property of emitting radiative photons through fluorescence emission. Generally, the labelled molecule is anchored on the affinity protein to monitor binding events or to control surface densities using labelled lectins.[167]

An example of GT fluorescence monitoring was published by Park & Shin in 2007.[175] They present a model of glycoarray for the assessment of a glycosylation process from a β-1,4-Galactosyltransferase using RCA 120 (*Ricinus Communis Agglutinin 120*) fluorescence lectin (Figure 4.9).

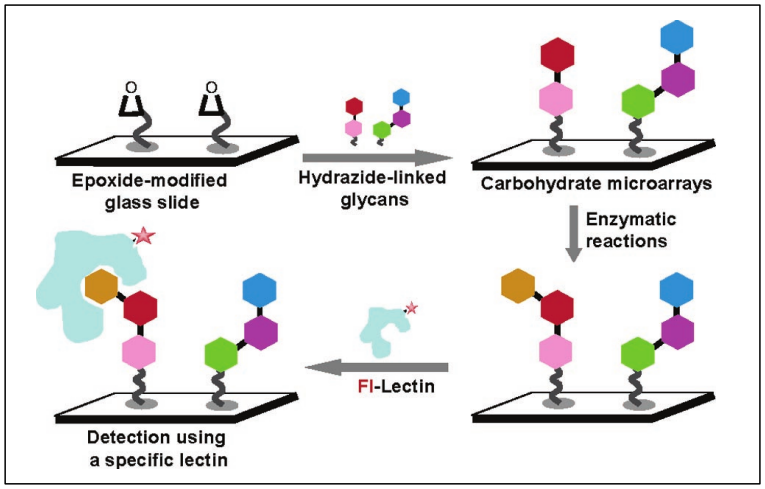

Figure 4.9: Diagram for the construction of carbohydrate microarrays to assay glycosyltransferases (β-1,4-Galactosyltransferase) with a label lectin by fluorescence detection. Image taken from Park *et al.*[175]

Within this experiment, a collection of twenty glycan structures, some of them with a galactose fragment (α/β-Gal, α/β-Glc, β-Lac, α/β-GlcNAc etc) were chemoselectively immobilized *via* hydrazide conjugation over epoxide-coated glass slides.

Then, the carbohydrate microarrays were incubated with the β-1,4- Galactosyltransferase in the presence of UDP-Galactose donor. Finally, the glycosylation level was evaluated by Cy3-tag RCA 120 lectin using fluorescence detection. The fluorescence pattern results concluded that both α- and β-GlcNAc were transferred a galactose molecule to form the corresponding α/β-LacNAc by the enzyme. This approach allows the detection of carbohydrate arrays with smaller quantities of acceptor substrates (picomoles) to assess GT activities. Furthermore, it provides a useful platform to explore new applications of enzymatic modifications with a large range of glycan probes.

Typically, fluorescence methods require an initial step dedicated to the chemical labelling of the target molecule or protein before each analysis that sometimes is difficult to apply. Moreover, the fluorophore itself is quite sensitive to light and relatively easy to be quenched or inactivated. Besides, the solid surface might produce an attenuation of the fluorescence background signal. However, the fluorescent detection represent a highly sensitive, cheaper and safer methodologies to monitor and quantify enzymatic modifications in glycoarrays platforms.

- **Radioactivity detection method**

Similar approaches use radioactive atoms as labelling species to detect and monitor glyco-enzymatic interactions. In this context, Shipp *et al.*[141] developed a plant cell wall glycoarray to study enzymatic activities of our model of fucosyltransferase (AtFUT1) involved in the xyloglucan biosynthesis. To that purpose, the tamarind xyloglucan ligand (XyG) trimer and cello-oligosaccharide forms (cello-heptaose) were functionalised with poly-D-lysine (PDL) *via* reductive amination and immobilised through photoactivatable aryldiazirine group over a glass slide. The enzymatic transfer reaction on the immobilize ligands was detected by incorporating radiolabelled GDP-[^{14}C]Fucose donor *via* phosphoimager scanner.

The great advantage of radioactive labelling methods relies on the capability of tracking enzymatic transformations with high sensitivity. That makes this analytical technique an effective way of screening glycan probes at low enzyme and substrate concentrations. However, the main drawback of this approach is the implicit hazard of working with radioactive substrates, which causes this technique to be replaced in many research laboratories by other non-invasive approaches. Moreover, this methodology is highly dependant on the commercial availability of radioactive nucleotide donors for glycosyltransferases, or other synthetic approach to label binding proteins such as lectins or antibodies, with the open access to get false positive and negative results.

Label-free Detection Methods

Labelling techniques have demonstrated to be quite sensitive at low concentration of label molecules (picomoles) and are still today reference techniques in biology. However, labelless detection methods have emerged to offer robust alternatives to explore binding interactions under native conformations (both proteins and glycans) on glycoarray platforms. Some examples of label-free techniques are typically identified with real-time QCM and SPR, or endpoint MALDI-ToF MS on solid phase with detection limits from nano- to femtomoles.[176] A great advantage of label-free methods rely on their great applicability over substrates difficult to labelled such as carbohydrates.[140]

- Quartz Crystal Microbalance, QCM

This label-free biosensor is a sensitive device able to measure minimal local changes in mass involved within a protein-glycan interactions from nano- to the microscale in real-time.[177] The signal transduction is gravimetric and achieved by a piezoelectric material (a type of material that generates electricity in response to mechanical stress) made of quartz crystals oscillating at a defined frequency (Figure 4.10 left side). This parameter is controlled by an electric current throughout metallic electrodes (typically gold) where the bioreceptor elements are immobilised. As a consequence of the biomolecular recognition, the mass onto the electrode surface changes, resulting in a negative linear-dependant variation of the initial-state oscillation frequency (Figure 4.10 right side).[37] Therefore, monitoring the variation in the resonance frequency can provide useful information in real-time about protein-ligand specificity and kinetic studies.[178]

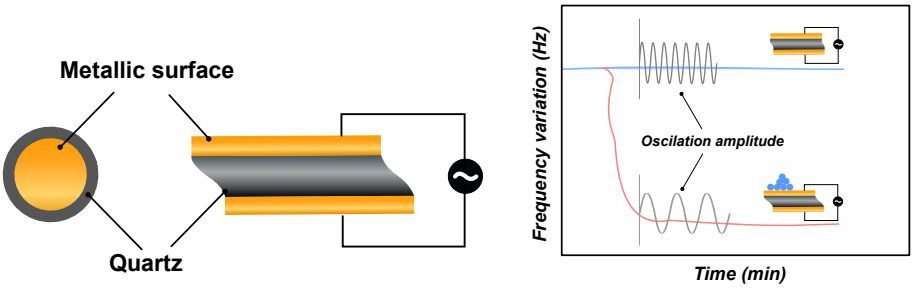

Figure 4.10: Representation a quartz crystal microbalance (QCM). The quartz crystal is attached onto metallic surface (typically gold) connected to a pair of electrodes (left). Sensorgram of the frequency variation (Hz) in the case of interaction on the sensor surface (red line). As a reference, no variation is detected in running buffer (blue line). Adapted from Liu *et al.*[37]

One interesting example for QCM was developed by Nishino *et al.*[179] In their study, they monitored the catalytic cleavage of an immobilised amylopectin substrate by a phosphorilase-*b* enzyme through QCM method. Furthermore, all the kinetic parameters were obtained by fitting the changes in frequency and mass against the time courses.

Currently, QCM assays are limited to miniaturization and not adapted for multiplexed assays in high throughput manner. Moreover, numerous side effects can be additionally measured to mass coupled with the solvent (water) or mass transport limitations, making the analysis harder.[180]

- Endpoint Mass spectrometry, MS

Similarly, mass spectrometry (MS) is a versatile and routinely technique that determines the mass of a sample mixture immobilized on electrically conducting surfaces with low detection limits (femtomoles).[140]

In glycoarrays where the glycan probes are immobilised on surfaces, the mass detection requires a chemical cleavage prior the proper analysis, which sometimes is not feasible. However, MALDI-Tof MS analysis represents an interrogation approach that enables the mass detection of the immobilization probes directly on conducting surfaces. Typically for protein-glycan interaction, gold surfaces are one of the most popular platforms for MALDI-Tof MS detection.[140] In this line, Ban *et al.* developed a label-free analytical assay to screen and identify new putative glycosyltransferase activities analysed by MS.[181] the Figure 4.11 illustrates the general strategy used by the authors for the array platform committed to the identification of new GTs.

The design of this screening approach combined the immobilization of glycan probes *via* SAM on gold with the MALDI-Tof MS analysis (named SAMDI). The glycan acceptors were coupled with the monolayers *via* alkanethiol reagents or thiol-functionalized glycans. Thanks to this methodology, around 60.000 individual reactions (GT, donor, acceptor) were evaluated by SAMDI assays giving 44 glycosylation products that finally yielded 4 new validated GTs.

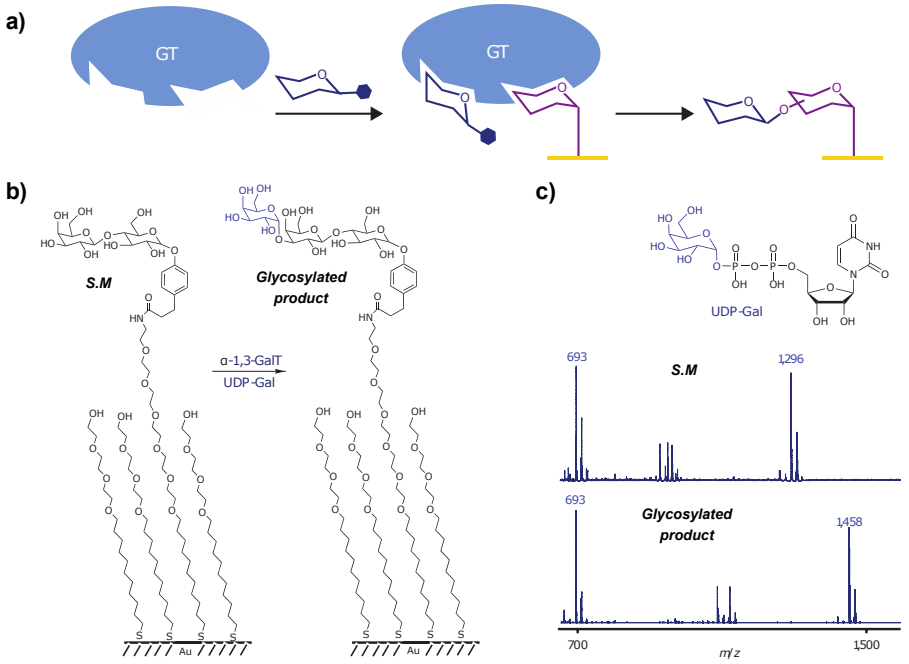

Figure 4.11: Representation of the general approach for the screening of new GTs.[181] a) GT reaction scheme (donor and GT in solution with immobilized sugar acceptor) b) Gold array platform formed by SAMs containing a lactose sugar immobilized. Galactosyltransferase reaction is depicted. c) Mass spectra called SAMDI of the starting material and the glycosylated product. Taken and adapted from Ban *et al.*[181]

- Surface Plasmon Resonance imaging, SPRi

Closing the most relevant label-free techniques, the surface plasmon resonance imaging or SPRi has emerged as a representative optical method with extensive applications in the field of biosensors.[34,180,182]

As we described in the Chapter 1, SPR is an optical method that enables the direct analysis of interacting biomolecules in real-time measurements without labelling.[34] The new updated version with an image processing (SPR imaging) allows the high throughput screening (HTS) analysis of multiple label-free samples visualizing the whole biochip in real-time *via* a CCD camera (Figure 4.13).

The physical concept of SPRi represents the electromagnetic oscillations of the free-electrons density wave throughout the gold metal. The idea of surface plasmons refers the propagation of evanescent waves (EWs) along the interface of the

gold, showing the maximum intensity at this point and decaying exponentially as it penetrate the media. The resonance phenomenon occurs at the surface level when the energy of the photons from the incident light matches the energy of the surface plasmons. This process, also called Surface Plasmon Polaritons (SPP), occurs at a certain angle of the incident light (SPR angle) under Total Internal Reflection (TIR) moment in which, the intensity of the reflected light is attenuated, drawing the plasmonic curve (Figure 4.12-a,b). The detection and readout is carried out at fixed angle of incident and the reflected light is collected by a CCD camera. This optical tool obtains an image or picture of the entire surface, enabling simultaneous multiplexed array analysis.

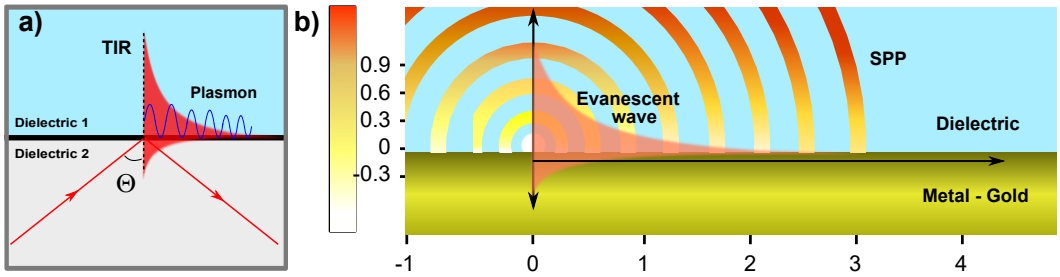

Figure 4.12: Principle of SPR phenomena. a) Specific condition for the formation of a Total Internal Reflection (TIR). b) Representation of the resonance effect forming the Surface Plasmon Polaritons (SPP) under TIR angle.

The most popular approach to produce the optical excitation of surface plasmons is the use of prisms to guide the incident light towards the gold layer. The optical configuration is displayed according to the Kretschmann geometry where the thin metal surface is localized on top of the glass prism in contact with two dielectric media with different refractive index (Figure 4.13). This configuration allows the generation of evanescence waves penetrating through the gold layer and the alignment with the surface plasmons at the SPR angle of the incident light.[36] Hence, the SPRi technology is able to detect simultaneously any physico-chemical event at few nanometres of the metal surface that alters the initial parameters of the light, proportionate to the mass changes.

SPR imaging system depicted in the Figure 4.13 works with intensity modulation (reflectivity-based SPRi) in which the reflectivity of a polarised incident light is measured at a single angle and wavelength. Two types of monochromatic incident light source are used to promote and optimise the SPRi conditions: the p-polarised (TM) and the s-polarised (TE). The p-polarised light permits the SPRi measurements generating the plasmon resonance event, and the s-polarised light is used as

a reference signal to minimise the background and artefacts.[183]

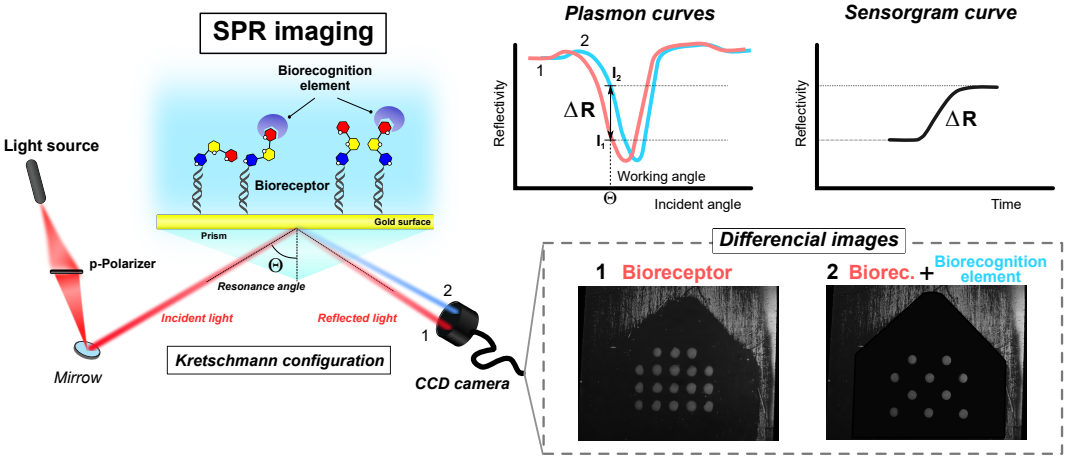

Figure 4.13: General scheme of the Surface Plasmon Resonance imaging (SPRi) technology under Kretschmann configuration. This optical device provides the visualization of each biomolecular interaction in a single experiment. The binding recognition is monitored in real time and without labelling. Initial reflectivity curve vs angle of incidence (plasmon curve) of bioreceptors is depicted in red (1) to identify the best working angle (θ) at maximum slope. Monitoring the shift in the reflectivity when a binding process occur (2) allows the direct visualization of the positive bioreceptor elements on the chip by the CCD camera and therefore, the kinetic curve of the binding event.

In order to transform these physico-chemical and optical responses into readable information, the CCD camera along with SPRi software detect and record all the minimal variations in the reflected intensity within the whole biochip. In SPRi, the output signals are collected simultaneously in the form of digital contrast image and sensorgram curves during the experiment, as shown in the Figure 4.13. In a typical assay, the changes in reflectivity signal are proportional to the mass attached on the surface. Looking closer to the sensorgram curve, quantitative and qualitative biochemical parameters can be obtained. Ideally, the analysis of the SPRi sensorgram provides a better understanding about the physico-chemical binding (either yes or no), the affinity or enzyme kinetic parameters (k_{on} and k_{off}) as well as equilibrium binding constants (K_A and K_D).

In the field of carbohydrates, the SPRi technique represents an optimal method highly compatible for glycoarray analysis. It provides a perfect design for the multiplexed interrogation and screening of protein-glycan recognition in real-time.[42] In this context, Fais *et al.* demonstrated the use of SPRi technique to address an array

of plant lectins to identify potential inhibitors of ricin toxin.[184] In another study, de Boer *et al.* constructed a microarrays containing *N*-glycans and glycolipids isolated from the pathogen *S. mansoni*. Then, SPR-based assays determined the profiles of serum antibodies as a potential markers for diagnosis screening purposes.[185]

- **Combination of label-free detection methods**

The use of gold surfaces on SPR and SPRi studies can open the window to exploit this assay with complementaries techniques as MALDI-Tof MS analysis.[143,176,186]

This approach was addressed by Zhi *et al.* which combine these two analytical techniques to extend the development of gold glycoarrays. It successfully exploit dual binding/mass information towards a better understanding protein-glycan interactions without any labels or cleavage.

Likewise, Remy-Martin *et al.* developed a new robust method of detection that couple a home-made SPRi chips and MALDI-Tof MS called "SUPRA-MS".[176] This strategy was envisioned as a proof-of-concept validation of SUPRA-MS for prognosis towards a potential marker of human breast cancer and tuberculosis (Figure 4.14).

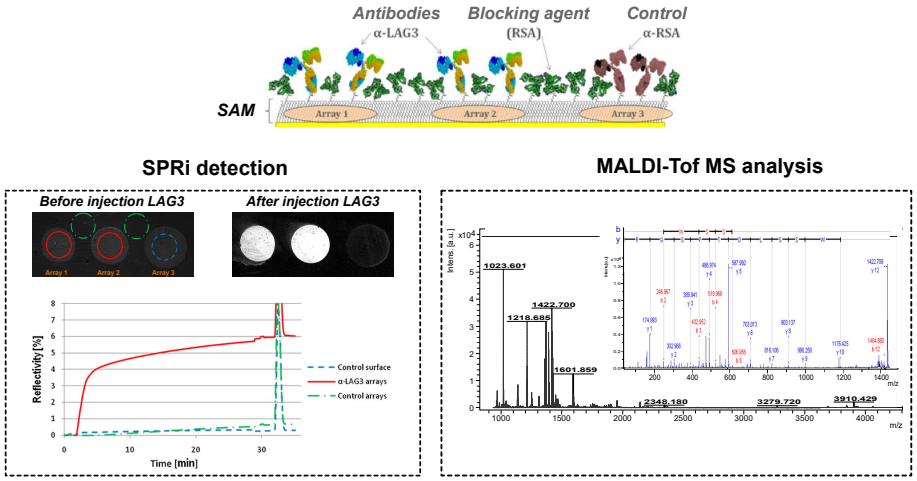

Figure 4.14: SUPRA-MS technique as a combination of SPRi detection and mass spectrometry characterization towards a potential breast cancer marker in human plasma. Top: Surface functionalization and array building. Left: SPRi detection of LAG3 protein in real-time. Right: MALDI-Tof MS analysis of the defined peptide distribution from the LAG3 proteins. Taken and adapted from Remy-Martin *et al.*[176]

In this study, the authors demonstrated the capacity of SUPRA-MS immunoarray to detect and characterize a specific LAG3 protein associated to the human breast cancer at femtomole scale. Briefly, the gold chip surface was functionalized by SAM and chemically activated with Sulfo-NHS /EDC. Then, the antigen (α-LAG3, positive control) and rat serum albumin (α-RSA, negative control) were spotted prior passivation with RSA blocking agent (Figure 4.14-top). The injection of human plasma containing the LAG3 antibody was monitored by SPRi in real-time (Figure 4.14-left side). Finally, the enzymatic digestion and matrix homogeneity for MALDI-Tof MS measurements allowed the characterization of a defined peptide distribution associated to the LAG3 protein (Figure 4.14-right side). Both analytical techniques were performed within the same biochip.

4.1.4 Analytical Techniques to Monitor Glycan Interactions in solution

Within this group of analytical methods for in-solution assays, we can find powerful technologies to characterise and monitor enzyme-glycan interactions such as Saturation-Transfer Difference NMR (STD-NMR),[187,188] Isothermal Titration Calorimetry (ITC)[189] or gel electrophoresis[190] among others.

Isothermal Titration Calorimetry

Isothermal titration calorimetry or ITC is considered one of the most modern and routinary label-free analytical technique widely used for studying biomolecular interactions in real-time. The main principle of this technique resides in measuring the heat exchange either by absorption (endothermic) or release (exothermic) involved in native reactions under isothermic conditions. In a single experiment, ITC offers valuable information about the affinity, thermodynamic, kinetic and stoichiometry interrogations associated to binding interactions in solution.[189,191] A general description of the ITC principle is depicted in the Figure 4.15.

The ITC setup (Figure 4.15a) is composed of two cells, one of which contains water and works as a reference cell and the other represents the sample cell containing usually, the enzyme solution of interest. Insulated by an adiabatic chamber, both cells are connected to a heat system isothermally controlled. This system is formed by two heaters (the reference and the feedback) and a thermocouple sensor to monitor the differences in temperature between cells. Finally, a stirred-injection syringe containing the ligand analyte is inserted and adjusted into the sample cell to trigger the titration process.

In the Figure 4.15-b, fixed volumes of ligand are injected multiple times until the enzyme gets saturated reducing the heat difference signal (Raw data). Finally,

the thermogram analysis in Figure 4.15c (heat of each injection versus molar ratio) provides crucial information about thermodynamic parameters (enthalpy (δH), entropy (δS) and free energy (δG)), equilibrium constant (K_D) and stoichiometry (n) specific of each particular enzyme.

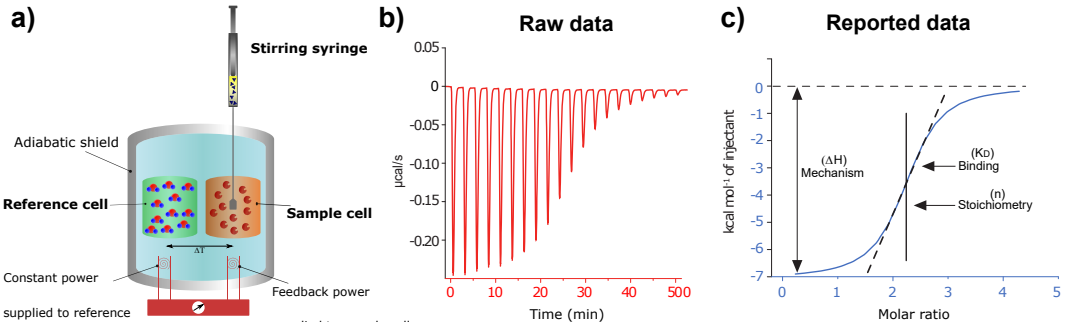

Figure 4.15: General principle of Isothermal Titration Calorimetry (ITC) technique. a) An adiabatic chamber where the titration process is taken place. b) An exothermic reaction releases heat after ligand injection giving ITC raw data. c) Integration of each peak is plotted against molar ratio.

Kinetic information is also a pivotal parameter to understand the intrinsic behaviour of biological samples during binding interactions.[189,191,192] It can provide useful information about the molar enthalpy of the reaction (δH_{app}) from the heat change (Q) and the number of moles of the product (n). Then, the reaction rate ($\delta P/\delta t$) is proportional to the heat flow ($\delta Q/\delta t$) under the equation X. As reaction rates are under steady-state conditions, the Michaellis-Menten plot provides the kinetic parameters k_{cat} and K_M.

Most of the relevant applications of ITC methodology are focused on the study of the enzyme-ligand recognition and catalysis/inhibition for drug discovery.[193,194] However, ITC assays have been well established towards many other biomolecules such as DNA-ligand interaction, Protein-metal ion complex formation or thermodynamic studies of monomer-dimer equilibrium among others, illustrated in the recent review from Margarita Menéndez.[189]

In glycoscience, the ITC contributes positively to enhance the comprehension of some classical family of proteins interacting with glycans such as glycan-binding proteins (lectins), degradation enzymes (glycosylhydrolases) or synthetic enzymes (glycosyltransferases), being the lectins the most popular family of proteins studied by ITC.[195,196]

Reynolds *et al.*[197] designed a multivalent gold glycocluster to improve the affinity binding for PA-IL lectin from *Pseudomonas aeruginosa*. This multivalent scaffold was displayed on gold nanoparticles and the lectin interaction was thermodynamically and kinetically described by ITC and SPR along with hemagglutination inhibition (HIA). The final results drop important insights in the use of gold-glycocluster nanoparticules to boost the binding affinity up to 3000-fold compared with monovalent distribution.

Likewise, the versatility of the ITC has been described to characterize molecular mechanism involved in enzyme-ligand complexes. Gooley *et al.*[198] described the joint action of ITC and NMR applied to monitor the differences in the kinetic behaviour of two forms of carbohydrate-binding modules (β1 and β2) from the AMP-kinase protein.

Finally, Sindhuwinata *et al.*[199] performed a thermodynamic screening of multiple substrates binding to a galactosyltransferase from human blood group B. All binding interactions were described using ITC experiments supplemented by SPR analysis and STD-NMR titration experiments revealing a binding process governed by mutual allosteric control.

Electrophoresis Gel for DNA probes

Commonly in biochemistry laboratories, electrophoresis allows the direct identification, quantification, and purification of many different macromolecules (DNA, RNA or proteins) in solution according to their mass and charge. The principle of this technique consists on applying an electric voltage that will serve as a driven-force to separate a mixture of biomolecules through a polymeric gel. The migration process will be determined by the nature of the sample (charge, conformation or size), the electrophoresis gel (chemical composition or porosity) and the temperature.

The electrophoresis gel is composed by a polymeric-based compound chemically synthesised *in situ* before the separation process (Figure 4.16a). The most widely used are the polyacrylamide-based gel (PAGE) for separating proteins and DNA fragments, and the agarose-based gel suitable for larger size of DNA fragments. Electrodes are displayed at both sides of the gel to promote the sample mobility exclusively by molecular size. For DNA architectures, the gel is stained by fluorescent compounds commercially available (SYBR^{TM}-gold, SYBR^{TM}-green). It interacts with the single/double-stranded DNA conformation by inserting between the nucleic acids and emitting fluorescence after irradiation (Figure 4.16b).

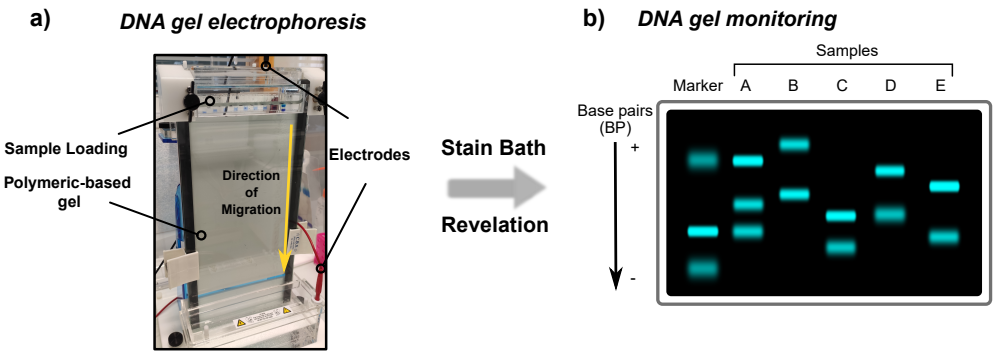

Figure 4.16: General procedure of DNA gel electrophoresis. a) Electrophoresis apparatus dedicated to the DNA separation over a polymeric-based gel. b) Example of DNA sample distribution after stain bath revelation.

The applicability of this technique is essential for routinise progression in biology and biochemistry research. In the field glycoscience, the COCs have been extensively studied thanks to the versatility of these architectures in glycoarrays platforms.[200] However, the study of these COCs scaffolds and further interactions with proteins are not typically monitored by DNA electrophoresis. Nevertheless, it can be found in the literature some examples of using DNA electrophoresis to control the production of COCs in solution.

Ikeda*et al.*[190] probed the stability of oligonucleotides bearing a functional carbohydrate moiety at the 3'-end against enzymatic degradation. The COCs were synthesised by a novel solid phase method to conjugate a galactose fragment at the 3'-end and a fluorescence-tag at the 5'-end. They developed a polyacrylamide gel electrophoresis followed by fluorescence scanning to monitor their stability in serum buffer.

In another interesting study, Matsui *et al.*[201] developed a novel trigonal COCs emulating the 3-dimensional scaffold of concanavalin A (ConA) for efficient multivalent interaction to lectins. Three DNA structures were enzymatically modified with maltose and lactose sugars at the 3'-end and then, hybridised to form the final trigonal architecture. Confirmation of each DNA building-block combination with and without the sugar fragment was monitored by polyacrylamide gel electrophoresis.

4.2 Proposed strategy

Within the last two chapters, we explored both the biochemistry and chemistry domains towards the production and purification of a model of glycosyltransferase. For this study, we chose the fucosyltransferase (AtFUT1) and its XyG ligand enzymatically hydrolysed in a set of building-blocks well-characterized. Furthermore, we chemoselectively modified the XyG ligands *via* reducing end with two complementary DNA sequences (I-A and I-B) at the 5'-terminal. Likewise, a pyrrole residue was chemically added to the sibling-strand DNA sequences (II-A and II-B) at 5'terminal for grafting purposes.

In this chapter, we aim for the conception, validation and study of a versatile biochip for the monitoring of interactions between XyG probes and proteins in real-time using SPRi assays (Figure 4.17). Complementary techniques in solution such as DNA electrophoresis gel or MALDI-Tof MS will support and validate the technique for future assays with other biological probes.

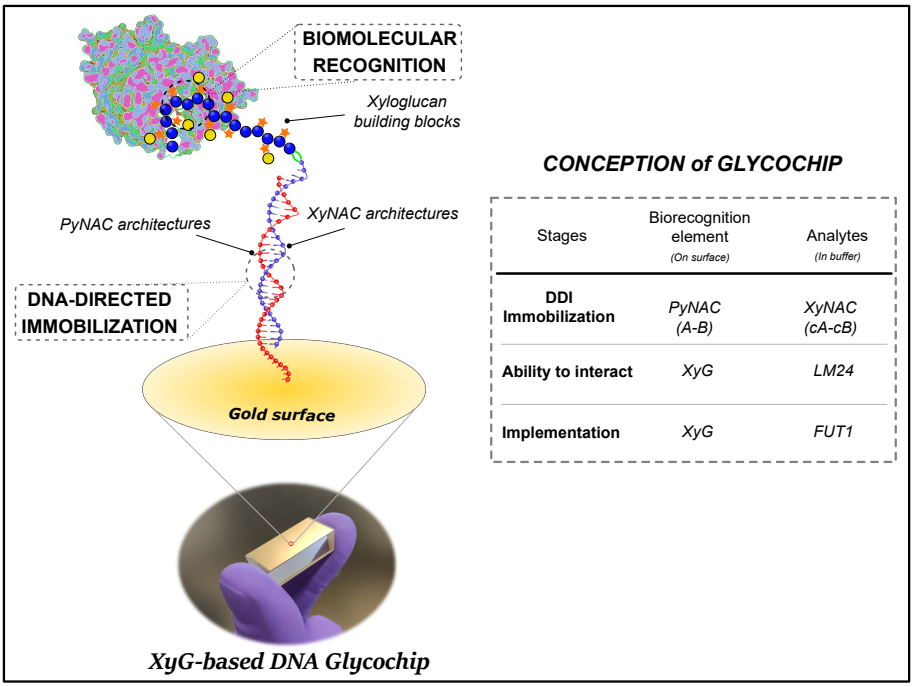

Figure 4.17: General scheme of the conception of XyG-based DNA glycochip for SPRi analysis. The attachment of XyG building-blocks is addressed by DNA-Directed Immobilization (DDI) approach. The glycochip is validated for biomolecular binding recognition with potential application towards glycosyltransferase specificity and activity measurements.

Thus, this original approach will be tackled in three stages:

Stage 1 This stage will describe the conception of a XyG-based DNA glycochip for monitoring protein-glycan interactions. The original DDI approach for the presentation of XyG-based DNA glycochip compatible with SPRimaging characterization will be described. DNA-electrophoresis gel technique will support the quality and the hybridization efficiency of the XyG-DNA probes in solution.

Stage 2 Within the second stage, our XyG-based glycochip will be validated by SPRi bioassays. The accessibility and integrity of the grafted XyG probes will be addressed using a rat monoclonal antibody (anti-XyG, LM24).

Stage 3 Finally, we will address the implementation of our glycochip platform towards the biorecognition of glycosyltransferases by SPRi. For this study, our model of plant fucosyltransferase (AtFUT1) will be evaluated against different sizes of XyG probes. In a first part, the FUT1 enzyme activity will be monitored by MALDI-Tof MS in solution prior the SPRi assays. Finally, kinetic ITC experiments will be explored with FUT1 enzyme against XyG polymer.

4.3 Conception of Xyloglucan-based Glycochip for Protein-Glycan Interactions. Stage 1

In this section, we tackled the original DDI approach to achieve a site-selective immobilization of XyG oligomers on gold surface for SPRi glycochip. DNA electrophoresis gel studies have been developed to address the formation of the duplex-DNA structures in solution. Finally, XyNAC probes were presented by DDI strategy and characterized by SPRi in real time.

4.3.1 DNA Electrophoresis Gel of duplex PyNAC and XyNAC architectures

We explored the selective hybridization process in solution of the XyNAC glycoconjugates prior evaluation on SPRi biosensor. The DNA electrophoresis gel was presented as a suitable technique enabling the visualization of duplex conformation of ODN samples in a single gel. With the advantage of having the XyG structures conjugated to ODN building-blocks, we were able to use the DNA as a "labelled" biomolecule to monitor the gel migration of the different XyNAC conjugates.

The specific hybridization process was addressed by DNA electrophoresis gel using different complementary XyNAC architectures (cB) over the same PyNAC architec-

ture(B) under native conditions. A mixture of bromophenol blue (BPB) / Xylene cyanol (XC) was used as a marker control.

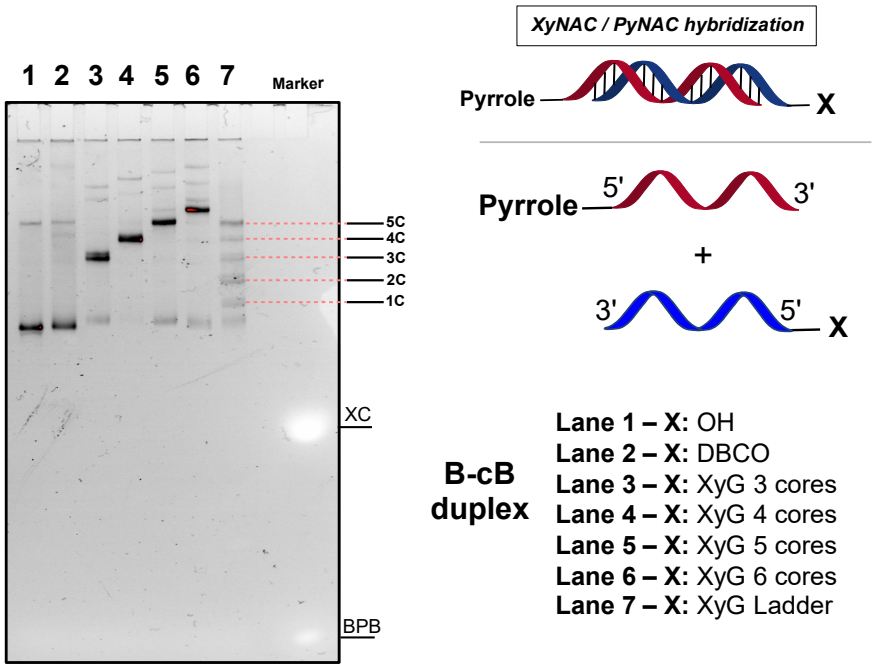

Figure 4.18: DNA electrophoresis gel of duplex XyNAC (cB) and PyNAC (B) architectures. The X represents the functional group coupled at the 5' end of each complementary oligonucleotide (cB). The gel was prepared in polyacrylamide gel at 20% and revealed with SYBR-Gold incubation for UV detection.

Duplex formation of XyNAC from 3 to 6 cores were evaluated by DNA gel electrophoresis (Figure 4.18). The electrophoresis gel analysis successfully revealed a selective hybridization event of the ODN conjugates (B-cB) having the XC/BPB markers as a references. Similarly to the single-strand ODN conjugates, we observed a remarkable size-distribution of ODN duplexes eminently determined by the size of XyG building-blocks.

To conclude this analysis, we demonstrated the feasibility of this routinely technique to monitor synthetic XyNAC with high sensitivity. Furthermore, we successfully addressed the selectivity and viability in the hybridization process from complex structures of XyNAC forming stable duplex architectures. These results confirmed the affinity interaction in solution between the complementary XyNAC probes that will be used to achieve the DDI approach on chip.

Overall, we emphasised the remarkable versatility in the use of tagged-ODN biomolecules as a labelling archetypes for monitoring glycoconjugates using a simple DNA electrophoresis gel.

4.3.2 XyNAC glycochip using DDI and characterization by SPR imaging

Previous works developed in our team over SPRi experiments have reported the specific immobilization of DNA probes using the DDI approach for monitoring biological interactions[41,148] or detecting damaged ODN duplexes.[169]

The reversibility in the DNA hybridization process envisions the goal of "catch-and-release" to address XyG glycochips construction (Figure 4.19) and further dehybridization using restriction enzymes[41] or denaturing agents such as NaOH.[169]

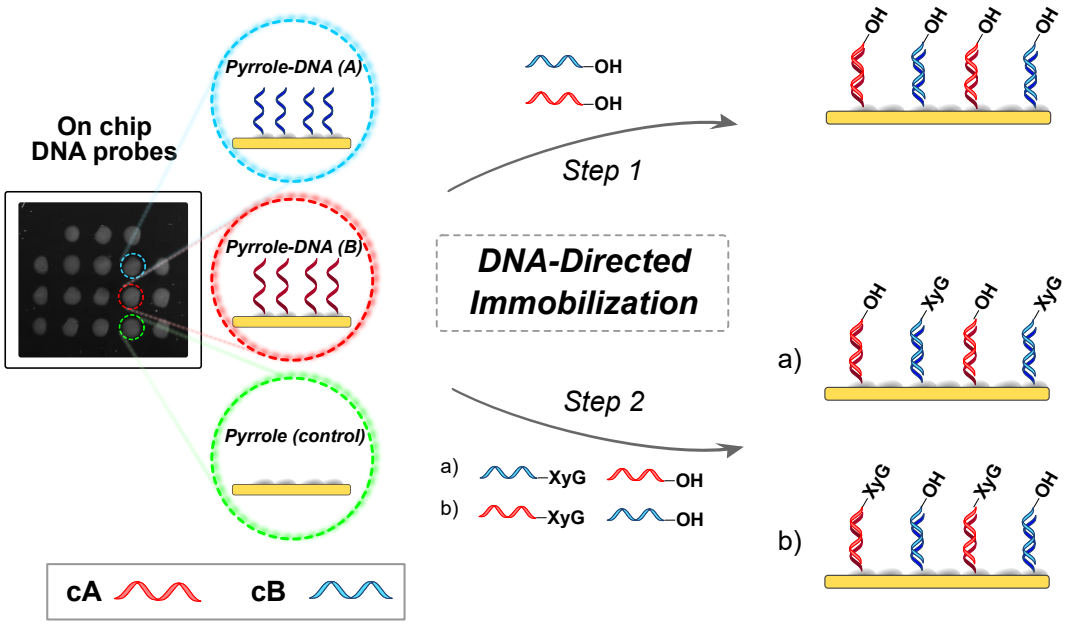

Figure 4.19: Conception of XyNAC glycochip construction *via* DDI approach. Step 1.- Selective hybridization of complementary ODN sequences (cA and cB). Step 2.- XyNAC architectures and unmodified cODN hybridization (cA and cB).

Two different PyNAC probes with the sequence A and B were directly immobilized on the gold surface by pyrrole electrocopolymerization in a defined spot pattern. A first step was dedicated to address the accessibility and the quality of

the ODN spots by injecting unmodified complementary ODN sequences (cA and cB). Then, a second step was committed to evaluate the specific immobilization of XyNAC architectures on the chip for the purpose of protein recognition.

The hybridization strategy was monitored by the injection of 500 nM for each cODN-1 (cA and cB sequences) at room temperature with a flow rate of 50 μL.min^{-1}. Running buffer at 10 mM HEPES with 150 mM of NaCl and 0.005% Tween 20 at pH 7,4.Furthermore, to prevent non-specific adsorption interactions, the gold surface was blocked with 1 % of Bovine-Serum Albumin (BSA) at the beginning of each experiment.

Oligonucleotides with non complementary ODN probes to the injected ODN probe served as a negative control. The reversibility of ODN duplexes allowed the regeneration of the glycochips by injecting denaturing agents after each SPRi analysis.

Selective hybridization using unmodified ODN structures. Step 1

The attachment of unmodified cODN-1 architectures on SPRi chip was explored by DDI strategy. The SPRi signals are illustrated in the Figure 4.20.

Based on the sensorgrams, both SPRi signals exhibited selective hybridization with the injected complementary sequence. In the first sensorgram (top), the injection of the sequence cA showed an increase in the SPRi signal over time with the pairing strand yielding an immobilized A-cA duplex on the chip. Furthermore, the presence of free ssODN (B) on the spot did not produce any cross-interaction with the ODN sequence cA injected.

Likewise, within the sensorgram at the bottom we observed a similar SPRi response with the grafted ODN-2 (B) sequences on the chip. The hybridization process of the cODN-1 structures (cB) showed a clear specificity for those pairing ODN-2 (B) spots on the chip. The injection of the cODN-1 (cB) sequence did not modify the SPRi response of the ssODN-2 (A) which remained dehybridized on the chip.

Overall, these findings confirmed and validated the accessibility of the grafted PyNAC architectures on gold surface towards the glycochip fabrication *via* DDI. Then, the SPRi results proved the selective hybridization with no cross-interactions detected. Therefore, this immobilization strategy can be tackled for the next assays with XyNAC architectures.

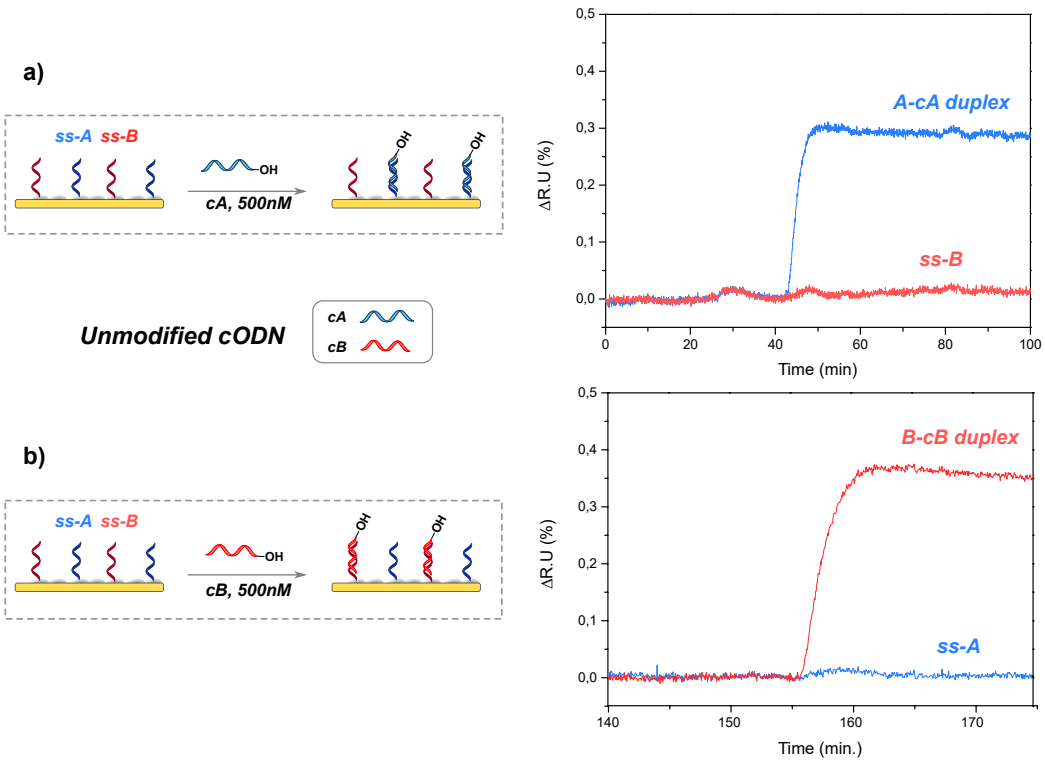

Figure 4.20: SPRi sensorgram curves for the selective immobilization of unmodified cODN sequences (cA and cB) at 500 nM by DDI approach. Running buffer at 10 mM HEPES with 150 mM of NaCl and 0.005% Tween 20 at pH 7,4. a) Hybridization sensorgram of A-cA duplex formation on chip. b) Hybridization sensorgram of B-cB duplex formation on chip.

Selective hybridization using XyNAc architectures. Step 2

The attachment of XyNAC architectures on SPRi chip was explored by DDI strategy. The experiment was developed by monitoring the SPRi signal after the injection of XyNAC architectures under the same experimental conditions. The non complementary ODN sequences served as a negative control.

First, the smaller XyG building-blocks were immobilized on the chip *via* DDI. The Figure 4.21 illustrates the sensorgrams of the XyNAC architectures containing 1 to 3 cores.

Similarly to the unmodified cODN-1, the three sensorgrams exhibited a specific hybridization with the complementary ODN sequences (cA). As a result, the binding response from the XyNAC probes showed a well-differentiated increase in the

SPRi curve until saturation forming the glycoconjugate A-cA duplex on the chip. The negative control ODN-2 probes remained as a single strand B on the chip.

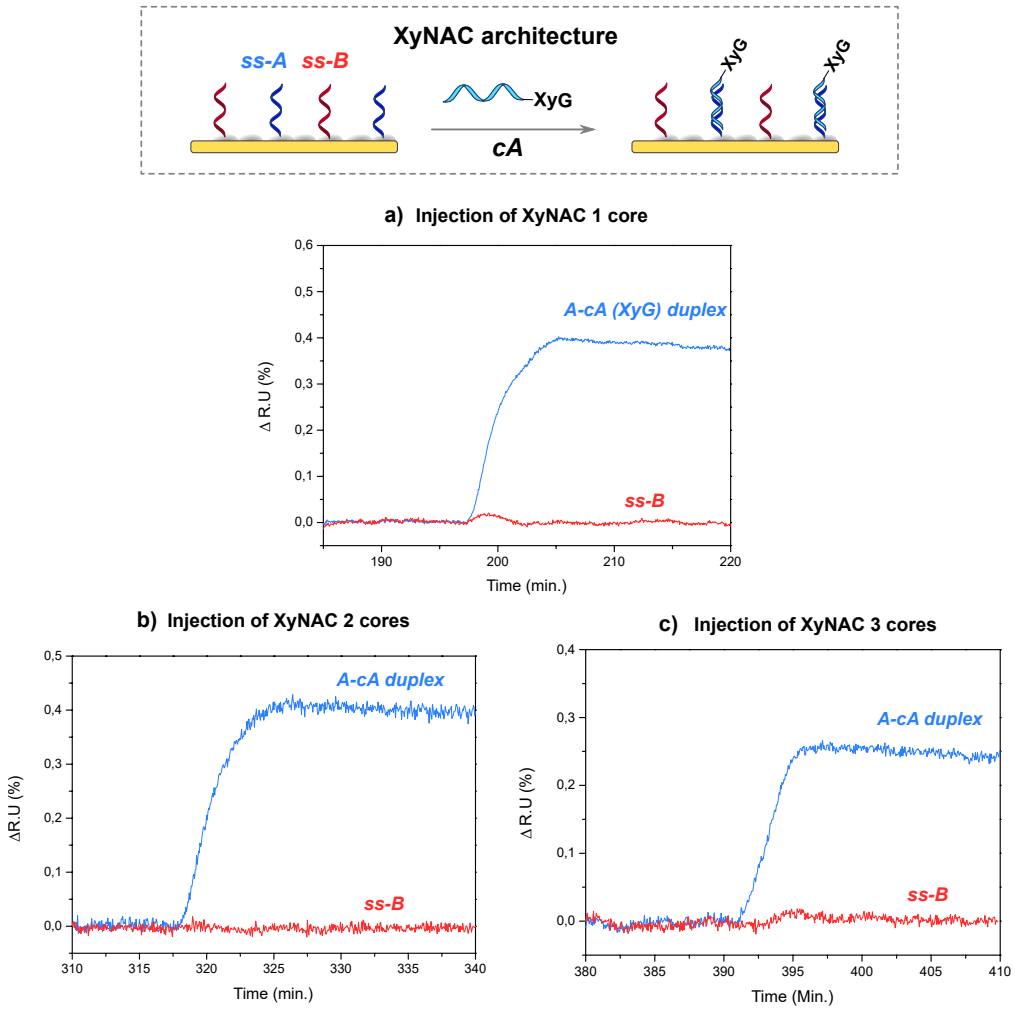

Figure 4.21: Specific immobilization of XyNAC architectures (XyG 1 to 3 cores) containing the cA-ODN sequence at almost saturation *via* DDI approach monitored by SPRi. Running buffer at 10 mM HEPES with 150 mM of NaCl and 0.005% Tween 20 at pH 7,4. a) Hybridization sensorgram of A-cA (XyG 1 core) duplex formation on chip. b) Hybridization sensorgram of A-cA (XyG 2 cores) duplex formation on chip. c) Hybridization sensorgram of A-cA (XyG 3 cores, 300nM) duplex formation on chip.

Likewise, the Figure 4.22 the SPRi analysis of the immobilization process for the larger XyG structures (from 3 to 5) with the opposite sequence.

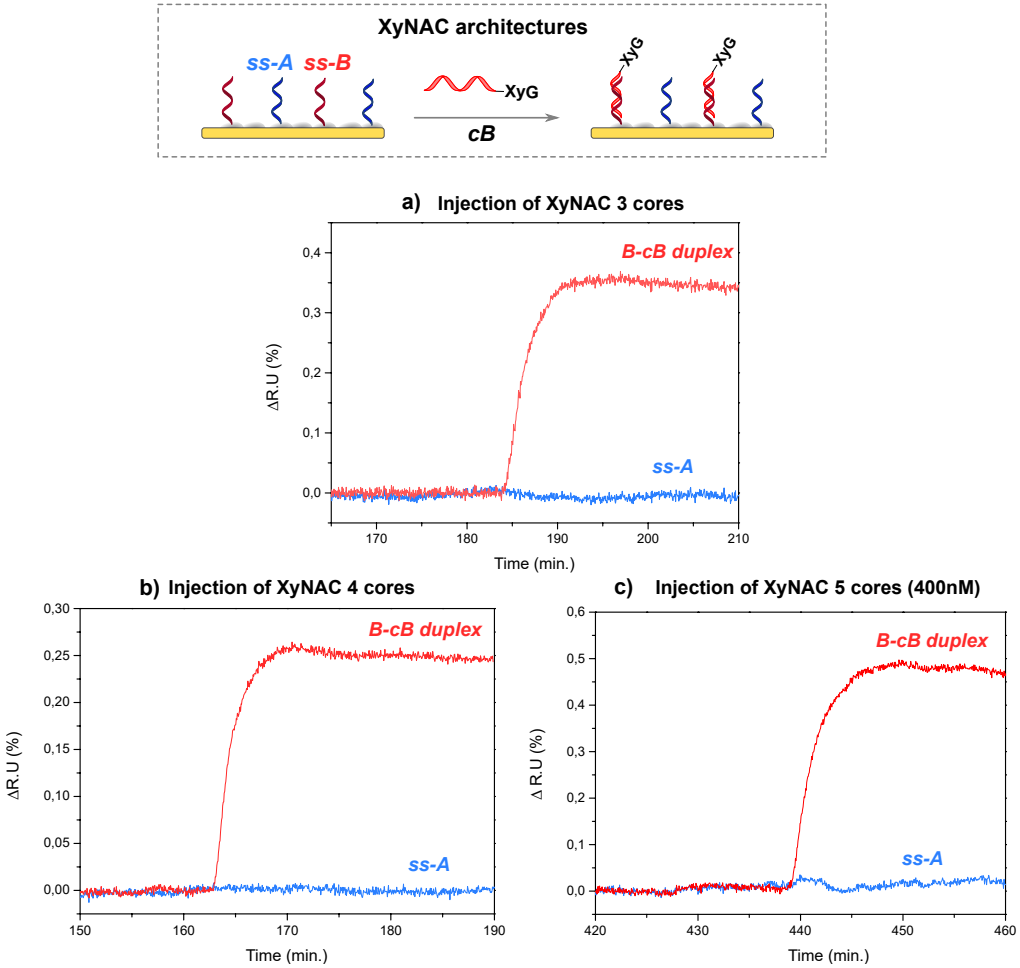

Figure 4.22: Specific immobilization of XyNAC architectures (XyG 3 to 5 cores) containing the cB-ODN sequence *via* DDI approach monitored by SPRi. Running buffer at 10 mM HEPES with 150 mM of NaCl and 0.005% Tween 20 at pH 7,4. a) Hybridization sensorgram of B-cB (XyG 3 core) duplex formation on chip. b) Hybridization sensorgram of B-cB (XyG 4 cores) duplex formation on chip. c) Hybridization sensorgram of B-cB (XyG 5 cores, 400nM) duplex formation on chip.

Larger XyNAC probes bearing the sequence cB were monitored by SPRi biosensor. The hybridization process of each sample injection provided selective and defined variation in the reflectivity signal on SPRi.

Knowing the selective hybridization of the XyNAC architectures, we explored the conception of the DDI approach over a stepwise injection of two XyNAC probes.

The efficiency and selectivity of DNA/DNA interactions were monitored by SPRi in real-time (Figure 4.23-a). The hybridization process was developed on a biochip containing 18 spots of ODN probes organized in a defined pattern (Figure 4.23-b). In this study, we immobilized the XyNAC architectures bearing 3 and 4 cores successively within the same experimental conditions.

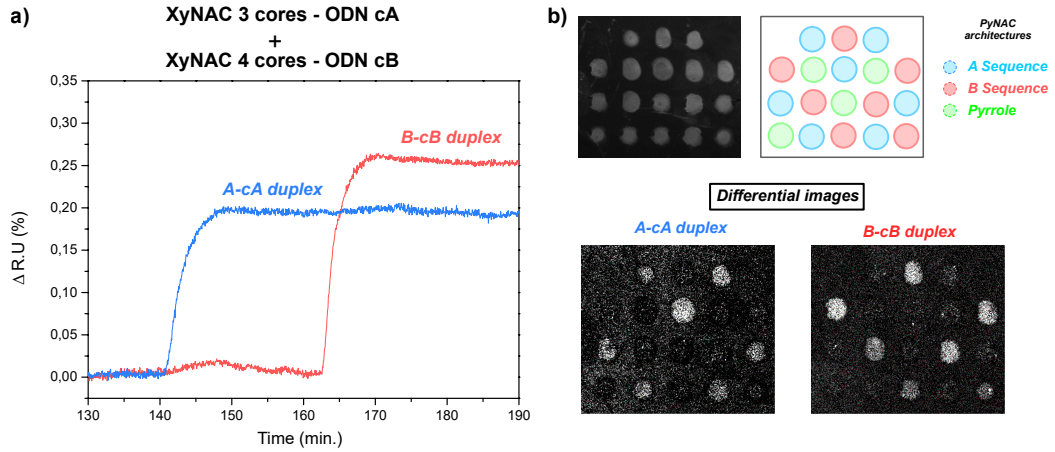

Figure 4.23: Real-time observation of the selective immobilization of XyNAC architectures (3 and 4 cores) *via* DDI approach monitored by SPRi. a) Sensorgrams obtained with the injections of XyNAC architecture with 3 cores (blue signal) and subsequent injection of XyNAC architecture with 4 cores (red signal). b) Schematic representation of the experimental glycochip composed by PyNAC architectures containing A sequences (blue), B sequences (red) and pyrrole (green) distributed in a defined pattern of 18 total spots. The SPRi differential images of the XyG glycochip after the injection of XyNAC 3 cores (cA) and 4 cores (cB) at 500 nM.

Regarding the sensorgram in the Figure 4.23-a, each complementary XyNAC architecture injected into the biosensor gave significant SPR responses with the respective ODN strands attached on the surface. The SPRi signals were detected with well-defined curves under a high signal-to-noise ratio.

Simultaneously, all the interacting spots were recorded by the CCD camera during the binding interaction in real time. The complementary hybridization of each spot were illuminated in response to the pairing hybridization at the sensor surface. In comparison with the spot reference image before injection, a selective immobilization pattern was captured for both XyNAC architectures interactions.

Overall, we have demonstrated a selective and specific DDI approach to anchor plant cell wall polysaccharide probes for the glycochip fabrication according to the literature.[147,148,169] Furthermore, the SPRi technique allowed the characterization

of the ODN hybridization process at the sensor surface in real-time. Therefore, this immobilization strategy provided the presentation of two different XyNAC architectures in a resolvable pattern for further multiplexed binding assays. Finally, the noncovalent but stable interaction of ODN duplexes allowed the regeneration and therefore, reuse of the biochip for further glycan-ODN hybridizations.

4.4 On Chip Validation of Grafted Xyloglucan Probes. Stage 2

The immobilization of XyNAC architectures was a pivotal step in the fabrication of XyG glycochip through DDI strategy. In this stage, a validation assay of the XyG's ability to interact (accessibility, orientation and integrity) was addressed using an antibody specific of XyG structure. We used for this experiment was the monoclonal anti-Xyloglucan LM24 (Rat Ig2a) and it was commercially available from PlantProbes, UK. The LM24 binds preferentially to the XLLG motif of xyloglucan structure according to the supplier specification.

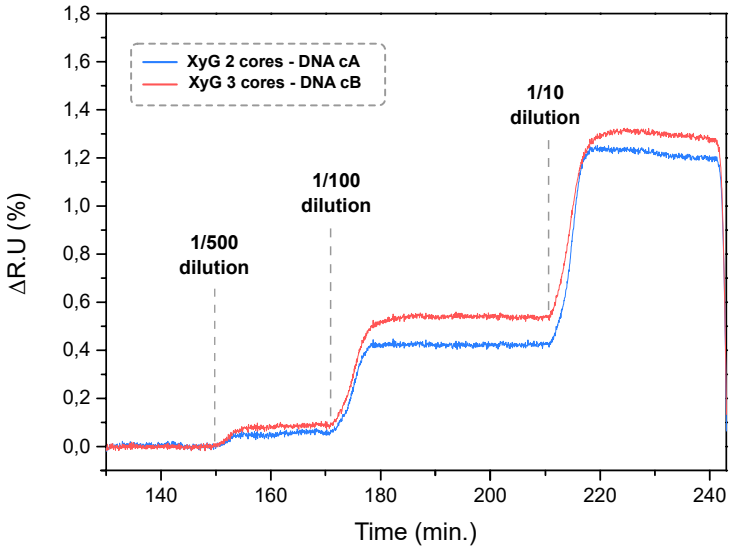

Figure 4.24: Sequential injections of LM24 dilutions (1/500; 1/100; 1/10) upon XyG probes (2 and 3) detected on SPRi.

A first assay was developed to estimate the optimal concentrations of the LM24 for SPRi monitoring. To that end, three different LM24 dilutions (1/500, 1/100 and 1/10) were injected successively and monitored by SPRi onto XyG structures with

two different building-blocks (2 and 3). The sensorgram is depicted in the Figure 4.24.

Results from the Figure 4.24 showed a sensorgram with gradual increase in reflectivity percentage on the XyG spots while the LM24 concentration increased. The most diluted injection (1/500) produced a too small signal. Considering the positive interaction of both 1/100 and 1/10 AB dilutions, we decided to use the higher AB dilution (1/100) to validate the accessibility of XyG probes on the glycochip.

For this experiment, two SPRi assays were developed to explore the binding recognition of LM24 antibody upon XyG building-blocks displayed on the surface (Figure 4.25). Unmodified ODN probes were used as a negative control for both SPRi assays.

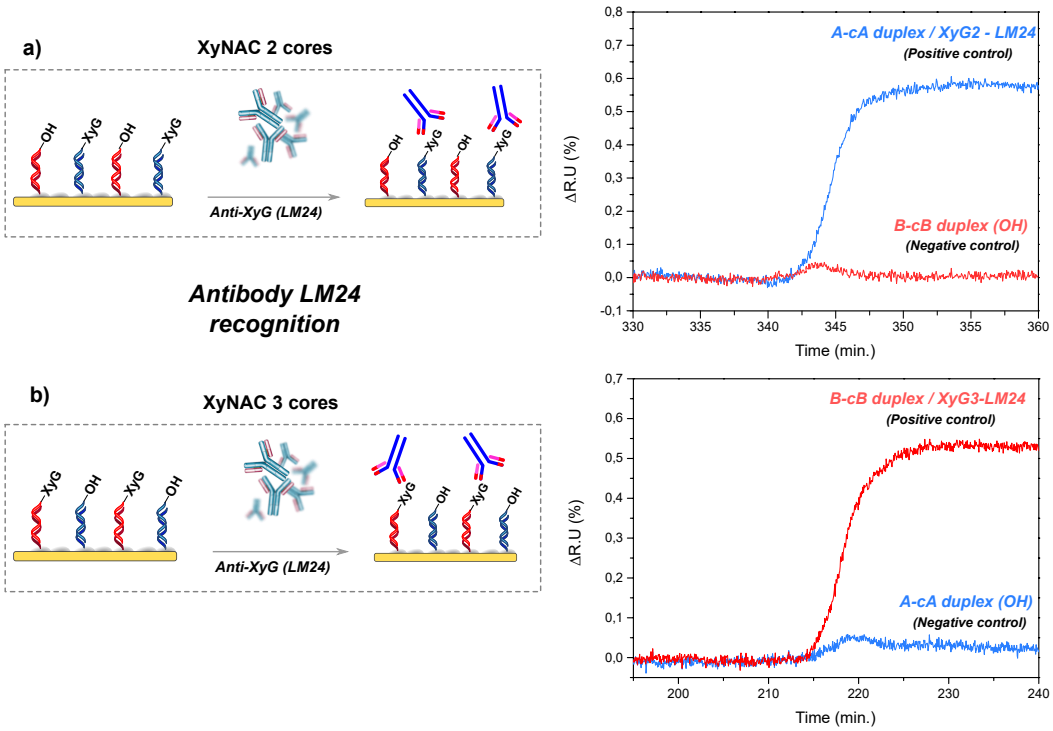

Figure 4.25: Validation of XyG probes accessibility on the glycochip by LM24 antibody (1/100 dilution) monitored by SPRi in real-time. a) Sensorgram of the selective LM24 recognition upon XyNAC 2 cores (positive control) versus unmodified cODN. b) Sensorgram of the selective LM24 recognition upon XyNAC 3 cores (positive control) versus unmodified cODN (negative control).

In the first assay (Figure 4.25-a), XyNAC architectures (2 cores) was anchored on the surface *via* DDI previously described. The sensorgram showed that the LM24 antibody recognized the XyG 2 probes with high specificity (blue curve) in comparison with the unmodified ODN probes. On the other hand, the second assay (Figure 4.25-b) was evaluated changing the ODN sequences and the XyG sample. In this case, XyG 3 cores and unmodified ODN were used instead. Similarly, the sensorgram revealed a specific binding recognition of the LM24 antibody upon the anchored XyG probes (red curve).

From our evaluations, we can conclude that the LM24 exhibited specific interactions with the XyG probes and no binding event on unmodified ODN pairing was observed. Furthermore, the LM24 proved the accessibility, orientation and integrity of XyG 2,3 oligosaccharides on the chip with no mismatch interactions with the negative control. Therefore, this assay conclude the operational viability of the glycochip for further interactions with XyG binding proteins.

4.5 Xyloglucan Glycochip Applications towards FUT1 Enzyme Interaction Recognition. Stage 3

This last section aims at the implementation of XyG-based glycochips for the direct monitoring on SPRi assays of a plant cell wall fucosyltransferase (FUT1) under native conditions of the enzyme. Complementary analytical techniques in solution such as MALDI-Tof MS analysis were carried out for a better comprehension of FUT1 binding recognition.

Within a first part of this section was dedicated to prove the activity of FUT1 on XyG enzymatic activity in solution using GDP-Fuc as acceptor molecule. For this study, MALDI-Tof MS analysis and ITC assays were employed prior the SPRi analysis. Finally, the FUT1-XyG binding recognition was interrogated against anchored XyG probes by SPRi analysis in real-time.

Activity detection of FUT1 enyzme by MALDI-TOF MS

Prior SPRi assays, the FUT1 enzyme was evaluated against the XyG 3 cores as a proof of activity by MALDI-Tof MS. Based on the literature[20] the FUT1 enzyme can only transfer 1 fucose molecule per core. Considering that XyG probes harbour an oligonucleotide structure, the corresponding XyNAC architecture was therefore tested against the enzyme. The single-strand ODN fragment is a polyanionic biomolecule with high molecular weight that somehow, could be a sensitive molecule for the enzyme by forming electrostatic interactions or exhibiting some

steric hindrance that alter the final transfer activity. Therefore, both XyG 3 cores and the XyNAC architecture were used as an acceptors molecules for the AtFUT1 enzyme. To monitor the fucosylation reaction, a mass analysis of two samples was evaluated after 2 and 24 hours of reaction.

The Figure 4.26 below illustrates the enzymatic reaction monitored by MALDI-Tof MS where three mass spectra were displayed over time within the same range of mass for comparative purpose.

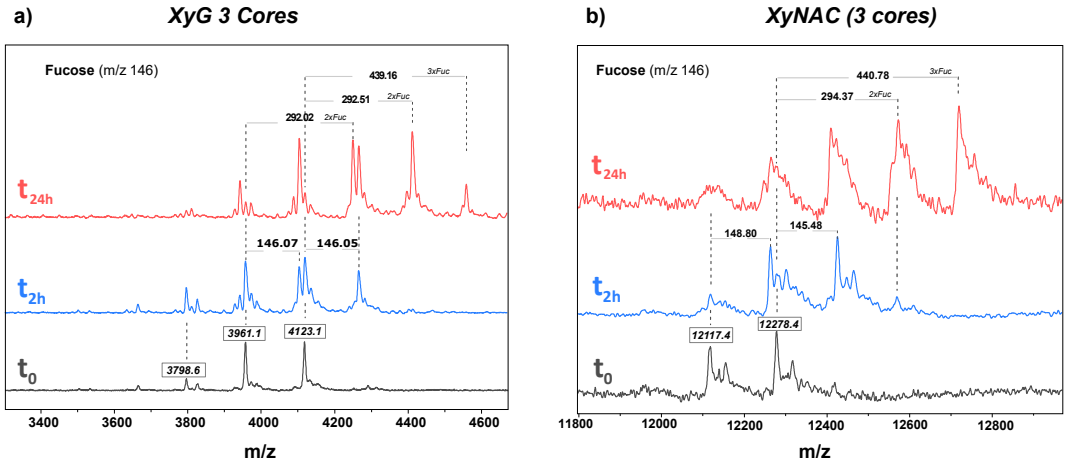

Figure 4.26: MALDI-Tof MS analysis of fucosylation transfer activity after 1 hour, 2 hours and overnight from AtFUT1 enzyme to XyG ligand. a) MALDI-Tof MS spectrum of XyG 3 cores ligand. b) MALDI-Tof MS spectrum of XyNAC architecture (3 cores).

Firstly, the fucosylation reaction over the XyG 3 cores was evaluated to serve as a positive activity control. In the Figure 4.26-a, the starting material (t_0) exhibited three main peaks well defined at m/z 3798.6, 3961.1 and 4123.1. After 2 hours of reaction (blue spectrum), new peaks appeared separated around 146 g/mol indicating a mono-fucosylation of the XyG ligand. Those peaks are shifted from the initial ones within an interval of 16 mass units. Finally, the MALDI-Tof spectrum during an overnight reaction (red spectrum) showed a reduction of the initial peaks and a successive progression in the fucose transfer yielding a XyG ligand harbouring 2 and 3 fucose per initial peak. Therefore, the mass analysis confirmed that: 1) the XyG 3 cores was a suitable acceptor molecule to explore binding interactions and 2) the positive control of the FUT1 activity over XyG acceptor.

A second enzymatic assay was performed in order to address the activity of FUT1 over XyG acceptor (3 cores) bearing the oligonucleotide structure. In the Figure

4.26-b, two main peaks were identified within the initial XyNAC architectures at 12117.4 m.u and 12278.4 m.u. Within the first two hours of reaction (blue spectrum), the mass of the XyNAC architecture was shifted 146 mass units indicating a mono-fucosylation of the starting peaks. The overnight enzymatic reaction provided a di-fucosylated and tri-fucosylated conjugates of the XyG acceptor domain. Overall, the accessibility of the enzyme upon the XyG domain was not affected when it is conjugated with an ODN scaffold.

Overall, the MALDI-Tof MS allowed the evaluation of the FUT1-XyG enzymatic transfer reaction as a positive proof of activity. Both XyG and XyNAC architecture with 3 cores were confirmed as a suitable acceptor molecules towards the biomolecular recognition by SPRi. The XyG containing 3 cores can only be observed 3 fucose maximum to saturate the XyG acceptor, which confirmed our findings as referred previously. Finally, although only the XyG 3 cores was explored in this section, similar results were experimentally confirmed for the XyG 4 and 6 cores.

Preliminary test of FUT1-Xyloglucan recognition on glycochip monitored by SPRi

MALDI-Tof MS analysis demonstrated the transfer activity of the FUT1 over different XyG acceptors. The implementation of the XyG glycochip was evaluated for the study of the interactions between XyG and FUT1. The binding recognition was characterized by SPRi assays under native conditions of the enzyme in real time.

The XyG glycochip was elaborated by the immobilization of XyNAC acceptor molecules using the validated DDI approach. For this assay, different sizes of XyNAC probes (3 and 4 cores) were simultaneously presented for FUT1 binding recognition. Pyrrole spots were defined as a negative control. The Figure 4.27 illustrates the SPRi sensorgram of the FUT1 interaction with the grafted XyG probes at 500 mM concentration.

The sensorgram in the Figure 4.27 showed an increase in the SPRi signal after injecting the enzyme. Both XyG probes exhibited a positive interaction with almost the same initial tendency in the association with the FUT1 enzyme. On the other hand, pyrrole spots exhibited less interaction with the FUT1 injection compared to the other spots containing a XyG fragment. However, the reproducibility of this assay need to be improved by presenting a set of different sizes of XyNAC architectures and other negative control (celloheptaose, maltodextrine) to address the binding interaction of the FUT1 by SPRi.

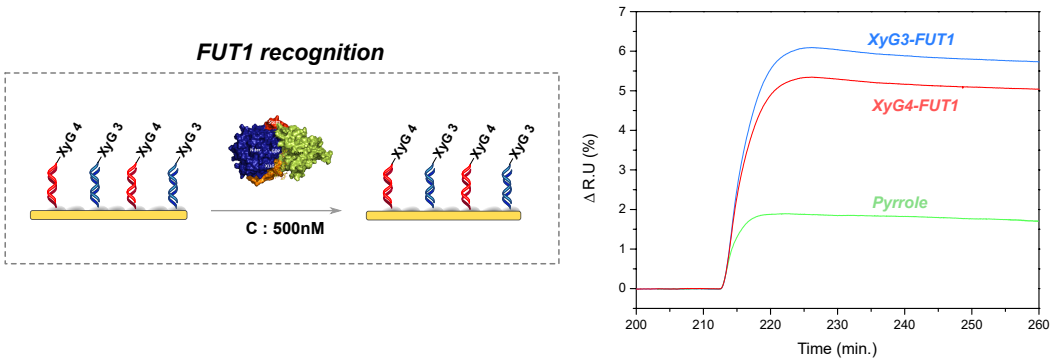

Figure 4.27: SPRi sensorgram of anchored XyG 3 and 4 cores for AtFUT1 fucosyltransferase enzyme recognition (500 nM).

The final strategy aimed to monitor glycan binding interactions by SPRi and analyse the modified product after dehybridization. A single experiment was attempted to do by monitoring the fucosylation transfer reaction. The glycochip was prepared by immobilizing a XyNAC architectures (acceptor) and, the subsequent unmodified ODN to define a negative fucosylation control. The FUT1 enzyme was mixed with the GDP-Fucose donor forming an enzyme-donor complex prior injection. Finally, to confirm the enzymatic transfer event on the glycochip, a dehybridization step was tried thanks to the noncovalent interaction of the ODN using a solution of NaOH 100 mM.

These SPRi results (data not shown) concluded that the FUT1 interacts unspecifically with the free ODN on the chip. However, the sample was unclear and difficult to defined the final fucosylated product. Nevertheless, these results encourages to optimized this dehybridization stage for further modification probes and having more product to be released to improve the mass detection. Since we only performed this experiment once, these results need to be reproduced and optimized multiple times using both, different probes and SPRi conditions to be more precise in the conclusions.

4.6 Conclusion

In the general process of understanding the biochemical functions of putative glycosyltransferase enzymes, the conception of glycoarray has emerged as a powerful alternative to cross the threshold in glycoscience.

The first stage was dedicated to the elaboration of XyG glycochip using a DDI approach characterized by SPRi assays.

Prior surface immobilization of XyNAC architectures, a quality control of the ODN probes as well as DNA/DNA hybridization process were successfully detected in solution by DNA electrophoresis gel. Then, the selectivity and specificity of the DDI approach were confirmed by SPRi assays in both single injections and stepwise injections. Furthermore, the CCD camera allowed the visualization in real-time assays of the site-selective immobilization of XyG probes at the sensor surface. In summary, DDI approach is consolidated as an original strategy to elaborate XyG glycochips in a resolvable pattern displayed on biochips compatible with SPRi technique for multiplexed binding assays.

A second stage was performed in order to characterize the glycochip. The LM24 antibody exhibited specific interactions with the XyG probes and no binding event on unmodified ODN pairing was observed. Furthermore, it proved the accessibility, orientation and integrity of XyG probes on the chip that conclude the operational viability for XyG binding proteins.

In the last stage, the XyG glycochip was adapted towards the FUT1 enzyme recognition by SPRi analysis. Prior on chip recognition, FUT1 activity test monitoring was evaluated using MALDI-Tof MS analysis. This technique allowed the mass detection of the fucosylated product over time from the XyG and the XyNAC architectures incubated with the FUT1 enzyme at 30°C. The results concluded with an active FUT1 enzyme over a set of XyG and XyNAC probes (data shown for the XyG 3cores).

Then, a very preliminary assay XyG glycochip was performed as a first approach in the FUT1 binding assessment. Although a FUT1 binding response was detected by SPRi, it has yet to be reproducible by presenting different probes and negative control in order to explore kinetic interactions.

Finally, the AtFUT1 enzyme has been studied in terms of binding recognition and transfer activity. We have explored the enzyme activity in solution and over time through MALDI-Tof MS analysis. These results have been tested with the XyG ligand and XyNAC architectures as a active molecules on the chip. All results in mass from the MALDI-Tof MS analyses exhibited a positive transfer activity from the AtFUT1 over both substrates indicating that the presence of ODN on the XyG conjugate did not alter the binding recognition of the XyG ligand.

5 Experimental procedures

This chapter describes the experimental procedures for the preparation, purification and characterization of the starting material which build the glycochip. It also details the heterologous expression and purification of the active and soluble AtFUT1 enzyme in insect cells. Then, the chemical synthesis of XyG-based ODN architectures is described. Finally, the SPRi set-up and working conditions are also detailed for the conception of glycochips towards protein-XyG interactions.

Contents

5.1 General Protocol for the Production of an Active and Soluble AtFUT1 enzyme

Unless otherwise stated, all chemicals were purchased from commercial sources and used without further purification. Preparation of biological samples and culture media were developed in aqueous solution using H_2O milliQ grade. Counting cells were followed using an haemocytometer (Brand?) and a microscope Olympus CK40 (x100). Nickel-sepharose resin (cOmplete™) was purchased from Sigma and nickel affinity column (HisTrap™Excel) was purchased from GE Healthcare. Purification step was carried out using NGC™chromatography system from BioRad. SDS-PAGE was performed with the BioRad electrophoresis kit. UV quantification was carried out by NanoDrop™2000 spectrophotometer (Thermo Scientific) at indicated wavelength. Activity test was developed with a GDP-Glo™kit supplied by Promega. Microplate Luminometer GloMax®from Promega was used for the bioluminescence assay. TECAN spectrophotometer was recorded for bioluminescence readout.

5.1.1 Heterologous expression of $His_{\Delta 68}$-AtFUT1 in insect cells

A truncated form of the plant cell wall enzyme fucosyltransferase 1 from *Arabidopsis thaliana* was expressed and purified, motivated by previous studies in our group of this particular enzyme.[44] The final gene sequence conformed the soluble and catalytic region of the enzyme structure missing 68 aminoacids residues from the N-terminus and providing an extra 6x Histidine tag to produce $His_{\Delta 68}$-AtFUT1 structure.

Preparation of EX-CELL 405 culture medium

A stock solution of 1 L of culture medium serum-free EX-CELL 405 was prepared by mixing 42.71 g/L of dry powder media and 0.35 g/L of $NaHCO_3$ until fully solution. The pH was adjusted to 6.2-6.4 with 1 N KOH or 1 N HCl solutions. Finally, the culture medium was left under stirring for 1 hour, filtered through 0.22 μm of sterile filter and finally, stored at 4°C prior use.

Production-loop of Insect Cells Culture in suspension

An insect cell line from *Trichoplusia ni* (High-Five™; Invitrogen) was thawed from liquid nitrogen to room temperature on a water bath at 35°C. Then, the cells were transferred to 10 mL of serum-free EX-CELL 405, equilibrated for 40 minutes and centrifuged at 500xG for 5 minutes. Finally, they were resuspended with another 10 mL of serum-free EX-CELL 405 supplied with 50 μg/mL of gentamicin in a 100 mL autoclaved Erlenmeyer at 22°C under shacking at 135 rpm with a final cell density of 0.5 millions of cells/mL (MC/mL). The cells were grown and split with fresh

culture medium for three weeks to get a final density estimation around 2 MC/mL in a 1,5 L of culture medium.

Estimation of the Cell Size from suspension cells

Cells were counted using a glass haemocytometer with a cover slip previously clean with ethanol at 70% under a microscope (x100). 50 μL fraction of cell suspension was taken and diluted in 40 μL of PBS and 10 μL of trypan blue in an Eppendorf tube. The cell suspension was mixed gently and placed on top of the glass by filling the gap underneath the cover slip by capillary action. The number of cells viability per millilitre was measured taking the average of living cells per grid multiply by 2, to correct the initial dilution factor 1:2, and multiply by 10^4.

Recombinant expression of His$_{\Delta 68}$-AtFUT1 with Baculovirus in suspension

A volume of 1.5 L containing the cells in suspension with around 2 MC/mL was harvested in presence of Baculovirus particles (PharMingen) containing the gen-of-interest. They were incubated for 4 days at 28°C under shaking at 110 rpm. On average, the counting on the number of living cells might be reduced below 20%. The multiplicity of infection factor was estimated between 2.5-5. The supernatant baculovirus-infected cells was transferred and centrifuged at 13000xG in a 1 L centrifuged bottles (Nalgene) for 30 minutes to remove the cell pellets and collect the AtFUT1 protein soluble within the culture medium. Finally, the medium was filtered through 0.22 μm filter and stored at -80°C for further purification.

Detection of His$_{\Delta 68}$-AtFUT1 by Nickel beads resin after Baculovirus infection

To assess the production of the His$_{\Delta 68}$-AtFUT1 protein after baculovirus infection, a Nickel-sepharose resin (GE Healthcare) solution was used. A small metal affinity purification was carried out in solution taking 50 μL of Nickel beads resuspended in a 2 mL Eppendorf tube. The beads were washed three times with 500 μL of water to remove the ethanol within the stock solution. Subsequently, 1 mL of culture medium (supernatant) was mixed with the beads and stirred for 2 hours at 4°C. Next, the sample was centrifuged at 6000 rpm for 1 minutes to pull the supernatant out. The Nickel-His$_{\Delta 68}$-AtFUT1 complex within the resin was rinsed twice first, with 1 mL of equilibrium buffer (NaCl 500 mM, HEPES 25 mM, pH 7.4) to adjust the beads to the new buffer solution; secondly, with 1 mL of washing buffer (NaCl 500 mM, HEPES 25 mM, imidazole 10 mM, pH 7.4) to remove non-specific binding protein interaction; and ultimately, with 35 μL of elution buffer (NaCl 500 mM, HEPES 25 mM, imidazole 500 mM) to rinse the protein from the nickel beads. Then, the resin was treated with 15 μL of denaturation buffer (50 mM of Tris-HCl, pH 6.8, glycerol 20 %, SDS 3 %, β-mercaptoethanol 2% and bromophenol blue

0.01%), heated at 95°C for 5 minutes and centrifuged at 6000 rpm for 2 minutes. Finally, the solution was loaded on 12% of acrylamide gel for SDS-PAGE separation and immobilized onto a nitrocellulose membrane for the Western-blot identification using the anti-Xpress antibody.

5.1.2 Purification by Immobilized Metal Affinity Chromatography, IMAC

The culture medium (around 1 L) containing the soluble fraction of $His_{\Delta 68}$-AtFUT1 protein was gently thawed in the fridge from -80°C to 4°C for 24 hours. The pH was adjusted to 6.8 with equilibrium buffer (NaCl 500 mM, HEPES 25 mM, pH 7.0), filtered through 0.22 μm and degassed. The purification process was carried out with 1 mL nickel HisTrap^{TM} Excel chromatography column and monitored the protein signal by NGC chromatography system from Bio-Rad at 280 nm. The nickel column was joined to the NGC system, pre-equilibrated with water and then, with equilibrium buffer using at least 5 times the volume of the column with a flow rate of 1 mL/mL before the sample injection. Then, all the supernatant was injected through the column with a flow rate of 0.5 mL/min overnight at 4°C and washed with equilibrium buffer afterwards. To recover selectively the protein attached to the nickel column, three different gradients of elution were performed with a flow rate of 0.5 mL/min using a mixture of equilibrium buffer and elution buffer (NaCl 500 mM, HEPES 25mM, imidazole 500 mM, pH 7.0) and keeping, both the running buffers (equilibrium and elution) and the nickel column at 4°C. The first gradient of elution was established between 0% to 5% of elution buffer (imidazole 25 mM) for 10 minutes to remove non-binding proteins. The second gradient of elution between 5% to 10% of elution buffer (imidazole 50 mM) for 10 minutes to detach proteins with low binding affinity to the nickel; and finally, a gradient of elution between 10% to 38% of elution buffer (imidazole 190 mM) for 5 minutes to elute the $His_{\Delta 68}$-AtFUT1 protein pure. All the elution steps were collected in 2 mL fractions and traced by SDS-PAGE 10% acrylamide. The fractions from the last step of elution (16 mL total volume) were identified as pure $His_{\Delta 68}$-AtFUT1.

Concentration and Quantification of $His_{\Delta 68}$-AtFUT1

All the fractions containing $His_{\Delta 68}$-AtFUT1 protein were concentrated using Vivaspin concentrators from Sartorius (MWCO 30.000) at 5000xG for 15 min at 4°C to reduce the final volume to 2 mL. Then, this 2 mL of sample were concentrated and washed 8 times with a stabilization buffer (NaCl 150 mM, HEPES 25 mM, pH 7.0) at 5000xG for 30 minutes at 4°C to obtain around 500 μL of pure $His_{\Delta 68}$-AtFUT1 protein. The concentration of FUT1 (MW 150 kDa) was measured by UV detection at 280 nm using a with a extinction coefficient of 89000 $M^{-1} \cdot cm^{-1}$

yielded 1.82 mg/mL of FUT1 pure. The enzyme was stored at -20°C for further experiments.

5.1.3 Activity Monitoring of AtFUT1 by Bioluminescence

These measurements were carried out with a prototype commercial test of GDP-Glo (Promega) under the recommended conditions gave by the supplier. In particular, ultra pure GDP-Fuc was employed from the mother solution which is kept under -20C. All experiments were developed using the buffer solution (HEPES/KOH 10 mM, $MnCl_2$ and $MgCl_2$ 5 mM, pH 7.4) in 25μL, in 96 plates (LUMITRAC 200, Greiner). The kinetic parameters were measured with 6 ng of AtFuT1 (150ng/mL) and concentrations from 62 to 2000 μM for GDP-Fuc and 3 mg/mL for XyG. After 30 min of incubation at room temperature, the reactions were stopped by adding 25μL of "GDP detection reagent" (reagent which contains the GDP-Glo enzyme and the luciferase). The luminescence readout was measured after 1 hour of incubation at room temperature with the Microplate Luminometer setup (Glomax Promega).

5.2 Preparation and Characterization of ODN-based XyNAC and PyNAC Architectures

Unless otherwise stated, all chemicals were purchased from commercial sources and used without further purification. Preparation of chemical and biological assays were developed in aqueous solution using H_2O milliQ grade. Solvents for purification were purchased in HPLC grade. Oligonucleotide substrates were purchased from Eurogentec. Size-exclusion chromatography (SEC) was carried out using Superdex S30 (3x columns serie) equipped with a digital refractometer IOTA 3 detector for XyG purification. De-salting and clean-up were performed by Sephadex prepacked gravity columns (PD MiniTrap G-10, GE Healthcare). NMR spectra were recorded on a Bruker AVANCE 400 MHz spectrometer in the solvent indicated. Agilent Technology RP HPLC was run with C18 column (250 mm x 4.6 mm x 5 μm) using TEAA 10 mM in a gradient of CH_3CN (0% to 22%) in 40 minutes at 40°C. Flow rate of 1 mL/min, UV detection using diode array at 260 and 310 nm. Mass spectroscopy analysis was addressed by MALDI-Tof MS (Bruker MicroFlex™) using a laser wavelength (Azote λ 337 nm) upon samples co-crystallized within an indicated matrix (2,5-dihydroxybenzoic acid, DHB matrix for oligosaccharide probes; 3-hydroxypicolinic acid, HPA for DNA and DNA conjugate probes). ESI mass spectra (ELECTROSPRAY source) were recorded on an Agilent Technology RP HPLC (C18 column 150 x 2 mm x 3 μm) using TEAA 10 mM in a gradient of CH_3CN (0% to 25%) in 40 minutes at 40°C. Flow rate of 0.1 mL/min, UV detection using diode at 260 nm. UV quantification was carried out by NanoDrop™spectrophotometer

(Denovix DS-11) at indicated wavelength. DNA electrophoresis gel preparation using polyacrylamide gel electrophoresis, PAGE (Sigma-Aldrich) and revelation using DNA intercalating agent SyBR gold (ThermoFisher Scientific) under gel documentation system (GelDoc XR+ BIORAD). Melting temperature of DNA duplex was determined by UV/Visible monitoring at 260 nm using Agilent Cary 100.

5.2.1 XyNAC. Chemical Elaboration Procedure

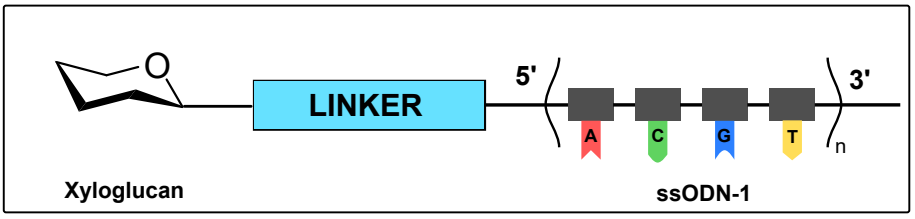

Figure 5.1: Chemical structure of the Architecture I formed by the xyloglucan oligosaccharide, a single-strand ODN scaffold and an organic molecule in between connected to both building-blocks.

Production and Purification of Xyloglucan building-blocks

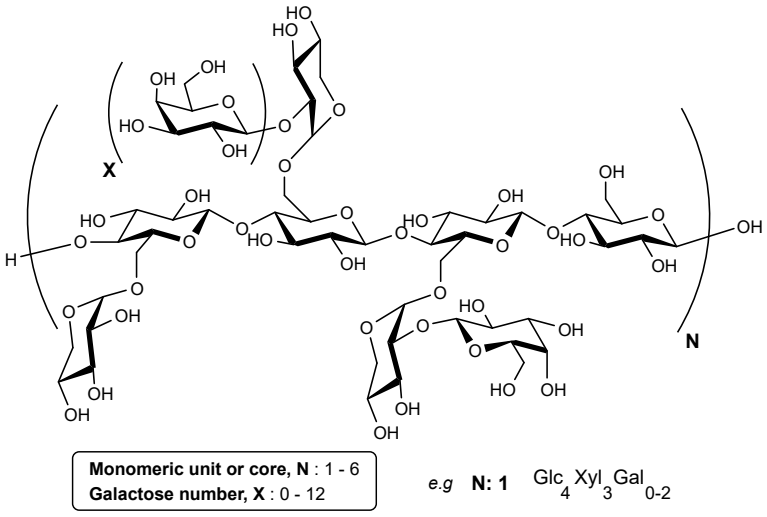

The Tamarin Xyloglucan polymer (250 mg, 575 kDa) was dissolved in 25 mL of warm water containing 5 mL of sodium azide 0.05% under strong stirring. The solution was adjusted with AcOH 4 N at pH 5.6 and then, 0.5 μL of an *endo*-cellulase (Megazyme, *endo*-1,4-β-glucananse) was added to digest the stirred solution of xyloglucan substrate for 5 minutes. Finally, the enzymatic reaction was quenched at 80 °C for 10 minutes, filtrated over 0.22 μm filter and lyophilized. For the purification by SEC Superdex S30, the dry sample was re-dissolved in 10 mL of deionized water, filtered through 0.22 μm filter and injected onto the column with a flow rate of 1.2 mL/min using 0.1 M of ammonium carbonate as mobile phase. The different building-blocks were monitored by refractive index according to their size and collected in fractions of 4 mL. All peaks of interest were and characterized by MALDI-Tof MS (DHB matrix) in positive mode and lyophilized to yield the final xyloglucan products (N:1-6, X:variable) organized in the Table 5.2-Annexe.

Functionalization of xyloglucan building-blocks by Oxime ligation

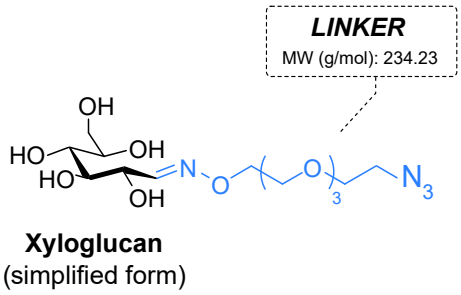

A solution of 1 mL mixture containing a xyloglucan building-block (0.1 μmol-1 μmol, 1 Eq) previously described, the aminooxy-triethylenglycol-azide (0.5 μmol-5 μmol, 5 Eq) and aniline (100 μL, 1 mM) in sodium acetate buffer (100 mM, pH 4.3) was stirred in the dark at 50°C for 48 hours. The reaction mixture was concentrated under reduced reassure and then, clean up and de-salted on Sephadex G-10 eluting with deionized water to yield the final aminooxylated products identified by MALDI-Tof MS (DHB matrix, positive mode) analysis (Table 5.3-Annexe). The final products were used without further purification.

Conjugation of xyloglucan-azide with ODN scaffold by copper-free click chemistry cycloaddition, SPAAC

Within an aqueous solution containing the xyloglucan-azide compound, a 5'-end modified single-strand DBCO-ODN sample solution (2 nmol, 1 Eq) was added and stirred in 100 μL of final volume in the dark at 40°C overnight. The reaction

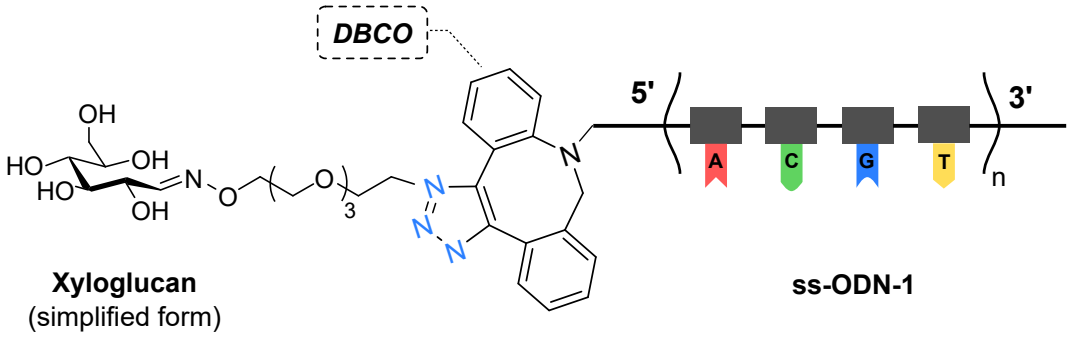

mixture was purified by RP HPLC UV monitoring at 260 nm and 310 nm; and the final product was identified by ESI-MS analysis. Finally, the XyNAC products were quantified by UV detection NanoDrop (260 nm) to afford quantitative yields. Mass analysis described on the Table 5.4-Annexe.

5.2.2 PyNAC. Chemical Elaboration Procedure

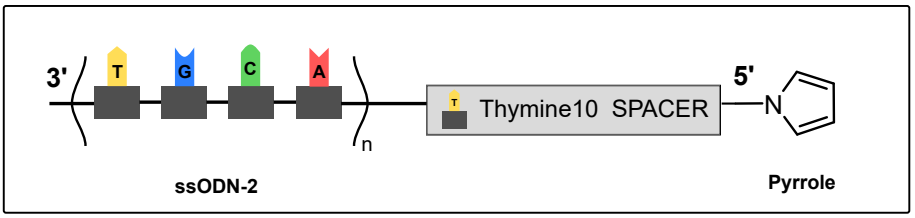

Figure 5.2: Chemical structure of the Architecture II formed by a single-strand ODN scaffold and a pyrrole organic molecule localized in the 5'-end separated by 10 thymine sequence as a spacer.

Synthesis of PyNAC architectures via NHS activated ester

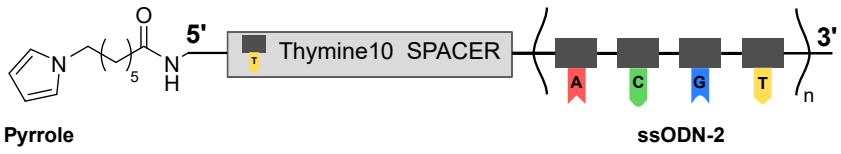

A solution of free-amine single-strand ODN (Eurogentec) (5 nmoles, 1 Eq) in potassium carbonate buffer (100 mM, pH 9.3) was added with pyrrole-NHS (250 nmoles,

50 Eq) solution. The reaction mixture was stirred at room temperature overnight and characterized by MALDI-Tof MS using HPA in negative mode (Table5.5-Annexe). The reaction mixture was purified by RP HPLC UV monitoring at 260 nm and the final PyNAC product was quantified by UV detection at 260 nm NanoDrop to afford quantitative yields.

5.3 Interaction Evaluations in solution

5.3.1 General Procedure for DNA-electrophoresis gel Detection of ODN-based substrates and ODN/ODN duplexes

The presence of ODN conjugates within architectures I and II was qualitatively addressed both in the form of single-strand ODN for quality control, and in the duplex form to evaluate the base pair complementarity. Sample solutions were prepared using an assay buffer (HEPES 10 mM, NaCl 150 mM, $MgCl_2$ 5 mM, pH 7.5) and loaded in 15% PAGE at room temperature. The migration was performed at 5 Watts using 40% solution of sucrose mixed with Xylene Cyanol (XC) and BromoPhenol Blue (BPB) as a dye references. Each solution contained around 8μL of the ODN-based sample and 2μL of the dye reference solution. Likewise, commercial ODN structures were also evaluated.

Quality control of single-strand ODN

Typically, 10 pmoles of ssODN substrate were prepared in an Eppendorf tube containing 20% solution of urea (7M) as denature agent. Then, the ssODN sample solution was heated at 95 °C for 5 minutes with further temperature stabilization prior sample loading. Finally, the dye reference were added to the sample solution, vortex and loaded into the gel. To reveal the samples, the gel was incubated in a diluted solution (1/10000) of SYBR Gold DNA intercalating agent for 5 minutes and characterized by GelDoc fluorescence detection.

Hybridization control ODN/ODN duplexes

Within an Eppendorf tube, 10 pmoles of the single-strand ODN-1 scaffold were incubated with 10 pmoles of PyNAC substrate with the complementary ODN-2 scaffold. Then, the sample mixture was heated at 90 °C for 5 minutes and settled down back to room temperature afterwards (Annealing process). Both the dye reference and 1 μL of the DNA intercalating agent (SYBR Gold) were added to the sample mixture, vortex and loaded into the gel. Finally, the gel was characterized by GelDoc fluorescence detection.

5.3.2 Melting temperature determination of Architectures I and II duplex formation

Within a 1 mL quartz cuvette (1 cm path length), 10 pmoles of the ODN-1 scaffold were incubated in assay buffer with 10 pmoles of PyNAC substrate with the complementary ODN-2 scaffold in a total volume of 100 μL. Melting profiles were obtained in annealing cycles from 20 °C to 85 °C (4x cycles) at a ramp rate of 1 °C /min and monitored by UV/Visible spectrophotometer detection at 260 nm (Agilent Cary 100). The first derivatives of the melting curves provided all the $T_M{}^o$ values for each sample mixture.

5.3.3 Activity of AtFUT1 toward XyG and XyNAC substrates determined by MALDI-Tof MS analysis

The AtFUT1 enzyme (2 pmoles) was mixed with a solution containing the Xyloglucan substrate (50 pmoles, 1 Eq) in ammonium citrate buffer (100 mM, pH 7.4) and the activated donor GDP-Fuc (750 pmoles, 15 Eq) was added to the reaction mixture. The enzymatic reaction was incubated at 30°C under stirring overnight. Samples were taken after 1 hour, 2 hours and overnight; and de-salted by 10μL Zip-Tip C18 micropipette. Finally, mass analysis of the AtFUT1 transfer activity was performed by MALDI-Tof MS in DHB (Xyloglucan building-blocks) and HPA (XyNAC) matrices.

5.4 Conception of DNA-based Glycochip by DDI using SPR Imaging Methodology

5.4.1 SPRi Materials

Chemical reagents and reactants

Unless otherwise stated, all chemicals were purchased from commercial sources (generally Sigma-Aldrich) and used without further purification. Preparation of SPRi buffers were developed in distilled water milliQ grade and filtered through 0.22 μm filters (Millipore). All buffers were stored at -20 °C and thawed at 4 °C prior to use.

- **Spotting buffer**: PBS 50 mM, NaCl 50 mM, 10% glycerol at pH 6.8;
- **SPRi running buffer composition**: HEPES 10 mM, NaCl 150 mM and Tween20 0.005% (v/v) at pH 7.4;
- **Regeneration buffer**: aqueous solution of NaOH 100 mM;

- **Blocking buffer**: solution of BSA (1%) in running buffer;

All the sample probes were dried out at the indicated concentration and re-dissolved in the SPRi running buffer to minimize signal mismatch, prior injection.

Probes and targets biomolecules

The conception of glycochip elaboration involved the DNA-Directed Immobilization and further biomolecular detection. This procedure required a set of probes and targets biomolecules described below. These samples were quantified by UV absorbance (NanoDrop 2000c) before SPRi experiments.

DDI approach was addressed using the ODN pairing sequences described in the Table 5.1 from the ODN-1 (commercial and XyNAC) the complementary ODN-2 (PyNAC) substrates previously synthesised.

DNA-Directed Immobilization. Probes sequences

Commercial and XyNAC	cA (3'-5'): CTG-GCC-ATA-CGC-TGG-ACC-ATA-CGC
cODN-1 probes	cB (3'-5'): ACG-CTA-GCG-TCG-CCA-TTG-GAC-TGG
PyNAC compl.	A (5'-3'): GAC-CGG-TAT-GCG-ACC-TGG-TAT-GCG
ODN-2 targets	B (5'-3'): TGC-GAT-CGC-AGC-GGT-AAC-CTG-ACC

Table 5.1: ODN pairing sequences from XyNAC and PyNAC substrates used for the selective hybridization process on SPRi glycochip

For the biomolecular recognition of the anchored xyloglucan probes, both the antibody LM24 (PlantProbes) and the purified AtFUT1 enzyme were used as xyloglucan binding protein.

5.4.2 SPRi Instrumentation Method Design

The customizable SPR imaging equipment from our laboratory was comprised of four central components: the SPRi optical system (GenOptics, Horiba Scientific), a laboratory air oven (Memmert oven), a fluidic units and finally, a PC monitoring as shown in Figure 5.3.

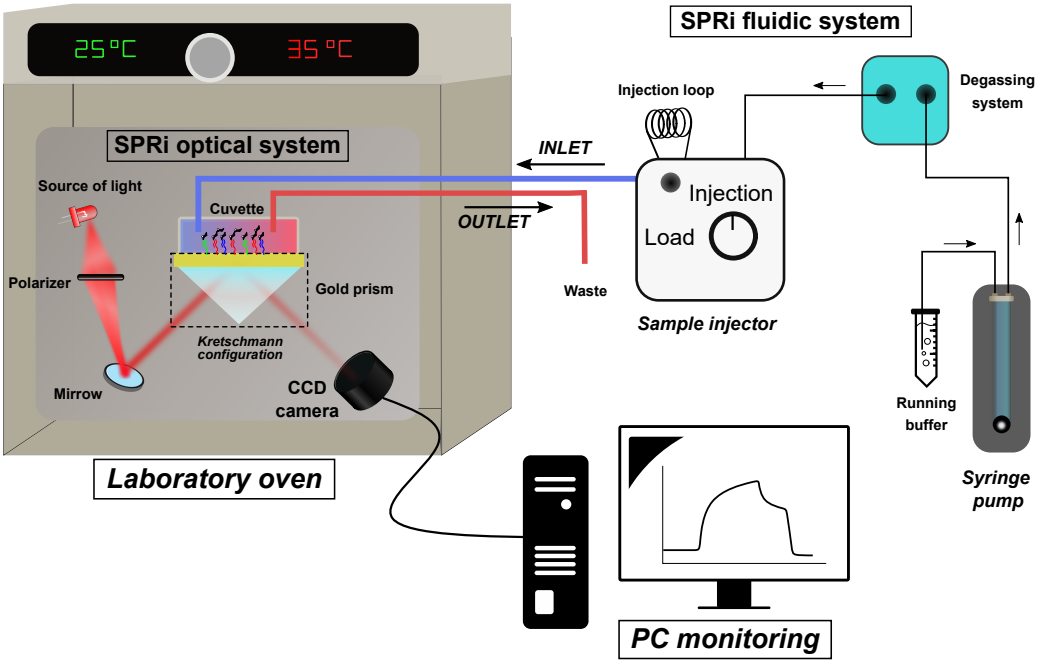

Figure 5.3: General diagram of the SPR imaging experimental design. It encompasses five main components separated in SPRi system inside the laboratory air oven (Memmert Oven), a sample injector, a syringe pump and a PC SPRi monitoring detection.

The SPRi detection system was composed by a SPRi-Biochip™prism coated with a bare 50 nm thick gold surface (HORIBA Scientific-GenOptics, France) suitable for DNA immobilization (DDI), an optical setup and a biomolecular detection system. Our glycochip was defined based on the classical Kretschmann-type optical configuration (Figure5.3) placed inside a laboratory air oven at 25 °C. Furthermore, a polariser was configured in the plane-polarized position to collimate the light at 635 nm passing through some lens and mirrors to illuminate the entire glycochip. All binding information at surface level was collected in real-time by CCD camera that enables a mapping process at defined region wherein a specific recognition occurs. Finally, a PC monitoring software (LabView) transformed the SPR images into a kinetic binding curves (sensorgrams) expressed as reflectivity changes (%) versus time (minutes) as described in the literature.[145,202]

Unified with the SPRi optical system, a cuvette was fixed on top of the gold prism as a closed reactor with a simple inlet and outlet tubes. The sample injector was defined to have two different positions whether to load the sample into the injection loop (100μL) or to inject the sample from the loop towards the glycochip. Within a

non-stop and steady flow rate of 50 μL/min, the running buffer was degassed before reaching the sample injector and circulated along the system with laminar flow via automated syringe pump (Cavro Scientific Instruments, USA). A central carousel served as a mechanism of joining together all the components.

The connection between components was carried out using a biocompatible poly ether ether ketone or, commercially known PEEK tubing with 0.03 mm of diameter.

5.4.3 Preparation of the Glycochip prior SPRi assays

Plasma Treatment of the Glycochip

Two days before use, the gold layer was treated by a plasma source as a powerful technique to clean and achieve a quality coating process. In physics, this treatment is called *Sputtering*, in which energized atoms hits the target surface and eliminates the contaminants off of the surface into the vacuum system. The energetic atoms used in sputter cleaning are created in a plasma state. The most commonly atom that is used in this process is an argon gas source since it is quite inert during the treatment of the surface. A general process of the plasma treatment is depicted in the Figure 5.4.

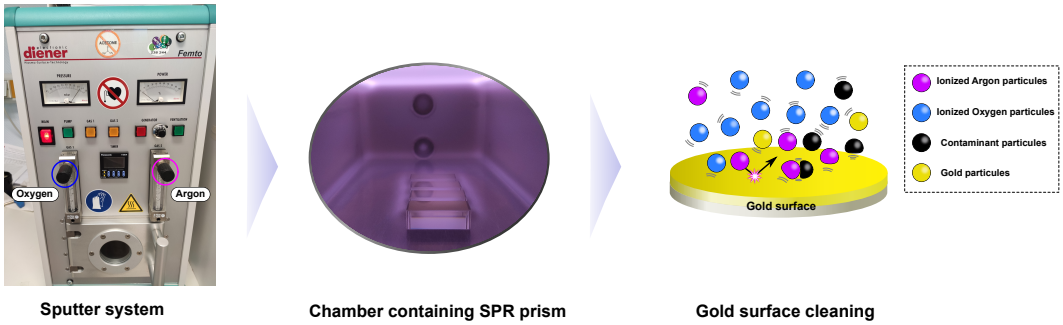

Figure 5.4: Physical procedure of gold surface cleaning via plasma ionization or sputtering. On the left, the sputter system dedicated to plasma treatment (Diener electronic). The gold prism are introduced inside the reactor chamber to be exposed to plasma ionization (Image in the middle). In particular, a mixture of oxygen and argon particles are ionized to both clean and activate the surface (Scheme on the right).

In our sputter system, Femto plasma cleaner from Diener electronics (Figure5.4left), the target biochip was introduced inside the reactor chamber and exposed under lower-vacuum system pump. Then, a source of oxidized plasma was leaked into the vacuum chamber composed by a mixture of Argon gas at 25% and oxygen gas at 75% for 3 minutes, controlled by two manometric valves. When the mixture of gases

were in the chamber, a negative electrical voltage was applied to the chamber (40 W) which strip an electron from the gas atoms (now ionized) that have enough speed to physically knock off individual atoms from the gold prism. This process formed the classical and beautiful plasma auras around the metallic surfaces observed in the Figure 5.4 in the centre. Nevertheless, the exposure time to ionized atoms not only clean the surface from unwanted particles, but also might produces the detachment of gold particles from the surface (Figure5.4 right). Therefore, after the plasma cleaning, the contact surface is highly activated for chemical functionalization.

Spotting of PyNAC substrates by Pyrrole Electrocopolymerization

From stock solutions, the PyNAC conjugates (2 μM) and free pyrrole solution (1 M) were mixed at specific probe density ratio (PyNAC:Pyrrole - 1:20.000) to get 500 nM of PyNAC per spot in spotting buffer according to the literature.[145] Finally, a solution of pyrrole (15 mM) was prepared as a spot reference. Overall, the gold prism presented simultaneously two ODN conjugates (sequence A and B) displayed within a define pattern.

Following the radical reaction in the Figure 5.5a, the electrochemical pyrrole polymerization was induced by supplying an electric pulse of 2 Volts for 100 ms leading to the formation of free-radicals cations on the monomeric pyrrole structures within the pyrrole solution.[151] The actual set-up is depicted in the Figure 5.5b.

The anode was directly in contact with the gold layer (working electrode) and the cathode was connected to a platinum wire (counter-electrode) inserted into a modified micropipette's tip containing the mixture of two solutions (PyNAC and free-pyrrole).[149] Then, these circuit was connected to a potentiostat and the micropipette was fitted in an automatic robotic arm to set precisely the position of each spot solution on the X and Y axis. According to the zoom-scale in the Figure 5.5c, to define the Z axis, the micropipette was manually placed so that the droplet was in contact with the gold surface allowing the formation of the polypyrrole film. Once the first spot has been formed, an automatic setup was configured to draw an array profile or map with all the probes to be spotted as it was depicted in the Figure 5.5d. Finally, the coated biochip was rinsed with deionized water (milliQ grade) and stored in the dark at 4 °C for 24 hours prior SPRi assays.

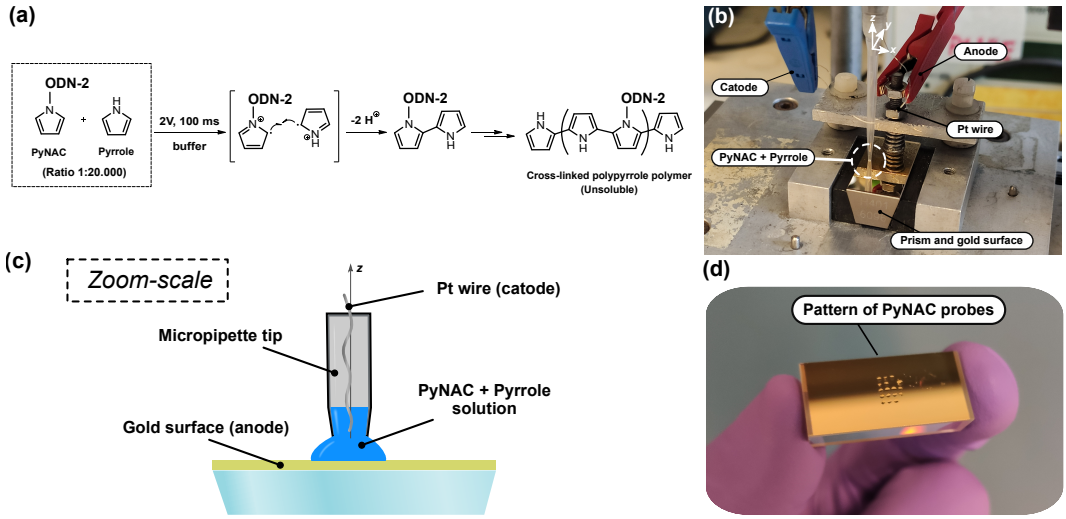

Figure 5.5: Chemical Immobilization of PyNAC architectures on gold surface. (a) Electrochemical Polymerization Reaction of PyNAC structures for gold immobilization. (b) Actual Experimental set-up of the electrocopolymerization of PyNAC architectures. (c) Scheme depicting the pyrrole electropolymerization solution at zoom-scale within the micropipette tip fixing the z-axis. (d) Actual SPRi-Biochip with PyNAC probes spotted onto the gold surface.

Finding the best operating angle

The angular scanning of the gold prism coated with the PyNAC substrates was monitored by the CCD camera which registered several images of each spot at different incident angles. The software provided an SPRi curve of each probe coated the surface showing the SPR-dip at the resonance angle (Figure5.6-a). Then, the definition of the working angle Φ_w is manually fixed close to the maximum slope (sensitive area for all spots) where the minimum variation of the resonance angle ($\delta\phi$) produces a maximum difference of reflectance intensity (δR). At this angle, the CCD camera reconstructs an entire visual image of the different probes (Region of interest, ROI) grafted onto the gold layer (Figure5.6-b). This image serves as a reference for addressing further biomolecular interactions via 2D-differential images response in the gold sensor.

5.4.4 SPRi protocol for the Glycochip Construction by DDI

The specific immobilization process of cODN-1 (commercial and XyNAC) over the grafted ODN-2 target sequences was monitored in real-time by SPRi assays. Prior ODN immobilization, a solution of blocking buffer was injected to minimize nonspecific interactions. Then, a first step of hybridization was carried out using a solution

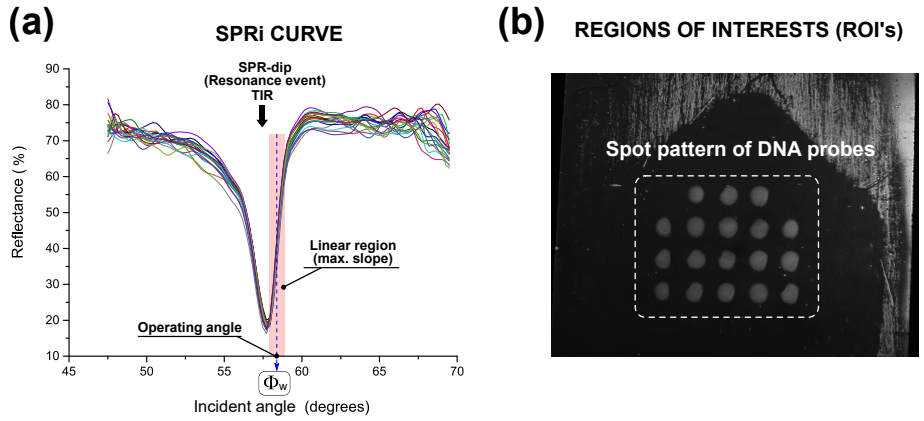

Figure 5.6: Real plasmon curve (part a) and glycochip image (part b) obtained from PyNAC probes prior a SPRi monitoring. This procedure helps to define the working angle and the region of interests wherein the SPRi monitor reflectivity values.

of commercial cODN-1 (1μM) in SPRi running buffer. Non complementary ODN sequence was configured as a negative control. After validation on the chip, a solution of XyNAC (0.5μM) was injected to confirm the specific immobilization of xyloglucan conjugates on the biochip. Finally, the DNA/DNA binding interactions were denatured using the regenerating buffer to remove the cODN-1 probes and re-use the biochip after each analysis.

5.4.5 SPRi Detection of anchored Xyloglucan probes. LM24 Antibody and AtFUT1 enzyme

Similar procedure was performed for the biomolecular recognition in terms of flow rate (50μL/min) and temperature (25 °C). Within a first stage, 500 nM solutions of both cODN-1 substrates (unmodified and XyNAC) were specifically immobilized by DDI previously described. The unmodified cODN-1 substrate was defined as a negative binding control. Then, a solution containing an antibody LM24 (1/100) was injected through the SPRi system to validate the glycochip by monitoring the accessibility of XyNAC conjugates on the surface. Finally, a regenerating buffer was injected to recover the initial configuration for further analysis.

Likewise, this experimental approach was reproduced to determine the binding recognition of the AtFUT1 enzyme. Thus, a stepwise hybridization process of XyNAC substrates (500 nM) were injected and successfully immobilized on the chip. Then, a solution of AtFUT1 enzyme (400 nM) in running buffer was injected on the chip and monitored the reflectivity variations by SPRi.

All SPRi data analysis was treated with Origin 9. Each duplicated spot species was firstly organized and the values were averaged out and plotted. Then, a subtraction of the reference signal to the other signals was developed. Finally, a correction to the zero-baseline was performed to visualize the SPRi curves at the same level enabling comparative studies.

5.5 ANNEXE. TABLE OF MASS ANALYSIS

5.5.1 Xyloglucan building-blocks Mass Analysis

Substrate	calc	found	Substrate	calc	found
N=1			**N=4**		
			X=3	4681,7	4679,8
X=0 (M+Na)	1085,3	1083,7	X=4	4843,8	4842,7
X=1 (M+Na)	1247,4	1246,4	X=5	5005,9	5005,1
X=2 (M+Na)	1409,4	1409,2	X=6	5167,9	5167,1
			X=7	5329,9	5329,1
			X=8	5492,0	5490,8
N=2			**N=5**		
			X=5	6050,3	6049,5
X=1	2268,7	2270,1	X=6	6212,3	6211,1
X=2	2430,7	2431,1	X=7	6374,4	6373,1
X=3	2592,8	2593,1	X=8	6536,5	6535,1
X=4	2754,8	2756,6	X=9	6698,5	6697,1
			X=10	6860,8	6859,4
N=3			**N=6**		
			X=6	7256,7	7254,2
X=2	3475,3	3474,8	X=7	7418,8	7418,2
X=3	3637,4	3637,1	X=8	7580,8	7581,5
X=4	3799,4	3799,0	X=9	7742,8	7743,6
X=5	3961,5	3961,2	X=10	7904,9	7904,6
X=6	4123,5	4123,1	X=11	8067,0	8064,5
			X=12	8229,1	8223,3

Table 5.2: MALDI-Tof MS $[M+H]^+$ assignment found for the xyloglucan building-blocks. The N describes the number of monomeric units (cores) and the X defines the number of galactose molecules within each N structure.

5.5.2 Oxime ligation

Substrate	calc	found	Substrate	calc	found
N=1			**N=4**		
X=0 (M+Na)	1301,3	1301,7	X=4	5059,8	5060,8
X=1 (M+Na)	1463,5	1464,2	X=5	5221,9	5222,4
X=2 (M+Na)	1625,6	1626,9	X=6	5383,9	5383,5
			X=7	5545,9	5544,4
			X=8	5708,0	5703,8
N=2			**N=5**		
X=1	2484,7	2488,0	X=6	6428,3	6428,8
X=2	2446,7	2648,9	X=7	6590,4	6588,1
X=3	2808,8	2811,0	X=8	6752,5	6751,0
X=4	2970,8	2973,6	X=9	6914,5	6916,3
			X=10	7076,8	7077,4
N=3			**N=6**		
X=2	3691,3	3691,4	X=8	7796,8	7801,3
X=3	3853,4	3851,9	X=9	7958,8	7960,8
X=4	4015,4	4012,8	X=10	8120,9	8118,8
X=5	4177,5	4174,7	X=11	8283,0	8276,6

Table 5.3: MALDI-Tof MS $[M+H]^+$ assignment found for the xyloglucan-azide reaction products. The N describes the number of monomeric units (cores) and the X defines the number of galactose molecules within each N structure.

5.5.3 Strain-Promote Azide Alkyne Cycloaddition, SPAAC

XyNAC (ODN-1)

cA sequence			cB sequence		
Substrate	calc. mass	found mass	Substrate	calc. mass	found mass
			N=3		
			X=5	12117	12117
			X=6	12280	12282
N=1			**N=4**		
X=1	9309	9309	X=4	13000	13002
N=2			X=5	13162	13164
X=3	10677	10677	X=6	13324	13326
X=4	10840	10841	X=7	13486	13488
N=3			**N=5**		
X=3	11722	11724	X=6	14368	14369
X=4	11884	11886	X=7	14530	14532
X=5	12046	12046	X=8	14692	14695
			X=9	14854	14857
			N=6		
			X=8	15737	15738
			X=9	15899	15901
			X=10	16061	16063
			X=11	16223	16227

Table 5.4: ESI-MS assignment found for XyNAC reaction products. The N describes the number of monomeric units (cores) and the X defines the number of galactose molecules within each particular N structure

5.5.4 PyNAC mass analysis

PyNAC (ODN-2)			
A sequence		B sequence	
calc.mass	found mass [a]	calc.mass	found mass [b]
10833.12	10832.61	10739.13	10738.93

Table 5.5: MALDI-Tof MS assignment of PyNAC architectures products crystallized with HPA matrix after desalting by NAP-10. [a]∼Calculated exact mass for $[M\text{-}H]^-$. [b]∼Calculated exact mass for $[M\text{-}H]^-$

5.6 ANNEXE. MALDI-TOF MS SPECTRA

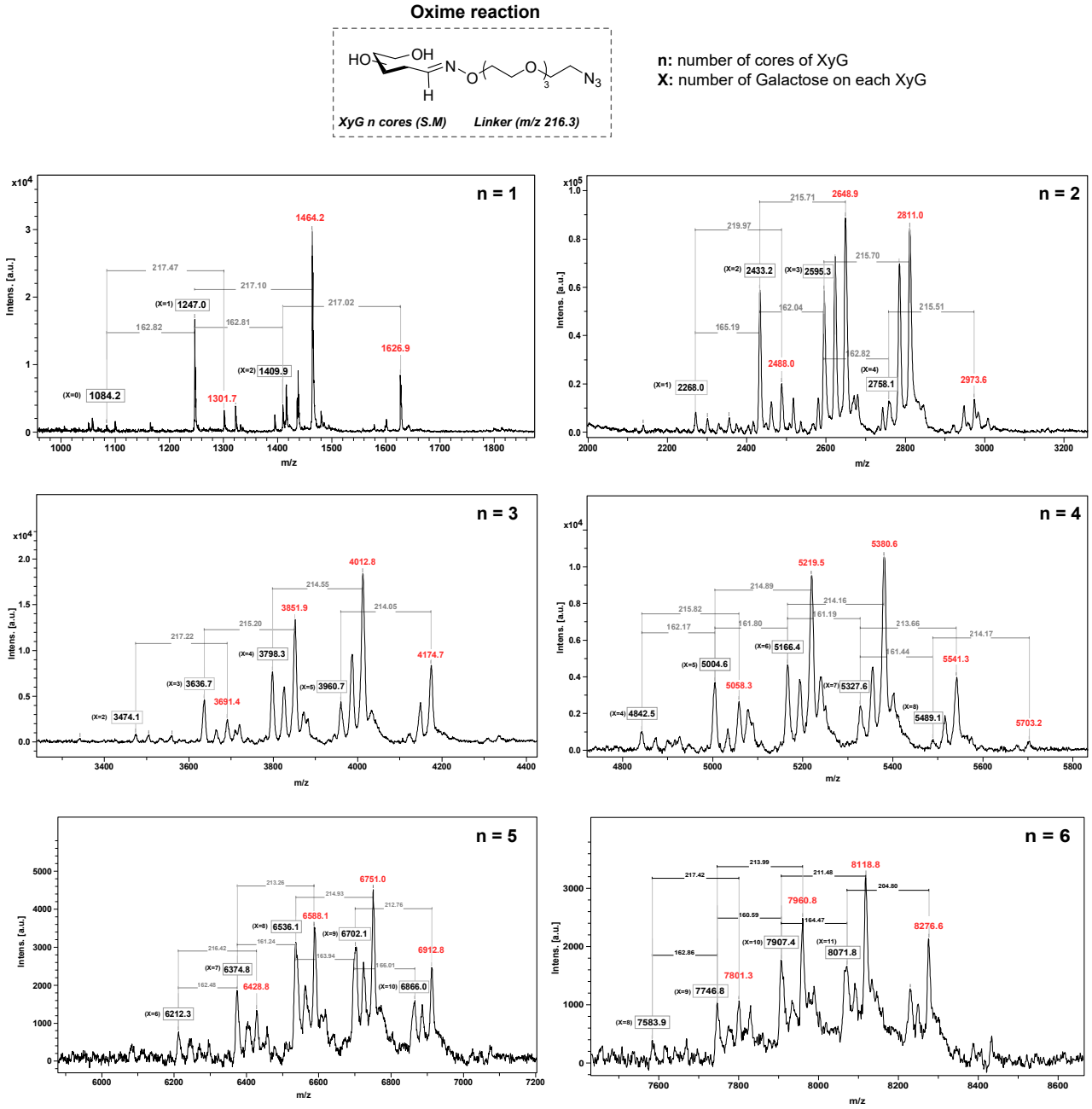

Figure 5.7: MALDI-Tof MS analysis of the XyG oxime product from 1 to 6 cores functionalized by the linker aminooxy-TEG-azide.

6 Conclusions and Future Perspectives

6.1 Final conclusions

This multidisciplinary PhD research project was involved in the Glycoscience framework to address the lack of biochemical information related to the glycosyltransferase enzymes (GT). This family of glycan active enzymes is intimately responsible for the biological glycosylation process in nature that contributes to the higher glycome complexity. Therefore, decoding enzyme-glycan binding interactions is of uttermost importance and priority in the Glycoscience, but yet to be a bottleneck.

To explore the role of this pivotal family of enzymes, we have driven this research project towards the design of an original approach for the elaboration of a versatile glycochip suitable for SPRi biosensor monitoring. The design of the glycochip was promoted by the selective immobilization strategy through selective DNA/DNA hybridization named DNA-Directed immobilization (DDI). Therefore, chemical approaches were established in order to conjugate the glycan probes with an oligonucleotide architecture forming carbohydrate-oligonucleotide conjugates (COCs). Finally, SPRi was chosen as a powerful optical detection technique to address real-time measurements of GT-glycan interactions under native conditions.

In particular, we have been studied throughout this manuscript as a model system of GT, a plant cell wall fucosyltransferase enzyme from *Arabidopsis thaliana* AtFUT1 involved in the last step of the biosynthetic pathway of the XyG hemicellulose ligand. This specific enzyme catalyses the biochemical transfer of a fucose residue from GDP-β-L-fucose donor to a galactose side-chain acceptor in the XyG to afford an α-1,2-fucosylated linkage.

6.1.1 Chapter 2. Active Expression of a Soluble AtFUT1 enzyme

A common challenge for the expression of this type of enzymes is to assess the efficiency of production and promote the biological folding and activity. We pursued in the Chapter 2 our first approach focused on the heterologous expression of an active and soluble form of AtFUT1 adapted for a large-scale of cell culture media (Exc-405). Therefore, a baculovirus-insect cell (High Five™cells) expression system was used for the suitable production in suspension of a truncated His-tagged AtFUT1

form to guarantee a proper enzyme folding. This truncated form corresponded to a recombinant AtFUT1 wherein the first 68 aminoacids residues from the N-terminal were deleted to exhibit enzymatic activity. The final production of the soluble form of AtFUT1 was successfully confirmed by SDS-PAGE and Western blot detection after preliminary capture assays using nickel beads resin.

Our second approach was dedicated to the purification process through IMAC. In particular, the large volume of Exc-405 culture media containing AtFUT1 enzyme in solution was purified using the HisTrap™Excel nickel chromatography column from GE Healthcare. As this method relies on the chelating complex formation between the nickel metal and the histidine sequence, the pH of the culture medium played an important role for a well-formed binding process. Therefore, the Exc-405 media was adjusted with a pH up to 7.1 in order to avoid salt precipitation. Furthermore, the temperature of the culture medium can be determining for the protein stability during the purification process, specially for large loading volumes of culture. Thus, the temperature remained at 4°C throughout the entire process of AtFUT1 purification. Under our current procedure, the AtFUT1 enzyme was recovered after three-steps non-isocratic gradient of imidazole elution (5%, 10% and 38%) for 10 minutes each, and concentrated through membrane under centrifugation.

Finally, we have demonstrated the enzymatic activity of the pure AtFUT1 enzyme using a new bioluminiscent assay from Promega adapted for Leloir-GTs kinetic analysis. For our enzyme of interest, the GDP-Fucose donor was used as an activated nucleotide sugar. This GDP-Glo™kit relies on the *in situ* transformation of GDP released after the transfer reaction into ATP nucleotide that is further detected and quantified using a luciferase/luciferin reaction by UV. Therefore, the indirect monitoring analysis of the light measured was proportional to the fucosylation reaction produced by the AtFUT1 which validate the enzymatic activity. Furthermore, this bioluminescent platform was used to determine the kinetic parameters of the enzyme based on the proportionality between the light readout and the reaction rate (δGDP/δt) at different concentration of the nucleotide donor. Overall, this technique offers a universal bioluminescent assay to measure most of the Leloir-GTs transfer activity or GT inhibition screening at low concentration of enzyme.

6.1.2 Chapter 3. Chemical Preparation of Architectures I and II towards the Glycochip Construction

After producing an active and soluble AtFUT1 enzyme, we focused our efforts to the initial preparation of the main partners involved in the XyG-based glycochip fabrication. In this sense, the Chapter 3 pursued the creation of starting materials containing complementary ODN structures highly motivated towards the original

glycochip elaboration *via* DDI strategy. For that purpose, this chapter entailed chemical approaches to prepare a pairing architectures bearing complementaries ODN scaffolds (ODN-1 and ODN-2):

- **Architecture I**. Comprise the chemical conjugation of XyG building-blocks and ODN-1 scaffold to form COCs.

- **Architecture II**. Comprise an ODN-2 scaffold chemically modified by a pyrrole functional group for further grafting purposes.

The first approach encompassed a synthetic design committed to the development of COCs to define the XyNAC architecture. Thus, a set of XyG building-blocks was obtained after an enzymatic digestion process optimized for the XyG polymer using an endo-cellulase (β-1,4-D-glucanase). As a result, XyG products from 1 to 6 cores were successfully purified by SEC and characterized by MALDI-Tof MS. Then, the chemical ligation of XyG and ODN compounds was carried out in two chemoselective reactions steps through a specific linker in between bearing dual functionalities to form the hybrid products. On the one side, an aminooxy group promoted the formation of the oxime ligation *via* reducing-end from the XyG building-block. This reaction yielded a XyG-linker compound purified by SEC and characterized by MALDI-Tof MS. The other side of the linker was defined by an azide group to facilitate the SPAAC reaction with a cyclooctyne-ODN derivative. The presence of the ODN scaffold allowed the proper purification and UV monitoring of the XyNAC compounds by RP HPLC with further characterization by LC-MS. Regarding the PyNAC architecture, a pyrrole group was successfully added to an ODN scaffold *via* activated ester coupling. Likewise, this architecture was purified by RP HPLC monitoring the UV absorbance readout through the ODN structure and characterized by MALDI-Tof MS.

Finally, the ODN entity from both architectures allowed the gel monitoring *via* DNA electrophoresis as a quality control prior hybridization. As a result, RP HPLC eluted conjugates were confirmed as pure compounds. Nevertheless, some commercial starting materials were not entirely pure and could have alter the final reaction yield. Besides, evaluation of the melting temperature (T_m°) in solution determined a typical hybridization process with no interference from the XyG side.

Based on our results, the conjugation of complex plant oligosaccharides onto ODN scaffolds through chemoselective reactions can offer a potential access to the formation of similar glycoconjugates with different oligosaccharide. Furthermore, we have demonstrated the huge contribution of having an oligonucleotide structure in conjugation to the polysaccharide. This staggering biomolecule modifies the chemical

properties of the glycoconjugate compound enabling the UV detection to enhance the purification and quantification step that otherwise would entail difficulties.

6.1.3 Chapter 4. XyG-based glycochip by DDI approach using SPRi

All partners previously obtained come together in this Chapter 4 towards the construction of a XyG-based ODN glycochip and further AtFUT1 preliminary results monitored by SPRi. Therefore, the architecture II was directly immobilized on the gold surface *via* electrocopolymerization of pyrrole structure in a defined pattern prior glycochip validation.

In our first approach then, the COCs were selectively hybridized on-chip upon the immobilized complementary ODN structure by the DDI approach. The selective hybridization was confirmed and monitored by SPRi assays in real-time and without any label. This findings were consistent with DNA electrophoresis gel assays developed in solution. Furthermore, an optical biorecognition assay by SPRi using LM24 antibody validated the characterization and the ability to interact of XyG probes on the glycochip. Although only two different ODN sequences were studied, these results confirmed the simultaneous analysis of immobilized glycans on the biochip.

Finally, an activity test of AtFUT1 over time were performed against the XyG building-blocks and COCs prior SPRi detection. MALDI-Tof MS findings revealed a fucosylation transfer upon both substrates in solution and confirmed an active AtFUT1 enzyme for XyG binding recognition. We performed some very preliminary SPRi assay for the study of the interactions between the immobilized XyG probes and AtFUT1 enzyme. Although the glycosyltransferase exhibited a SPRi binding response with the XyG probes, the interaction was maybe non specific and further experiences need to be reproduced and optimized to tackle this conclusion.

Once again, we have to highlight the pivotal role of the ODN as a driving force in the selective immobilization of glycan structures on solid support (gold in our case). Moreover, the noncovalent interactions between ODN strands allow the reversibility of the hybridization to recover the interacting product as well as the subsequent reuse of the glycochip.

6.2 Future Perspectives

This ambitious project can be scoped at various future perspectives depending on the scientific demand and be adapted to different biorecognition probes. However,

our PhD approach envisions in a long term strategy, the standardization of a potential high-throughput screening tool for Glycoscience to characterize novel putative GTs, detect transferase activities or identify new GT glycan acceptors in real-time monitoring by SPRi methodology. The compatibility of our glycochip for SPRi assays can contribute in the interrogation of different carbohydrate probes (modified and nonmodified glycans) to investigate biochemical processes such as glycan biosynthesis, recognition or competence interactions in real time with no need of labelling step. This glycochip might be also combined and compatible with a MALDI-Tof MS analysis directly on the chip after the SPRi measurements.

Some achievements have been developed in different scientific domains to contribute positively in the conception of SPRi glycoarray. Thus, in the biological domain, our procedure, motivated from Ciceron *et al.*,[44] for the expression and purification of the AtFUT1 enzyme could also be adapted for the production of new GTs under heterologous expression. Moreover, the enzymatic digestion that we optimized for the XyG polymer might serve as a reference in further treatments of analogue structures (cellulose, pectin, xylan, arabinoxylan etc) towards the study of physico-chemical properties or glycan binding interaction monitoring.

Then, within the chemistry domain we provided a versatile approach for the chemoselective conjugation, purification and characterization of plant oligosaccharides bearing an ODN structure. Our original idea was to proceed a bottom-up approach and steer this concept towards the construction of any COCs combination for the attachment of these glycoconjugates by DDI approach.

Finally, within the physics domain we validated the conception of DDI approach for the construction of glycochips by SPRi assays. This powerful strategy might offer a potential scope for the multiplexed array by displaying a diverse combination of COCs simultaneously on the chip simply by modifying the ODN sequences. Therefore, the consistent DNA glycoarray can be an attractive approach for the high-throughput screening of new GT binding events by SPRi detection.

In particular for our project, a very preliminary interaction assay was performed with the AtFUT1 enzyme with no conclusive results. Therefore, the future perspectives in this matter might be orientated to the optimization of critical parameters such as AtFUT1 concentration, flow rate, detection limit or mass transport effect. Furthermore, this project pursues the direct monitoring of enzymatic transfer activity of AtFUT1 enzymes in SPRi experiments. Either in complex with the GDP-fucose donor or in a stepwise addition, the AtFUT1 transfer reaction will be detected in real-time directly on the glycochip via fucose-binding lectin (*Ralstonia solanacearum*, RSL). The versatility of the DNA/DNA hybridization will allow the

cleavage of the noncovalent interaction (either selective with restriction enzymes or nonselective with denature compounds) for further analysis by mass spectrometry.

The extension of our glycochip design can also be exploited as a powerful screening tool for the identification of Leloir-GTs or glycosidases enzymes inhibitors with potential applications from pathogen binding to cancer and drug discovery, similarly to other scientific research.[203–206] Likewise, this study might be extended to the interrogation of other important glycan-binding proteins like lectins. This family of proteins plays also a central role in the glycan recognition and biochemical identification to steer a bit further toward a better understanding of the glyco-code mystery.

Complementary techniques can also be accepted in the evaluation of GTs activity. The ITC is a nice example to be explored using the different sizes of XyG already obtained in this thesis project. Also, this technique can be exploitable in terms of kinetic evaluation approaches to provide full comprehension about the enzyme activity parameters.

Reproducing the statement of Emil Fisher lecture (Nobel Prize in Chemistry, 1902) and one of the pioneer scientist in the world of carbohydrates said[207] ...

Herman Emil Fischer

"... the chemical enigma of Life will not be solved until organic chemistry has mastered another, even more difficult subject, the proteins, in the same way as it has mastered the carbohydrates."

Herman E. Fisher
Nobel Prize 1902

The ironic point is that he never knew that nowadays carbohydrates have become one of the central piece of the Life's puzzle to be deciphered.

Hopefully, my research work through this doctoral manuscript involved in a multidisciplinary domain at the interfaces between biology, chemistry and physics will favourably contribute and encourage further studies that help to the comprehension of this fascinating world of sugars.

Bibliography

[1] H. Ghazarian, B. Idoni, and S. B. Oppenheimer, "A glycobiology review: Carbohydrates, lectins and implications in cancer therapeutics," *Acta Histochem.*, vol. 113, no. 3, pp. 236–247, 2011.

[2] A. Varki, "Biological roles of glycans," *Glycobiology*, vol. 27, no. 1, pp. 3–49, 2016.

[3] A. Varki, R. D. Cummings, J. D. Esko, and et al., "Chapter 1: Historical background and overview in essentials of glycobiology [internet]," Cold Spring Harbor (NY): Cold Spring Harbor Laboratory Press, 2017.

[4] C. Reily, T. J. Stewart, M. B. Renfrow, and J. Novak, "Glycosylation in health and disease," *Nat. Rev. Nephrol.*, vol. 15, no. 6, pp. 346–366, 2019.

[5] F. Corolleur, A. Level, M. Matt, and S. Perez, "Innovation potentials triggered by glycoscience research," *Carbohydr. Polym.*, vol. 233, p. 115833, 2020.

[6] P. Valverde, A. Ardá, N. C. Reichardt, J. Jiménez-Barbero, and A. Gimeno, "Glycans in drug discovery," *MedChemComm*, vol. 10, no. 10, pp. 1678–1691, 2019.

[7] K. T. Schjoldager, Y. Narimatsu, H. J. Joshi, and H. Clausen, "Global view of human protein glycosylation pathways and functions," *Nat. Rev. Mol. Cell Biol.*, vol. 21, no. 12, pp. 729–749, 2020.

[8] L. Casalino, Z. Gaieb, J. A. Goldsmith, C. K. Hjorth, A. C. Dommer, A. M. Harbison, C. A. Fogarty, E. P. Barros, B. C. Taylor, J. S. McLellan, E. Fadda, and R. E. Amaro, "Beyond shielding: The roles of glycans in the SARS-CoV-2 spike protein," *ACS Cent. Sci.*, vol. 6, no. 10, pp. 1722–1734, 2020.

[9] C. Breton, L. Šnajdrová, C. Jeanneau, J. Koča, and A. Imberty, "Structures and mechanisms of glycosyltransferases," *Glycobiology*, vol. 16, no. 2, pp. 29R–37R, 2005.

[10] L. Lairson, B. Henrissat, G. Davies, and S. Withers, "Glycosyltransferases: Structures, functions, and mechanisms," *Annu. Rev. Biochem.*, vol. 77, no. 1, pp. 521–555, 2008.

[11] C. Lizak, S. Gerber, S. Numao, M. Aebi, and K. P. Locher, "X-ray structure of a bacterial oligosaccharyltransferase," *Nature*, vol. 474, no. 7351, pp. 350–355, 2011.

[12] D. A. Jové and M. E. Guerin, "The conformational plasticity of glycosyltransferases," *Curr. Opin. Struct. Biol.*, vol. 40, pp. 23–32, 2016.

[13] K. W. Moremen and R. S. Haltiwanger, "Emerging structural insights into glycosyltransferase-mediated synthesis of glycans," *Nat. Chem. Biol.*, vol. 15, no. 9, pp. 853–864, 2019.

[14] K. Keegstra and N. Raikhel, "Plant glycosyltransferases," *Curr. Opin. Plant Biol.*, vol. 4, no. 3, pp. 219–224, 2001.

[15] C. Breton, J. Mucha, and C. Jeanneau, "Structural and functional features of glycosyltransferases," *Biochimie*, vol. 83, no. 8, pp. 713–718, 2001.

[16] A. Oikawa, C. H. Lund, Y. Sakuragi, and H. V. Scheller, "Golgi-localized enzyme complexes for plant cell wall biosynthesis," *Trends Plant Sci.*, vol. 18, no. 1, pp. 49–58, 2013.

[17] V. Lombard, H. G. Ramulu, E. Drula, P. M. Coutinho, and B. Henrissat, "The carbohydrate-active enzymes database (CAZy) in 2013," *Nucleic Acids Res.*, vol. 42, no. D1, pp. D490–D495, 2013.

[18] J. Ati, P. Lafite, and R. Daniellou, "Enzymatic synthesis of glycosides: from natural O- and N-glycosides to rare C- and S-glycosides," *Beilstein J. Org. Chem.*, vol. 13, pp. 1857–1865, 2017.

[19] A. Ardèvol and C. Rovira, "Reaction mechanisms in carbohydrate-active enzymes: Glycoside hydrolases and glycosyltransferases. insights from *ab Initio* Quantum mechanics/molecular mechanics dynamic simulations," *J. Am. Chem. Soc.*, vol. 137, no. 24, pp. 7528–7547, 2015.

[20] B. R. Urbanowicz, V. S. Bharadwaj, M. Alahuhta, M. J. Peña, V. V. Lunin, Y. J. Bomble, S. Wang, J. Y. Yang, S. T. Tuomivaara, M. E. Himmel, K. W. Moremen, W. S. York, and M. F. Crowley, "Structural, mutagenic and in silico studies of xyloglucan fucosylation in Arabidopsis thaliana suggest a water-mediated mechanism," *Plant Journal*, vol. 91, no. 6, pp. 931–949, 2017.

[21] C. Breton, S. F. Gigleux, and M. M. Palcic, "Recent structures, evolution and mechanisms of glycosyltransferases," *Curr. Opin. Plant Biol.*, vol. 22, no. 5, pp. 540–549, 2012.

[22] D. A. Jové, F. Mendoza, A. R. Unzueta, F. G. Bel, J. O. Cifuente, S. Urresti, N. Comino, H. Gómez, J. Romero-García, J. M. Lluch, E. S. Vaello, X. Biarnés, A. Planas, P. Merino, L. Masgrau, and M. E. Guerin, "A native ternary complex trapped in a crystal reveals the catalytic mechanism of a retaining glycosyltransferase," *Angew. Chem. Int. Ed.*, vol. 54, no. 34, pp. 9898–9902, 2015.

[23] D. A. Jové, M. Á. S. Polo, A. Marina, and M. E. Guerin, "Structural snapshots of α-1, 3-galactosyltransferase with native substrates: Insight into the catalytic mechanism of retaining glycosyltransferases," *Angew. Chem. Int. Ed.*, vol. 129, no. 47, pp. 15049–15053, 2017.

[24] O. von Ahsen, U. Voigtmann, M. Klotz, N. Nifantiev, A. Schottelius, A. Ernst, B. M. Tiemann, and K. Parczyk, "A miniaturized high-throughput screening assay for fucosyltransferase VII," *Anal. Biochem.*, vol. 372, no. 1, pp. 96–105, 2008.

[25] M. Kopp, C. Rupprath, H. Irschik, A. Bechthold, L. Elling, and R. Müller, "SorF: A glycosyltransferase with promiscuous donor substrate specificity in vitro," *ChemBioChem*, vol. 8, no. 7, pp. 813–819, 2007.

[26] N. Laurent, J. Voglmeir, A. Wright, J. Blackburn, N. T. Pham, S. C. C. Wong, S. J. Gaskell, and S. L. Flitsch, "Enzymatic glycosylation of peptide arrays on gold surfaces," *ChemBioChem*, vol. 9, no. 6, pp. 883–887, 2008.

[27] G. K. Wagner and T. Pesnot, "Glycosyltransferases and their assays," *ChemBioChem*, vol. 11, no. 14, pp. 1939–1949, 2010.

[28] B. T. Houseman and M. Mrksich, "Carbohydrate arrays for the evaluation of protein binding and enzymatic modification," *Chem. Biol.*, vol. 9, no. 4, pp. 443–454, 2002.

[29] D. Pihíková, P. Kasák, and J. Tkac, "Glycoprofiling of cancer biomarkers: Label-free electrochemical lectin-based biosensors," *Open Chem.*, vol. 13, no. 1, 2015.

[30] V. Perumal and U. Hashim, "Advances in biosensors: Principle, architecture and applications," *J. Appl. Biomed.*, vol. 12, no. 1, pp. 1–15, 2014.

[31] N. Bhalla, P. Jolly, N. Formisano, and P. Estrela, "Introduction to biosensors," *Essays Biochem.*, vol. 60, no. 1, pp. 1–8, 2016.

[32] T. Puvirajesinghe and J. Turnbull, "Glycoarray technologies: Deciphering interactions from proteins to live cell responses," *Microarrays*, vol. 5, no. 1, p. 3, 2016.

[33] S. Park, J. C. Gildersleeve, O. Blixt, and I. Shin, "Carbohydrate microarrays," *Chem. Soc. Rev.*, vol. 42, no. 10, pp. 4310–4326, 2013.

[34] P. Damborský, J. Švitel, and J. Katrlík, "Optical biosensors," *Essays Biochem.*, vol. 60, no. 1, pp. 91–100, 2016.

[35] J. Homola, "Electromagnetic theory of surface plasmons. In: Springer series on chemical sensors and biosensors," pp. 3–44, Springer Berlin Heidelberg, 2006.

[36] J. Homola, "Surface plasmon resonance sensors for detection of chemical and biological species," *Chem. Rev.*, vol. 108, no. 2, pp. 462–493, 2008.

[37] Y. Liu, A. Jaiswal, M. A. Poggi, and W. D. Wilson, "Chemosensors. Chapter 16: Surface plasmon resonance and quartz crystal microbalance methods for detection of molecular interactions," pp. 329–344, John Wiley & Sons, Inc., 2011.

[38] B. Prabowo, A. Purwidyantri, and K. C. Liu, "Surface plasmon resonance optical sensor: A review on light source technology," *Biosensors*, vol. 8, no. 3, p. 80, 2018.

[39] M. Perenon, H. Bonnet, T. Lavergne, J. Dejeu, and E. Defrancq, "Surface plasmon resonance study of the interaction of N-methyl mesoporphyrin IX with G-quadruplex DNA," *Phys. Chem. Chem. Phys.*, vol. 22, no. 7, pp. 4158–4164, 2020.

[40] E. Dausse, A. Barré, A. Aimé, A. Groppi, A. Rico, C. Ainali, G. Salgado, W. Palau, E. Daguerre, M. Nikolski, J. J. Toulmé, and C. D. Primo, "Aptamer selection by direct microfluidic recovery and surface plasmon resonance evaluation," *Biosens. Bioelectron.*, vol. 80, pp. 418–425, 2016.

[41] R. Bombera, L. Leroy, T. Livache, and Y. Roupioz, "DNA-directed capture of primary cells from a complex mixture and controlled orthogonal release monitored by SPR imaging," *Biosens. Bioelectron.*, vol. 33, no. 1, pp. 10–16, 2012.

[42] G. Safina, "Application of surface plasmon resonance for the detection of carbohydrates, glycoconjugates, and measurement of the carbohydrate-specific interactions: A comparison with conventional analytical techniques. A critical review," *Anal. Chim. Acta*, vol. 712, pp. 9–29, 2012.

[43] J. S. Weerakkody, S. Brenet, T. Livache, C. Herrier, Y. Hou, and A. Buhot, "Optical index prism sensitivity of surface plasmon resonance imaging in gas phase: Experiment versus theory," *J. Phys. Chem. C*, vol. 124, no. 6, pp. 3756–3767, 2020.

[44] F. Cicéron, J. Rocha, S. Kousar, S. F. Hansen, V. Chazalet, E. Gillon, C. Breton, and O. Lerouxel, "Expression, purification and biochemical characterization of

AtFUT1, a xyloglucan-specific fucosyltransferase from Arabidopsis thaliana," *Biochimie*, vol. 128–129, pp. 183–192, 2016.

[45] J. Rocha, F. Cicéron, D. de Sanctis, M. Lelimousin, V. Chazalet, O. Lerouxel, and C. Breton, "Structure of Arabidopsis thaliana FUT1 reveals a variant of the GT-B class fold and provides insight into xyloglucan fucosylation," *Plant Cell*, vol. 28, no. 10, pp. 2352–2364, 2016.

[46] J. P. Joseleau and S. Pérez, "The plant cell wall," 2016.

[47] B. S. Valent and P. Albersheim, "The structure of plant cell walls," *Plant Physiol.*, vol. 54, no. 1, pp. 105–108, 1974.

[48] A. Driouich, M. L. F. Gueye, S. Bernard, S. Kousar, L. Chevalier, M. V. Gibouin, and O. Lerouxel, "Golgi-mediated synthesis and secretion of matrix polysaccharides of the primary cell wall of higher plants," *Front. Plant Sci.*, vol. 3, p. 79, 2012.

[49] R. Perrin, C. Wilkerson, and K. Keegstra, "Golgi enzymes that synthesize plant cell wall polysaccharides: Finding and evaluating candidates in the genomic era," *Plant Mol. Biol.*, vol. 47, pp. 115–130, 2001.

[50] M. Pauly and K. Keegstra, "Biosynthesis of the plant cell wall matrix polysaccharide xyloglucan," *Annu. Rev. Plant Biol.*, vol. 67, no. 1, pp. 235–259, 2016.

[51] J. C. Cocuron, O. Lerouxel, G. Drakakaki, A. P. Alonso, A. H. Liepman, K. Keegstra, N. Raikhel, and C. G. Wilkerson, "A gene from the cellulose synthase-like C family encodes a β-1,4 glucan synthase," *PNAS*, vol. 104, no. 20, pp. 8550–8555, 2007.

[52] A. Faik, N. J. Price, N. V. Raikhel, and K. Keegstra, "An Arabidopsis gene encoding an alpha-xylosyltransferase involved in xyloglucan biosynthesis," *PNAS*, vol. 99, no. 11, pp. 7797–7802, 2002.

[53] O. A. Zabotina, U. Avci, D. Cavalier, S. Pattathil, Y. H. Chou, S. Eberhard, L. Danhof, K. Keegstra, and M. G. Hahn, "Mutations in multiple XXXT genes of Arabidopsis reveal the complexity of xyloglucan biosynthesis," *Plant Physiol.*, vol. 159, no. 4, pp. 1367–1384, 2012.

[54] S. Vuttipongchaikij, D. Brocklehurst, C. S. King, D. A. Ashford, L. D. Gómez, and S. J. M. Mason, "Arabidopsis GT34 family contains five xyloglucan α-1,6 xylosyltransferases," *New Phytol.*, vol. 195, no. 3, pp. 585–595, 2012.

[55] N. Mansoori, A. Schultink, J. Schubert, and M. Pauly, "Expression of heterologous xyloglucan xylosyltransferases in Arabidopsis to investigate their role in determining xyloglucan xylosylation substitution patterns," *Planta*, vol. 241, no. 5, pp. 1145–1158, 2015.

[56] S. C. Fry, W. S. York, P. Albersheim, A. Darvill, T. Hayashi, J. P. Joseleau, Y. Kato, E. P. Lorences, G. A. Maclachlan, M. McNeil, A. J. Mort, J. S. G. Reid, H. U. Seitz, R. R. Selvendran, A. G. J. Voragen, and A. R. White, "An unambiguous nomenclature for xyloglucan-derived oligosaccharides," *Physiol. Plant.*, vol. 89, no. 1, pp. 1–3, 1993.

[57] X. Li, I. Cordero, J. Caplan, M. Mølhøj, and W. D. Reiter, "Molecular analysis of 10 coding regions from Arabidopsis that are homologous to the MUR3 xyloglucan galactosyltransferase," *Plant Physiol.*, vol. 134, no. 3, pp. 940–950, 2004.

[58] M. Madson, C. Dunand, X. Li, R. Verma, G. F. Vanzin, J. Caplan, D. A. Shoue, N. C. Carpita, and W. D. Reiter, "The MUR3 gene of Arabidopsis encodes a xyloglucan galactosyltransferase that is evolutionarily related to animal exostosins," *Plant Cell*, vol. 15, no. 7, pp. 1662–1670, 2003.

[59] J. K. Jensen, A. Schultink, K. Keegstra, C. G. Wilkerson, and M. Pauly, "RNA-seq analysis of developing nasturtium seeds (tropaeolum majus): Identification and characterization of an additional galactosyltransferase involved in xyloglucan biosynthesis," *Mol. Plant*, vol. 5, no. 5, pp. 984–992, 2012.

[60] R. M. Perrin, "Xyloglucan fucosyltransferase, an enzyme involved in plant cell wall biosynthesis," *Sci.*, vol. 284, no. 5422, pp. 1976–1979, 1999.

[61] O. Lerouxel, D. M. Cavalier, A. H. Liepman, and K. Keegstra, "Biosynthesis of plant cell wall polysaccharides - a complex process," *Curr. Opin. Plant Biol.*, vol. 9, no. 6, pp. 621–630, 2006.

[62] G. F. Vanzin, M. Madson, N. C. Carpita, N. V. Raikhel, K. Keegstra, and W. D. Reiter, "The mur2 mutant of Arabidopsis thaliana lacks fucosylated xyloglucan because of a lesion in fucosyltransferase AtFUT1," *PNAS*, vol. 99, no. 5, pp. 3340–3345, 2002.

[63] R. A. Amos and D. Mohnen, "Critical review of plant cell wall matrix polysaccharide glycosyltransferase activities verified by heterologous protein expression," *Front. Plant Sci.*, vol. 10, p. 915, 2019.

[64] A. Faik, M. B. Peled, A. E. DeRocher, W. Zeng, R. M. Perrin, C. Wilkerson, N. V. Raikhel, and K. Keegstra, "Biochemical characterization and molecular cloning of an α-1,2-fucosyltransferase that catalyzes the last step of cell wall xyloglucan biosynthesis in pea," *J. Biol. Chem.*, vol. 275, no. 20, pp. 15082–15089, 2000.

[65] O. Lerouxel, T. S. Choo, M. Séveno, B. Usadel, L. Faye, P. Lerouge, and M. Pauly, "Rapid structural phenotyping of plant cell wall mutants by enzymatic oligosaccharide fingerprinting," *Plant Physiol.*, vol. 130, no. 4, pp. 1754–1763, 2002.

[66] R. M. Perrin, Z. Jia, T. A. Wagner, M. A. O'Neill, R. Sarria, W. S. York, N. V. Raikhel, and K. Keegstra, "Analysis of xyloglucan fucosylation in Arabidopsis," *Plant Physiol.*, vol. 132, no. 2, pp. 768–778, 2003.

[67] M. J. Soto, B. R. Urbanowicz, and M. G. Hahn, "Plant fucosyltransferases and the emerging biological importance of fucosylated plant structures," *Crit. Rev. Plant Sci.*, vol. 38, pp. 327–338, 2019.

[68] D. B. Jordan, M. J. Bowman, J. D. Braker, B. S. Dien, R. E. Hector, C. C. Lee, J. A. Mertens, and K. Wagschal, "Plant cell walls to ethanol," *Biochem. J.*, vol. 442, pp. 241–252, 2012.

[69] A. Mishra and A. V. Malhotra, "Tamarind xyloglucan: A polysaccharide with versatile application potential," *J. Mater. Chem*, vol. 19, p. 8528, 2009.

[70] L. Mazzarino, G. L. Neckel, L. dos Santos Bubniak, F. Ourique, I. Otsuka, S. Halila, R. C. Pedrosa, M. C. S. Silva, E. L. Senna, E. C. Muniz, and R. Borsali, "Nanoparticles made from xyloglucan-block-polycaprolactone copolymers: Safety assessment for drug delivery," *Toxicol. Sci.*, vol. 147, pp. 104–115, 2015.

[71] V. A. Erdmann, S. Jurga, and J. Barciszewski, "RNA and DNA diagnostics," Springer International Publishing, 2015.

[72] T. Hermann, "Adaptive recognition by nucleic acid aptamers," *Sci.*, vol. 287, no. 5454, pp. 820–825, 2000.

[73] S. K. Silverman, "DNA as a versatile chemical component for catalysis, encoding, and stereocontrol," *Angew. Chem. Int. Ed.*, vol. 49, no. 40, pp. 7180–7201, 2010.

[74] F. Teles and L. Fonseca, "Trends in DNA biosensors," *Talanta*, vol. 77, no. 2, pp. 606–623, 2008.

[75] E. Defrancq, Y. Singh, and N. Spinelli, "Chemical strategies for oligonucleotide-conjugates synthesis," *Curr. Org. Chem*, vol. 12, no. 4, pp. 263–290, 2008.

[76] P. H. Seeberger and D. B. Werz, "Synthesis and medical applications of oligosaccharides," *Nature*, vol. 446, no. 7139, pp. 1046–1051, 2007.

[77] J. R. Bishop, M. Schuksz, and J. D. Esko, "Heparan sulphate proteoglycans fine-tune mammalian physiology," *Nature*, vol. 446, no. 7139, pp. 1030–1037, 2007.

[78] M. Mammen, S. K. Choi, and G. M. Whitesides, "Polyvalent interactions in biological systems: Implications for design and use of multivalent ligands and inhibitors," *Angew. Chem. Int. Ed.*, vol. 37, no. 20, pp. 2754–2794, 1998.

[79] Y. Singh, O. Renaudet, E. Defrancq, and P. Dumy, "Preparation of a multitopic glycopeptide-oligonucleotide conjugate," *Organic Letters*, vol. 7, no. 7, pp. 1359–1362, 2005.

[80] J. D'Onofrio, L. Petraccone, L. Martino, G. D. Fabio, A. Iadonisi, J. Balzarini, C. Giancola, and D. Montesarchio, "Synthesis, biophysical characterization, and anti-HIV activity of glyco-conjugated g-quadruplex-forming oligonucleotides," *Bioconjugate Chem.*, vol. 19, no. 3, pp. 607–616, 2008.

[81] D. Boturyn, E. Defrancq, G. T. Dolphin, J. Garcia, P. Labbe, O. Renaudet, and P. Dumy, "RAFT nano-constructs: surfing to biological applications," *J. Pept. Sci.*, vol. 14, no. 2, pp. 224–240, 2008.

[82] T. Akasaka, K. Matsuura, and K. Kobayashi, "Transformation from block-type to graft-type oligonucleotide-glycopolymer conjugates by self-organization with half-sliding complementary oligonucleotides and their lectin recognition," *Bioconjugate Chem.*, vol. 12, pp. 776–785, 2001.

[83] Y. Singh, P. Murat, and E. Defrancq, "Recent developments in oligonucleotide conjugation," *Chem. Soc. Rev.*, vol. 39, no. 6, p. 2054, 2010.

[84] C. Pifferi, G. C. Daskhan, M. Fiore, T. C. Shiao, R. Roy, and O. Renaudet, "Aminooxylated carbohydrates: Synthesis and applications," *Chem. Rev.*, vol. 117, no. 15, pp. 9839–9873, 2017.

[85] J. Kalia and R. Raines, "Hydrolytic stability of hydrazones and oximes," *Angew. Chem. Int. Ed.*, vol. 47, no. 39, pp. 7523–7526, 2008.

[86] S. Ulrich, D. Boturyn, A. Marra, O. Renaudet, and P. Dumy, "Oxime ligation: A chemoselective click-type reaction for accessing multifunctional biomolecular constructs," *Chem. A Eur. J.*, vol. 20, no. 1, pp. 34–41, 2013.

[87] W. P. Jencks, "Studies on the mechanism of oxime and semicarbazone formation1," *J. Am. Chem. Soc.*, vol. 81, no. 2, pp. 475–481, 1959.

[88] W. P. Jencks, "Mechanism and catalysis of simple carbonyl group reactions in progress in physical organic chemistry," pp. 63–128, John Wiley & Sons, Inc., 1964.

[89] H. Egberink and C. V. Heerden, "The mechanism of the formation and hydrolysis of cyclohexanone oxime in aqueous solutions," *Anal. Chim. Acta*, vol. 118, no. 2, pp. 359–368, 1980.

[90] E. H. Cordes and W. P. Jencks, "General acid catalysis of semicarbazone formation," *J. Am. Chem. Soc.*, vol. 84, no. 22, pp. 4319–4328, 1962.

[91] E. H. Cordes and W. P. Jencks, "Nucleophilic catalysis of semicarbazone formation by anilines," *J. Am. Chem. Soc.*, vol. 84, no. 5, pp. 826–831, 1962.

[92] S. Morales, J. L. Aceña, J. L. G. Ruano, and M. B. Cid, "Sustainable synthesis of oximes, hydrazones, and thiosemicarbazones under mild organocatalyzed reaction conditions," *J. Org. Chem.*, vol. 81, no. 20, pp. 10016–10022, 2016.

[93] A. Dirksen, T. M. Hackeng, and P. E. Dawson, "Nucleophilic catalysis of oxime ligation," *Angew. Chem. Int. Ed.*, vol. 118, no. 45, pp. 7743–7746, 2006.

[94] S. Wang, D. Gurav, O. P. Oommen, and O. P. Varghese, "Insights into the mechanism and catalysis of oxime coupling chemistry at physiological pH," *Chem. A Eur. J.*, vol. 21, no. 15, pp. 5980–5985, 2015.

[95] H. C. Kolb, M. G. Finn, and K. B. Sharpless, "Click chemistry: Diverse chemical function from a few good reactions," *Angew. Chem. Int. Ed.*, vol. 40, no. 11, pp. 2004–2021, 2001.

[96] R. Huisgen, "1,3-dipolar cycloadditions. Past and future," *Angew. Chem. Int. Ed.*, vol. 2, no. 10, pp. 565–598, 1963.

[97] V. Rostovtsev, L. Green, V. Fokin, and K. B. Sharpless, "A stepwise huisgen cycloaddition process: Copper(I)-catalyzed regioselective "ligation" of azides and terminal alkynes," *Angew. Chem. Int. Ed.*, vol. 41, no. 14, pp. 2596–2599, 2002.

[98] B. T. Worrell, J. A. Malik, and V. V. Fokin, "Direct evidence of a dinuclear copper intermediate in Cu(i)-catalyzed azide-alkyne cycloadditions," *Sci.*, vol. 340, no. 6131, pp. 457–460, 2013.

[99] N. J. Agard, J. A. Prescher, and C. R. Bertozzi, "A strain-promoted [3+2] azide-alkyne cycloaddition for covalent modification of biomolecules in living systems," *J. Am. Chem. Soc.*, vol. 126, no. 46, pp. 15046–15047, 2004.

[100] J. C. Jewett and C. R. Bertozzi, "Cu-free click cycloaddition reactions in chemical biology," *Chem. Soc. Rev.*, vol. 39, no. 4, p. 1272, 2010.

[101] A. B. Neef and C. Schultz, "Selective fluorescence labeling of lipids in living cells," *Angew. Chem. Int. Ed.*, vol. 121, no. 8, pp. 1526–1529, 2009.

[102] P. V. Chang, J. A. Prescher, E. M. Sletten, J. M. Baskin, I. A. Miller, N. J. Agard, A. Lo, and C. R. Bertozzi, "Copper-free click chemistry in living animals," *PNAS*, vol. 107, no. 5, pp. 1821–1826, 2010.

[103] D. H. Ess, G. O. Jones, and K. N. Houk, "Transition states of strain-promoted metal-free click chemistry: 1,3-dipolar cycloadditions of phenyl azide and cyclooctynes," *Org. Lett.*, vol. 10, no. 8, pp. 1633–1636, 2008.

[104] J. M. Baskin, J. A. Prescher, S. T. Laughlin, N. J. Agard, P. V. Chang, I. A. Miller, A. Lo, J. A. Codelli, and C. R. Bertozzi, "Copper-free click chemistry for dynamic in vivo imaging," *PNAS*, vol. 104, no. 43, pp. 16793–16797, 2007.

[105] J. A. Codelli, J. M. Baskin, N. J. Agard, and C. R. Bertozzi, "Second-generation difluorinated cyclooctynes for copper-free click chemistry," *J. Am. Chem. Soc.*, vol. 130, no. 34, pp. 11486–11493, 2008.

[106] J. Dommerholt, S. Schmidt, R. Temming, L. J. A. Hendriks, F. P. J. T. Rutjes, J. C. M. van Hest, D. J. Lefeber, P. Friedl, and F. L. van Delft, "Readily accessible bicyclononynes for bioorthogonal labeling and three-dimensional imaging of living cells," *Angew. Chem. Int. Ed.*, vol. 49, no. 49, pp. 9422–9425, 2010.

[107] X. Ning, J. Guo, M. A. Wolfert, and G. J. Boons, "Visualizing metabolically labeled glycoconjugates of living cells by copper-free and fast huisgen cycloadditions," *Angew. Chem. Int. Ed.*, vol. 120, no. 12, pp. 2285–2287, 2008.

[108] E. M. Sletten and C. R. Bertozzi, "A hydrophilic azacyclooctyne for Cu-free click chemistry," *Org. Lett.*, vol. 10, no. 14, pp. 3097–3099, 2008.

[109] M. F. Debets, C. W. J. van der Doelen, F. P. J. T. Rutjes, and F. L. van Delft, "Azide: A unique dipole for metal-free bioorthogonal ligations," *ChemBioChem.*, vol. 11, no. 9, pp. 1168–1184, 2010.

[110] A. Kuzmin, A. Poloukhtine, M. A. Wolfert, and V. V. Popik, "Surface functionalization using catalyst-free azide-alkyne cycloaddition," *Bioconjugate Chem.*, vol. 21, no. 11, pp. 2076–2085, 2010.

[111] L. S. C. Verduyn, L. Mirfeizi, A. K. Schoonen, R. A. Dierckx, P. H. Elsinga, and B. L. Feringa, "Strain-promoted copper-free click chemistry for 18f radiolabeling of bombesin," *Angew. Chem. Int. Ed.*, vol. 50, no. 47, pp. 11117–11120, 2011.

[112] J. Dommerholt, F. P. J. T. Rutjes, and F. L. van Delft, "Strain-promoted 1,3-dipolar cycloaddition of cycloalkynes and organic azides," *Top. Curr. Chem.*, vol. 374, no. 2, p. 16, 2016.

[113] T. S. Zatsepin and T. S. Oretskaya, "Synthesis and applications of oligonucleotide-carbohydrate conjugates," *Chem. Biodivers.*, vol. 1, no. 10, pp. 1401–1417, 2004.

[114] N. Spinelli, E. Defrancq, and F. Morvan, "Glycoclusters on oligonucleotide and PNA scaffolds: synthesis and applications," *Chem. Soc. Rev.*, vol. 42, no. 11, pp. 4557–4573, 2013.

[115] A. Novoa and N. Winssinger, "DNA display of glycoconjugates to emulate oligomeric interactions of glycans," *Beilstein J. Org. Chem.*, vol. 11, pp. 707–719, 2015.

[116] S. Akhtar, A. Routledge, R. Patel, and J. M. Gardiner, "Synthesis of mono- and dimannoside phosphoramidite derivatives for solid-phase conjugation to oligonucleotides," *Tetrahedron Lett.*, vol. 36, no. 40, pp. 7333–7336, 1995.

[117] M. Adinolfi, G. Barone, L. D. Napoli, L. Guariniello, A. Iadonisi, and G. Piccialli, "Solid phase glycosidation of oligonucleotides," *Tetrahedron Lett.*, vol. 40, no. 13, pp. 2607–2610, 1999.

[118] J. Hunziker, "Synthesis of 5-(2-amino-2-deoxy-β-d-glucopyranosyloxymethyl)-2'-deoxyuridine and its incorporation into oligothymidylates," *Bioorg. Med. Chem. Lett.*, vol. 9, no. 2, pp. 201–204, 1999.

[119] K. Matsuura, M. Hibino, M. Kataoka, Y. Hayakawa, and K. Kobayashi, "Phosphoramidite solid-phase synthesis of site-specifically glycosylated oligodeoxynucleotides," *Tetrahedron Lett.*, vol. 41, no. 39, pp. 7529–7533, 2000.

[120] M. Karskela, P. Virta, M. Malinen, A. Urtti, and H. Lönnberg, "Synthesis and cellular uptake of fluorescently labeled multivalent hyaluronan disaccharide conjugates of oligonucleotide phosphorothioates," *Bioconjugate Chem.*, vol. 19, no. 12, pp. 2549–2558, 2008.

[121] A. M. Jawalekar, N. Meeuwenoord, J. S. G. O. Cremers, H. S. Overkleeft, G. A. van der Marel, F. P. J. T. Rutjes, and F. L. van Delft, "Conjugation of nucleosides and oligonucleotides by [3+2] cycloaddition," *J. Org. Chem.*, vol. 73, pp. 287–290, 2008.

[122] C. Bouillon, A. Meyer, S. Vidal, A. Jochum, Y. Chevolot, J. P. Cloarec, J. P. Praly, J. J. Vasseur, and F. Morvan, "Microwave assisted "click" chemistry for the synthesis of multiple labeled-carbohydrate oligonucleotides on solid support," *J. Org. Chem.*, vol. 71, no. 12, pp. 4700–4702, 2006.

[123] Z. Ye, K. Cheng, R. V. Guntaka, and R. I. Mahato, "Targeted delivery of a triplex-forming oligonucleotide to hepatic stellate cells," *Biochemistry*, vol. 44, no. 11, pp. 4466–4476, 2005.

[124] S. Sando, K. Matsui, Y. Niinomi, N. Sato, and Y. Aoyama, "Facile preparation of DNA-tagged carbohydrates," *Bioorg. Med. Chem. Lett.*, vol. 13, no. 16, pp. 2633–2636, 2003.

[125] D. Forget, O. Renaudet, E. Defrancq, and P. Dumy, "Efficient preparation of carbohydrate–oligonucleotide conjugates (COCs) using oxime bond formation," *Tetrahedron Lett.*, vol. 42, no. 44, pp. 7829–7832, 2001.

[126] A. Meyer, N. Spinelli, P. Dumy, J. J. Vasseur, F. Morvan, and E. Defrancq, "Oligonucleotide sequential bis-conjugation via click-oxime and click-huisgen procedures," *J. Org. Chem.*, vol. 75, no. 11, pp. 3927–3930, 2010.

[127] Y. B. Park and D. J. Cosgrove, "Xyloglucan and its interactions with other components of the growing cell wall," *Plant Cell Physiol.*, vol. 56, no. 2, pp. 180–194, 2015.

[128] T. J. Styslinger, N. Zhang, V. S. Bhatt, N. Pettit, A. F. Palmer, and P. G. Wang, "Site-selective glycosylation of hemoglobin with variable molecular weight oligosaccharides: Potential alternative to PEGylation," *J. Am. Chem. Soc.*, vol. 134, no. 17, pp. 7507–7515, 2012.

[129] S. Park, M. R. Lee, and I. Shin, "Chemical tools for functional studies of glycans," *Chem. Soc. Rev.*, vol. 37, no. 8, p. 1579, 2008.

[130] F. Nicotra, L. Cipolla, F. Peri, B. L. Ferla, and C. Redaelli, "Chemoselective neoglycosylation," *Adv. Carbohydr. Chem. Biochem*, pp. 353–398, 2007.

[131] L. L. Kiessling and R. A. Splain, "Chemical approaches to glycobiology," *Annu. Rev. Biochem*, vol. 79, no. 1, pp. 619–653, 2010.

[132] M. B. Thygesen, H. Munch, J. Sauer, E. Clo, M. R. Jorgensen, O. Hindsgaul, and K. J. Jensen, "Nucleophilic catalysis of carbohydrate oxime formation by anilines," *J. Org. Chem*, vol. 75, no. 5, pp. 1752–1755, 2010.

[133] J. Heinze, B. A. F. Uribe, and S. Ludwigs, "Electrochemistry of conducting polymers persistent models and new concepts," *Chem. Rev.*, vol. 110, no. 8, pp. 4724–4771, 2010.

[134] S. Cunningham, J. Q. Gerlach, M. Kane, and L. Joshi, "Glyco-biosensors: Recent advances and applications for the detection of free and bound carbohydrates," *Analyst*, vol. 135, no. 10, p. 2471, 2010.

[135] S. Park and I. Shin, "Fabrication of carbohydrate chips for studying protein-carbohydrate interactions," *Angew. Chem. Int. Ed.*, vol. 114, no. 17, pp. 3312–3314, 2002.

[136] D. Wang, S. Liu, B. J. Trummer, C. Deng, and A. Wang, "Carbohydrate microarrays for the recognition of cross-reactive molecular markers of microbes and host cells," *Nat. Biotechnol.*, vol. 20, no. 3, pp. 275–281, 2002.

[137] F. Fazio, M. C. Bryan, O. Blixt, J. C. Paulson, and C. H. Wong, "Synthesis of sugar arrays in microtiter plate," *J. Am. Chem. Soc.*, vol. 124, no. 48, pp. 14397–14402, 2002.

[138] O. Blixt, S. Head, T. Mondala, C. Scanlan, M. E. Huflejt, R. Alvarez, M. C. Bryan, F. Fazio, D. Calarese, J. Stevens, N. Razi, D. J. Stevens, J. J. Skehel, I. van Die, D. R. Burton, I. A. Wilson, R. Cummings, N. Bovin, C. H. Wong, and J. C. Paulson, "Printed covalent glycan array for ligand profiling of diverse glycan binding proteins," *PNAS*, vol. 101, no. 49, pp. 17033–17038, 2004.

[139] S. Serna, S. Yan, M. M. Lomas, I. B. H. Wilson, and N. C. Reichardt, "Fucosyltransferases as synthetic tools: Glycan array based substrate selection and core fucosylation of Synthetic N-glycans," *J. Am. Chem. Soc.*, vol. 133, no. 41, pp. 16495–16502, 2011.

[140] C. J. Gray, M. J. Weissenborn, C. E. Eyers, and S. L. Flitsch, "Enzymatic reactions on immobilised substrates," *Chem. Soc. Rev.*, vol. 42, no. 15, p. 6378, 2013.

[141] M. Shipp, R. Nadella, H. Gao, V. Farkas, H. Sigrist, and A. Faik, "Glyco-array technology for efficient monitoring of plant cell wall glycosyltransferase activities," *Glycoconj. J.*, vol. 25, no. 1, pp. 49–58, 2007.

[142] Z. L. Zhi, A. K. Powell, and J. E. Turnbull, "Fabrication of carbohydrate microarrays on gold surfaces: Direct attachment of non derivatized oligosaccharides to hydrazide-modified self-assembled monolayers," *Anal. Chem.*, vol. 78, no. 14, pp. 4786–4793, 2006.

[143] Z. L. Zhi, N. Laurent, A. K. Powell, R. Karamanska, M. Fais, J. Voglmeir, A. Wright, J. M. Blackburn, P. R. Crocker, D. A. Russell, S. Flitsch, R. A. Field, and J. E. Turnbull, "A versatile gold surface approach for fabrication and interrogation of glycoarrays," *ChemBioChem.*, vol. 9, no. 10, pp. 1568–1575, 2008.

[144] M. Ogiso, K. Matsuoka, T. Okada, T. Imai, M. Itoh, T. Imamura, Y. Haga, K. Hatanaka, and N. Minoura, "Immobilization of carbohydrate clusters on a quartz crystal microbalance sensor surface," *J. Colloid Interface Sci.*, vol. 393, pp. 257–263, 2013.

[145] P. Guedon, T. Livache, F. Martin, F. Lesbre, A. Roget, G. Bidan, and Y. Levy, "Characterization and optimization of a real-time, parallel, label-free, polypyrrole-based DNA sensor by surface plasmon resonance imaging," *Anal. Chem*, vol. 72, pp. 6003–6009, 2000.

[146] S. Kim, L. K. Jang, H. S. Park, and J. Y. Lee, "Electrochemical deposition of conductive and adhesive polypyrrole-dopamine films," *Sci. Rep.*, vol. 6, no. 1, p. 30475, 2016.

[147] T. Livache, E. Maillart, N. Lassalle, P. Mailley, B. Corso, P. Guedon, A. Roget, and Y. Levy, "Polypyrrole based DNA hybridization assays: study of label free detection processes versus fluorescence on microchips," *J. Pharm. Biomed. Anal.*, vol. 32, no. 4-5, pp. 687–696, 2003.

[148] E. Maillart, K. B. Pesce, D. Capela, A. Roget, T. Livache, M. Canva, Y. Levy, and T. Soussi, "Versatile analysis of multiple macromolecular interactions by SPR imaging: application to p53 and DNA interaction," *Oncogene*, vol. 23, no. 32, pp. 5543–5550, 2004.

[149] L. Grosjean, B. Cherif, E. Mercey, A. Roget, Y. Levy, P. N. Marche, M. B. Villiers, and T. Livache, "A polypyrrole protein microarray for antibody–antigen interaction studies using a label-free detection process," *Anal. Biochem.*, vol. 347, no. 2, pp. 193–200, 2005.

[150] E. Bulard, A. B. Spinelli, P. Chaud, A. Roget, R. Calemczuk, S. Fort, and T. Livache, "Carbohydrates as new probes for the identification of closely related Escherichia Coli strains using surface plasmon resonance imaging," *Anal. Chem.*, vol. 87, no. 3, pp. 1804–1811, 2015.

[151] B. Schweiger, J. Kim, Y. Kim, and M. Ulbricht, "Electropolymerized molecularly imprinted polypyrrole film for sensing of clofibric acid," *Sensors*, vol. 15, no. 3, pp. 4870–4889, 2015.

[152] E. Mercey, R. Sadir, E. Maillart, A. Roget, F. Baleux, H. L. Jacob, and T. Livache, "Polypyrrole oligosaccharide array and surface plasmon resonance imaging for the measurement of glycosaminoglycan binding interactions," *Anal. Biochem.*, vol. 80, no. 9, pp. 3476–3482, 2008.

[153] L. Newton, T. Slater, N. Clark, and A. Vijayaraghavan, "Self assembled monolayers (SAMs) on metallic surfaces (gold and graphene) for electronic applications," *J. Mater. Chem. C*, vol. 1, no. 3, pp. 376–393, 2013.

[154] E. T. Gedig, "Handbook of surface plasmon resonance. Chapter 6: Surface chemistry in SPR technology," pp. 171–254, Royal Society of Chemistry, 2017.

[155] M. Frasconi, F. Mazzei, and T. Ferri, "Protein immobilization at gold–thiol surfaces and potential for biosensing," *Anal. Bioanal. Chem.*, vol. 398, no. 4, pp. 1545–1564, 2010.

[156] Y. Jung, J. M. Lee, H. Jung, and B. H. Chung, "Self-directed and self-oriented immobilization of antibody by protein G-DNA conjugate," *Anal. Chem.*, vol. 79, no. 17, pp. 6534–6541, 2007.

[157] J. M. Lee, H. K. Park, Y. Jung, J. K. Kim, S. O. Jung, and B. H. Chung, "Direct immobilization of protein G variants with various numbers of cysteine residues on a gold surface," *Anal. Chem.*, vol. 79, no. 7, pp. 2680–2687, 2007.

[158] F. Cheng and D. M. Ratner, "Glycosylated self-assembled monolayers for arrays and surface analysis in methods in molecular biology. In: Methods in molecular biology," pp. 87–101, Humana Press, 2011.

[159] T. Feizi and W. Chai, "Oligosaccharide microarrays to decipher the glyco code," *Nat. Rev. Mol. Cell Biol.*, vol. 5, no. 7, pp. 582–588, 2004.

[160] S. Fukui, T. Feizi, C. Galustian, A. M. Lawson, and W. Chai, "Oligosaccharide microarrays for high-throughput detection and specificity assignments of carbohydrate-protein interactions," *Nat. Biotechnol.*, vol. 20, no. 10, pp. 1011–1017, 2002.

[161] N. Laurent, J. Voglmeir, and S. L. Flitsch, "Glycoarrays-tools for determining protein-carbohydrate interactions and glycoenzyme specificity," *ChemComm*, no. 37, p. 4400, 2008.

[162] C. D. Rillahan and J. C. Paulson, "Glycan microarrays for decoding the glycome," *Annu. Rev. Biochem.*, vol. 80, no. 1, pp. 797–823, 2011.

[163] X. Song, J. H. Molinaro, R. D. Cummings, and D. F. Smith, "Chemistry of natural glycan microarrays," *Curr. Opin. Chem. Biol.*, vol. 18, pp. 70–77, 2014.

[164] K. Godula, D. Rabuka, K. T. Nam, and C. R. Bertozzi, "Synthesis and microcontact printing of dual end-functionalized mucin-like glycopolymers for microarray applications," *Angew. Chem. Int. Ed.*, vol. 121, no. 27, pp. 5073–5076, 2009.

[165] K. Godula and C. R. Bertozzi, "Synthesis of glycopolymers for microarray applications via ligation of reducing sugars to a poly(acryloyl hydrazide) scaffold," *J. Am. Chem. Soc.*, vol. 132, no. 29, pp. 9963–9965, 2010.

[166] M. G. Alteen, C. Gros, R. W. Meek, D. A. Cardoso, J. A. Busmann, G. Sangouard, M. C. Deen, H. Y. Tan, D. L. Shen, C. C. Russell, G. J. Davies, P. J.

Robinson, A. McCluskey, and D. J. Vocadlo, "A direct fluorescent activity assay for glycosyltransferases enables convenient high-throughput screening: Application to O-GlcNAc transferase," *Angew. Chem. Int. Ed.*, vol. 132, no. 24, pp. 9688–9696, 2020.

[167] Y. Chevolot, C. Bouillon, S. Vidal, F. Morvan, A. Meyer, J. P. Cloarec, A. Jochum, J. P. Praly, J.-J. Vasseur, and E. Souteyrand, "DNA-based carbohydrate biochips: A platform for surface glyco-engineering," *Angew. Chem. Int. Ed.*, vol. 119, no. 14, pp. 2450–2454, 2007.

[168] R. Meyer, S. Giselbrecht, B. E. Rapp, M. Hirtz, and C. M. Niemeyer, "Advances in DNA-directed immobilization," *Curr. Opin. Chem. Biol.*, vol. 18, pp. 8–15, 2014.

[169] C. Corne, J. B. Fiche, D. Gasparutto, V. Cunin, E. Suraniti, A. Buhot, J. Fuchs, R. Calemczuk, T. Livache, and A. Favier, "SPR imaging for label-free multiplexed analyses of DNA N-glycosylase interactions with damaged DNA duplexes," *Analyst*, vol. 133, no. 8, p. 1036, 2008.

[170] Y. Chevolot, E. Laurenceau, M. P. Goutorbe, V. Monnier, E. Souteyrand, A. Meyer, T. Géhin, J. J. Vasseur, and F. Morvan, "DNA directed immobilization glycocluster array: applications and perspectives," *Curr. Opin. Chem. Biol.*, vol. 18, pp. 46–54, 2014.

[171] C. M. Niemeyer, L. Boldt, B. Ceyhan, and D. Blohm, "DNA-directed immobilization: Efficient, reversible and site-selective surface binding of proteins by means of covalent DNA-streptavidin conjugates," *Anal. Biochem.*, vol. 268, no. 1, pp. 54–63, 1999.

[172] C. Boozer, J. Ladd, S. Chen, and S. Jiang, "DNA-directed protein immobilization for simultaneous detection of multiple analytes by surface plasmon resonance biosensor," *Anal. Chem.*, vol. 78, no. 5, pp. 1515–1519, 2006.

[173] C. F. W. Becker, R. Wacker, W. Bouschen, R. Seidel, B. Kolaric, P. Lang, H. Schroeder, O. Müller, C. M. Niemeyer, B. Spengler, R. S. Goody, and M. Engelhard, "Direct readout of protein-protein interactions by mass spectrometry from protein-DNA microarrays," *Angew. Chem. Int. Ed.*, vol. 44, no. 46, pp. 7635–7639, 2005.

[174] H. Song, K. Kerman, and H.-B. Kraatz, "Electrochemical detection of kinase-catalyzed phosphorylation using ferrocene-conjugated ATP," *Chem. Commun.*, no. 4, pp. 502–504, 2008.

[175] S. Park and I. Shin, "Carbohydrate microarrays for assaying galactosyltransferase activity," *Org. Lett.*, vol. 9, no. 9, pp. 1675–1678, 2007.

[176] F. Remy-Martin, M. E. Osta, G. Lucchi, R. Zeggari, T. Leblois, S. Bellon, P. Ducoroy, and W. Boireau, "Surface plasmon resonance imaging in arrays coupled with mass spectrometry (SUPRA–MS): proof of concept of on-chip characterization of a potential breast cancer marker in human plasma," *Anal. Bioanal. Chem.*, vol. 404, no. 2, pp. 423–432, 2012.

[177] E. Casero, L. Vázquez, A. M. P. Alfambra, and E. Lorenzo, "AFM, SECM and QCM as useful analytical tools in the characterization of enzyme-based bioanalytical platforms," *Analyst*, vol. 135, no. 8, p. 1878, 2010.

[178] B. Becker and M. A. Cooper, "A survey of the 2006-2009 quartz crystal microbalance biosensor literature," *J. Mol. Recognit.*, vol. 24, no. 5, pp. 754–787, 2011.

[179] H. Nishino, A. Murakawa, T. Mori, and Y. Okahata, "Kinetic studies of AMP-dependent phosphorolysis of amylopectin catalyzed by phosphorylasebon a 27 MHz quartz-crystal microbalance," *J. Am. Chem. Soc.*, vol. 126, no. 45, pp. 14752–14757, 2004.

[180] M. Wilczewski, A. V. der Heyden, O. Renaudet, P. Dumy, L. C. Guérente, and P. Labbé, "Promotion of sugar–lectin recognition through the multiple sugar presentation offered by regioselectively addressable functionalized templates (RAFT): a QCM-d and SPR study," *Org. Biomol. Chem.*, vol. 6, no. 6, p. 1114, 2008.

[181] L. Ban, N. Pettit, L. Li, A. D. Stuparu, L. Cai, W. Chen, W. Guan, W. Han, P. G. Wang, and M. Mrksich, "Discovery of glycosyltransferases using carbohydrate arrays and mass spectrometry," *Nat. Chem. Biol.*, vol. 8, no. 9, pp. 769–773, 2012.

[182] S. Scarano, M. Mascini, A. P. Turner, and M. Minunni, "Surface plasmon resonance imaging for affinity-based biosensors," *Biosens. Bioelectron.*, vol. 25, no. 5, pp. 957–966, 2010.

[183] M. Puiu and C. Bala, "SPR and SPR imaging: Recent trends in developing nanodevices for detection and real-time monitoring of biomolecular events," *Sensors*, vol. 16, no. 6, p. 870, 2016.

[184] M. Fais, R. Karamanska, S. Allman, S. A. Fairhurst, P. Innocenti, A. J. Fairbanks, T. J. Donohoe, B. G. Davis, D. A. Russell, and R. A. Field, "Surface plasmon resonance imaging of glycoarrays identifies novel and unnatural carbohydrate-based ligands for potential ricin sensor development," *Chem. Sci.*, vol. 2, no. 10, p. 1952, 2011.

[185] A. R. de Boer, C. H. Hokke, A. M. Deelder, and M. Wuhrer, "Serum antibody screening by surface plasmon resonance using a natural glycan microarray," *Glycoconjugate J.*, vol. 25, no. 1, pp. 75–84, 2008.

[186] A. Rouleau, M. Osta, G. Lucchi, P. Ducoroy, and W. Boireau, "Immuno-MALDI-MS in human plasma and on-chip biomarker characterizations at the femtomole level," *Sensors*, vol. 12, no. 11, pp. 15119–15132, 2012.

[187] B. Meyer and T. Peters, "NMR spectroscopy techniques for screening and identifying ligand binding to protein receptors," *Angew. Chem. Int. Ed.*, vol. 42, no. 8, pp. 864–890, 2003.

[188] A. Blume, J. Angulo, T. Biet, H. Peters, A. J. Benie, M. Palcic, and T. Peters, "Fragment-based screening of the donor substrate specificity of human blood group B galactosyltransferase using saturation transfer difference NMR," *J. Biol. Chem.*, vol. 281, no. 43, pp. 32728–32740, 2006.

[189] M. Menendez, "Isothermal titration calorimetry: Principles and applications," pp. 113–127, Wiley, 2020.

[190] Y. Ikeda, D. Kubota, and Y. Nagasaki, "Simple solid-phase synthesis and biological properties of carbohydrate-oligonucleotide conjugates modified at the 3'-terminus," *Bioconjugate Chem.*, vol. 21, no. 9, pp. 1685–1690, 2010.

[191] P. Dumas, E. Ennifar, C. D. Veiga, G. Bec, W. Palau, C. D. Primo, A. Piñeiro, J. Sabin, E. Muñoz, and J. Rial, "Methods in enzymology. Chapter 7: Extending ITC to kinetics with kinITC," pp. 157–180, Elsevier, 2016.

[192] J. M. D. Trani, N. Moitessier, and A. K. Mittermaier, "Measuring rapid timescale reaction kinetics using isothermal titration calorimetry," *Anal. Chem.*, vol. 89, no. 13, pp. 7022–7030, 2017.

[193] H. Su and Y. Xu, "Application of ITC-based characterization of thermodynamic and kinetic association of ligands with proteins in drug design," *Front. Pharmacol.*, vol. 9, 2018.

[194] E. C. Hulme and M. A. Trevethick, "Ligand binding assays at equilibrium: validation and interpretation," *Brit. J. Pharmacol.*, vol. 161, no. 6, pp. 1219–1237, 2010.

[195] T. K. Dam and C. F. Brewer, "Thermodynamic studies of lectin-carbohydrate interactions by isothermal titration calorimetry," *Chem. Rev.*, vol. 102, no. 2, pp. 387–430, 2002.

[196] T. K. Dam and C. F. Brewer, "Lectins. Chapter 4: Applications of isothermal titration calorimetry to lectin-carbohydrate interactions," pp. 75–101, Elsevier, 2007.

[197] M. Reynolds, M. Marradi, A. Imberty, S. Penadés, and S. Pérez, "Multivalent gold glycoclusters: High affinity molecular recognition by bacterial lectin PA-IL," *Chem. A Eur. J.*, vol. 18, no. 14, pp. 4264–4273, 2012.

[198] P. R. Gooley, A. Koay, and J. I. Mobbs, "Methods in molecular biology. Chapter 6: Applications of NMR and ITC for the study of the kinetics of carbohydrate binding by AMPK beta-subunit carbohydrate-binding modules," pp. 87–98, Springer New York, 2018.

[199] N. Sindhuwinata, L. L. Grimm, S. Weißbach, S. Zinn, E. Munoz, M. M. Palcic, and T. Peters, "Thermodynamic signature of substrates and substrate analogs binding to human blood group B galactosyltransferase from isothermal titration calorimetry experiments," *Biopolymers*, vol. 99, no. 10, pp. 784–795, 2013.

[200] B. Gerland, A. Goudot, C. Ligeour, G. Pourceau, A. Meyer, S. Vidal, T. Gehin, O. Vidal, E. Souteyrand, J. J. Vasseur, Y. Chevolot, and F. Morvan, "Structure binding relationship of galactosylated glycoclusters toward Pseudomonas aeruginosa Lectin LecA using a DNA-based carbohydrate microarray," *Bioconjugate Chem.*, vol. 25, no. 2, pp. 379–392, 2014.

[201] M. Matsui and Y. Ebara, "Enhanced binding of trigonal DNA–carbohydrate conjugates to lectin," *Bioorg. Med. Chem. Lett.*, vol. 22, no. 19, pp. 6139–6143, 2012.

[202] A. Delices, D. Moodelly, C. Hurot, Y. Hou, W. L. Ling, C. S. Pierre, D. Gasparutto, G. Nogues, P. Reiss, and K. Kheng, "Aqueous synthesis of DNA-functionalized near-infrared $AgInS_2$/ZnS core/shell quantum dots," *ACS Appl. Mater. Interfaces*, vol. 12, no. 39, pp. 44026–44038, 2020.

[203] J. S. Helm, Y. Hu, L. Chen, B. Gross, and S. Walker, "Identification of active-site inhibitors of MurG using a generalizable, high-throughput glycosyltransferase screen," *J. Am. Chem. Soc.*, vol. 125, pp. 11168–11169, 2003.

[204] P. Compain and O. Martin, "Design, synthesis and biological evaluation of iminosugar-based glycosyltransferase inhibitors," *Curr. Top. Med. Chem.*, vol. 3, pp. 541–560, 2003.

[205] E. E. Carlson, J. F. May, and L. L. Kiessling, "Chemical probes of UDP-galactopyranose mutase," *Chem. Bio.*, vol. 13, pp. 825–837, 2006.

[206] J. R. Brown, B. E. Crawford, and J. D. Esko, "Glycan antagonists and inhibitors: A fount for drug discovery," *Crit. Rev. Biochem. Mol. Biol.*, vol. 42, pp. 481–515, 2007.

[207] E. Fischer, "Syntheses in the purine and sugar group," 1902.